Half-sandwich Complexes of Ruthenium Supported by N-Heterocyclic Carbene Ligands: Synthesis and Application to Catalysis

Van Hung Mai

M.Sc

Chemistry

Thesis submitted to the Faculty of Graduate Studies

In partial fulfillment of the requirements

For the Ph.D. degree in chemistry

Chemistry Department

Faculty of Mathematics and Science

Brock University

St. Catharines, Ontario

Feb, 2017

Abstract

This thesis presents the preparation and catalytic reactivity of novel half-sandwich ruthenium complexes supported by N-Heterocyclic Carbene (NHC) ligands. The cationic half-sandwich ruthenium complexes $[Cp(IPr)Ru(CH_3CN)_2]^+$ show interesting reactivities toward the transfer hydrogenation of different unsaturated substrates, such as ketones, olefins, N-heterocycles, and nitriles. Kinetic studies disclose that a neutral trishydride ruthenium complex is actually involved in the catalytic cycle, playing the role as a resting state.

Further investigations on the sub-class of trishydride ruthenium complexes bearing NHC ligands ($Cp'(NHC)RuH_3$) reveal that these complexes have an unusual and great catalytic performance toward the hydrodefluorination (HDF) of fluorinated aromatic and aliphatic compounds. The combined kinetic studies, cross-over experiments and rate law analysis suggest an unusual mechanistic pathway for the $Cp^*(IPr)RuH_3$ catalyzed HDF. This study is one of the rare examples where isopropanol is employed as a reducing agent for the metal-mediated HDF reaction.

A class of silyl dihydride ruthenium complexes, derived from $Cp(IPr)RuH_3$ are prepared. These silyl hydrido derivatives are great compounds for the study of the inter ligand hypervalent interaction (IHI), an interesting phenomenon for many non-classical silane complexes. This study also suggests that the replacement of phosphines by their isolobally analogous NHC ligands result in stronger IHI interactions in the corresponding compounds.

Another type of non-classical interaction was systematically scrutinized in a

series of new cationic and neutral silane sigma complexes of ruthenium bearing different silyl moieties. These new NHC-supported ruthenium complexes allow for direct comparation with the known phosphine analogues, which reveals interplay of steric and electronic factors on the extent of Si-H complexation to metal and the extent of additional interligand interactions between Ru-Cl and chlorosilane ligand.

Finally, new trishydride ruthenium complexes bearing NHC ligands (Cp'(NHC)RuH_3) catalyze the H/D exchange reaction of various N-heterocycle substrates; their catalytic performance can be considered as one of the mildest, and most efficient approaches.

Manuscripts based on this work

1. Mai, V. H.; Kuzmina, L. G.; Churakov, A. V.; Korobkov, I.; Howard, J. A. K. "NHC carbene supported half-sandwich hydridosilyl complexes of ruthenium: the impact of supporting ligands on Si···H interligand interactions" *Dalton Trans*, **2015**, *45*, 208.

2. Mai, V. H.; Korobkov, I.; Nikonov, G. I. "Half-sandwich silane σ-complexes of ruthenium supported by NHC carbene", *Organometallics*, **2016**, *35*, 936.

3. Mai, V. H.; Nikonov, G. I.; "Transfer hydrogenation of nitriles, olefins, and N-heterocycles catalyzed by an NHC-supported half-sandwich complex of ruthenium" *Organometallics*, **2016**, *35*, 943.

4. Mai, V. H.; Nikonov, G. I.; "Hydrodefluorination of fluoroaromatics by isopropanol catalyzed by a ruthenium NHC complex. An unusual role of the carbene ligand", *ACS Catalysis*, **2016**, *6*, 7956.

5. Mai, V. H.; Nikonov, G. I.; "Half sandwich, NHC supported, tris-(hydride) ruthenium catalysts for H/D exchange reactions" (Manuscript in preparation).

Acknowledgements

To my deepest gratitude, I would like to thank my supervisor Professor Georgii Nikonov for all of his support, patience, and guidance. For the last several years, what I have learned from him is not only his passion about chemistry but also his devotion to the high academic standards. I must admit that his brilliant ideas are very intriguing, and his pedagogical approach is very nice and pleasant, which nourished and encouraged me to become an independent scientist. I am forever in debt for what you have done in the past several years to support my study and life.

In addition, I would like to express my gratitude to my committee members at Brock University, Prof. Martin Lemaire, Prof. Heather Gordon, and Prof. Melanie Pilkington, for not only their support and valuable suggestions, but also critical comments on my research. Prof. Travis Dudding and Prof. Art van der Est are thanked for their participation in my Ph.D candidacy examination. In addition, I want to thank Prof. Costa Metallinos for his interesting NMR lectures. Indeed, all of my administrative paperwork cannot be done without the help of Prof. Tony Yan, Ms. Chris Skorski, Ms. Marie Harris, Ms. Barbara Daly, and Ms. Beulah Alexander, therefore, I would like to thank all of you for that.

Honestly, I cannot imagine how my research could progress without the helping hand of our NMR technologist Razvan Simionescu. I would like to acknowledge you (Razvan) again for your great assistance with various NMR experiments, and for our conversations not only about NMR but also on other interesting scientific subjects. I am grateful to Dr. Sergio Paone for assisting me with my teaching duties; your great advice and effort made the TA become my enjoying

time. I also appreciate the great work of John and Jordan Vandenhoff (Glassblowing Shop) and Steve Crumb and his team (Machine Shop). In addition, I am thankful to Irene Palumbo, Jenn Roberts, and Alison Smart (Science Store) for giving us a friendly environment and great help. I would like to acknowledge Brock University, the OGSST program and sponsors, in particular, Gail Neff for the Gail I. Neff Award and NSERC for their financial support. I am very grateful to our collaborators, Dr. Ilia Korobkov (University of Ottawa), Prof. Judith A. K. Howard, Dr. Lyudmila G. Kuzmina and Dr. Andrey V. Churakov who professionally performed X-rays studies for my compounds.

In addition, I would like to thank Prof. Tom Baker for his unconditional support on reading and revising my thesis, as well as travelling such a long trip from Ottawa to Brock for my thesis defense. For such a great thing like that, I cannot imagine in my life that a very busy professor can do for me. I also want to thank Prof. David Ditor and Prof. Kirill Samokhin for being Chair and Internal Examiner for my thesis defense.

Furthermore, I would like to thank the previous and present members of Prof. Nikonov's research group for their great help and being great friends, Dr. Terry Chu, Dr. Kseniya Revunova, Nick McLeod, Dr. Sun Hwa Lee, Kayla Jacobsson, John Lortie, Irina Alshakova, Minh Tho Nguyen, Jan-Willem Lamberink, Josh Clarke, Joseph Cartwright, and others. Particularly, I would like to express my grateful to Dr. Terry Chu for all of his contributions to our lab and thank for all good memories and things you have done in the last five years.

In addition, I thank all graduate students of other research groups, especially the Hudlicky, Metallinos, Tony Yan, Lemaire, Stamatatos, Pilkington, Atkinson and

Dudding groups in Chemistry Department. It has been a privilege to have a good friendship with amazing and talented people. Thank you very much for being such good friends.

Finally, I have never expressed in words how much love my family gives to me; in these tiny texts, I would like to cherish your sacrifices and support during all these years. You have given me so much, and I in turn so little. Especially, to my wife and little son, you provide me a great shelter, called HOME.

To my wife, Thu Phuong Tong

to my son, Mai Hai Nam

& to my parents

Contents

List of Figures, Schemes, and Tables

Abbreviations

Å	Angstrom
acac	Acetylacetonate
AN	Acetonitrile
ACHN	1,1’-azobis(cyclohexanecarbonitrile)
Ar	Aryl
AH	Asymmetric hydrogenation
ATH	Asymmetric transfer hydrogenation
atm	Atmosphere (1atm = 101.3 kPa)
b	Broad (in NMR)
$BArF_4^-$	$B(C_6F_5)_4^-$
BAF	$[B[3,5\text{-}(CF_3)_2C_6H_3]_4]^-$
Bu	Butyl
*t*Bu	Tert-butyl
Calc.	Calculated
cat	Catalyst
Conv.	Conversion
cod	Cyclooctadiene
coe	Cyclooctene
ºC	Degrees Celsius
3c-2e	Three centre – two electron

Cp	η^5-C_5H_5
Cp_2Ru	Ruthenocene
Cp*	η^5-C_5Me_5
Cp’	η^5-C_5H_5 or η^5-C_5Me_5, unless specified
d	Doublet (in NMR)
DCD	Dewar-Chatt-Duncanson
DCM	Dichloromethane
DFT	Density functional theory
DME	1,2-dimethoxyethane
DMF	Dimethylformamide
DMSO	Dimethyl sulphoxide
DPPE	1,2-Bis(diphenylphosphino)ethane
EA	Elemental analysis
Et	Ethyl
Equiv.	Equivalents
EPR	Electron paramagnetic resonance
Exc.	Excess
FLP	Frustrated Lewis Pair
h	Hour
Hz	Hertz

IPA	Isopropanol
IPr	1,3-bis(2,6-diisopropylphenyl)imidazol-2-yliden
IPrHCl	1,3-bis-(2,6-diisopropylphenyl)imidazolinium chloride
IPr=S	1,3-bis(2,6-diisopropylphenyl)-1H-imidazole-2(3H)-thione
IMes	1,3-bis(2,4,6-trimethylphenyl)imidazol-2-yliden
IMesHCl	1,3-bis(2,4,6-trimethylphenyl)imidazolium chloride
IMes=S	1,3-dimesityl-1H-imidazole-2(3H)-thione
IMes(-1)HCl	1,3-bis(2,6-dimethylphenyl)imidazolium chloride
IMes(-1)=S	1,3-bis(2,6-dimethylphenyl)-1H-imidazole-2(3H)-thione
ItBu	1,3-di-tert-butylimidazol-2-ylidene
ItBuHBF$_4$	1,3-di-tert-butylimidazolinium tetrafluoroborate
ItBu=S	1,3-di-tert-butyl-1H-imidazole-2(3H)-thione
IiPr	1,3-diisopropylimidazol-2-ylidene
IiPrHPF$_6$	1,3-diisopropylimidazolium hexafluorophosphate
IiPr=S	1,3-diisopropyl-1H-imidazole-2(3H)-thione
J	Coupling constant (in NMR)
Hantzsch ester	Diethyl-1,4-dihydro-2,6-dimethyl-3,5 pyridinedicarboxylate
HBpin	Pinacolborane
HBcat	Catecholborane

HD	H/D exchange reaction
HDF	Hydrodefluorination
TH	Transfer hydrogenation
TE	Trans esterification
IHI	Interligand hypervalent interactions
IR	Infrared
L_n	Ligands
M	metal
m	Meta
m	Multiplet (in NMR)
min	minute
Me	Methyl
Mes	Mesityl
MO	Molecular orbital
MVP	Meerwein-Ponndorf-Verley reaction
NHC	N-heterocyclic carbene
NMR	Nuclear magnetic resonance
o	Ortho
OTf	triflate
p	Para

Ph	Phenyl
PMHS	Polymethylhydrosiloxane
^{i}Pr	isopropyl
Py	Pyridine
PDMS	Polydimethylsiloxane
q	Quartet (in NMR)
RT	Room temperature
s	Singlet (in NMR)
sat	Satellite (in NMR)
Sept	Septet (in NMR)
SISHA	secondary interactions between silicon and hydrogen
t	Triplet (in NMR)
t	tertiary
TMDS	Tetramethyldisiloxane
TMP	2,2,6,6-tetramethylpiperidine
TBAF	Tetrabutylammonium fluoride
TMAF	Tetramethylammonium fluoride
TOF	Turnover frequency
TON	Turnover number
VT	Variable temperature

UV	Ultraviolet
δ	Chemical shift, ppm (in NMR)
σ	Sigma
η	Eta
2c/2e	2 centre 2 electrons
3c/2e	3 centre 2 electrons
9BBN	9-Borabicyclo[3.3.1]nonane

I. Introduction

Reduction is one of the crucial transformations in the organic synthesis,[1-4] and includes such methods as hydrogenation,[5-9] hydrosilylation,[10-13] hydroboration,[14-18] transfer hydrogenation,[5, 8, 19-23] hydrogenolysis.[24] Unquestionably, the catalytic reduction is the most important reaction in a wide range of reduction transformations, judging by the fact that several Nobel prizes have been awarded for work in this area.[25] Since the discovery of finely-divided metal hydrogenation catalysts by Sabatier et al., who received a Nobel prize for this work, catalytic reduction has been vastly developed on both laboratory and production scales for a wide variety of chemicals.[25-27] Notably, not only have heterogeneous catalysts been used in this catalytic reduction, but homogeneous and enzyme-based catalysts have also been involved in the field.[26-39] Owing to their convenience (easily prepared and separated), heterogeneous catalytic systems have shown excellent results for the reduction of various unsaturated functional groups.[7-9, 19, 22-23] There are several well-known heterogeneous catalysts for reduction, such as Raney, Lindlar, and Pd/C catalysts.[19, 36, 40-41] Regrettably, heterogeneous systems are less effective in asymmetric synthesis than homogeneous ones, which was highlighted by the fact that a Nobel prize were awarded to Noyori and Knowles for their achievement in catalytic homogeneous asymmetric hydrogenation.[22, 26-27, 42-46] With the aid of homogeneous catalytic reduction methods, an enormous library of compounds, bearing diverse functional groups, has been reduced to high degrees of regio, stereo, and chemoselectivity to obtain many complex molecules, which then are used in many fields, such as military, polymer, pharmaceutical, agricultural and space applications.[28, 30-32, 34-39, 47-49]

It is widely acknowledged that homogeneous catalytic hydrogenation is the

most preferred method for reducing unsaturated bonds, owing to its atom efficiency, broad substrate scope, and well-developed approaches. Along the development path for homogeneous catalytic hydrogenation systems, there have been significant efforts to investigate the mechanisms of this unique transformation. In 1965, Sir Wilkinson, a future Nobel laureate, presented one of the first homogeneous systems, using phosphine based rhodium catalysts, which is still an inspiration to many chemists today.[50] This work could be considered a milestone in mechanistic understanding of catalytic hydrogenation, as based on similar systems, Halpern et al. suggested several fundamental steps in this catalytic cycle (Figure I-1).[51-52]

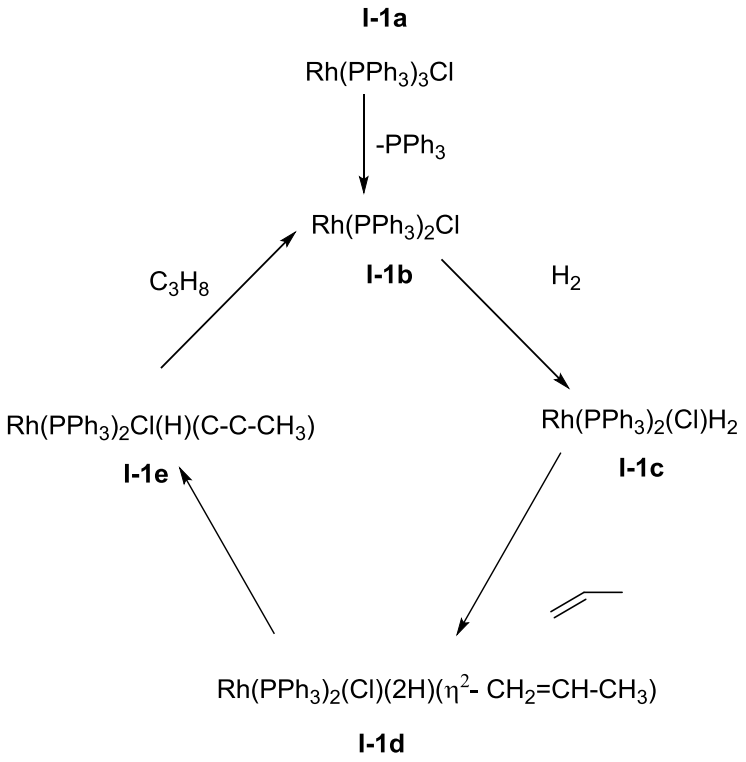

Figure I- 1. Halpern's catalytic cycle for hydrogenation of olefins

Briefly, the catalytic cycle begins with the dissociation of one phosphine

ligand from **I-1a** to form the unsaturated 14e rhodium complex **I-1b**, from which hydrogen is cleaved homolytically across the metal centre to generate a dihydride complex.[50, 53-55] Then, the olefin coordinates to this newly formed dihydride rhodium complex to produce a π-coordinated olefin complex (**I-1d**); and the following steps include olefin insertion into the Rh-H bond (**I-1e**) and reductive elimination that will regenerate the Rh(I) complex (**I-1b**), and release alkane to complete the cycle. It is also worth mentioning that this catalytic cycle is useful to explain the stereoselectivity control of chiral-version catalysts, using the quadrant model to predict enantioselectivity in homogeneous hydrogenation (Figure I-2). The chiral determining steps normally take place upon the coordination of olefin (or substrates in general), and requires additional interactions, controlled by the steric and electronic environment around the metal centre, to achieve the highest recognition for chiral selectivity.[26-27, 43-46]

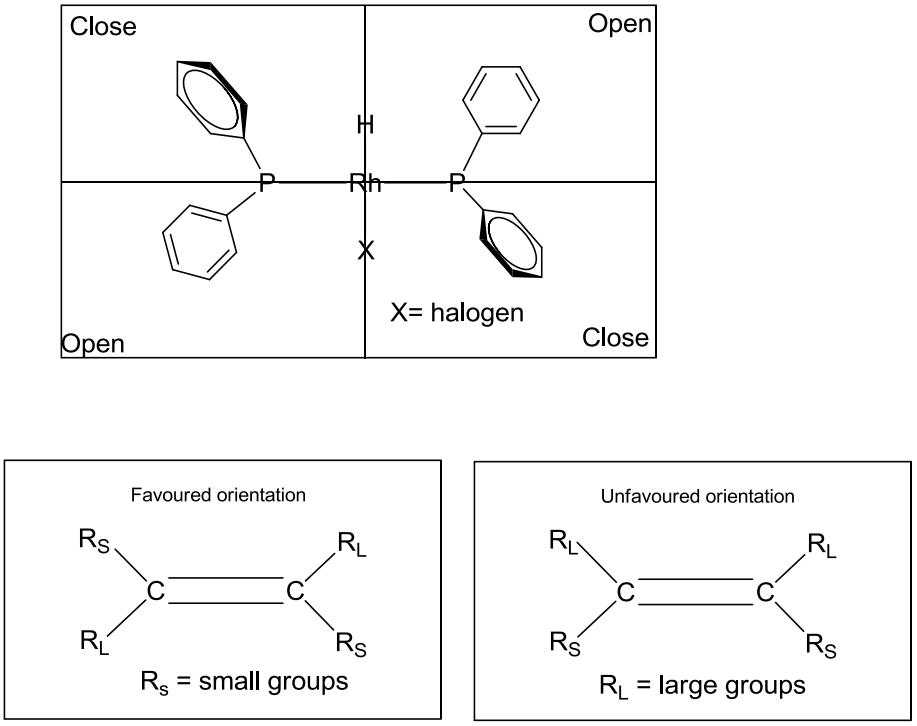

Figure I- 2. The quadrant model to predict enantioselectivity

It must be noted that other reduction methods have also contributed significantly to obtain a variety of regio-, enantio-, chemo- directed and functionalized compounds.[11-13, 56-60] For examples, transfer hydrogenation is an important method for catalytic reduction; which allows for small scale syntheses, milder conditions, and simple laboratory setup and avoids the elevated pressure and safety issues of hydrogenation by molecular H_2.[5, 8, 19, 22-23, 28, 61-62] Also considered as a hydrogen transfer method is the Meerwein-Ponndorf-Verley (MVP) reaction,[63] which will be mentioned in chapter II of this thesis. The MVP is an attractive alternative method for the reduction of aldehydes and ketones using alcohol as the reducing agent. This method has been used in the fine and specialty chemicals for fragrance and pharmaceutical industries.[26, 28, 30-31, 34-35, 42, 47-48] In the 1990s, breakthrough discoveries in the field of catalytic transfer hydrogenation were

established by several pioneers, such as Noyori, Burk, and Kagan; they designed a plethora of chiral ligands (mostly phosphine based), such as BINAP,[64] DIOP,[65] Duphos,[66] and DIPAMP.[67] Once these ligands are associated with Ru, Rh, or Ir metal centre, many active complexes could be formed, which led to great improvement on the catalytic transfer hydrogenation in terms of achieving higher yield and enantioselectivity.[28, 42-46, 62, 68-69] More details related to the mechanisms of transition metal catalyzed transfer hydrogenation reactions, will also be mentioned in chapter II of this thesis; a general mechanism for metal catalyzed transfer hydrogenation involves two significant steps:[5, 8, 23] 1) hydride and proton are transferred from substrates to the metal centre (and/or basic sites on ligands), 2) then the hydride and proton would be transferred into the unsaturated substrate (Figure I-3).

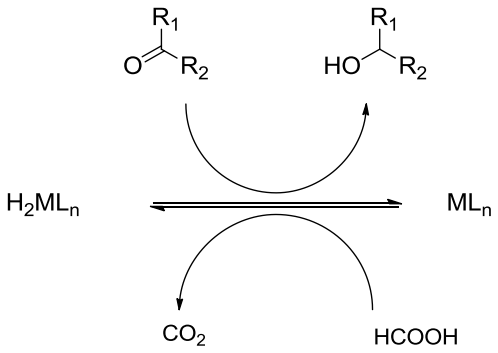

Figure I- 3. Transfer hydrogenation pathway

So far, half sandwich π-complexes of ruthenium,[61, 70-79] rhodium,[67, 80-81] and iridium[1, 82-84] show great activity toward transfer hydrogenation in both asymmetric and non-asymmetric versions. As a part of our interest in catalytic reduction, we investigated the preparation of Cp' (Cp and Cp*) ruthenium complexes[85-89] and examined them toward transfer hydrogenation using alcohol[21, 90] and formate as reducing agent.[91] We also performed kinetic studies related to these catalytic

systems.[21, 91]

Another popular approach to reducing unsaturated compounds is catalytic hydrosilylation,[10-13, 60, 92-97] which allows for access to a large collection of important silicon-based materials,[98] such as sealants, adhesives, coating, and silicon polymers.[99-100] The first transition metal catalyzed hydrosilylation of olefins can be dated back to a study by Chalk and Harrod in 1965 (Figure I-4).[52] Using group VIII transition metal complexes as catalysts for the hydrosilylation of 1-hexene, these authors suggested the first mechanism for catalytic hydrosilylation of C=C bonds, which are involved in the (M^n/M^{n+2}) catalytic cycle. Importantly, in this study, they suggested that the activation of the Si-H bond by the transition metal was fast and could proceed before the coordination of the olefin (even in the presence of large excess of olefin), therefore the silyl hydride metal complexes would be the kinetically favored intermediates. The silylated product could be generated from the reductive elimination of the alkyl, silyl hydride metal complexes. The proposed mechanism, suggested by Ojima et al (Figure I-5),[101-102] for the hydrosilylation of carbonyl groups, is slightly different from that of olefins, in which the end-on coordination of carbonyl and the insertion of carbonyl into the M-Si bond take place.

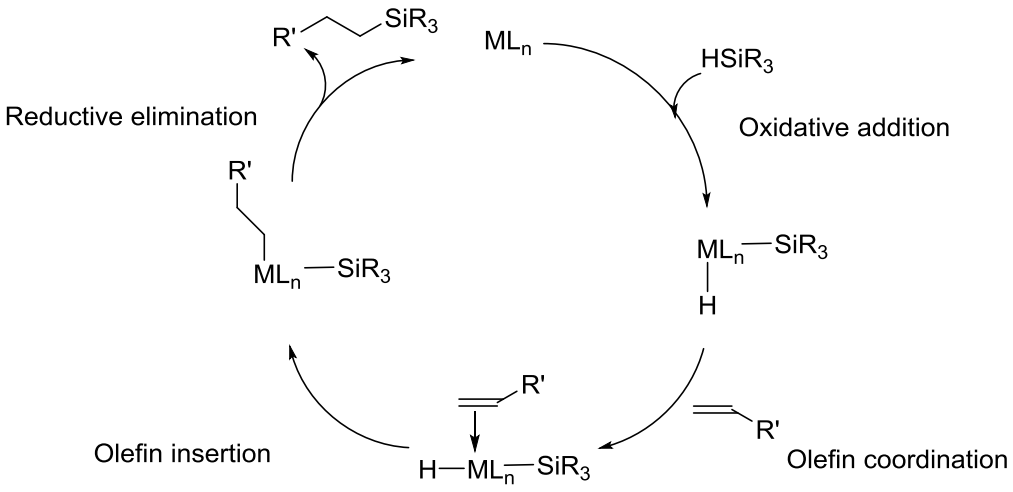

Figure I- 4. Chalk-Harrod hydrosilylation mechanism

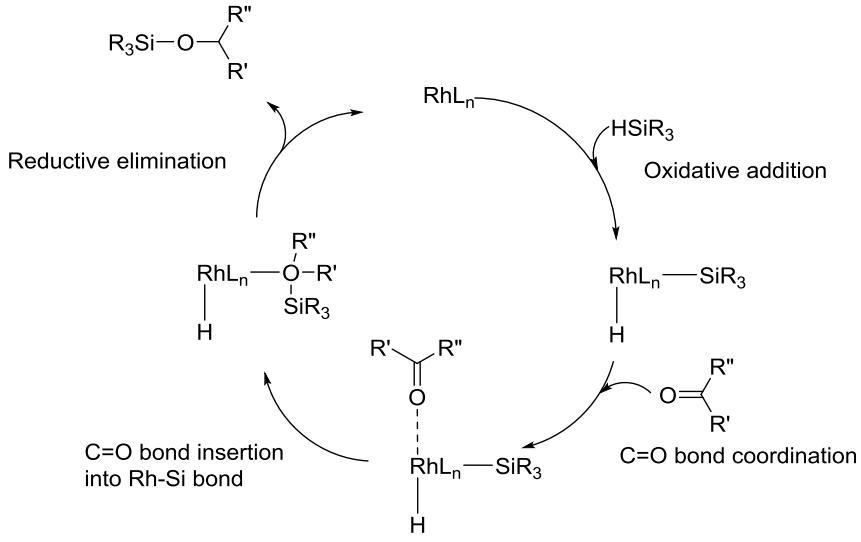

Figure I- 5. Ojima's carbonyl hydrosilylation mechanism

Due to the common features of the transition metal catalyzed hydrosilylation such as the activation of the Si-H bond, and the formation of silyl hydride intermediates,[103] investigations of the Si-H-M interaction can be considered as a very important subject, which allows for a better understanding of catalyst behavior and makes its improvement and modification more directed.[20, 85, 89, 96, 104-111] In general,

the addition of silane to the transition metal centre can go through several stages (Figure I-6), including weak σ-interaction, α-agostic, and hypervalent interligand interaction to fully oxidized and classical 2c/2e product.[94, 103, 112-114] Except for the latter species, which is a classical hydride silyl complex, all intermediates of silane addition can be classified as having non-classical interactions (details about non-classical interaction will be mentioned in section VIII), of which the 3c/2e type of bond is most known.[87]

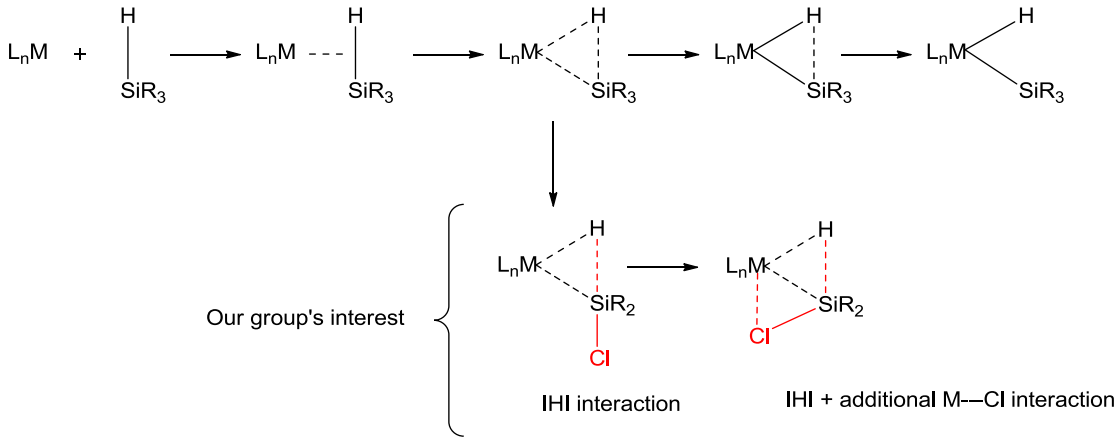

Figure I- 6. SiH bond addition to metal centre

Our group has pioneered studies on one specific type of nonclassical silane complexes, the Interligand Hypervalent Interactions (IHI).[85, 87, 89, 115-118] This phenomenon has been observed for early transition metal (Ti,[115] Nb,[119] Ta,[120] and V[121]) to late transition metal complexes (Ru[87, 116-117, 122-123], and Fe[122]). Recently, our group found that ruthenium complexes bearing Cp' and phosphine ligands have great reactivity toward the catalytic hydrosilylation of nitriles,[108, 124] pyridine,[125] and N-heterocycles.[91, 126] These are very important transformations, considering that it is a great synthetic challenge to selectively add a Si-H bond to the robust C≡N bond in nitrile and the C=N bond in aromatic cyclic compounds such as pyridine and N-

heterocycles. We found that η^2-silane chloride complexes supported by the $Cp(PR_3)Ru$ fragment can have an unusual secondary Si---Cl interaction between the chloride and silane moieties in addition to the non-classical Si---H bonding in the silane ligand (Figure 6, bottom scheme).[85, 87, 89, 117, 127-128]

As a continuation of previous Nikonov group research, we are interested in exploring the reactivity of new half sandwich ruthenium complexes supported by N-Heterocyclic carbene (NHC) ligands toward catalytic reductions, such as hydrosilylation, transfer hydrogenation, and other transformations (Scheme I-1). Moreover, we would like to examine the effect of replacement of the phosphine ligand by a stronger σ-donating NHC carbene ligand on the nature and strength of Si-H interactions in the silyl Cp/Ru/NHC systems, and how this change will impact the activity of these new complexes in catalytic reactions.

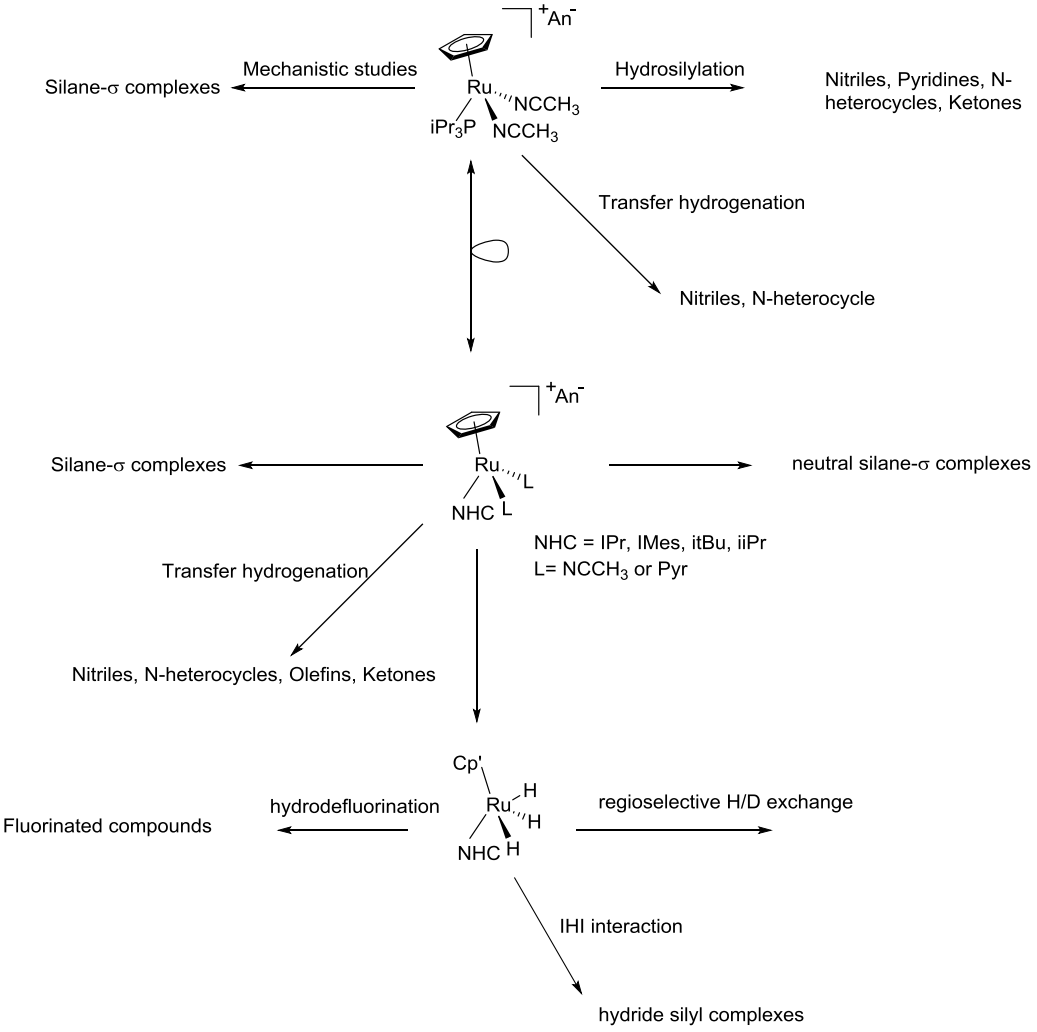

Scheme I- 1. Ruthenium chemistry from our group

Literature review:

II. Transition metal catalyzed transfer hydrogenation of unsaturated compounds

The reduction of unsaturated compounds into the corresponding saturated ones is one of the fundamental transformations in chemistry.[1, 3-4, 129] These transformations can be achieved either by direct reactions with stoichiometric reagents such as $LiAlH_4$, $NaBH_4$,[130] silanes,[131] boranes[14, 17, 132] or by metal catalyzed reductions.[133-135] In terms of atom economy, direct hydrogenation with pressurized hydrogen gas is the best choice. However, the use of the potentially explosive H_2 gas requires significant capital cost, presents serious hazards, and is inconvenient for laboratory applications.[6-9, 67, 136] In sharp contrast, transfer hydrogenation reactions, in which the addition of hydrogen from hydrogen donor molecules, typically an alcohol or formic acid, can be an attractive alternative route to access a wide range of hydrogenated substrates. Transfer hydrogenation thanks to its ease of handling, low cost, and ready availability of hydrogen donors has emerged as a core process in hydrogenation studies.[5, 8, 19-20, 23, 137]

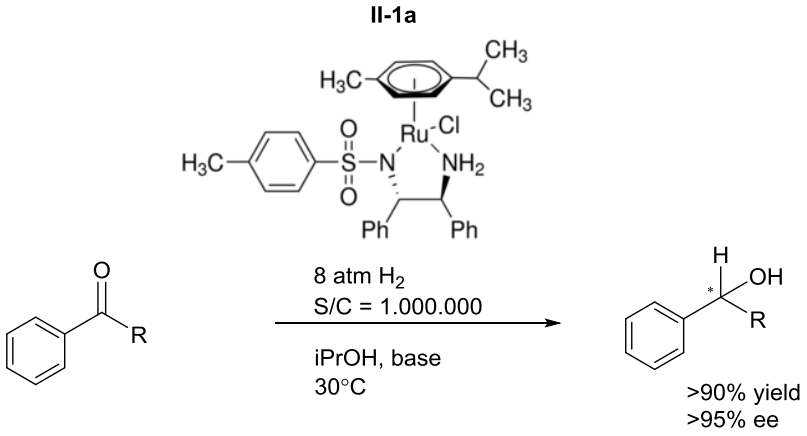

Figure II- 1. Noyori's catalyst for asymmetric hydrogenation

Dating back to the great discovery by Noyori and Ikariya et al., who developed the highly efficient asymmetric transfer hydrogenation (ATH) of ketones at room temperature by Ru(II)-arene/ TsDPEN (**II-1a**) systems, numerous studies have been carried out on both the transfer hydrogenation (TH) and asymmetric transfer hydrogenation with different catalysts, various hydrogen donors and a wide range of substrates (Figure II-1).[27, 33, 64, 138-142] Significant advances have been made with the catalyzed transfer hydrogenation of carbonyls and imines in both asymmetric and non-asymmetric processes.[22, 143-144]

Unfortunately, there are several compounds less likely to be subjected to the transfer hydrogenation method, such as those bearing C≡N triple bond or C-F bonds. They are very hard to reduce due to the high bond activation energies. Non-activated olefins should also be added to this list, due to the lack of directing group for better enantioselectivity. In this historical review, we will mainly discuss the transfer-hydrogen reduction of these substrates either by stoichiometric reductions or by catalyzed transformations in both heterogeneous and homogeneous systems, including several highlights about the catalytic mechanism.

II.1 Historical background

Reduction of organic compounds is one of the most important synthetic methods for laboratory and industrial applications.[1-4, 129-130, 145] There are various methods for effecting reduction, such as i) hydrogenation,[6-9, 136, 146] the addition of hydrogen to unsaturated groups, such as ketones, aldehydes, imines, and ii) hydrogenolysis,[147-157] the replacement of a functional group / an element by hydrogen, iii) hydrosilylation,[10-13, 59, 92, 95, 124, 158-159] hydroborylation,[14-18] the addition of Si-H (B-H) bonds across unsaturated bonds. In 1903, Knoevenagel group[160] discovered the reduction of dimethyl 1,4-dihydroterephthalate to dimethyl terephthalate with the aid of palladium black, which is now classified as a hydrogen transfer reaction (Figure II-2).

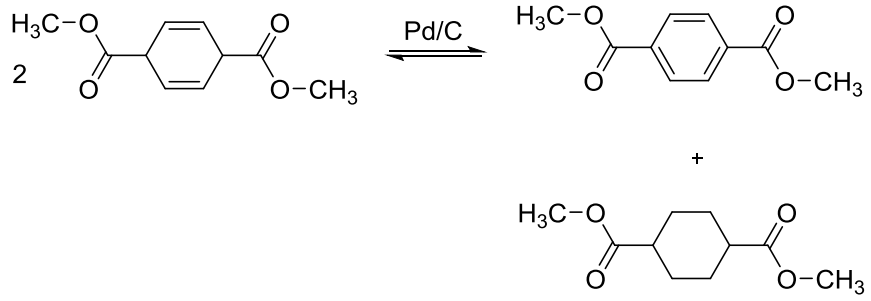

Figure II- 2. Knoevenagel's discovery

However, compared to the catalytic reduction with molecular hydrogen or metal hydrides,[3] this hydrogen transfer reduction method was underutilized due to such drawbacks as poor yields, long reaction times, and limited substrate scope as observed in early studies. Since 1964, the utility of transfer hydrogenation has

dramatically changed thanks to the striking discovery by the Braude group[161] (Figure II-3), who reported that ethylenic and acetylenic linkages could be efficiently reduced in high yield and selectivity in the presence of palladium black with cyclohexene as the hydrogen donor. Since then, the application of hydrogen transfer has increased owing to its prevailing advantages,[5, 8, 23] such as no special gas container is needed, simple stirring of solutions is all that is required, and a large selection of hydrogen donor molecules may be used.

Transfer hydrogenation was initially employed in heterogeneous systems, where Pd/C was a favourite choice for the reduction of many organic compounds. There was a long list of functional groups which could be reduced by the Pd/C system, including nitro, azo, azoxy, azomethine and carbonyl groups.[19] Nitriles, known as the less active substrates, were also successfully reduced to amines with the same Pd/C system.[162] Although more and more substrates were found to be reduced by the transfer hydrogenation method, the utility of homogeneous systems was not well studied until several decades later.

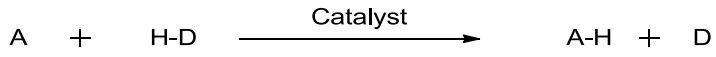

Figure II- 3. Transfer hydrogenation pathway

This could be associated to the widespread interest of chemists in heterogeneous catalytic reduction systems. However, there were several studies highlighting the mechanism of heterogeneous catalysis, setting the cobblestones to build a road of well-known "inner - outer sphere" mechanisms later. In the mid-1920s, Meerwein−Schmidt,[63] Ponndorf,[163] and Verley,[164] from three different

groups, reported the highly selective reduction of carbonyls to alcohols under mild conditions with the aid of $Al(O^iPr)_3$, and isopropanol as the hydrogen donor source (Figure II-4). It was not a very efficient reaction as it required the use of superstoichiometric amounts of $Al(O^iPr)_3$ as a reagent. Regardless of how inefficient the reaction was, authors came up with the brilliant idea about a six-membered ring transition state (Figure II-4, bottom) for its proposed mechanism, which was a great aesthetic pleasure. Even though this mechanism originally was applied to the non-transition metal reactions, it has been a great candidate for later mechanistic proposals for homogeneous transition metal catalyzed transfer hydrogenations. It now can be classified as a direct H-transfer mechanism. According to this mechanism, both hydrogen donor and acceptor were simultaneously coordinated to the same metal centre to form a six-membered cyclic transition state, then the hydride is transferred directly from the donor to the acceptor without the formation of any metal hydride species. Later computational work provided support to this mechanism for some transition metal catalysts.

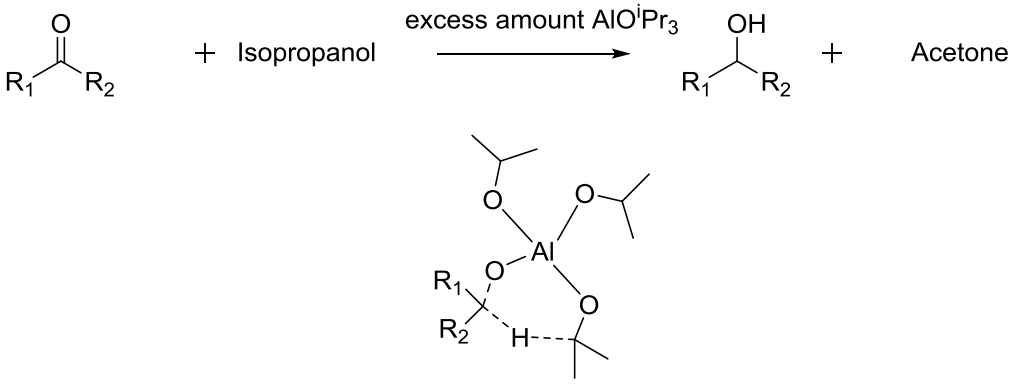

Figure II- 4. MVP transfer hydrogenation and direct H^- transfer transition state

Soon after this mechanism had been proposed, an alternative mechanism pathway was suggested, firstly by Bäckvall,[165] and later by Handgraaf[166] as well as by Baratta.[167-168] Well-designed labeling experiments from the Bäckvall's group demonstrated that hydrogen was transferred from donor to acceptor through a monohydride mechanism (Figure II-5) rather than by the dihydride mechanism. These studies lead to the coinage of the "inner sphere" mechanism, where metal alkoxide complexes are the most important intermediates for hydride transfer between donor and acceptor.

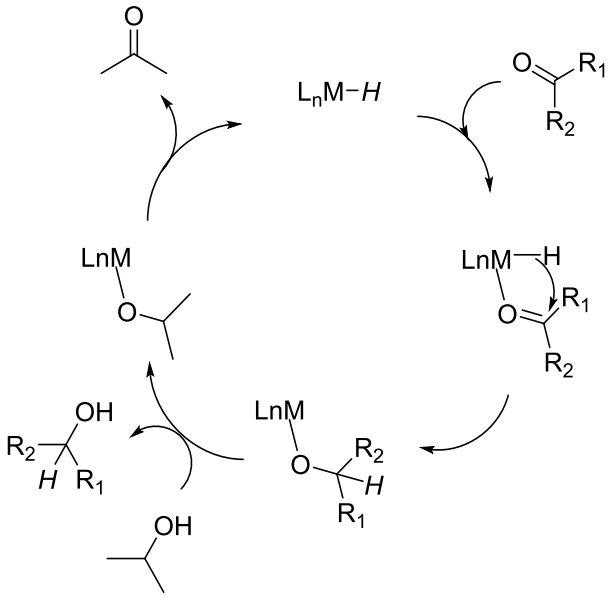

Figure II- 5. Monohydride mechanism

However, these mechanisms could not explain the remarkable accelation hydrogenation and transfer hydrogenation by NH-amino complexes of ruthenium studied by Noyori et al.,[27,33] who suggested the involvement of both the metal

hydride and a proton on an amine ligand in the formation of a six-membered transition structure (Figure II-6). In a cooperative way, the substrate could slip easily into the favourite chiral quadrant site of the metal sphere, which was determined to be the result of hydrogen bond between the carbonyl group of substrate and the amine proton of the ligand.

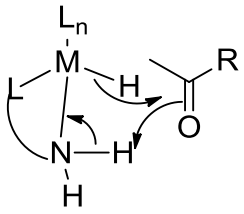

Figure II- 6. Six-membered transition state in Noyori's bifunctional catalyst

This model also allowed Noyori to explain why the TsDPEN/Ru system exhibited high enantioselectivity with the ee of up to 99% and the high yield for carbonyl reduction, which was attributed to the very selective recognition of polar C=O bonds by the polar NH functionality. In addition to this great discovery of the TsDPEN/Ru system, Noyori's work led to the development of two remarkable and unconventional concepts:[27, 33, 73, 169] 1) the substrate does not bind directly to the metal centre during the whole hydride transfer process, but interacts with the ligand only, according to the "outer sphere" mechanism; and 2) the proton transfer between the donor and acceptor could be facilitated by a hydrogen bond between the acceptor and a basic site (which could be N-, S-, or O-based) on the ligand, the so-called metal-ligand bifunctional catalysis. These two concepts were experimentally verified through the isolation and characterization of presumed intermediates.

However, very recently Dub and Gordon have performed detailed DFT calculations of the Noyori system and proposed an alternative explantion for the

activation of carbonyls (acetophenone) in asymmetric hydrogenation of (Figure II-6b, top). This mechanism laso emphasizes the importance of hydrogen bond formation between the substarte and the NH site but also involves the homolytic splitting of H_2 via the formation of a six-membered ring transition state, in which the appended substrate essentially plays the role of an internal base. Therefore, the whole activation process has a significant contribution of the reagent, ligand, and the metal (Figure II- 6a, bottom).[33b]

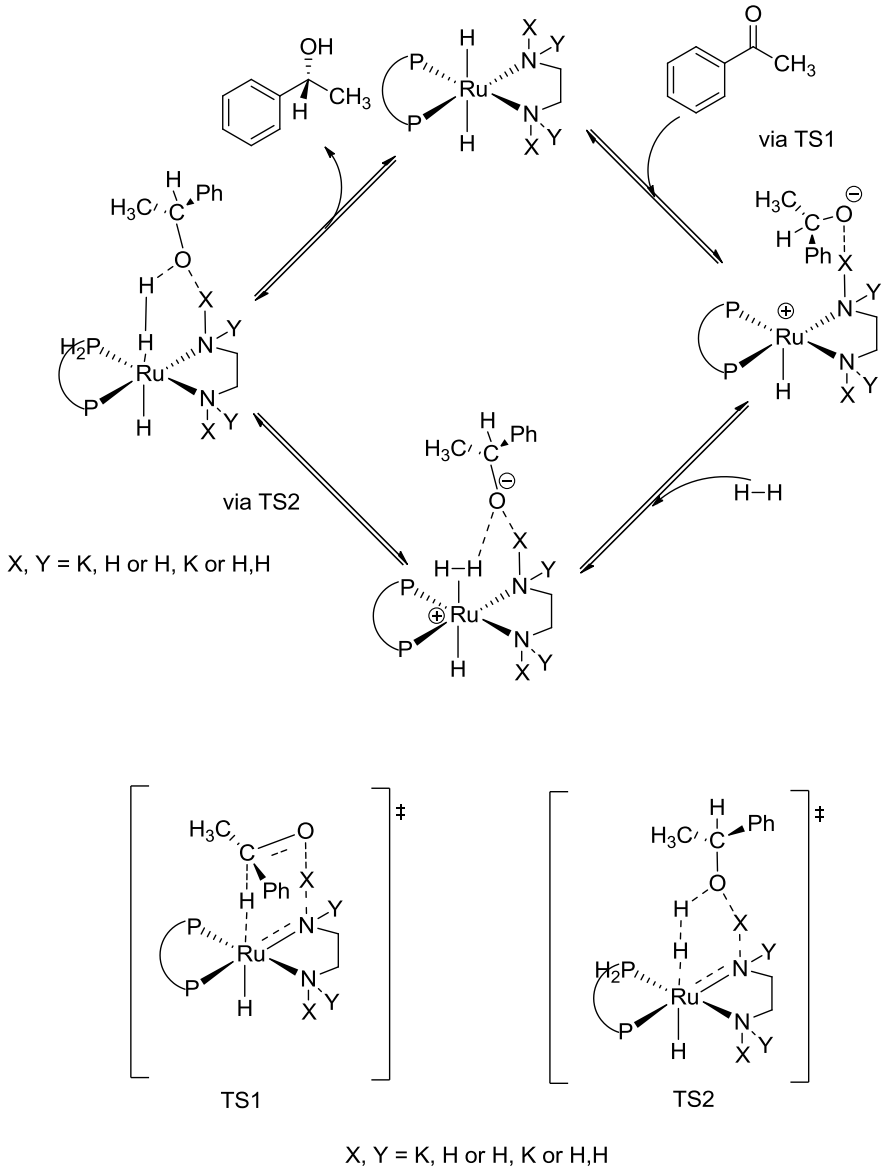

Figure II- 6a. Dub and Gordon's mechanism.

All these five mechanisms are currently accepted by the chemical community, and depending on the nature of the ligand and the metal centre, a certain pathway would be preferred over others.

II.2 Nitriles

II.2.1 Reductions of nitriles

The reduction of nitriles to amines or imines is one of the key processes for the synthesis of agro- and pharmaceuticals, dyes, as well as numerous fine chemicals.[29, 170] Conventionally, nitriles are reduced by using stoichiometric amounts of metal hydrides $LiAlH_4$ or $NaBH_4$, hydrosilanes, or Hantzsch ester.[38, 171] However, these methods are usually accompanied with some drawbacks such as poor atom efficiency, low selectivity, expensive and hazardous reagents, less tolerance of different functional groups, and wasteful by-products (Figure II-7).

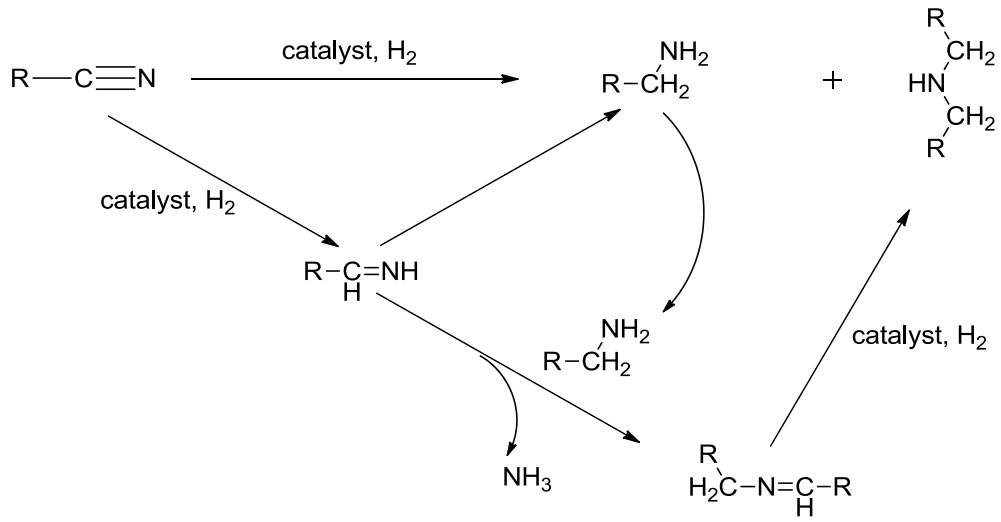

Figure II- 7. Hydrogenation of nitriles, and possible by-products proposed by Adkins

To perform this transformation in cheaper, greener and atom-economic ways, the catalyzed hydrogenation with pressurized hydrogen gas is the best choice. Previously, heterogeneous systems, employing Raney-Ni and -Co catalysts,[41, 170, 172] have been applied for industrial production of amines from nitriles. However, these systems also suffer from the need of additives, instability of catalysts, high temperature and/or high-pressure operation, and a limited substrate scope. Recently, to achieve the goal of Green Chemistry synthesis, there have been two competing trends in the reduction of nitriles, which are transition metal mediated hydrogenation and catalytic transfer hydrogenation. In this mini historical review, we would like to cover the recent progress in hydrogenation and transfer hydrogenation of nitriles with both heterogeneous and homogeneous systems.

II.2.2 Transition metal catalyzed TH of Nitriles

One of the first examples of the metal-catalyzed reduction of nitriles was reported by Szantay's group.[173b] In this work, Pd/C was utilized as a catalyst, with p-menthene or tetralin as hydrogen donors. This reaction required very harsh conditions to reduce some α,β -unsaturated nitriles to give a mixture of amines. The author also pointed out that aliphatic nitriles were more resistant to reduction by the same catalytic system. In fact, previous reports on reductions of nitriles were very divergent, and usually, the reduction stopped at the formation of imines. Another challenge with the hydrogenation of nitriles is the low selectivity of this reaction. As stated in their study, Adkins et al.[174] explained the reasons why this transformation leads to different products including amines and imines (Figure **II- 7**). Firstly, R-C≡N would be hydrogenated to give the corresponding imine. This imine intermediate could be further reduced to yield the wanted primary amine, or

followed by a coupling reaction with the newly formed amine to give the secondary amine and ammonia (in the presence of hydrogen). In further steps, di-substituted and trisubstituted amines could be formed through an analogous reaction path.

The first efficient nitrile reduction system was demonstrated by Bishop's group,[175] who reduced sebaconitriles completely in the presence of Raney Nickel catalyst under high pressure of H_2 (1500psi). Indeed, high temperature and the utility of additives were also demanded this transformation. These harsh conditions actually were a typical problem for heterogeneous catalytic hydrogenation of nitriles. One of the early examples of homogeneous catalysis was patented by Levering[176] in 1964, in which the carbonyl complexes $Fe(CO)_5$ and $Ni(CO)_4$ were employed as catalysts for the hydrogenation of nitriles under very high temperature and pressure (~200 °C, ~140 bar H_2). Inspired by these first examples, more and more studies have focused on the development of new catalytic systems with different metal centres.

II.2.3 Ruthenium catalysts

A preferable industrial process of the ruthenium catalyzed nitrile hydrogenation was developed in 1999 by Beatty and Paciello,[177] who patented it using 0.1 mol % of $[RuH_2(H_2)_2(PCy_3)_2]$ under rather harsh catalytic conditions (50−70 bar H_2, 100 °C). Unfortunately, this patent did not disclose any information about the reaction mechanism, only the technical parameters. The first well-defined ruthenium catalyzed hydrogenation of nitriles was found accidentally by Hidai's group[178] (Figure II-8).

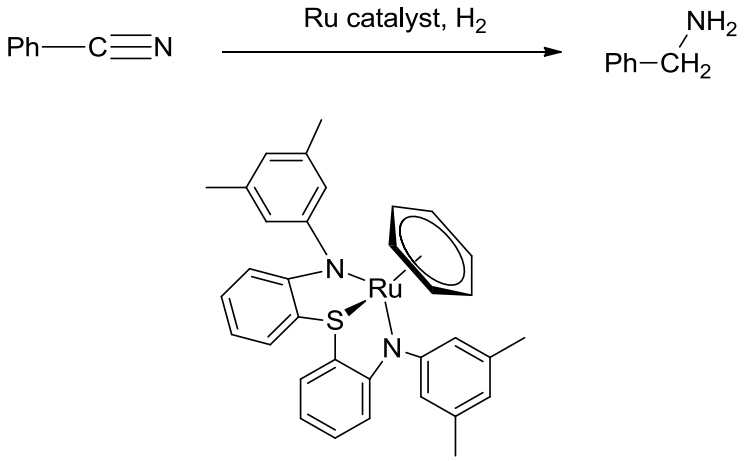

Figure II- 8. Hidai's ruthenium catalyst

Detoured from their original goal to activate dinitrogen molecules, these authors realized that their ruthenium complexes tailored with bis(diarylamido)/thioether ligands (Figure II-8, bottom) could be also used as efficient catalysts for the hydrogenation of aromatic nitriles. In the presence of 1 mol % catalyst, benzonitrile was smoothly hydrogenated at 80 °C in THF under 30 atm of H_2. Originally, within only 18 h, the reaction was completed to yield mainly benzylamine (72%) together with benzylidene benzylamine (27%) and a trace amount of dibenzylamine. However, upon the addition of an external base EtONa (10 mol %), the selectivity toward primary amine was remarkably enhanced (92%) and only traces of other products were obtained.

Giannelli et al.[179] published one of the first mechanistic studies about the ruthenium catalyzed hydrogenation of benzonitrile. Known as effective catalysts for the hydrogenation of olefins, several dihydride ruthenium complexes such as $RuH_2(CO)_2(P^nBu_3)_2$, $RuH_2(CO)_2(PPh_3)_2$, $RuH_2(PPh_3)_4$ complexes, were chosen as catalysts in their kinetic study (Figure II-9).

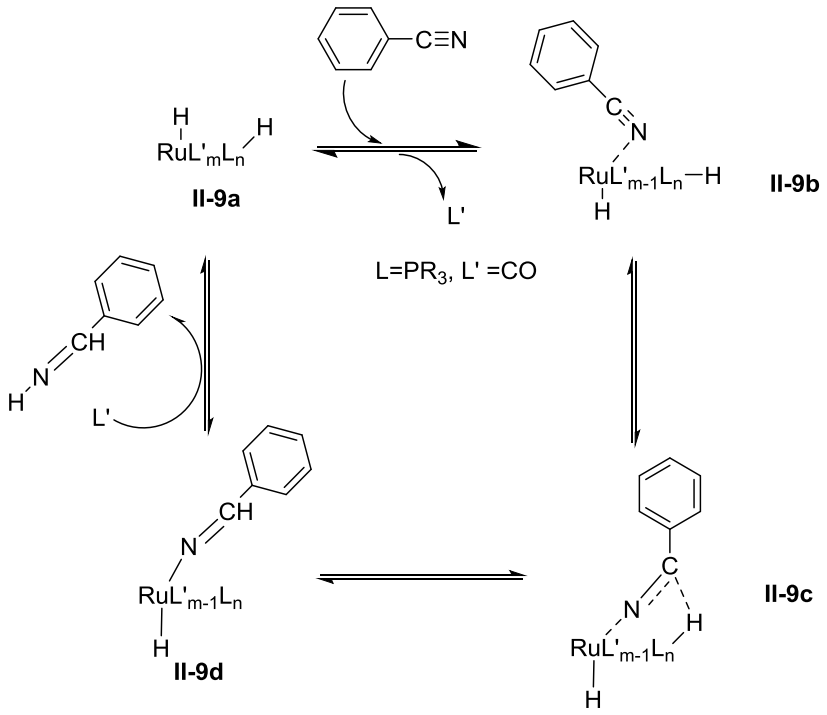

Figure II- 9. Giannelli 's catalytic pathway

The kinetic and thermodynamic data of this study suggested the following mechanism. In the first step, one of the phosphine ligands is replaced by a benzonitrile to form the complex (**II-9b**). The insertion of the C≡N bond into the Ru–H then takes place through a four-centre intermediate (**II-9c**) to generate an imino Ru complex (**II-9d**). In the next step, the regeneration of the original catalyst (**II-9a**) and formation of imine were completed through the hydrogenolysis of the complex (**II-9d**). The hydrogenation of newly formed imine to yield a primary amine would occur in a similar pathway, through a new dihydroimino ruthenium intermediate.

This mechanism was then supported by the isolation of benzamide RuH_2(NHCOPh) complexes by Morris et al.[180] in 2007. In addition, they proposed that nitrile hydrogenation could proceed via an outer sphere mechanism, and this

pathway was also supported by the theoretical calculation.

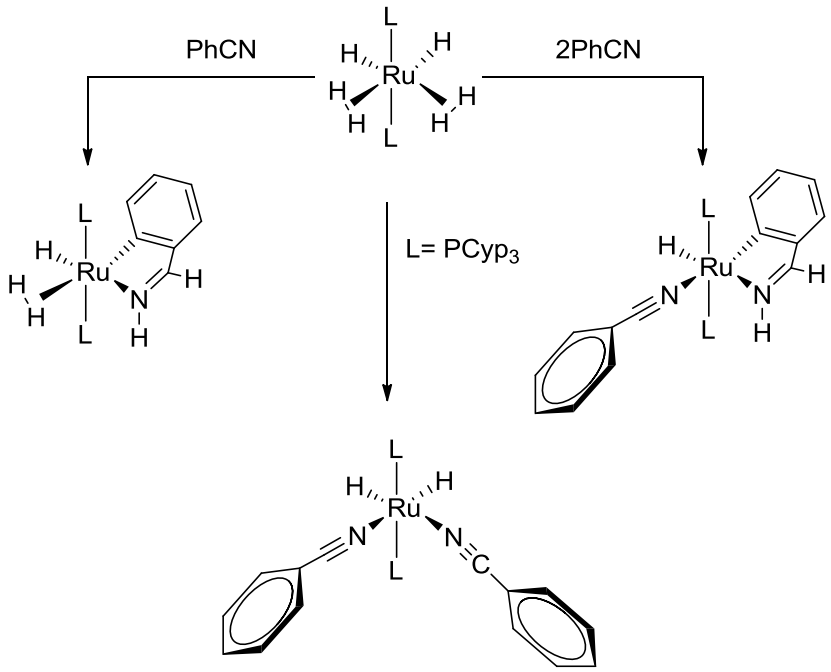

Figure II- 10. Sabo-Etienne's ruthenium catalyst

Another useful insight into the nitrile hydrogenation mechanism was provided later in 2010 by Sabo-Etienne et al.[76] The first intermediate in the benzonitrile hydrogenation (Figure II-10) was isolated and characterized by X-ray analysis. Thanks to the *ortho*-directed C−H activation within the aryl group, the catalyst resting state was quickly generated through the cyclometalation of imine and ruthenium centre. This phenomenon explained the effectiveness of this catalytic system toward benzonitrile hydrogenation under very mild conditions (99% yield, 0.5 mol% catalyst, 22°C, and 3bar H_2). However, in this study, benzonitrile was the only examined substrate.

In 2008, Beller et al.[181] reported an easy-to-adopt ruthenium catalytic system

(Figure II-11) for the homogeneous hydrogenation of nitriles, both aromatic and aliphatic, with excellent catalyst activity and high chemoselectivity. Within 10 min, most nitriles could be hydrogenated selectively to give primary amines, even at a low catalyst loading (0.125 mol %), albeit at a higher temperature (140°C). Remarkably, this catalytic system also tolerated different functional groups such as amino-, ester-, and bromo-benzonitriles.

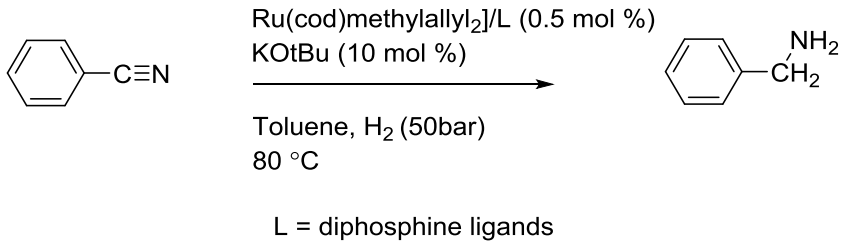

Figure II- 11. Beller's Ru/Diphosphine catalytic systems

In late 2008, Beller and co-workers[182] reported another catalytic system with a cheap triphenylphosphine ligand, and commercially available [$RuCl_2(PPh_3)_3$] compound as the catalyst (Figure II-12). Even though this system did not show a significant improvement in the catalytic reactivity, their procedure can be considered as an environmentally benign pathway to hydrogenate nitriles to give selectively

primary amines with a catalyst easily assembled *in situ*.

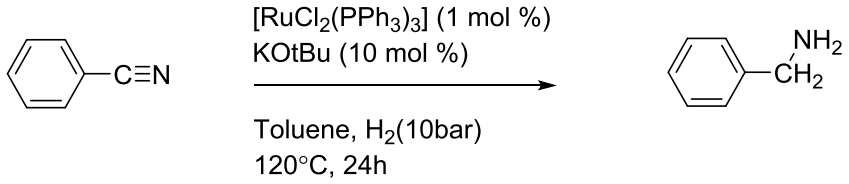

Figure II- 12. Beller's $[RuCl_2(PPh_3)_3]$ catalytic system

Moreover, the first ruthenium/ NHC carbene catalytic system was also discovered by the Beller group[183] (Figure II-13). In the presence of an excess external base (10 mol% KO^tBu), the combination of various imidazolium salts (0.5 mol %) with [Ru(cod)methylallyl$_2$] (**II-13**) (0.5 mol %) was examined for the hydrogenation of benzonitrile. Ru/SIMesBF$_4$ was the best pair to yield the highest yield of benzylamine (99%) under mild conditions (80 °C, 1 h, 35 bar H_2), however, the substrate scope of this Ru/carbene catalytic systems was very limited as

compared to their Ru/phosphine systems.

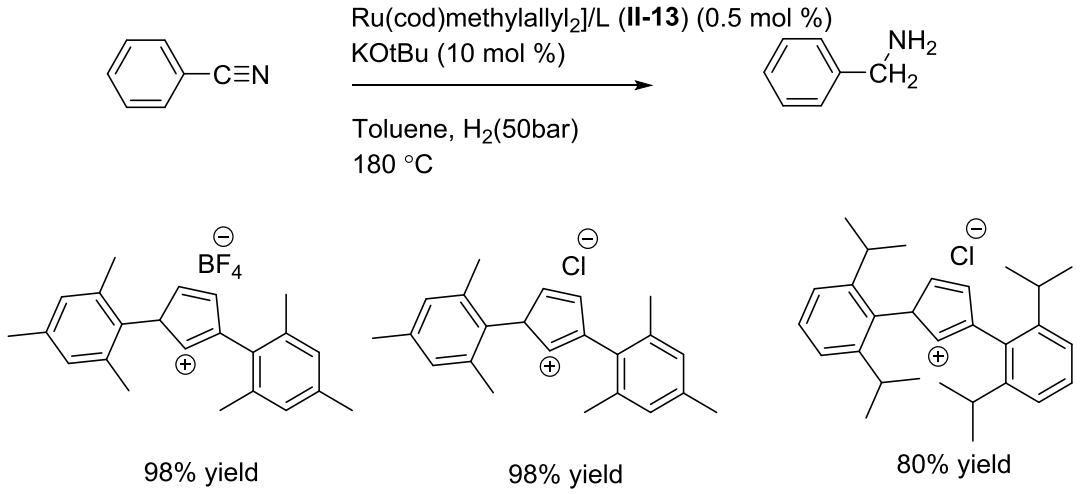

Figure II- 13. Beller's Ru/NHC catalytic systems for hydrogenation of nitrile

In the last decade, despite many reports on the application of ruthenium pincer complexes in the hydrogenation of unsaturated substrates bearing C=O, C=C, or C=N bonds, there have been a limited number of studies focusing on Ru/pincer systems in catalytic hydrogenation of the C≡N bond.[184] In 2011, the group of Leitner[185] used a non-classical hydride PNP pincer/Ru complex for the reduction of nitriles (Figure II-14). The results of this system were not promising, as very harsh conditions were needed to completely reduce nitriles to amines (135 °C, 75bar H_2, >45h). Surprisingly, the presence of a trace amount of water in their catalytic system actually enhanced the selectivity and conversion toward the formation of primary amines.

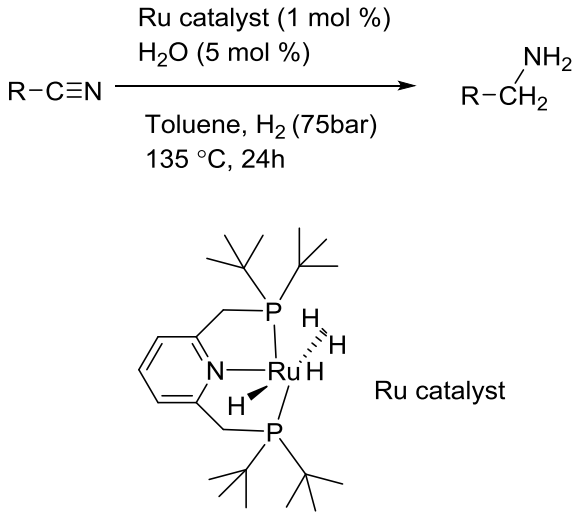

Figure II- 14. Leitner's pincer ruthenium catalyst

In 2015, Milstein et al. developed tridentate PNN and PNP Ru(II) pincer complexes (Figure II-15) supported with pyridine- and acridine- backbones, which showed imine-selective hydrogenation of nitriles under mild, neutral conditions (70 °C, 4bar H_2, <50h).[186] This is the first example that imines can be selectively formed by the hydrogenative coupling of nitriles and added amines to obtain unsymmetrical imines.

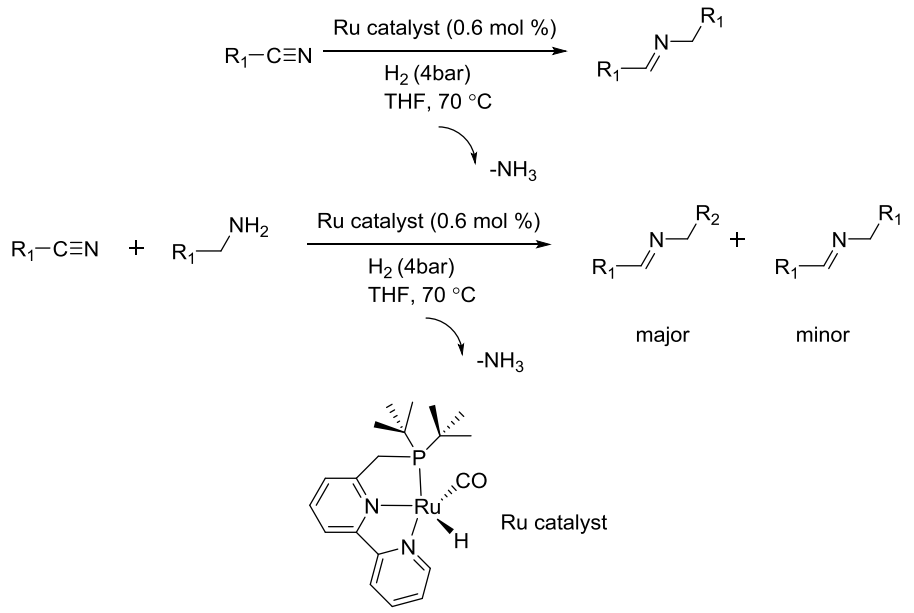

Figure II- 15. Milstein's pincer ruthenium catalyst

Actually, a few months earlier than our first paper about transfer hydrogenation of nitriles, Beller and co-workers published the first example of a heterogeneous catalytic system for the transfer hydrogenation of nitriles.[187] They found that, using Pd/C (10 mol%) as a heterogeneous catalyst and the HCOOH–NEt_3 azeotropic mixture as the hydrogen source, a variety of (hetero)aromatic nitriles could be reduced smoothly under mild conditions (98 % yield, 25 °C, <2h) (Figure II-16). Interestingly, ester and amide substituted nitriles were hydrogenated with a high chemoselectivity under the same catalytic conditions.

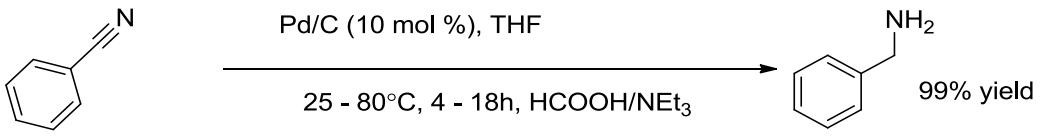

Figure II- 16. Beller's Pd/C catalyzed transfer hydrogenation of nitriles

II.2.4 Rhodium and Iridium catalysts

Surprisingly, as compared to a range of ruthenium catalysts, there has been a very limited number of rhodium and iridium-based catalytic systems for the hydrogenation of nitriles. The first example of rhodium-catalyzed nitrile reductions could be dated back to 1979, when Otsuka[188] and Yoshida showed that rhodium hydrides, [RhH(P^iPr_3)] and [$Rh_2H_2(\mu\text{-}N_2)$(P(cyclohexyl)$_3$] were active catalysts in this transformation with a low catalyst loading (1 mol%) under ambient conditions (20 °C, 1atm H_2, 20h) to gain 100% yield to amines. However, the substrate scope of this efficient system was limited to only several alkyl nitriles. The first iridium-catalyzed hydrogenation of nitriles was mentioned in 1992 by Chin and Lee.[189] Unfortunately, the selectivity of this system was not good, as a mixture of products was obtained (Figure II-17). Moreover, a common decomposition pathway with iridium catalysts was also observed with this system, as iridium clusters were formed in the presence of molecular hydrogen.[190]

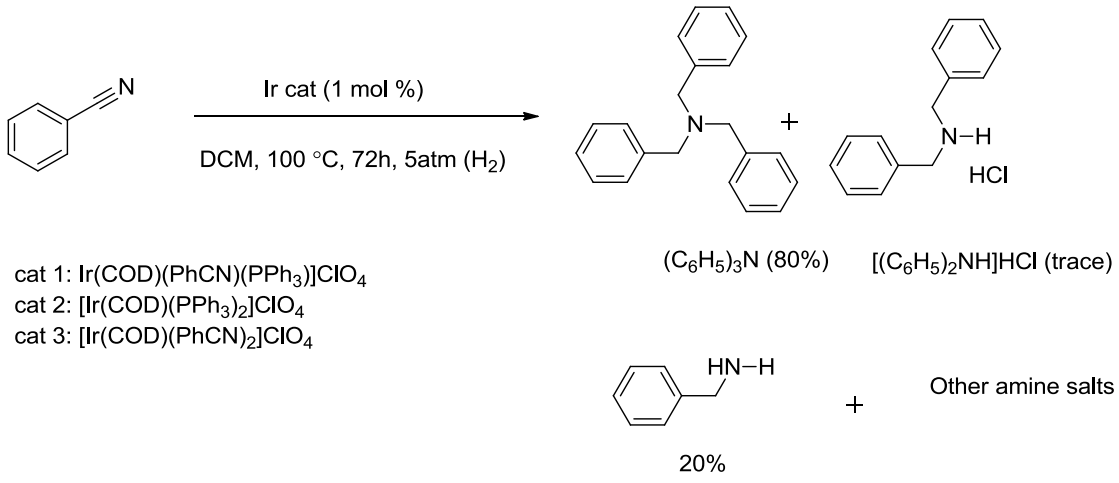

Figure II- 17. Chin and Lee's iridium catalysts

Early this year, Ikariya[191] and Sato reported that new cationic iridium and

rhodium complexes based on the C−N chelating motif ([Cp*M(NCCH$_3$){κ^2(N,C)-NH$_2$CR$_2$-2-C$_6$H$_4$}]$^+$SbF$_6^-$, M = Rh or Ir) could catalyze the hydrogenation of aromatic and cyclic-alkyl nitriles in the presence of $AgSbF_6$ and $N(C_2H_5)_3$ as additives (Figure II-18). Noteworthy, secondary amines were obtained as the main products (up to 81 % yield), and the details for this unique selectivity remain unclear at this point.

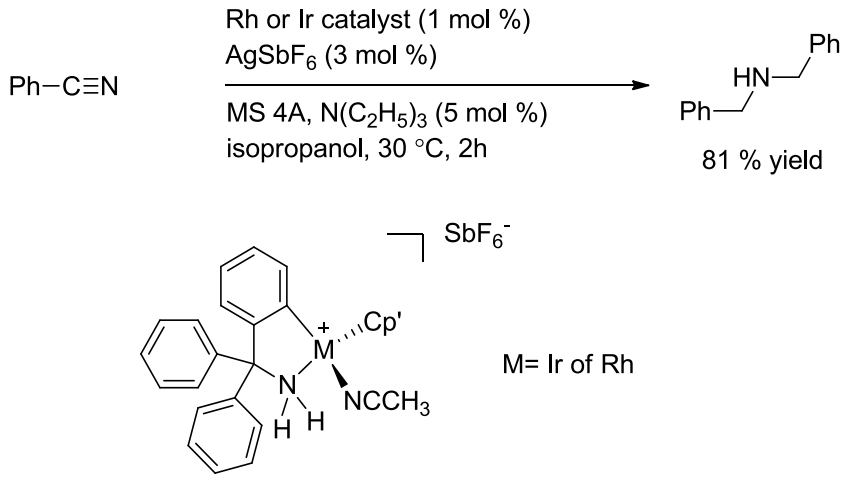

Figure II- 18. Sato's iridium and rhodium catalysts

II.2.5 Earth-abundant transition metal catalysts

In recent years, the rising prices of precious metals have brought about significant interest in the catalysis by earth abundant transition metals. The Beller group was the first to apply a base-metal catalyst to the hydrogenation of nitrile when in 2014 they introduced a novel well-defined iron PNP pincer complex for hydrogenation of aryl, alkyl, heterocyclic nitriles and dinitriles (Figure II-19).[192] This system was also characterized by its good tolerance to such functional groups as ester, ether, acetamido, and amines.

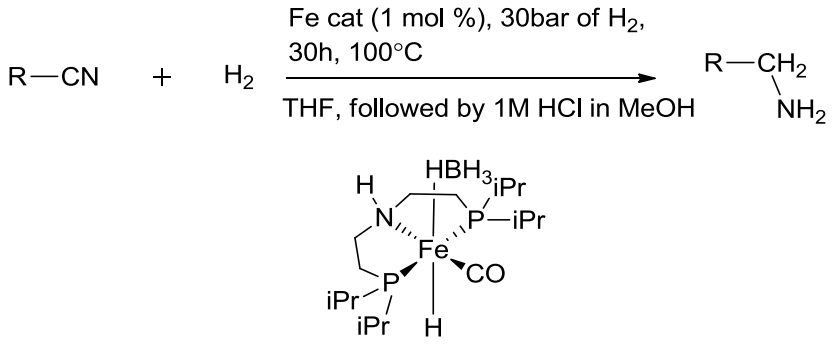

Figure II- 19. Beller's iron pincer catalyst

A year later, 2015, new iron and cobalt pincer complexes bearing rigid-backbone-NPN ligands were introduced by the Milstein group.[186, 193-194] These complexes were found to be active catalysts for the hydrogenation of nitriles to primary amines with high selectivity and yield; however, high temperature (140°C) and pressure (60 bar H_2) conditions were still required for this transformation (Figure II-20).

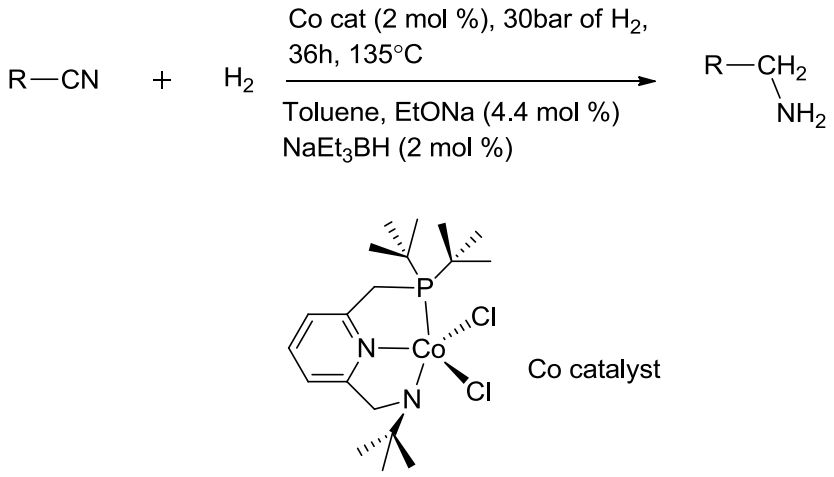

Figure II- 20. Milstein cobalt pincer catalyst

In 2016, Beller et al. developed two catalytic systems based on earth abundant transition metals (Mn and Co) for the hydrogenation of nitriles. In the first system[195] (Figure II-21), a series of well-defined manganese pincer complexes were prepared using PNP ligands. Various nitriles (including aromatic, aliphatic and dinitriles) were successfully hydrogenated at the same catalytic conditions (120 °C, 50bar H_2, 24-60h) to yield 100% primary amines in the presence of an external base (NaOtBu 10 mol %). Mechanistic study of the manganese system suggested an outer-sphere mechanism which takes place through the simultaneous transfer of the hydride from the Mn centre (Mn−H) and the proton from the nitrogen (N−H) to the nitrile to give the corresponding imine, similar to other bifunctional catalyst systems.

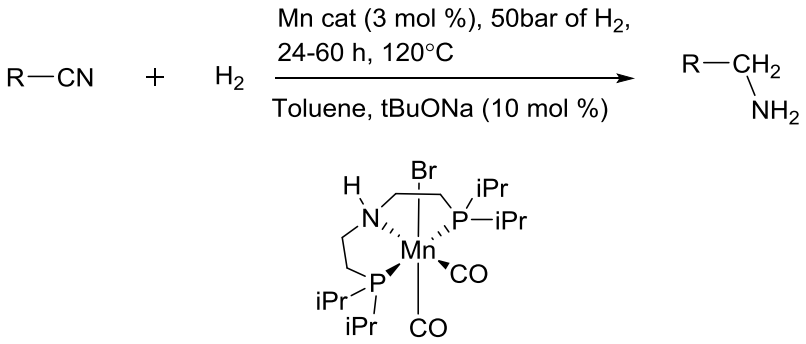

Figure II- 21. Beller's manganese catalytic system

In their second catalytic system,[196] novel heterogeneous cobalt-based catalysts were prepared by the pyrolysis of cobalt $Co(OAc)_2 \cdot 4H_2O$ with nitrogen ligands on different inorganic supports. This system worked quite well with a good tolerance to a variety of functional groups, using milder conditions (100 °C, 20bar H_2, <20 h) when compared to the previous manganese catalyst. Moreover, thanks to its heterogeneous nature, these cobalt catalysts could be separated easily from the reaction mixture and reused efficiently. In fact, recycling experiments showed that the catalysts retained their activity after eight cycles (Figure II-22).

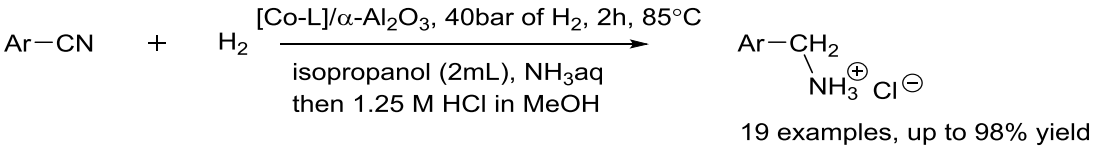

Figure II- 22. Beller's heterogeneous cobalt catalytic system

II.2.6 Perspective

There is no doubt that the future of homogeneous catalysis will involve the earth abundant transition metals. With the proper design of ligands, iron, nickel, manganese and cobalt complexes could replace precious metals such as Ir, Rh, Ru, and Pt in homogenous catalysis. In particular, this trend can be foreseen with many recent studies using pincer-type complexes for the hydrogenation of nitriles. Substrate scope of this transformation has been also lately expanded with good functional groups tolerance. In addition, the reaction conditions and work-up have also become milder and greener. The combination of hydrogenation of nitriles and other coupling reactions is another great subject for synthetic chemists because it allows for access to a variety of high-value products.

In the chapter V, new Ru complexes are prepared and characterized and tested for transfer hydrogenation of nitriles.

II.3 N-heterocycles

Even though chiral N-heteroarene derivatives are important building blocks for synthesizing many biologically relevant molecules, such as alkaloids, inhibitors, and receptors[197] (Figure II-23), the asymmetric hydrogenation (AH) of N-heteroaromatic compounds has been much less studied than other types of unsaturated systems. This situation may be caused by the three following reasons:[198] (1) deactivation or poisoning of catalyst due to the presence of nitrogen atoms in heteroarene compounds; (2) the high stability of N-heteroaromatic compounds, requiring high temperature, and pressure for the AH at these extreme conditions which may hamper the enantioselectivity; (3) simple N-heteroaromatic compounds do not contain a secondary coordinating functional group to assist in the interaction with the metal centre.

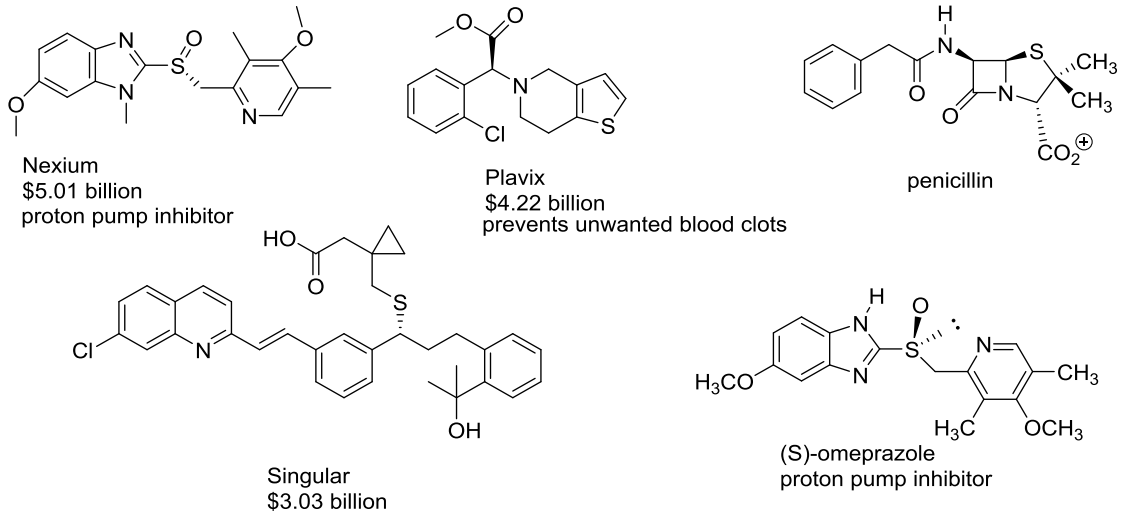

Figure II- 23. Pharmaceutical products which bear N-heterocycle building blocks.

Despite the obstacles mentioned above, the search for metal catalyzed AH of

N-heteroarenes within the last fifteen years has achieved significant progress in terms of yield, enantioselectivity and substrate scope.[199-203] The limited number of studies for the asymmetric transfer hydrogenation of N-heterocycles[200] could be attributed to the success of asymmetric hydrogenation processes using precious metals such as iridium and rhodium, and new trends in using non-metal catalyzed hydrogenation of N-heterocycles, for example by FLP systems.[204-206] In this section, we would like to highlight several advances in the asymmetric hydrogenation of N-heterocycles and recent progress toward the development of asymmetric transfer hydrogenation of these substrates.

II.3.1 Ir, Rh, and Ru-catalyzed AH of N-heterocycles

The first attempt to use homogeneous chiral catalysts for the asymmetric hydrogenation of N-heteroarenes was reported in 1987 by Murata and co-workers.[207] They employed Rh[(S, S)-DIOP]H with ethanol as the solvent for the catalytic asymmetric hydrogenation of 2-methylquinoxaline. However, the reaction was not enantioselective, with only 2% ee achieved at room temperature and 7 atm of hydrogen gas.

In 1998, a very significant improvement was achieved by the Bianchini group[208] by using an ortho-metallated dihydride iridium complex in the hydrogenation of 2-methylquinoxaline to 1,2,3,4-tetrahydro-2-methylquinoxaline with up to 90% ee. Remarkably, this was the first example of AH of N-heteroarenes with >90% ee. These pioneering works initiated a rapid growth of research activities in the asymmetric hydrogenation of N-heteroarenes over the past two decades. Following that, many novel and efficient strategies such as relay catalysis, substrate activation, and catalyst activation, while employing different hydrogen sources, were developed for the successful AH of N-heteroarenes.

In 2003, Zhou et al. discovered the first catalyst for the enantioselective hydrogenation of quinolines using [Ir(COD)Cl]/(R)-MeO-BiPhep/I_2/toluene as the catalytic system.[209-210] A series of quinoline derivatives was also screened by using this catalyst system, and all of them were hydrogenated efficiently to the corresponding products with high yield (83-97%) and excellent enantioselectivity (76%-96% ee) (Figure II-24). It is worth noting that this catalyst system also performed well in the AH of isoquinolines, one of the most challenging substrates for AH. Until now, this catalyst system has been the only successful example for an

AH transformation of isoquinoline.

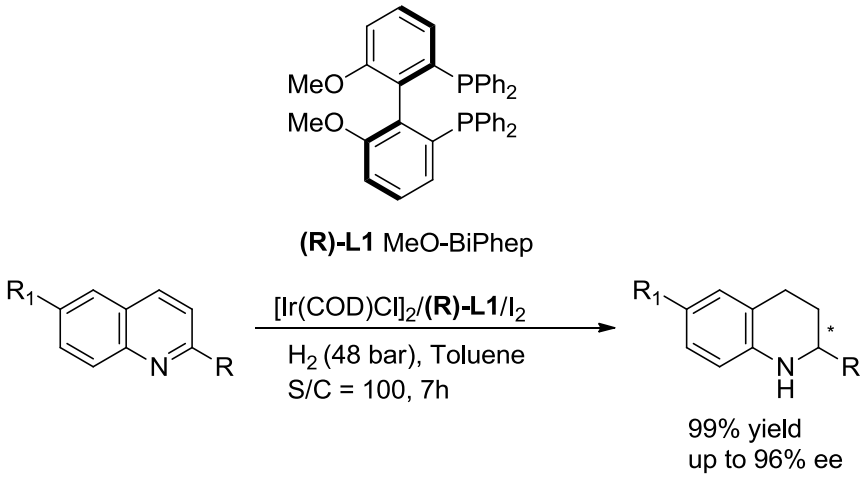

Figure II- 24. Zhou iridium catalytic systems for AH of N-heterocycles

After the impressive results of the Zhou catalyst system, much attention has been focused towards the AH of quinolines and other N-heteroarene substrates utilizing different methodologies such as chiral transition metal catalysts and organocatalysts under both homogeneous and heterogeneous conditions. Several efficient catalytic systems have been successfully developed for the AH of N-heteroarenes, using H_2 gas as the hydrogen source, as summarized in Table II-1.

So far, iridium chiral catalysts have dominated the area of metal-catalyzed asymmetric hydrogenation of N-heteroaromatic compounds and non-functionalized olefins. However, two key reasons for the continuous search of new catalysts in this field are the recognized toxicity and the volatile price of iridium metal.[211] Within seven years (from 2005 to 2011), the price of iridium metal increased by eight-fold. Additionally, iridium is not considered a bio-compatible metal.[211]

Substrates	Catalyst systems	[a]S/C	ee (%)	Reference
2-substituted quinolines	P-P*/Ir	43.000	99	[212]
2,3-disubstituted quinolines	P-P*/Ir	50	86	[213]
3-substituted quinolines	No example			
2-substituted indoles + PG	N-P*/Ir	100	99	[214-215]
2,3-disubstituted indoles + PG	Ph-TRAP/Rh	100	98	[216]
	N-P*/Ir	100	98	[215]
3-substituted indoles + PG	PhTRAP/Ru	100	72	[217]
	P-P*/Pd	50	98	[217]
Isoquinoline	P-P*/Ir	100	83	[218]
Quinoxaline	P-P*/Ir	5000	98	[219]
Pyridines + EWG	P-P*/Ir	1000	99	[220]
Pyrrole	Ph-TRAP/Ru	40	99	[221]
Imidazole +PG	Ph-TRAP/Ru	200	98	[222]

[a]S/C and ee indicate the highest values; P-P*: chiral bisphosphine ligand; N-P*: chiral bidentate nitrogen phosphine ligand; Ph-TRAP: 2,20-bis-[(diphenylphos-phino)ethyl]-1,10-biferrocene; PG: protecting group; EWG: electron withdrawing groups

Table II-1. Highly efficient catalyst systems for AH of N-heteroarenes using H_2 gas as hydrogen source

II.3.2 Earth abundant metal-catalyzed hydrogenation of N-heterocycles

Surprisingly, compared to other precious transition metal complexes, the use of earth abundant transition metal complexes in asymmetric reactions has been underdeveloped, although these metals have been known for their availability, biocompatibility, and low cost.[223] Currently, there are no examples of earth abundant transition metal catalysts for the asymmetric hydrogenation of N-heterocycles.[200] However, several recent studies on the hydrogenation of N-heterocycles suggest the possibility of future use of iron complexes as catalysts for asymmetric hydrogenation.[224] Thus, in 2014, Jones et al.[225a] reported a well-defined iron complex supported by a PNP type bis(phosphino)amine pincer ligand (Figure II-25) that could be used as a catalyst for the hydrogenation of N-heterocycles. Notably, good to excellent yields can be achieved (up to 90%) with seven examples of N-heterocycles, proceeding at 80°C, using low catalyst loadings (3% mol) and low pressure of H_2 gas (5-10 bar), in 24 hours.

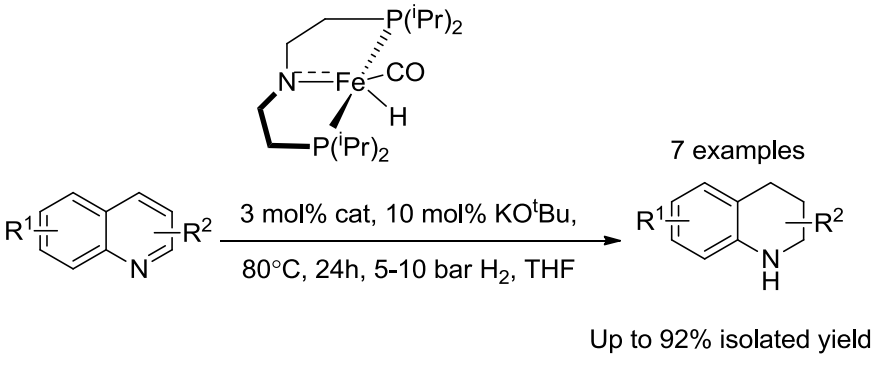

Figure II- 25. Jones' iron pincer catalyst for hydrogenation of quinolines

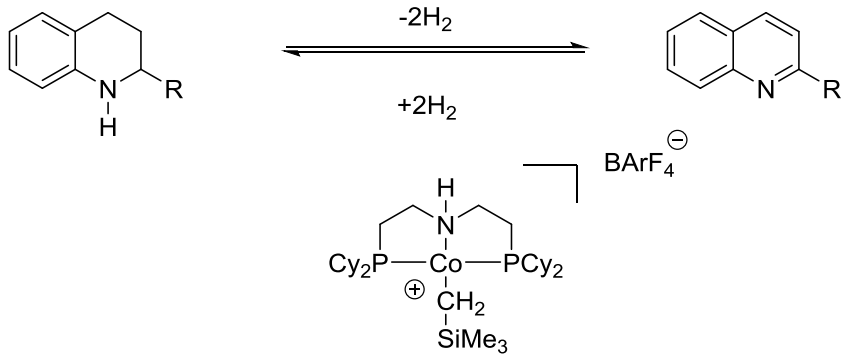

Figure II- 26. Jones' cobalt pincer catalyst

The Jones group also developed new pincer based cobalt catalysts for hydrogenation (Figure II-26).[225b] One of the special features about this catalytic system is that it can effectively catalyze both the acceptorless dehydrogenation and hydrogenation of different N-heterocycles under relatively mild conditions. With a catalyst loading of 10 mol %, quinaldine could be hydrogenated to 1,2,3,4-tetrahydro-quinaldine at 120 ^{o}C under low pressure of H_2 gas (10 atm) in 48 hours. Regrettably, the authors did not provide any details about the mechanism of this transformation.

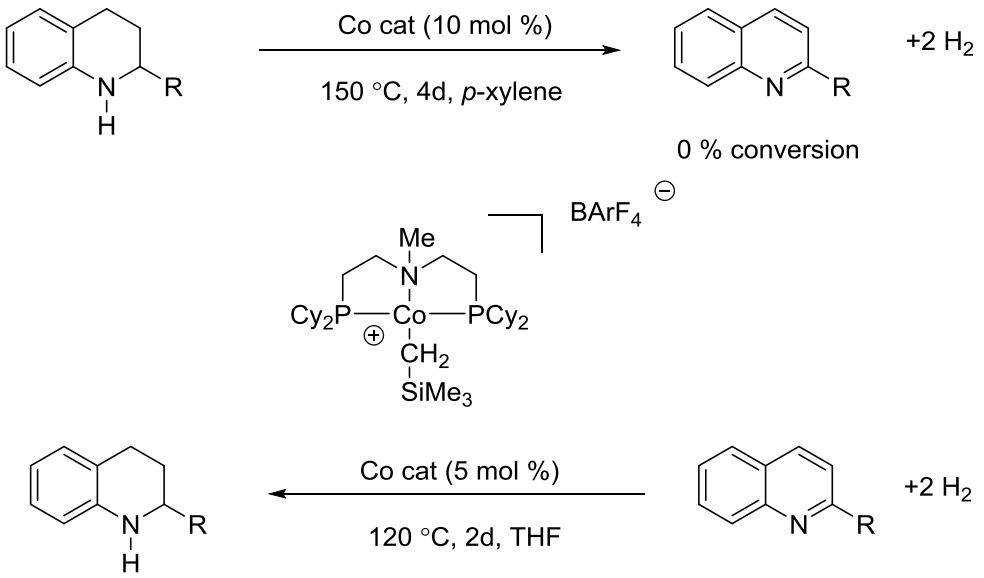

Figure II- 27. Jones' cobalt pincer with methyl moiety on N-atom

In 2015, the Jones' group introduced a new pincer cobalt catalyst for the hydrogenation of N-heterocycles.[225c] Even in the absence of a hydrogen acceptor, this catalytic system could mediate reversible dehydrogenation/hydrogenation reactions of N-heterocycles. Interestingly, upon the replacement of the N−H moiety in the pincer ligand by N-Me, the activity of this cobalt catalyst was reduced significantly for the dehydrogenation path, but still retained its hydrogenation activity (Figure II-27). Noteworthy, these authors suggested that to release the second hydrogen from the dehydrogenative reaction of N-heterocycles, there are two possible pathways related to the cleavage of two C-H bonds. The first scenario is a direct alkane dehydrogenation by cobalt from the partially oxidized substrate, and the second one is related to isomerization of the initially formed C=N to C=C, followed by a second dehydrogenation from the secondary amine fragment. Based on substrate-driven mechanistic studies, they were be able to rule out the first pathway based on direct alkane dehydrogenation. These results highlighted the applicability of new earth-abundant transition metal complexes for the AH reaction

of N-heteroarenes. Summarizing what has been accomplished for the application of earth-abundant metals in the hydrogenation of nitriles and N-heterocycles, we can forecast that in the future catalyst development will mainly focus on the adjustment of these catalysts toward the asymmetric synthesis[224]. Another trend for the asymmetric hydrogenation of N-heterocycles is the development of metal-free catalytic systems such as FLP. [225d]

II.3.2 Ir, Rh, and Ru-catalyzed TH of N-heterocycles

Compared to the surge of activity in the hydrogenation of N-heterocycles, efforts to improve the related transfer hydrogenation reaction have been much weaker. Nevertheless, transfer hydrogenation has also been applied in several significant studies. While conducting a mechanism study for their asymmetric hydrogenation of quinoline, in 2007 Zhou et al.[226] accidentally found that 1,4-dihydropyridines (Hantzsch esters) could be aromatized in the presence of iodine as an additive and $[Ir(COD)Cl]_2$/MeO-BiPhep as a catalyst, accompanied by the release of hydrogen gas. Based on this finding, these authors then accomplished the iridium-catalyzed asymmetric transfer hydrogenation of quinolines using Hantzsch ester as a reductant. The results of this study were very promising, as their reaction occurred under milder conditions and high enantioselectivity. By using just 1 mol % of $[Ir(COD)Cl]_2$ catalyst, the (*S*)-SegPhos ligand (2.2 mol %)I_2 (5 mol %), and the Hantzsch ester (2.0 equiv), quinoline and its derivatives could be selectively hydrogenated to achieve up to 98 % yield and up to 88% ee (Figure II-28).

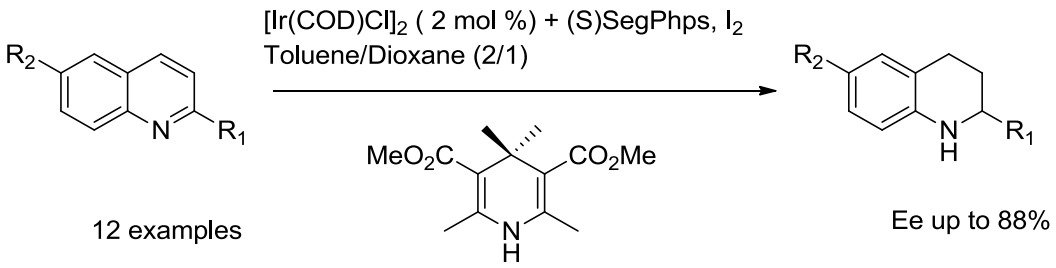

Figure II- 28. Zhou's iridium catalyzed ATH of quinolines

In 2010, Zhou et al. also introduced for the first time the combination of silanes and water as the hydrogen source for the asymmetric hydrogenation of quinoline

(Figure II-29). [227a] The results obtained by using this new hydrogen source were very promising, as a series of quinoline was hydrogenated selectively by $Ir(COD)Cl]_2$/(*S*)-SegPhos / I_2 as the catalytic system to obtain up to 93% ee.

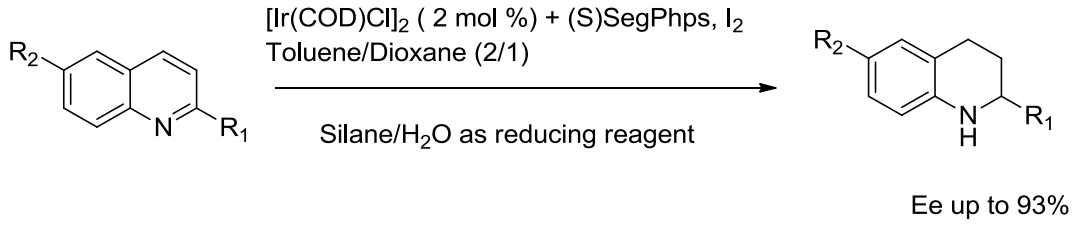

Figure II- 29. Zhou iridium catalytic systems with silane/H_2O as hydrogen sources

In 2012, Xiao et al.[227b] suggested that an aqueous solution of HCO_2H/NEt_3 could also be used as a hydrogen source for the reduction of N-heterocycles (Figure II-30). With these reaction conditions – 0.01 mol % $[Cp^*RhCl_2)_2]$ catalyst, 40 ^oC, 1.5eq KI, in HCO_2H/NEt_3 azeotrope solution – the reduction of quinolines, isoquinolines and quinoxalines happened smoothly with very high yields (98%) in about 24h, but with very low enantiomeric excess (ee) values. The low enantioselectivity of this reaction might be explained by its mechanism and the lack of chiral centres in this catalytic cycle. In the course of their study, the same catalytic system also showed great activity toward the transfer hydrogenation of pyridine salts, and again, it was a non-asymmetric transformation. It is very crucial to stress the importance of iodide, which facilitated the charge and hydride transfer to the pyridium (Figure II-30, bottom).

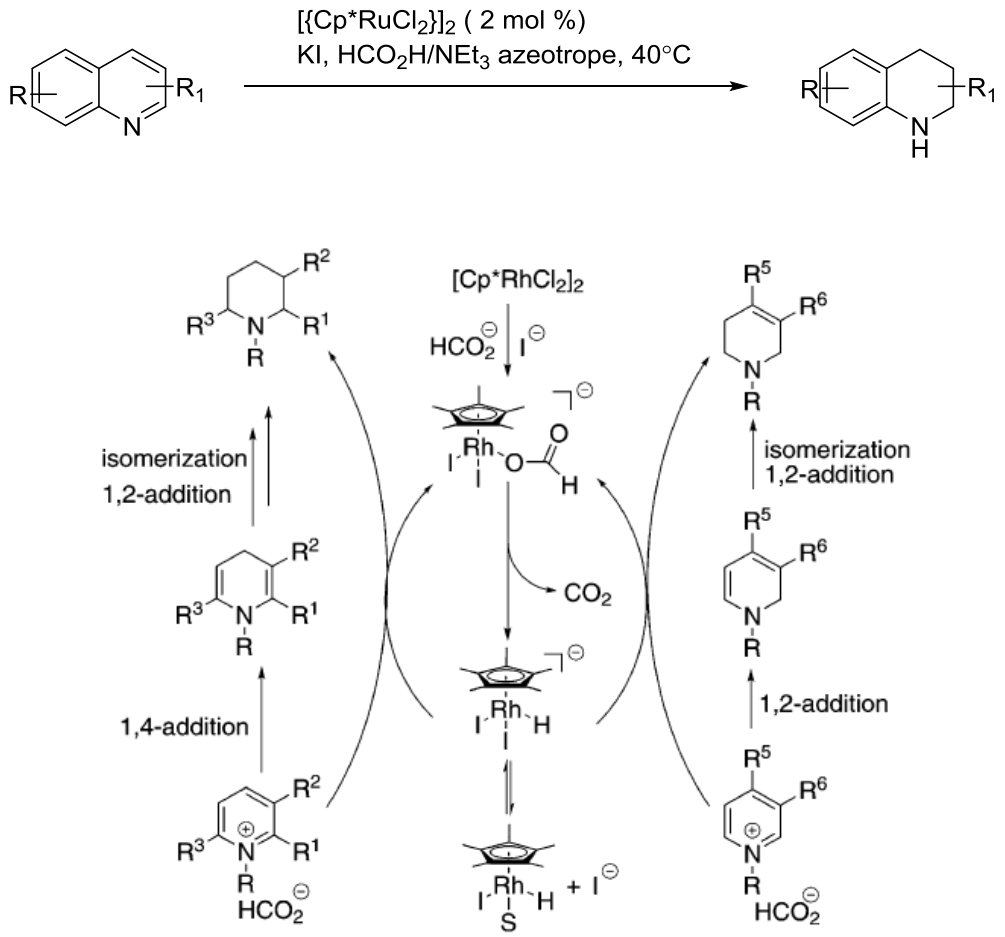

Figure II- 30. Xiao's ruthenium catalytic system

Also by using formic acid as the hydrogen source, in 2016 Jones et al. introduced a mild and efficient transfer hydrogenation of N-heterocycles (Figure II-31).[228] They discovered that, under ligand-free conditions, $[Cp^*IrCl_2]_2$ could catalyze the transfer hydrogenation of a variety of 2-substituted and 2,9-disubstituted 1,10-phenanthrolines by formic acid in 1,4 dioxane to yield 1,2,3,4-tetrahydro-1,10-phenanthroline products in high yields. They also found that the *in situ* formed catalyst, generated from introducing chiral ligands to $[Cp^*IrCl_2]_2$, showed excellent reactivity and enantioselectivity (up to 96% yield and >99% ee), but the conditions were slightly different from the previous system using isopropanol as the hydrogen

source.

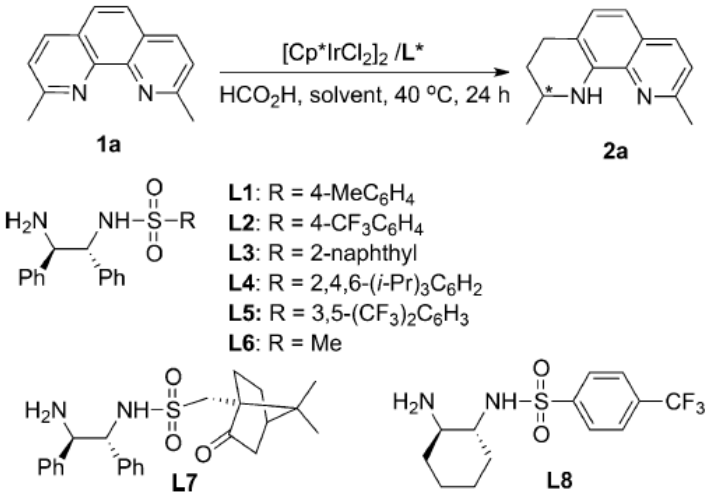

Figure II- 31. Jones' iridium catalysts

Compared to iridium, ruthenium catalysts for the asymmetric transfer hydrogenation (ATH) of N-heterocycles have not been much developed, so there have been only several examples in the literature. The first ruthenium-based catalytic system for the ATH was developed by the Wills group in 2010 (Figure II-32) .[229] A series of tethered ruthenium complexes was prepared and screened for the above transformation. The authors demonstrated that these complexes were active catalysts for the asymmetric reduction of quinolines and substituted quinolines with 5:2 formic acid/NEt_3 azeotrope mixtures as the reducing agent. Compared to iridium systems, the conversion was low (<80 %), although its mild conditions and high enantioselectivity (28 °C, 24h to yield up to 94% ee) should be noted.

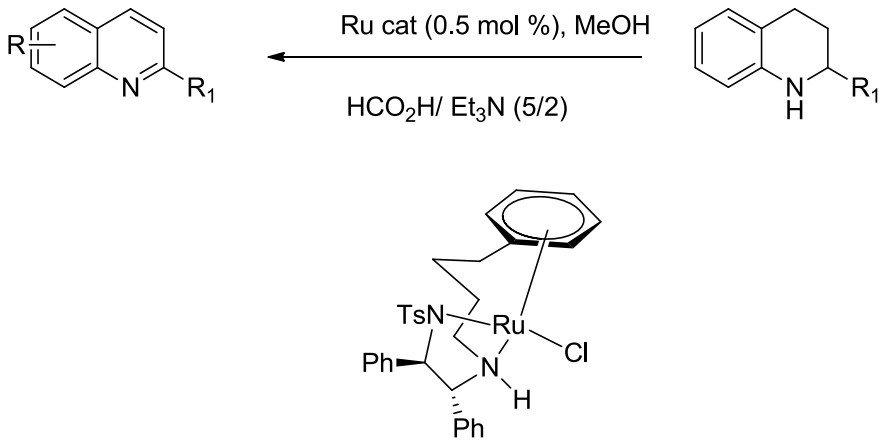

Figure II- 32. Wills' ruthenium catalytic systems

Later, our group found that half sandwich ruthenium complexes bearing NHC carbene ligands show good activity in the transfer hydrogenation of several N-heterocycles with the use of isopropanol as the reducing agent.[230] These results suggested the possibility of ruthenium-catalyzed TH of N-heterocycles in both asymmetric and non-asymmetric variants. These pioneering studies may ignite further research in the development of the chiral reduction of N-heterocycles by the transfer-hydrogen pathway.

II.3.3 Perspective on hydrogenation of N-heterocycles

Even though precious metal based catalysts have recently been employed in many laboratory and industrial syntheses, the urgent need to replace these precious metals by less expensive and more environmentally benign earth-abundant metals has been acknowledged by synthetic chemists.

Research attention has shifted to the iron, nickel, cobalt, manganese catalyzed hydrogenation systems. These results have actually ignited further studies on related reduction methods for unsaturated compounds. There are several ongoing trends in the hydrogenation of N-heterocycles, of which the most important ones are the use of new earth-abundant catalysts, the search for new hydrogen donors, the improvement of reaction selectivity, and the design of novel ligands. Thanks to the divergent catalytic reactivities of organometallic species, the opportunities, and possibilities of improving the current reaction are immense.

In the chapter V, new Ru complexes are prepared and characterized and tested for transfer hydrogenation of N-heterocycles.

II.4 Reduction of non-functionalized olefins

There are many available reagents for the reduction of olefins, such as silanes, boranes, hydrogen gas, to name just a few.[231-232] Molecular H_2 is the best choice for the reduction of olefins owing to its atomic efficiency and cost.[6-8, 67, 146, 177, 233] Although the hydrogenation of olefins is a thermodynamically favorable reaction, the reaction will not proceed without the addition of a catalyst due to the high activation energy.[231] In fact, all hydrogenation processes start with the activation of the H-H bond, which has the dissociation energy of 104 kcal/mol.[234] Hydrogen gas can be activated either by transition metal complexes or by Frustrated Lewis Pair (FLP) systems.[204] This section is mainly focused on transition metal catalyzed reactions. A brief overview of the activation of H_2 by transition metals will be presented, to give a clearer picture of hydrogenation.

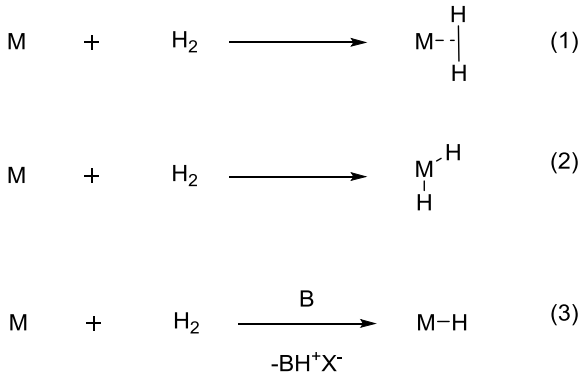

Figure II- 33. Activation of H_2 by transition metals

As shown in (Figure II-33), H_2 can be activated by transition metals in three ways: 1) the formation of an η^2 metal complex, in which the covalent bond of H-H is weakened but still significant, and can be described in terms of a three centre-two

electron interaction; 2) the complete addition of H_2 to a metal centre to form a dihydride complex; 3) the heterolytic cleavage of H-H by the metal and a basic site of the ligand (as in bifunctional catalysts) or by an external base to yield a metal monohydride. Depending on the nature of the ligands, and the electronic and steric situations around the metal centre, the activated hydrogen can be transferred from the resulting metal hydride complex to an unsaturated substrate in a controlled fashion, e.g. regioselectively and/or enantioselectively.

II.4.1 Ir, Ru and Rh catalysts

During the last 40 years, homogenous transition metal-catalyzed asymmetric hydrogenation has been used for the synthesis of numerous chiral compounds due to its high efficiency and cost-effectiveness.[6-8, 22, 67, 136, 177, 200, 231, 233] A plethora of substrates were hydrogenated asymmetrically by employing catalysts based on precious metals such as rhodium, ruthenium and iridium catalysts (Figure II-34).[108a, 109] Despite the huge progress, the efficiency of AH of the C=C bond by rhodium and ruthenium catalysts is still dictated by the presence of a coordinating functional group, such as amide, ester, alcohol, adjacent to the C=C bond.[27, 33, 73, 139, 235]

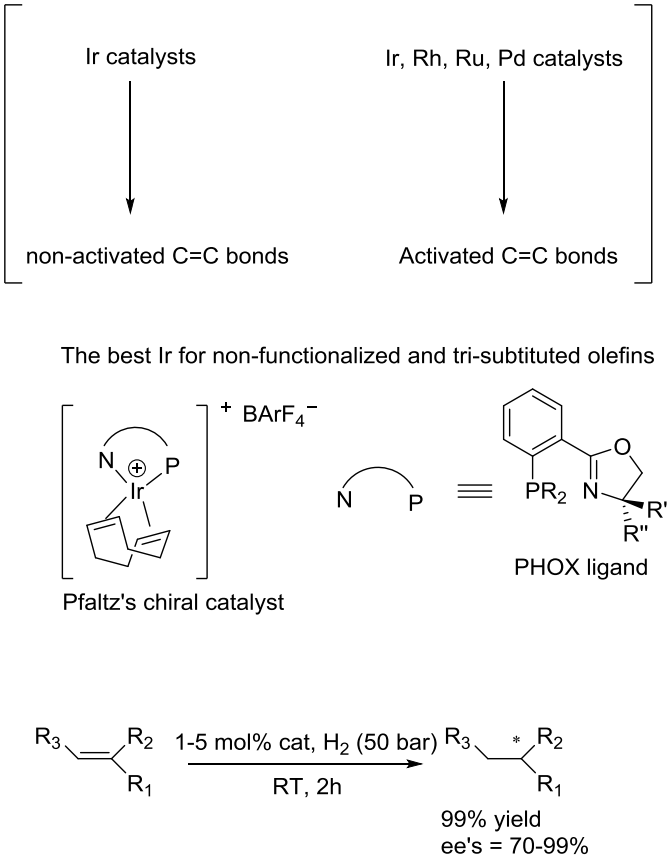

Figure II- 34. Catalytic systems for the AH of C=C bonds

Therefore, the application of these catalysts has been largely restricted to limited families of substrates, such as amino acid derivatives or allylic alcohols. Because unfunctionalized aryl/alkyl tri- or tetra-substituted olefins do not have a directing group (or another coordination site), their asymmetric hydrogenation is much harder to achieve. And for this reason, they constitute the most desirable target for this process.[28, 62, 69]

The first homogeneous hydrogenation of olefins was discovered by the Nobel Prize Laureate Sir Geoffrey Wilkinson, who showed the utility of $RhCl(PPh_3)_3$ as a catalyst.[55] Wilkinson's catalyst laid the foundation for further development by such scientists as Horner, Knowles, and Kagan. The first introduction of chiral phosphine

ligands was done independently by Horner and Knowles;[236] however, the optical purity of hydrogenated olefins was low (3-15% ee). Kagan accomplished a true breakthrough in this area with the design of the DIOP ligand (2,3-*O*-isopropylidene-2,3-dihydroxy-1,4-bis(diphenylphosphino)butane). This new Rh/DIOP system could catalyze the hydrogenation of activated olefins (bearing an adjacent acid or ester group) to obtain products with high enantioselectivity (up to 80 % ee)(Figure II-35).[237] However, these Rh-based systems failed to hydrogenate non-functionalized olefins.

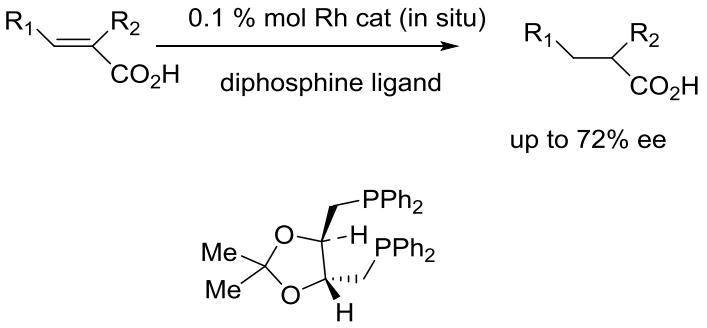

Figure II- 35. Kanga's Rh catalytic system.

In 1993, a chiral titanocene complex, which was the first successful chiral metallocene catalyst for the asymmetric reduction of unfunctionalized tri-substituted olefins, was reported by Buchwald's group[238] (Figure II-36), using the chiral 1,1'-binaphth-2,2-diolate ligand. The chiral titanocene catalyst gave high enantioselectivities (ee's ranging from 83% to >99%) in the AH of several trisubstituted olefins, although high catalyst load (6-10 % mol), high pressure of hydrogen (140 bars), elevated temperature (65^{o}C), and a long reaction time (several days) are required to achieve reasonable yields. Moreover, this chiral titanocene

catalyst is highly unstable and needs to be handled under inert atmosphere conditions.

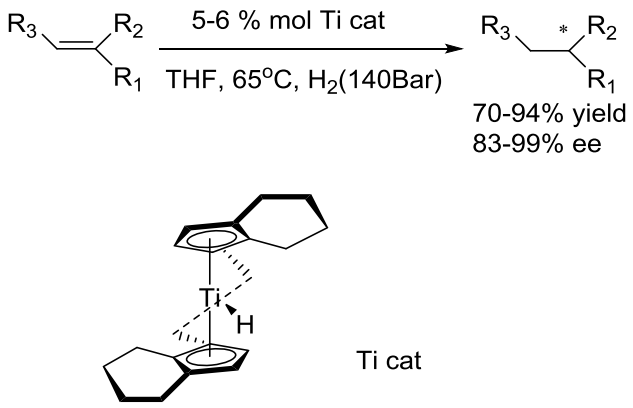

Figure II- 36. Buchwald's titanocene catalysts for AH of olefins

Six years later, based on the idea that cationic metal complexes, due to their high electrophilicity, should be particularly effective at binding highly substituted olefins, Buchwald and co-workers introduced a chiral cationic zirconocene catalyst for the AH of tri- and tetra-substituted olefins.[239] This chiral cationic zirconocene catalyst displayed better catalytic activity than the neutral titanocene analog, resulting in a shorter reaction time (13-21 h), lower temperature (25°C), and lower pressure of hydrogen (80 bars) (Figure II-37).

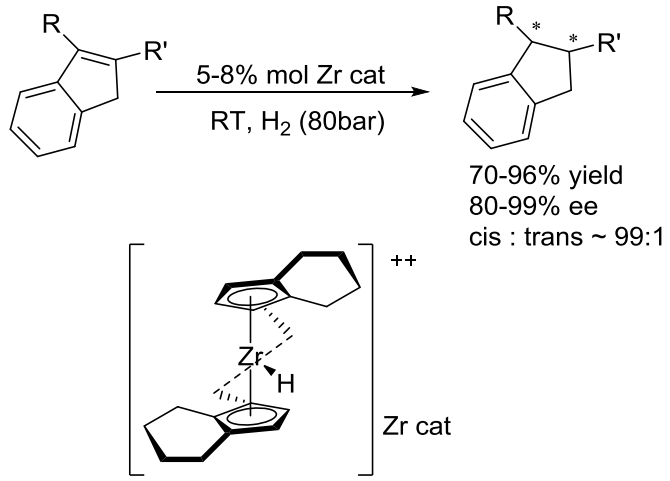

Figure II- 37. Zirconocene catalyst for AH of olefins

In an early work of Crabtree and coworkers[240], the complex [Ir(pyridine)(PCy_3)(COD)]PF_6 (**II-38a**) was found to be a very efficient catalyst for the hydrogenation of hindered olefins (Figure II-38). However, a known problem of Crabtree's catalyst is the deactivation of the active catalyst (**II-38b**) due to the formation of an inactive trinuclear iridium-hydride cluster (**II-38c**). In 1997, one of the biggest breakthroughs in the AH of non-functionalized olefins was the report by Pfaltz and coworkers[241] on the preparation of chiral iridium complexes [Ir(COD)(PHOX)][BAF] (**II-38d**).[242] These complexes, featuring bidentate phosphinooxazoline (PHOX) ligands and the $[B[3,5\text{-}(CF_3)_2C_6H_3]_4]^-$ anion, abbreviated as [BAF], can be considered as chiral analogs of the Crabtree's catalyst. The borate counter ion was used in place of hexafluorophosphate used in Crabtree's catalyst. The performance of Pfaltz's catalysts was much improved compared to the chiral metallocene catalysts discussed above, as they could operate at room temperature, under low hydrogen pressure (50 bars), short reaction time (full conversion in 2h), and gave high ee's (80-99%). Moreover, the chiral iridium

catalysts had further significant advantages as they displayed a good activity at very low catalyst loadings (0.02 mol %) and were also less sensitive to moisture than the parent Crabtree's catalyst.

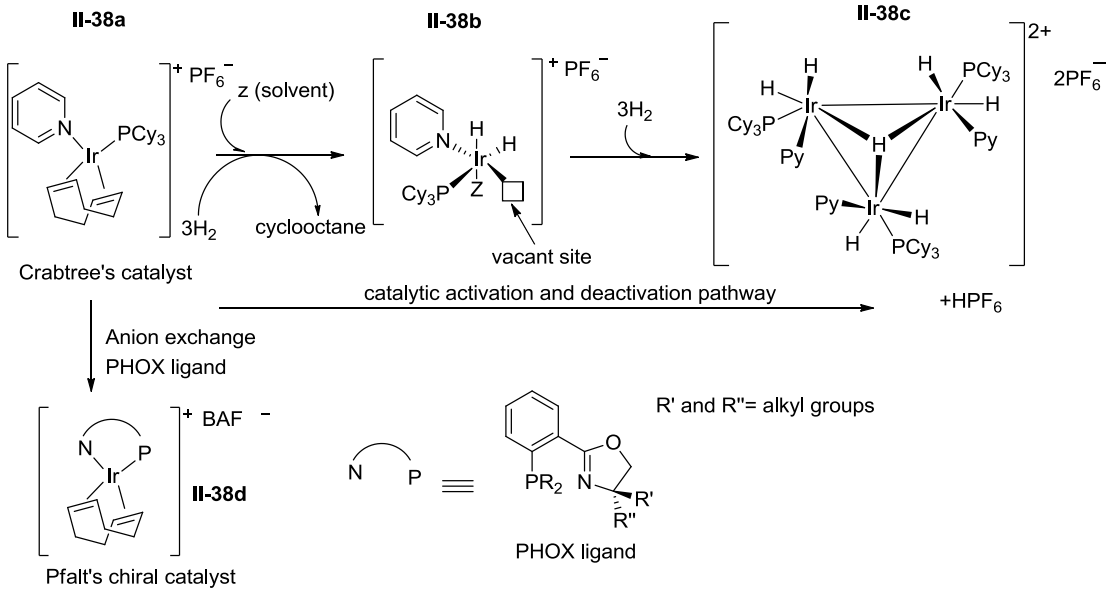

Figure II- 38. Crabtree based catalysts

Recently developed iridium catalysts show exceptionally high enantioselectivity toward the hydrogenation of unfunctionalized olefins (including the tri- and even tetra-substituted olefins). Significantly, chiral monofluorides and trifluoromethyl groups were achieved by Anderson's group[68] with the use of iridium catalysts. However, harsh conditions, with high temperature and pressure, were required for these catalytic systems. Moreover, the occurrence of a dehalogenation by-process brings about another issue for the asymmetric hydrogenation of vinyl fluoride olefins.[48]

In general, iridium-based catalysts have dominated the arena of asymmetric

hydrogenation of non-functionalized olefins. An effective and iridium-free process for the AH of non-functionalized olefins has been a target for many synthetic chemists, and the answer for this search may be found in earth abundant transition metal catalysis, or other metal-free methods.

II.4.2 Earth-abundant metal catalyzed hydrogenation of olefins

In 2004, Chirik et al.[243a] reported a well-defined iron complex (Figure II-39) featuring tridentate pyridinediimine (PDI) ligands for the hydrogenation of simple mono- and di-substituted olefins. This iron catalyst displayed an impressive activity with fast conversion time (12 minutes), low temperature (22°C), and low hydrogen pressure (4 atm) for the hydrogenation of 1-hexene. Mechanistic studies (Figure II-39, bottom) suggested that the active iron catalyst is formed upon dissociation of both dinitrogen molecules to form an unsaturated iron complex. Afterward, olefin coordination takes place, followed by oxidative addition of hydrogen to form an 18-electron complex. The iron alkyl complex is then formed through the insertion of the olefin into the M-H bond and subsequent reductive elimination to furnish the alkane and regenerate the active complex.

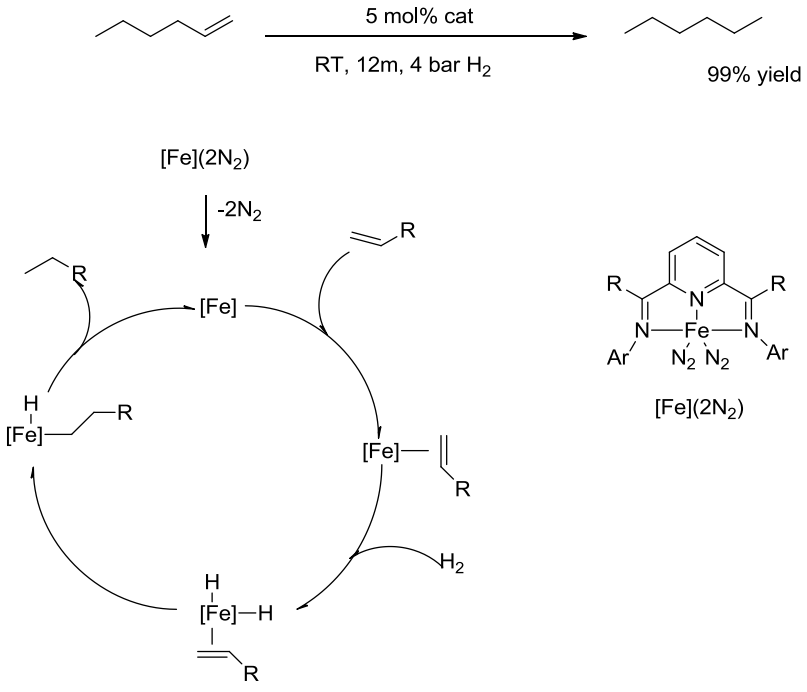

Figure II- 39. Chirik's iron catalyst

In the same year, Peters' group[243b] presented another well-defined iron catalyst supported by a tris(phosphino)borate ligand for the hydrogenation of 1-hexene. Compared to Chirik's system, this iron catalyst did not show significant improvements. However, a mechanistic study of the catalytic cycle suggested a very interesting cycle which may help chemists to start the development of new generations of iron catalysts for hydrogenation. The common belief in the field had been that the catalytic activity of iron complexes required the Fe(0)/Fe(II) redox pair, involving a low oxidation state Fe(0) species. In contrast, Peters and Daida's group considered the possibility of the Fe(II)/Fe(IV) redox as a feasible pathway, avoiding the low valent Fe(0)/Fe(II) cycle (Figure II-40).

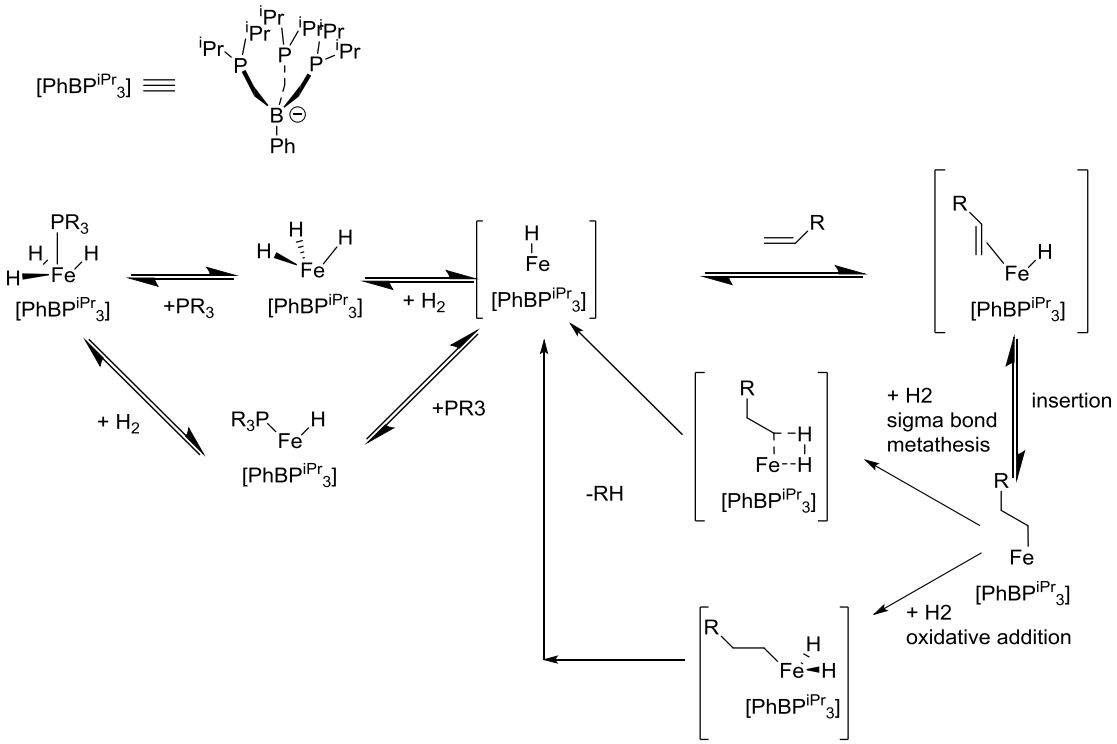

Figure II- 40. Peters and Daida's iron catalytic system for hydrogenation of olefins

In 2013, one of the most important breakthroughs in earth-abundant metal catalysis was accomplished by the Chirik group,[244] who introduced cobalt-based systems that could catalyze the asymmetric hydrogenation of an activated olefin, methyl 2-acetamidoacrylate (Figure II-41). The best catalytic conditions were 5 mol % of catalyst and 34 atm H_2 to completely hydrogenate the above substrate in 12h at room temperature with the enantioselectivity up to 92.7 % ee. Although this efficiency of this catalyst is still lower than with precious metal systems, this reaction was the first example of an earth-abundant metal catalyzing asymmetric hydrogenation of olefins. No doubt, this result will motivate future studies on developing the sustainable catalytic processes.

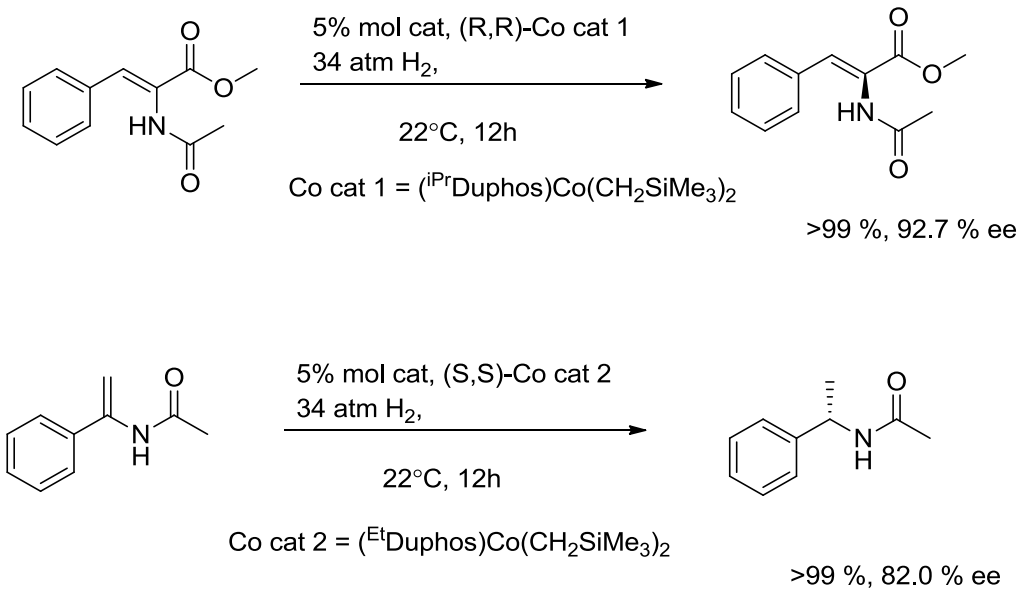

Figure II- 41. Chirik's cobalt catalytic system

A year later, Wangelin et al. suggested another cobalt complex, which was

able to catalyze the hydrogenation of non-activated di-substituted olefins (Figure II-42).[245] Furthermore, this system displayed a good activity under milder conditions, such as 1 mol % cat, 1 bar of H_2, 20 °C, and 3 h to obtain 100% conversion of olefins. Mechanistic studies suggested that the availability of many π-donor sites (as seen in benzene or anthracene ligands) actually stabilized the intermediate hydrido cobaltate or alkyl cobalt (I) hydride species.

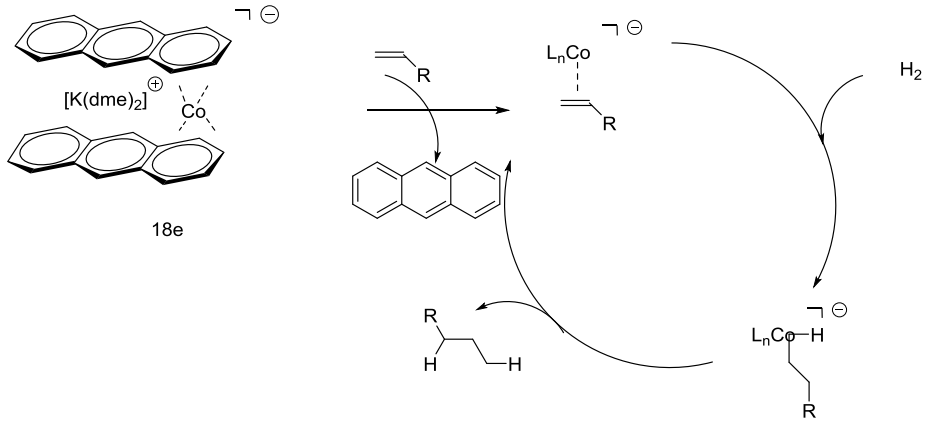

Figure II- 42. Wangelin's cobalt catalytic mechanism

In 2016, Jones' group[228] described pincer iron catalysts which could catalyze the hydrogenation of non-activated olefins under ambient conditions (1 atm of H_2, 20 °C) at 5 mol % catalyst load to achieve complete conversion of olefins within only 24 h (Figure II-43). The suggested catalytic cycle, supported by DFT calculations, involved a metal−ligand cooperative pathway, similar to what had been observed in nickel and cobalt systems developed by Hanson and co-workers.[246]

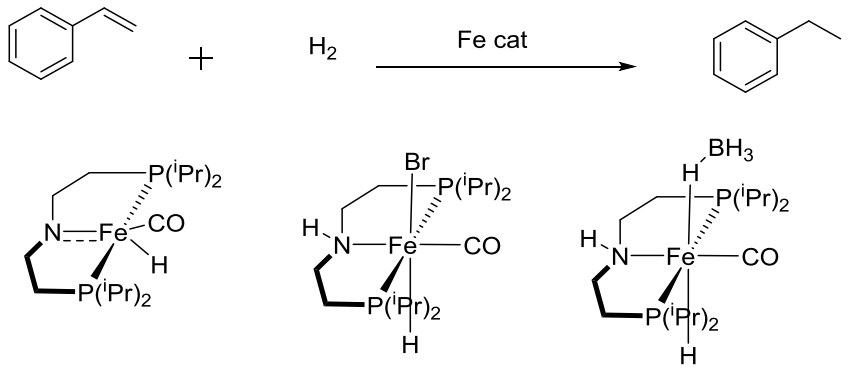

Figure II- 43. Jones' iron PNP pincer catalysts

II.4.3 Transition metal catalyzed TH of non-activated olefins

Compared to hydrogenation by H_2, the transition metal catalyzed transfer hydrogenation of alkenes is underdeveloped; there have been very few examples of such transformations. One of the first homogeneous systems for the above transformation was reported in 2008 by Grutzmacher et al.[247] (Figure II-44), who employed an unusual hydrogen donor, ethanol, for the reduction of acrylic acid methyl ester with Rh(I) diolefin amide [Rh($trop_2$N)-(PPh_3)] as a catalyst. Unfortunately, the substrate scope of this study was very narrow, as acrylic acid methyl ester was the sole tested olefin.

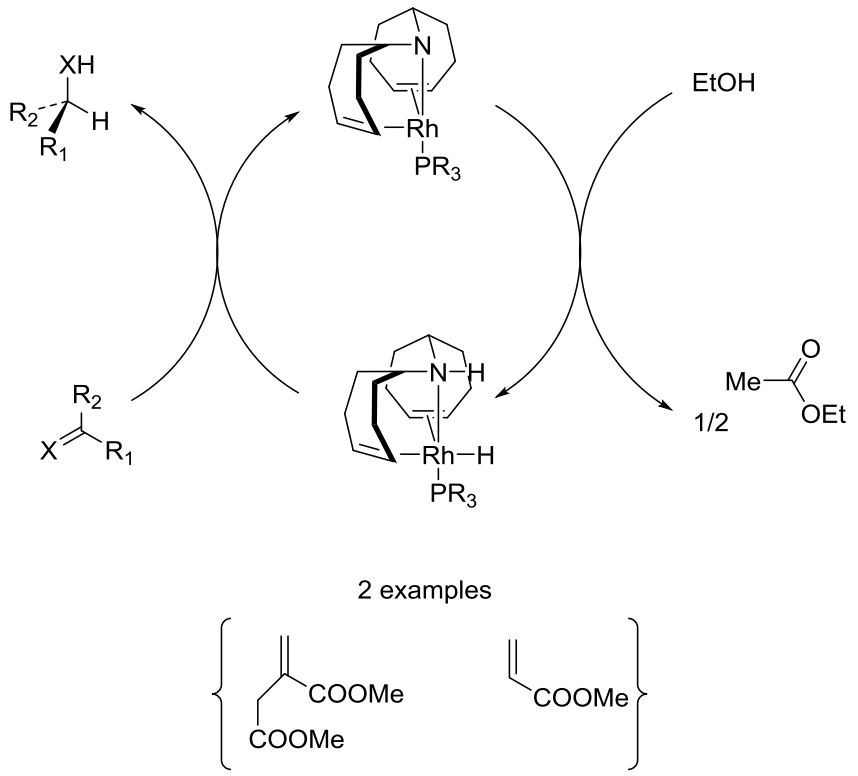

Figure II- 44. Grutzmacher's rhodium catalytic system

In 2011, Albrecht et al.[248] developed several catalytic systems for the transfer hydrogenation of mono and di-substituted olefins, using isopropanol as the hydrogen source. These catalysts were generated by mixing *in situ* ruthenium precursors and N-heterocyclic carbenes (Figure II-45). There were several significant parameters for this system to be active, including repetitive substrate addition and a high temperature (80 ^{o}C) of operation.

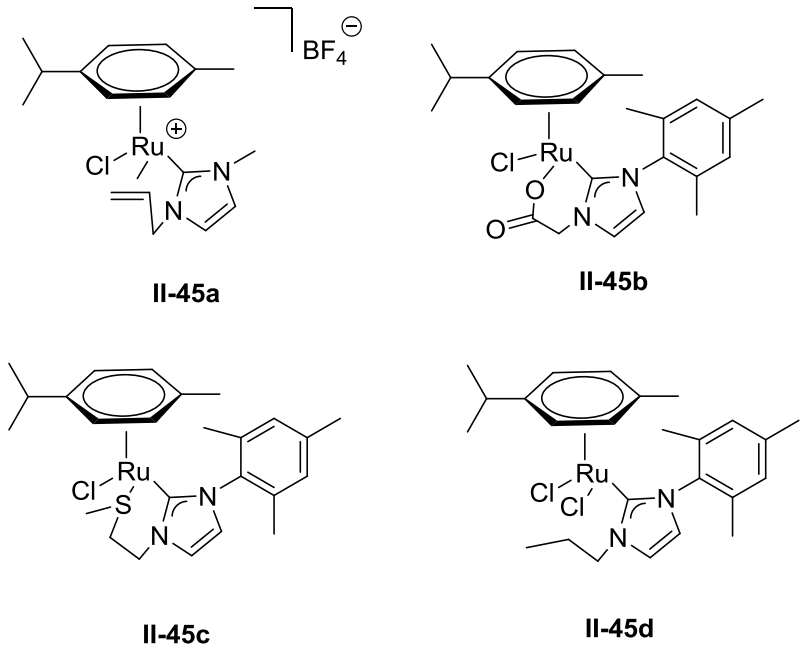

Figure II- 45. Albrecht's Ru/NHC catalysts

Reported in 2016, the first transfer hydrogenation of olefins catalyzed by cobalt-based systems was developed by Tan et al. (Figure II-46).[249] They also found that this catalytic system could tolerate different functional groups and, surprisingly, the presence of water in the reaction mixture did not affect the reactivity. In general, a variety of olefins were successfully reduced with moderate to high yields of the corresponding alkanes under mild conditions.

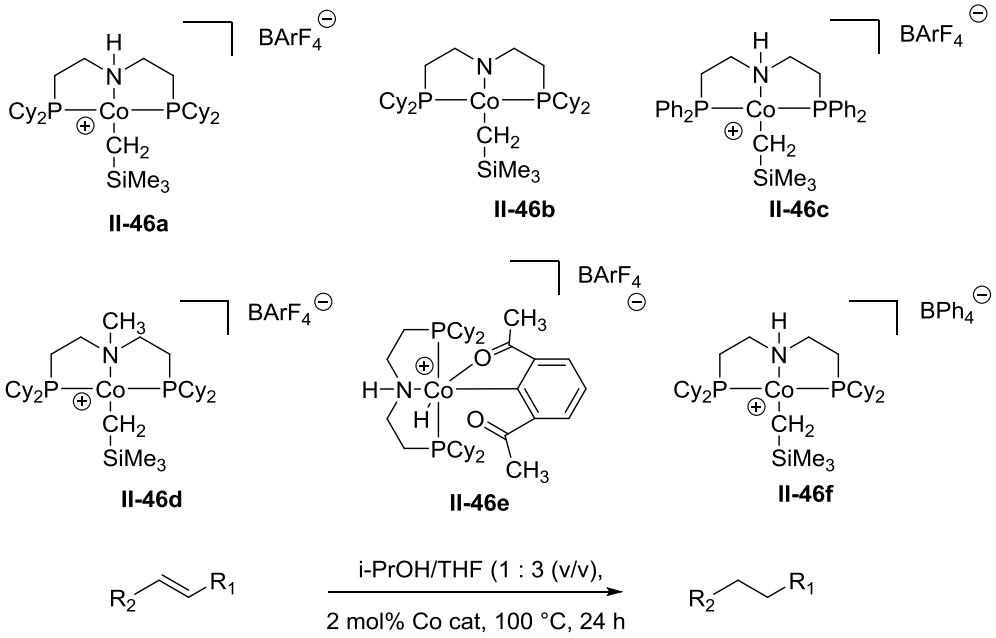

Figure II- 46. Tan's cobalt catalysts

II.4.4 New trends in TH of non-activated olefins

The transfer hydrogenation of olefins remains a relatively underdeveloped field, which offers significant opportunities for the application of new and earth-abundant catalysts, such as cobalt-, nickel-, and iron-based systems. Further investigation can improve the atom economy, utilize inexpensive reducing agents, and lead to a greater enantioselectivity in the transition metal-catalyzed asymmetric transfer hydrogenation of olefins, which can make this reaction amenable for industrial applications. The enantioselective transfer hydrogenation of non-functionalized (or non-activated) olefins is still an active area of application of new catalysts.

In the chapter V, new Ru complexes are prepared and characterized and tested for transfer hydrogenation of olefins.

III. Hydrodefluorination of fluorinated compounds.

Since its discovery in 1886 by the Nobel Laureate, Henry Moissan, the element fluorine has found limited application in synthetic chemistry due to its extraordinary properties, such as a large oxidation potential, the highest electronegativity, as well as exceptional toxicity.[250] Since the late 1930s, the utility of fluorine has been mainly limited to military applications. For example, uranium hexafluoride (UF_6), which bears special physicochemical properties, was used in the separation of fissible U-235 from the heavier isotope U-238 via centrifugation.[251] The first attempt to introduce fluorine in medicinal chemistry was done by Fried and Sabo in 1953,[252] who studied the correlation between the size of the halogen atom and the bioactivity of 9α-halo cortisones. Unexpectedly, they found that fluorinated cortisones showed a remarkable bioreactivity compared other halogen analogs and the parent hormones. Since then, fluorine chemistry has greatly contributed to many fields, such as polymer, pharmaceutical, medicinal, agricultural, and military applications. As stated in a recent review about the fluorine chemistry, half of the top ten selling drugs contain C-F bonds. About 20% of all pharmaceuticals and 30 - 40% of agrochemicals are fluorinated compounds.[251, 253-260]

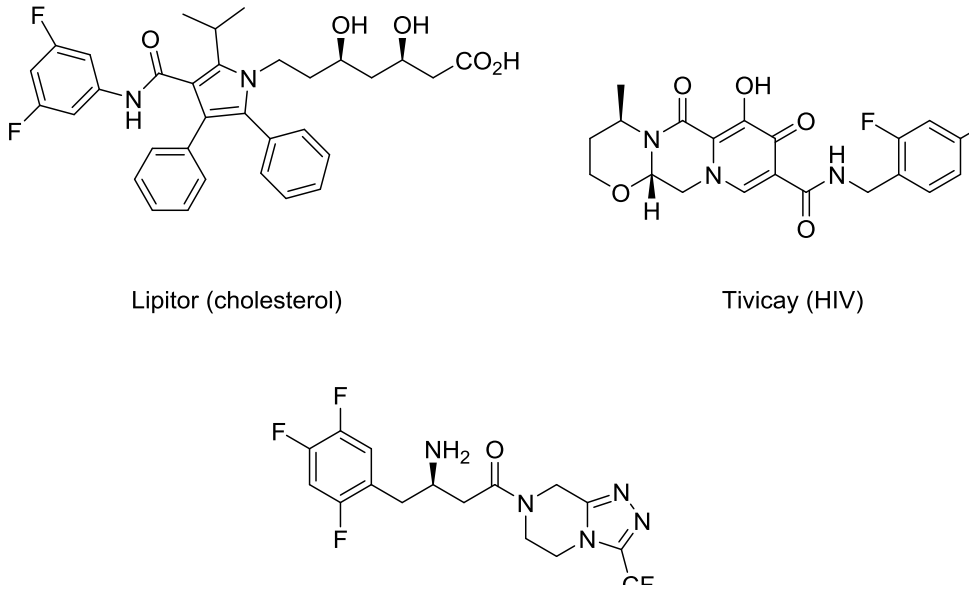

Figure III-1. Examples of high-value fluorinated compounds

The rapid growth of fluoroorganic chemistry brought about several synthetic strategies to prepare high-value compounds containing just a few fluorine groups (Figure III-1). These strategies, usually used for late-stage fluorination, include nucleophilic or electrophilic fluorination, difluoromethylation, and difluoromethylenation.[261-262] These methods could be used for a direct installation of fluorine atoms into biologically relevant molecules and are particularly useful for making compounds featuring an ^{18}F label for medical imaging applications. However, they also encounter several drawbacks, such as the high cost of fluorinating reagents, poor atom economy, and limited substrate scope.[263] In contrast, perfluorinated compounds are much easier to prepare and, actually, many are available from industrial processes. Therefore, they can serve as accessible fluorinated building blocks. For this reason, an alternative strategy could be to displace fluorine atoms in these precursors by a new group.[148, 155-156, 264-265]. However, examples of this transformation are scarce due to the poor ability of fluoride to serve

as a leaving group.[263] One solution to this problem is to perform the reaction in two separate steps (Figure III-2): first, remove excessive fluorines in selective hydrodefluorination of C-F bonds (HDF), and then functionalize the newly formed C-H bonds. The HDF has been intensively investigated over the past two decades, with the application of many different reducing agents and various catalysts, such as silylium,[151] and phosphonium ions,[92, 266] other main group elements,[154, 157, 267-268] or by transition metal complexes.[150, 152, 155, 264, 269-275] In the latter set of catalytic reactions, ruthenium, rhodium, palladium, copper, and gold catalysts have received significant attention.

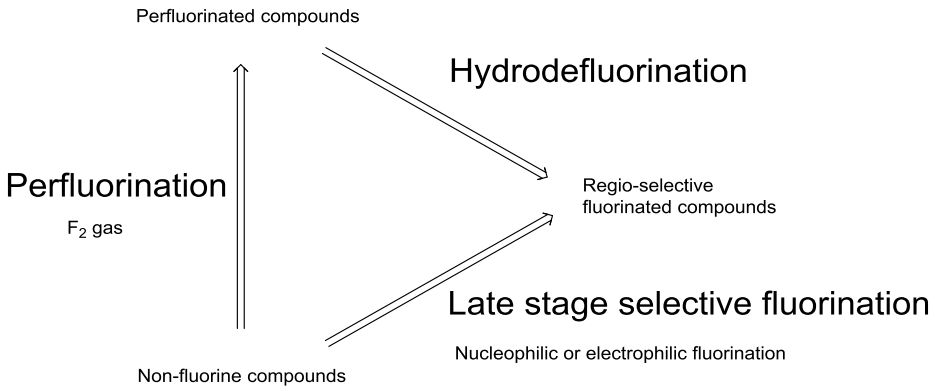

Figure III-2. Fluorination pathways

There are several comprehensive reviews on this subject;[148, 154-155, 264, 271, 276] covering *inter alia* reaction mechanisms for various metal catalysts, the role of metal hydrides, metal fluorides, details of various oxidative addition steps; therefore, these aspects of HDF reactions will not be considered here. Instead, to help in the subsequent discussion of the HDF by transfer hydrogenation, this micro review will focus only on late transition metal (groups 8-9) catalyzed reactions and their relevant mechanisms.

III.1 Late transition metal catalyzed HDF

Thermodynamic data for M–F bonds from "Comprehensive Handbook of Chemical Bond Energies" show that late transition metals have a lower affinity for fluorine than early transition metals, and thus their bonds to fluorine are less thermodynamically favorable than those of early transition metals.[277] The weaker M-F bonds of late transition metals make the cleavage of C–F bond by these metals harder; but in the HDF reaction, it may actually become beneficial as the conversion of the less stable fluorido complex into the corresponding hydride complex becomes easier.[262] Furthermore, to compensate for breaking strong C–F bonds, a strong E–F bond (E= H, P, Si, or B) should be formed to make the overall reaction an energetically favorable process.[264] This simple consideration helps to understand why there are so many successful examples of late transition metal based HDF systems utilizing boranes, silanes, and hydrogen gas as reductants.[262] In short, this process is similar to what is observed in the C-H activation by late transition metals, which has been extensively studied for the last several decades.

III.2 Rh, Ru, and Pd catalysts

Interestingly, the first literature report on the use of a late transition metal system in catalytic HDF dates back to a report by Swarts[278] in 1920, who reported the utility of a heterogeneous catalytic system, a Pt/Ni alloy, for the HDF of mono fluorinated arenes by hydrogen gas. Unfortunately, this catalytic system required a very high temperature (130 ^{o}C) and pressure (120 atm) for the HDF of fluorobenzene. This research field had been dormant until 1994 when the Milstein group introduced a new strategy to use silanes as reducing agents and scavengers for the fluorine atom.[279] They suggest a homogeneous rhodium catalyst and postulated a catalytic cycle, with [Rh($SiMe_2Ph$)(PMe_3)$_3$] as a pre-catalyst (Figure III-3). Thanks to the strong affinity between silicon and fluorine atoms, [Rh($SiMe_2Ph$)(PMe_3)$_3$] reacts quickly with perfluoro benzene to cleave one C–F bond and form [Rh(C_6F_5)(PMe_3)$_3$] as the active catalyst. When introduced into the systems, $(EtO)_3Si{-}H$ oxidatively adds to the Rh centre to form a hydrido silyl complex Rh(III). The subsequent reductive elimination from this Rh(III) intermediate yields C_6F_5H and generates a Rh(I) silyl complex. To complete the cycle, oxidative addition of new C_6F_6 to this Rh silyl complex, followed by reductive elimination of a fluorosilane, regenerates [Rh(C_6F_5)(PMe_3)$_3$] (Figure III-3).

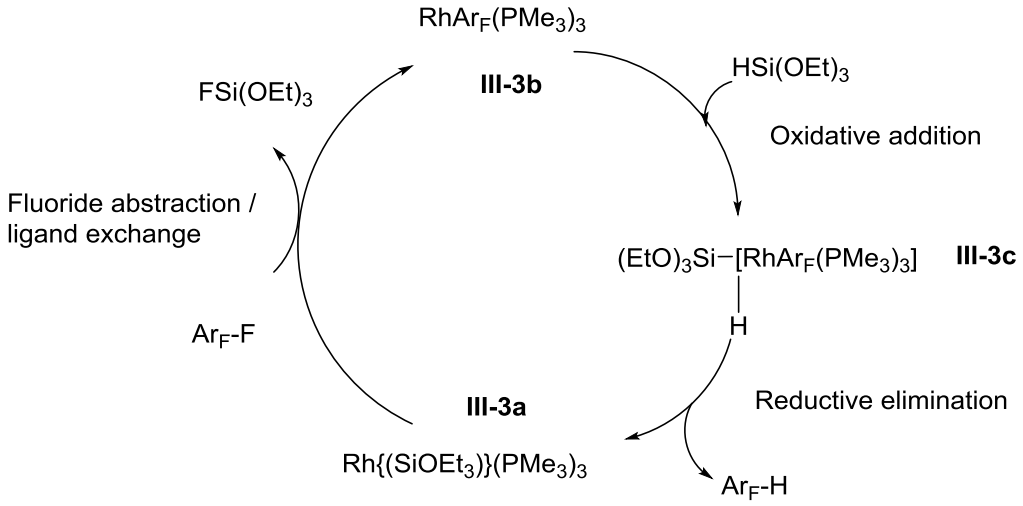

Figure III- 3. Milstein's Rh silyl HDF catalytic systems

Even though the turnover number (TON) for this system was only 38 for C_6F_6 and 33 for C_6F_5H, this new homogeneous reaction has become a source of inspiration for many later studies. The HDF reaction was also tested for the possibility of using hydrogen gas as the fluorine acceptor, and once formed in the reaction mixture, the HF can be consumed by a base. This approach significantly increased the activity of the [Rh($SiMe_2Ph$)(PMe_3)$_3$] system up to 114 TON.

One of the earliest mechanistic studies to investigate the activity of the Rh complex toward the C-F bond cleavage was carried out by the Jones group in 1997 (Figure III-4).[280] Based on a combination of well-designed kinetic studies and successful isolation of important intermediates, these researchers suggested that, in the presence of a base (F^- or pyridine), complex (**III-4a)** was deprotonated to form an anionic Rh complex. The nucleophilic aromatic substitution takes place between this anionic Rh complex and a fluorine substrate to form a fluoroaryl rhodium hydride complex and generates the fluoride anion, which is consumed quickly by the conjugated acid formed at the first stage (Figure III-4). Jones et al. also ruled out

the possibility of a radical pathway because adding a radical trap (9,10-dihydroanthracene) did not have any effect on the reaction rate.

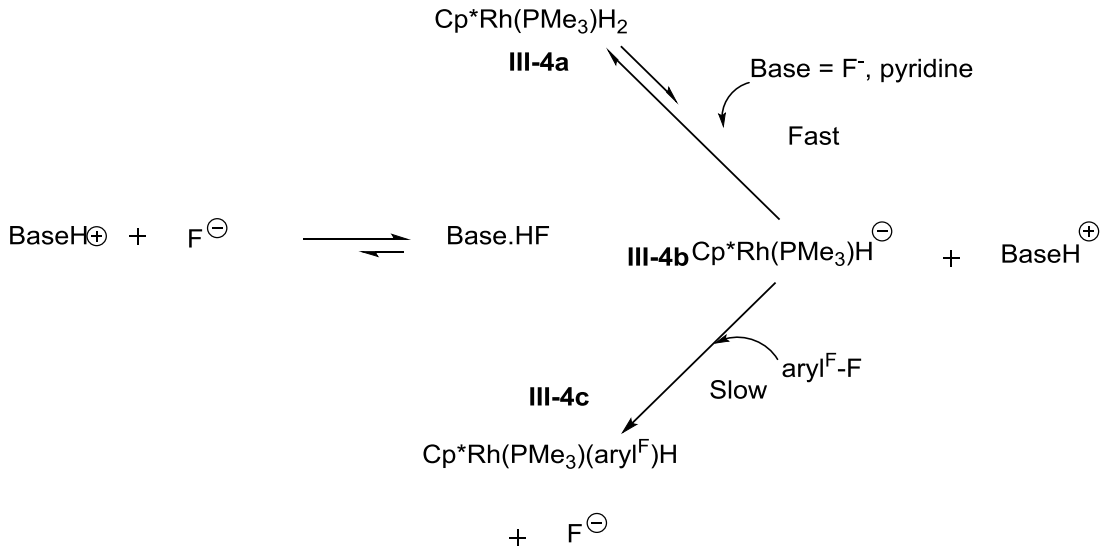

Figure III- 4. Jones' rhodium catalytic system for the HDF of perfluorinated aromatic compounds

A little later, in 1996, activation of the C-F bond by ruthenium complexes was studied by Whittlesey et al. (Figure III-5, top).[281] They found that cis-Ru(dmpe)H_2 reacts with tetra-, penta- and hexafluoro benzene at room temperature to generate *trans* fluoroaryl ruthenium hydride complexes. Surprisingly, there was no evidence of C-H activation in the hydridofluoro substrates, such as C_6F_5H and $C_6F_4H_2$. The authors ruled out the mechanism based on the oxidative addition of fluoroarene to the [Ru(dmpe)$_2$] fragment, because a reaction of **III-5a** and C_6F_6H yielded only the *trans*-isomer **III-5c**, while the *cis*- isomer **III-5c** should be the main product of oxidative addition. Instead, they proposed a radical mechanism for this transformation (Figure III-5, bottom). A caged radical species is believed to be

involved in the electron transfer pathway, which is initiated by electron transfer from **III-5a** (an electron rich complex) to C_6F_6 having a strong electron affinity. The concurrent loss of HF and radical combination steps yield [Ru(dmpe)$_2$(C_6F_5)H] (**III-5b**).

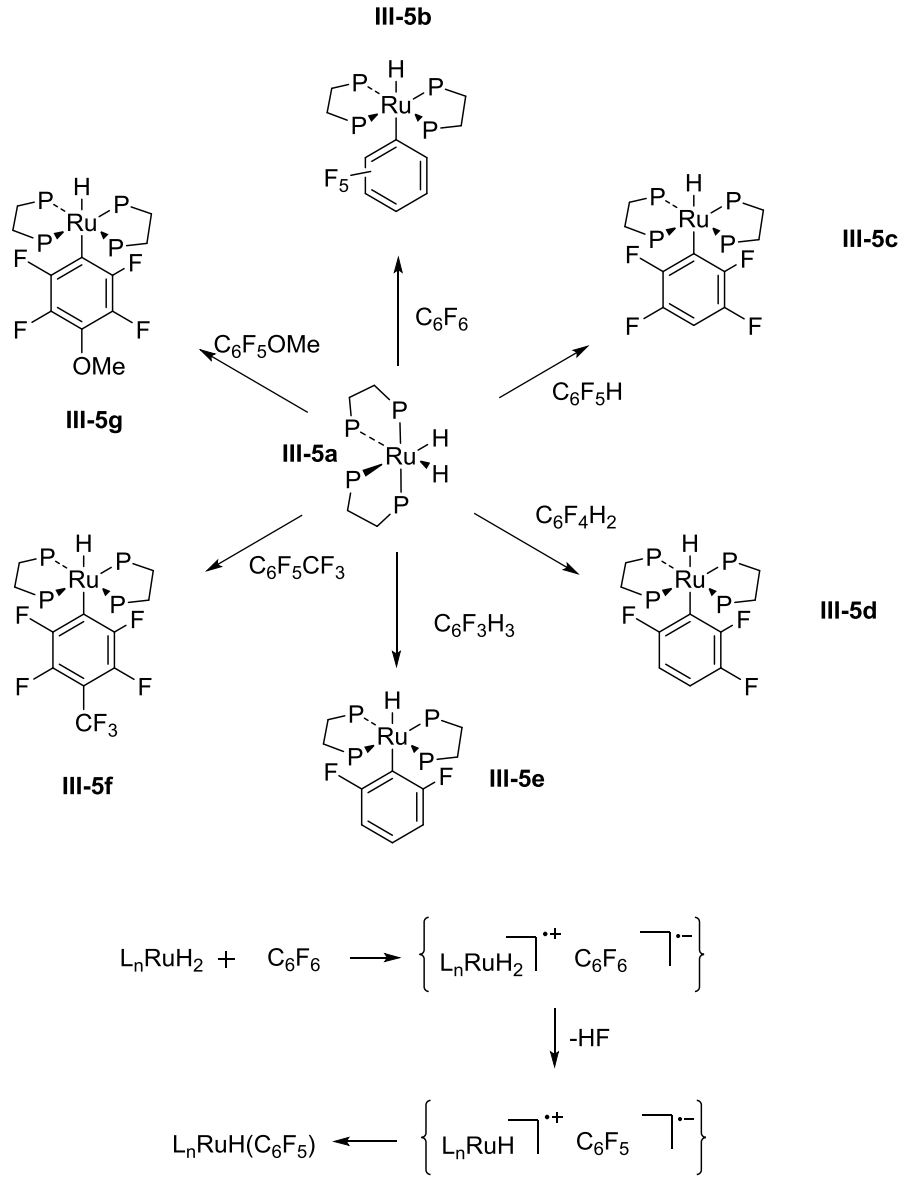

Figure III- 5. C-F and C-H addition reactions to [Ru(dmpe)H_2]

In 2009, the same group[282] reported a series of NHC-supported hydride complexes of ruthenium which react with $Et_3N{\cdot}3HF$ to form fluoride ruthenium

complexes, found to be active catalysts for the HDF of many fluorinated benzenes by silanes as a reducing reagent (Figure III-6). However, monofluorobenzenes are inactive under these conditions.

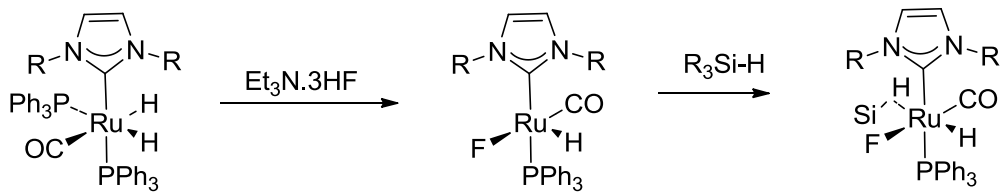

Figure III- 6. Whittlesey's NHC ruthenium catalysts for HDF

Stoichiometric reactions were carried out to elucidate the mechanism and it was proposed that the reaction goes via the formation of a silane σ-complex **III-6c** (Figure III-6). Because isolation and characterization of the important intermediate **III-6c** were not possible even at very low temperature (204 K), these authors did not come up with any solid conclusion for the mechanism of this reaction. Therefore, the mechanism still remained unclear until 2011, when based on the combination of DFT calculations and kinetic studies, they suggested[283] a refined mechanism (Figure III-7) involving the key steps: 1) the initial dissociation of phosphine to form an unsaturated 16e ruthenium complex (**III-7b**), which then coordinates C_6F_5H to form a η^2-arene ruthenium intermediate; 2) the subsequent metathesis affords **III-7e**, which then undergoes an F^- transfer from the ring to the metal to yield **III-7f**, followed by the reverse hydride transfer from metal to the ring to furnish the formation of **III-7g** ; 3) the hydrogenation of **III-7g** produces **III-7h**, followed by the dissociation of fluorinated products to generate **III-7k**; 4) in the final steps silane

adds to give a silane σ-complex and the cycle is completed by Si-F elimination to regenerate **III-7b**.

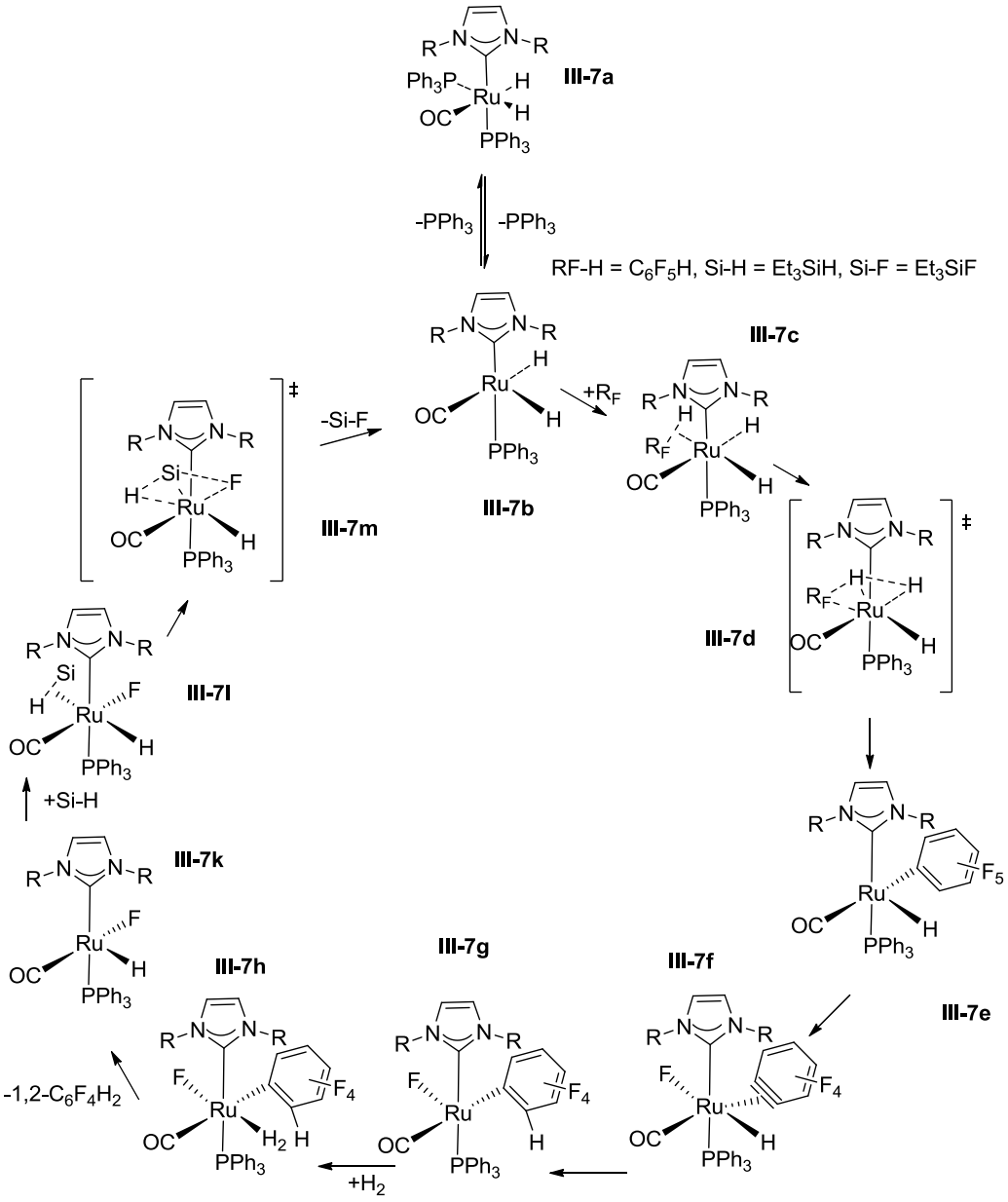

Figure III- 7. Whittlesey's NHC/Ru-catalyzed HDF mechanism

In 2013, Braun et al.[284] attempted to isolate a highly fluxional η^2-silane hydrido complex [Rh(H)(η^2-HSiEt$_3$)(dippp)] (dippp= $^{i}Pr_2P(CH_2)_3PiPr_2$), which was believed to be an important intermediate in the catalytic cycle of HDF using silanes.

But this species remained elusive. For some catalytic systems, Braun et al.[285] showed that pentafluoropyridine could be selectively reduced to form 2,3,5,6-tetrafluoropyridine. Interestingly, in 2007 Perutz et al.[286] reported that HDF of pentafluoropyridine by $[(PMe_3)_3RhSiPh_3]$ as the catalyst results in ortho-selectivity, i.e. 2,3,4,5-tetrafluoropyridine forms exclusively. To account for the specific regioselectivity, Peruz postulated the preferred coordination of the N atom of pentafluoropyridine. However, experimental and computational studies by Braun et al.[278a] suggested a silyl-assisted C–F activation mechanism, in which the preference of the 2-position in the C–F bond activation of pentafluoropyridine was dictated by the interaction between the silyl ligand and fluorine, as well as by the additional interaction between Rh and N atoms (Figure III-8).

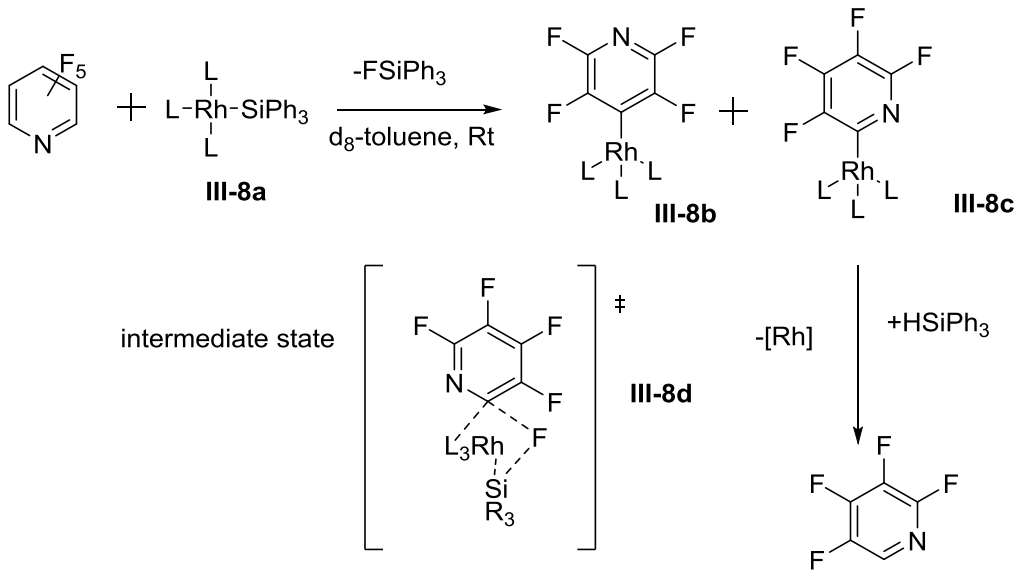

Figure III- 8. Braun's proposed intermediate states for Rh-catalyzed HDF.

Palladium

In 2001, Braun et al.[287b] showed that phosphine supported Pd complexes are active in the HDF of pentafluoropyridine. Improved Pd systems with HBpin as

reducing reagent showed an interesting catalytic activity, but the TOF was still very low (0.33/h). When silanes were used as reductants, the TOF significantly increased (2.6/h) (Figure III-9).

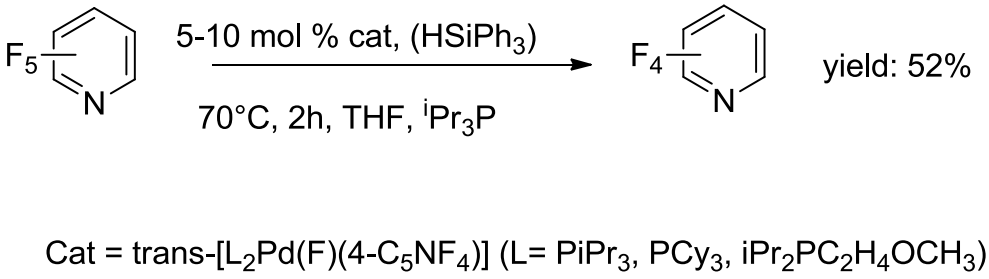

Figure III- 9. Braun's palladium catalyzed HDF using silanes as reducing reagent

An innovative approach was introduced by Zhang et al.[288] who used a directing group to achieve highly selective reduction of the ortho positions of perfluoroarenes. As explained in their proposed mechanism, with the help of a directing group, Pd(0) can quickly coordinate to the substrate through the oxidative addition pathway. Then the insertion of Pd into the C-F bond generates a fluoride complex of Pd (II). Fluoride abstraction by silane leads to the formation of a hydride Pd complex, which undergoes reductive elimination to regenerate the original Pd(0) species (Figure III-10).

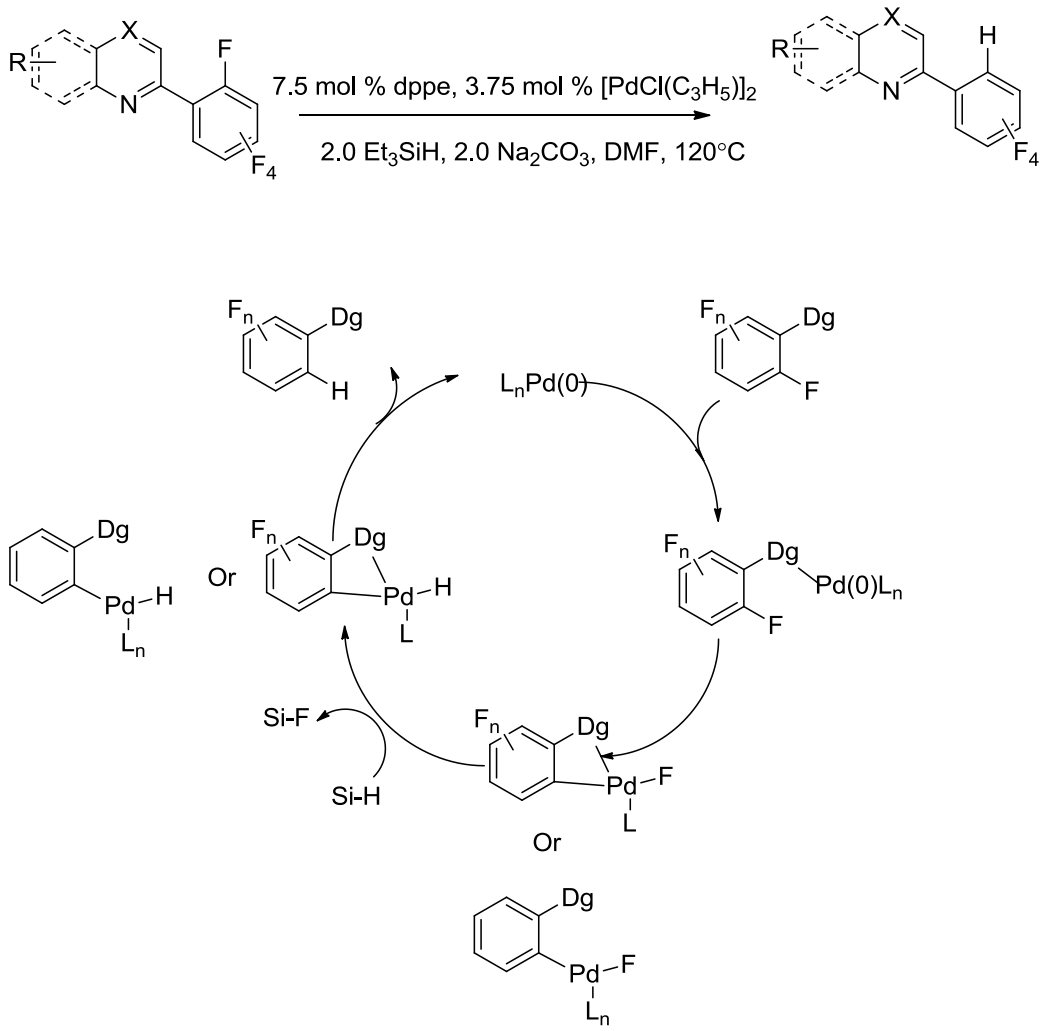

Figure III- 10. Zhang's Pd catalytic system.

In 2013, Peris et al.[289] reported the first homogeneous HDF by isopropanol catalyzed by a Ru/Pd bimetallic complex (1 mol %, 1h, 80 °C). This catalyst happened to be very efficient even for benzenes with a low extent of fluorine substitution (Figure III-11) and showed up to 660 TON for several substrates. Interestingly, this system was completely inactive when either ruthenium or palladium complex alone was employed as the catalyst, suggesting a synergistic effect.

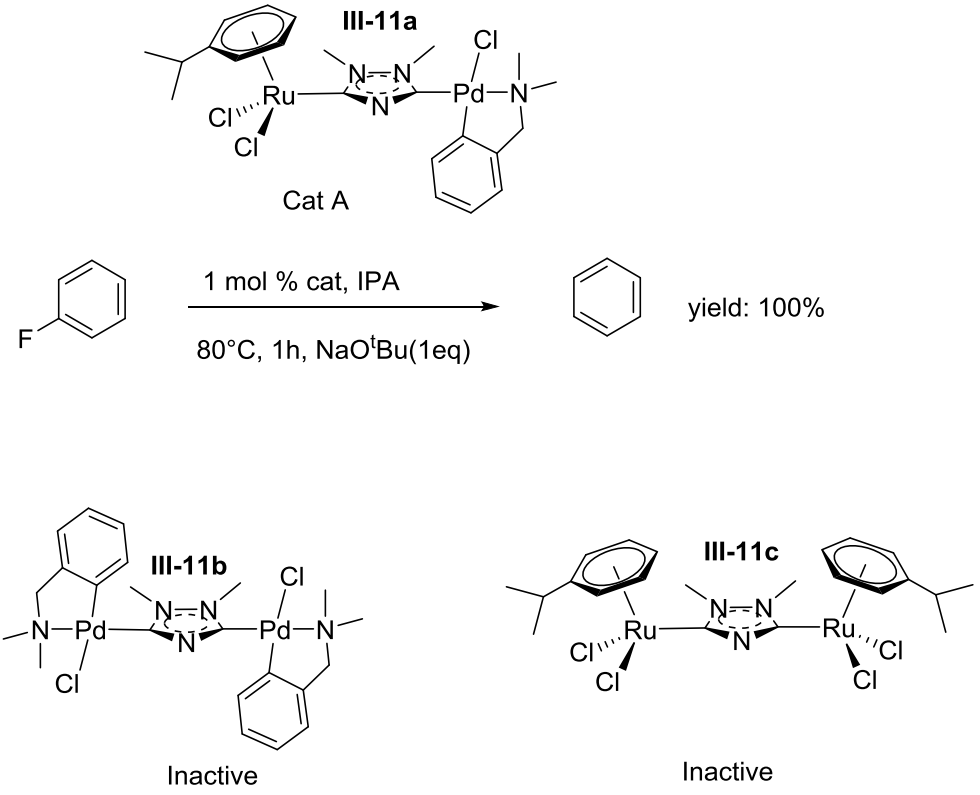

Figure III- 11. Peris' Ru and Pd bimetallic catalysts.

III.3 Fe, Co, and Ni catalysts

Nickel

The first example of C-F bond activation by a nickel complex was reported in 1977 by Mahan et al.[290] These authors found that, in the presence of phosphine ligands, bis(1,5-cyclooctadiene) nickel(0) undergoes oxidative addition of various aryl halides to form aryl Ni(II) halide complexes (Figure III-12, top). Based on the same nickel(0) system, Perutz et al.[291] found that these nickel complexes can activate selectively the C-F bond in the ortho position of 2,3,4,5-tetrafluoropyridine, even in the presence of the more labile C-H bond (Figure III-12, bottom).

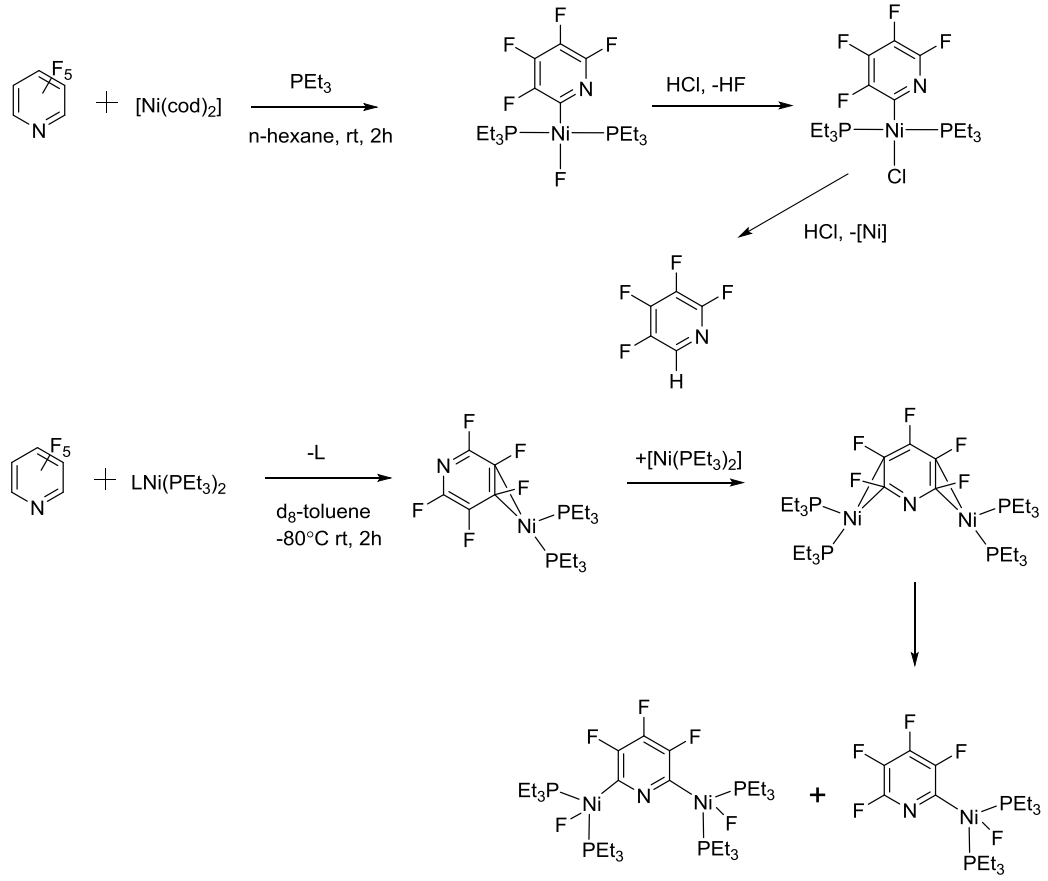

Figure III- 12. Mahan's nickel complexes for the activation of C-F bonds

There were many studies elucidating the mechanism of CF activation on nickel complexes and the unusual selectivity of this transformation. It is believed that phosphine ligands actually assist the activation of ortho C-F bonds through the generation of an unusual metallophosphorane intermediate. The para C-F bond did not have this additional chelating effect. An alternative mechanism was proposed by Johnson et al.,[292-293] who suggested a radical pathway for this C-F activation. Their arguments were based on the observation of an EPR active species and the successful isolation of a nickel(I) species from the reaction mixture (Figure III-13). Even though phosphines might play an important role in these earlier nickel-catalyzed HDF of perfluoroaromatics, a recent report from the Radius group highlights the activity of phosphine-free nickel systems.[294] In 2012, they applied $[Ni_2(^iPr_2Im)_4(COD)]$ (Pr_2Im = 1,3-bis(isopropyl)imidazolin-2-ylidene) as a catalyst for the HDF of polyfluoroaromatics using hydrosilanes. Based on combined computational and experimental studies,[294-296] they suggested a Ni(0)/Ni(II) catalytic cycle, which involves two classical important steps: the oxidative addition of the C-F bond and reductive elimination of the C-H bond. Silane in this catalytic system behaves as a reducing and fluorine abstraction reagent.

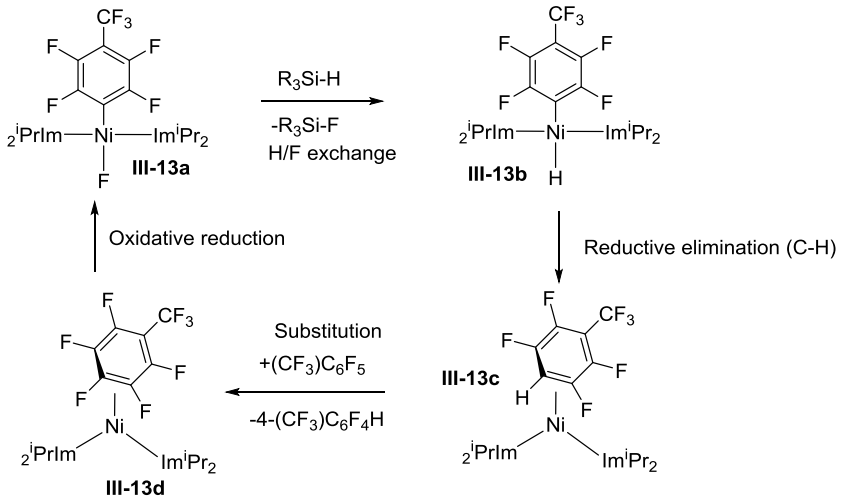

Figure III- 13. Johnson's nickel catalytic systems for the HDF of perfluorinated compounds

Stronger reducing reagents, such as zinc, alkali metal alkoxides, aluminum hydrides, boron hydrides, were also utilized in the nickel-catalyzed HDF systems. These studies also suggested the Ni(0)/Ni(II) redox cycle, as exemplified by the catalytic system reported by Adonin et al. (Figure III-14).[297-298]

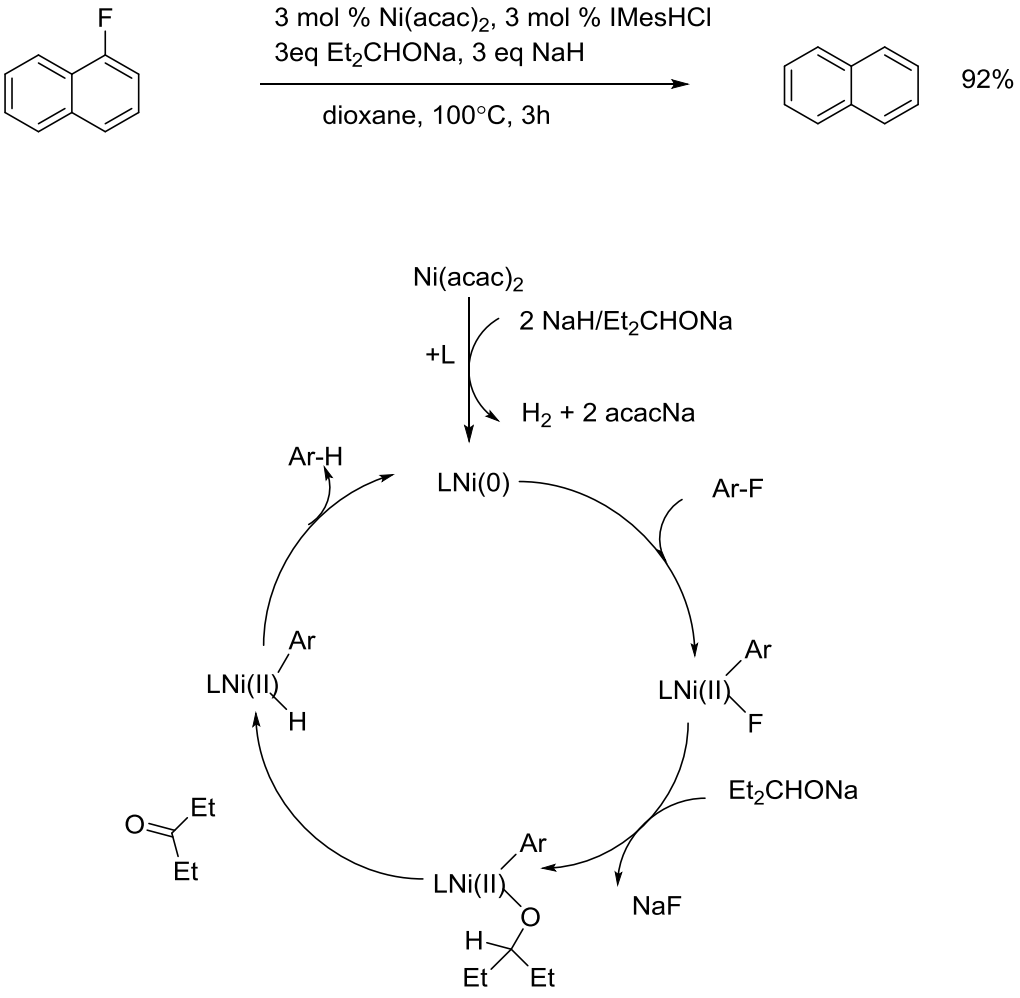

Figure III- 14. Adonin's nickel catalytic system

Remarkably in 2011, Cao et al.[299] reported that complete defluorination of perfluoroarenes could be achieved in the presence of excess $LiEt_3BH$ with a simple $NiCl_2$ catalyst without any additional ligands. The drawbacks of this system were the high loading of catalyst (40 mol %) and expensive $LiEt_3BH$ reagent.

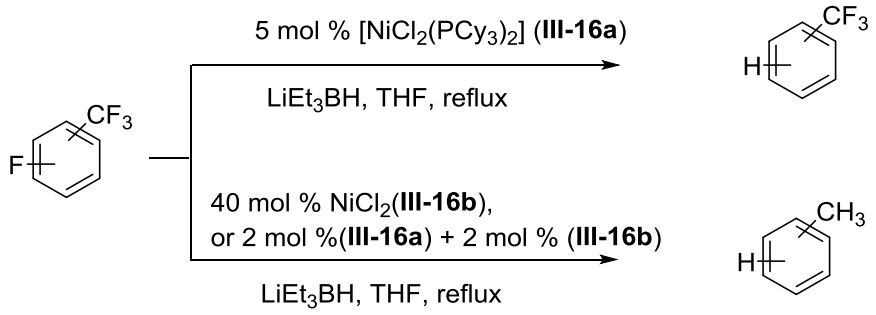

Figure III- 15. Cao's nickel catalytic system

Cobalt

Compared to nickel-catalyzed HDF reactions, cobalt systems have been developed later. In 2009, Ding and coworkers[300] attempted to use low-coordinate cobalt complexes for activating the C-F bond of perfluorobenzene and pentafluoropyridine in the presence of triethylsilane. Unfortunately, unlike their iron analogs, these cobalt complexes did not show any reactivity in test reactions. The reason for this inactivity can be rationalized by the instability of cobalt hydrides, which are believed to be the key intermediates in this catalytic cycle. The Klein and Li groups[77, 301-303] reported phosphine-supported cobalt complexes active toward C-F activation of perfluorinated arenes; however, none of them could be considered as effective catalysts, as they only reacted with the substrate in stoichiometric amounts.

Recently, Li et al.[304] reported that [$Co(PMe_3)_4$] could activate C-F bonds in perfluorinated arenes (Figure III-15). They found that a combination of low-valent cobalt complex and trimethylphosphine ligand was the key factor in this process and that the role of trimethylphosphine was not limited to being a supporting ligand but also it played an unusual role of fluorine scavenger. The authors suggested that reaction proceeded via initial C-H activation, and followed by C-F activation in the substrate by means of σ-bond metathesis with the Co-H bond. Even though several

intermediate complexes were successfully isolated and characterized, the overall mechanism is still not clear.

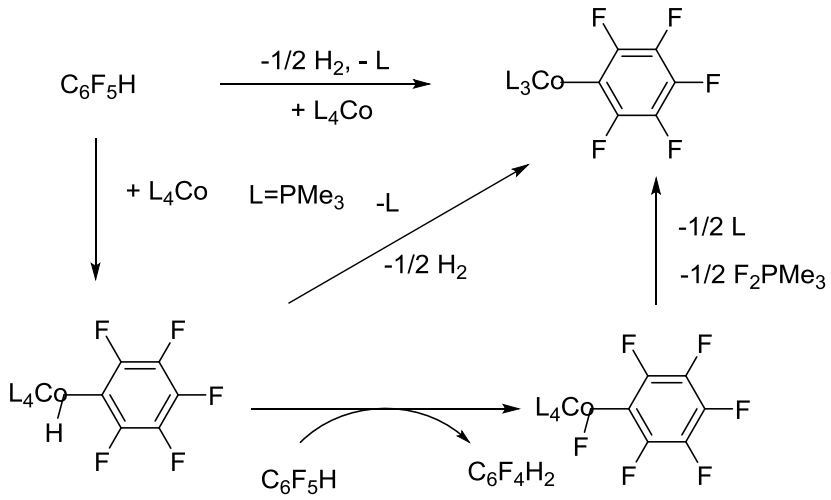

Figure III- 16. Li's cobalt catalytic system for HDF reaction

The first cobalt catalyzed HDF was again found by the Li group[305]. When sodium formate was used as the reducing agent, the reactivity of this system increased, but the reaction stopped at the maximum TON of 9. The authors proposed that this catalytic cycle goes through the Co(0)/Co(II) redox cycle, with the evolution of CO_2 and the release of NaF being the driving force for this reaction (Figure III-16).

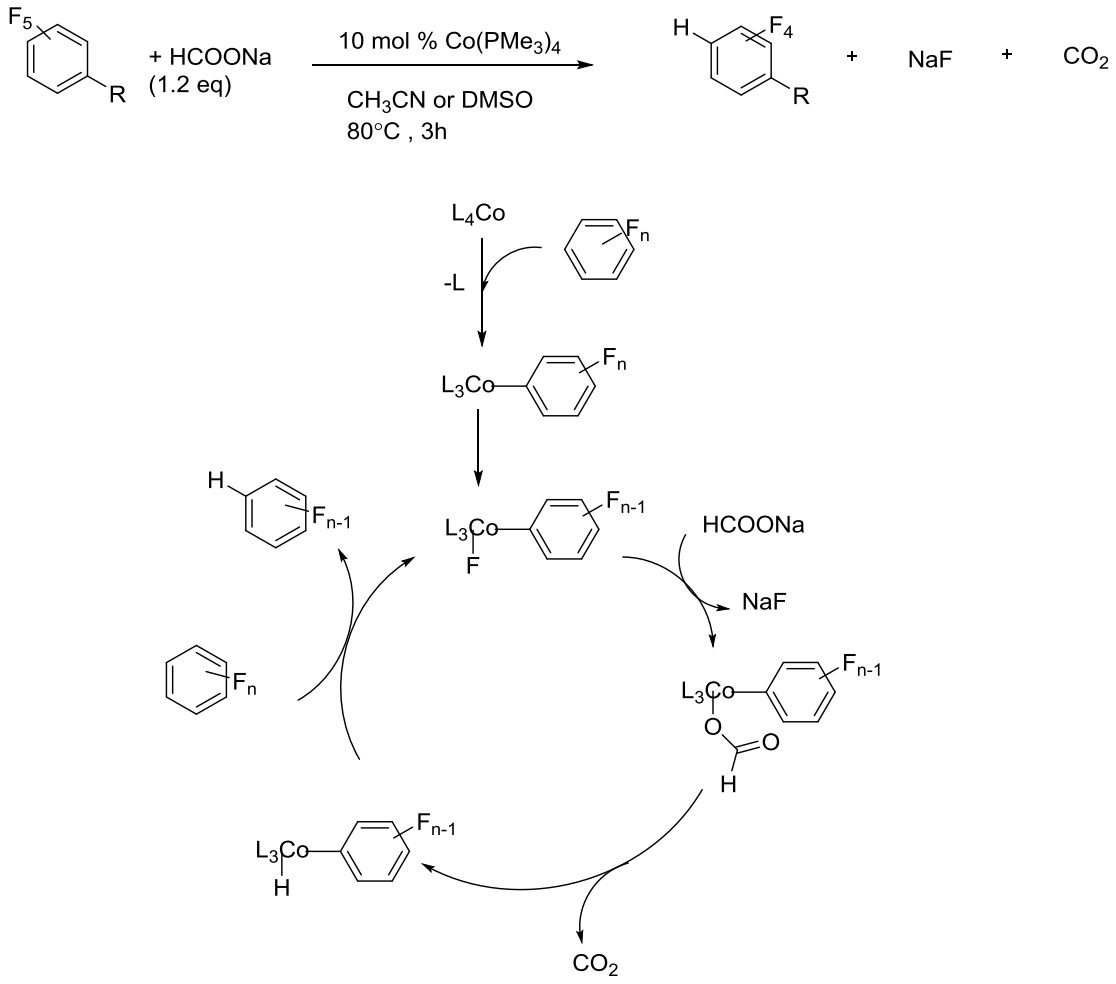

Figure III- 17. Li's cobalt catalytic systems using HCOONa as reducing reagent

Iron

As found by Holland et al.,[306] compared to analogous cobalt complexes, low-coordinate iron(II) fluorido compounds (Figure III-19) are active in the catalytic HDF of perfluorinated arenes in the presence of silanes. The authors suggested that an iron fluoride (**III-19a**) complex is part of the catalytic cycle, and dimeric hydrido complexes (**III-19b**) are considered as the resting state of the proposed catalytic cycle. Unfortunately, due to the instability of intermediates, it was impossible to draw a clear mechanistic proposal. Despite the fact that there are a limited number of studies using iron as a catalyst in the HDF reaction, the potential use of this earth

abundant metal in the near future is expected because of its low price and bio-compatibility[262, 264].

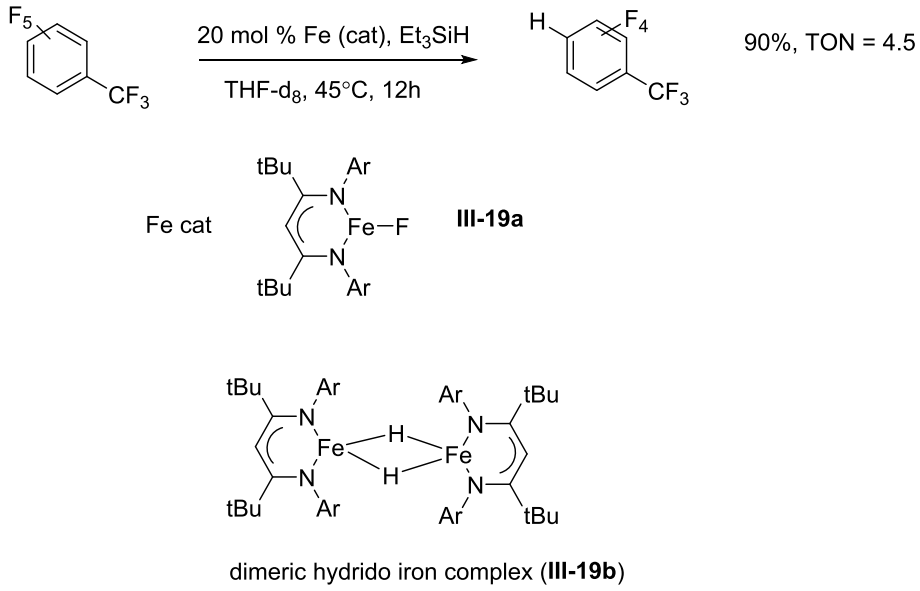

Figure III- 18. Holland's iron catalytic system for HDF of perfluorinated compounds

III.4 New directions in HDF reactions

In the near future, optimizing the reagents, broadening substrate scope, increasing selectivity, and enhancing reactivity will be active subjects for chemists involved in the field of HDF. Furthermore, there are limitations with current HDF systems, which makes these reactions succeed in the activation of C-F (sp^2) bonds, while C-F (sp^3) bonds still remained intact or less studied.

Another interesting trend could relate to the use of earth-abundant metals such as iron, molybdenum, cobalt in the catalytic HDF reaction. Current catalysts, based on these metals, have not been well developed, which becomes a big opportunity to investigate on this research stream. To overcome present obstacles related to the design of suitable HDF based on these metal, new ligands may be a great way to modify the electronic and steric properties of the corresponding catalysts for better HDF reactivity. Mechanistic studies, related to these HDF reactions, have also become interesting pursuits, as they might reveal insight of what really happens in these catalytic HDF systems.

Thanks to the high value of fluorinated pharmaceuticals and agrochemicals, the combination of HDF and other coupling reactions, such as borylation, silylation or functionalization, could become a hot topic for current research. These coupling reactions could let us reach for a variety of fluorinated compounds, which might have interesting reactivity or even bio-reactivity. Furthermore, as integrated with asymmetric syntheses, more and more chiral fluorinated products can be made for further use.

In the chapter VI, new cationic and neutral Ru complexes are prepared and characterized and tested for transfer hydrogenation of olefins.

IV. Ruthenium silane complexes, Si-H interactions, and H/D exchange

The investigation of nonclassical inter ligand interactions received significant impetus after the seminal discovery of Kubas in 1984.[307] who for the first time prepared the complex $W(CO)_3(PiPr_3)_2(H_2)$ with a hydrogen molecule trapped at the intermediate (arrested) stage of oxidative addition (Scheme IV-1).

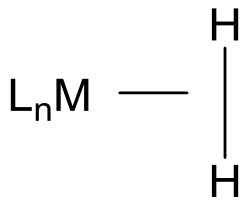

Scheme IV- 1. Kubas finding of dihydrogen sigma complex

This new η^2-coordinated H_2 complex showed very unusual structural features, such as an elongated H-H bond (0.84 Å, measured by neutron diffraction) compared to the usual free H_2 gas bond (0.73 Å) and large H-D coupling constant of a partially deuterated com plex, $W(CO)_3(PiPr_3)_2(HD)$, comparable with the normal H-D coupling value of H-D gas. These phenomena could not be explained by the formation of classical hydride compounds with 2c/2e bonds. It took a few years until Kubas' discovery was recognized by the chemistry community and the new mode of ligand coordination by donation of the σ-bond became accepted.[20, 308-309] Surprisingly, though, the idea of non-classical ligand bonding started almost two decades earlier than the first characterization of dihydrogen complexes by Kubas. In 1969, Graham et al. reported the first evidence of a non-classical Si-H interaction in a silane rhenium complex.[310] Remarkably, even without a neutron diffraction study, the combination of X-ray crystallography, NMR, and IR spectroscopy allowed them to identify this phenomenon and introduce one of the greatest recent concepts in

coordination chemistry. As stated in their seminal work "*each silicon-hydrogen bond functions as a two-electron donor to rhenium, effectively taking the place of a carbonyl group; the interaction could be described as a three centre, two-electron bond with the two electrons supplied by the original Si-H bond*".[103] This statement is the first example of what later became known as a 3 centre-2 electron model (3c/2e) (Figure IV-1) for a non-classical metal-ligand bond.[103] Since then, it has become common to depict non-classical interactions as σ-type interactions and to show delocalization of σ-bonds over three or more centres.

Figure IV- 1. 3 centre 2 electron model for transition metal silane sigma complexes

The widely accepted model for the description of σ-complexes is the adaptation of the Dewar-Chatt-Duncanson model (DCD),[311] which was originally suggested for the description of metal-olefin π-bonding. Interestingly, this model can be easily applied to most σ-complexes, including hydrogen, silane, and borane σ-complexes. Within this model, the coordination of a σ bond to a transition metal centre involves the donation from a σ bonding orbital of X-Y (Si-H, H-H, or B-H) to an empty d orbital of the metal, supported by back donation from a filled d orbital of the metal to the antibonding orbital σ* of X-Y (Figure IV-1, left). The inter-relationship between the donation and back donation actually dictates the extent of addition of the X-Y bond to the metal centre. There are two extreme situations which can be explained by this model. If there is a relatively strong donation from σ of X-

Y and but only weak or no back-donation, it will result in the formation of a weakly bound σ-complexes (a 2e/3c form). On the other hand, if there is a strong back-donation from the metal centre to the antibonding orbital of the X-Y bond, cleavage of the X-Y bond will occur, resulting in the formation of 2e/2c bonds between X, Y and M. For σ dihydrogen complexes, these two extreme states can be easily observed in dihydride and dihydrogen metal complexes. Likewise, for silane σ complexes various intermediate stages of Si-H addition to metal form depending on the metal complex and substitution at silicon.[103, 312]

As a result of the difference between hydrogen and silicon, silane σ-complexes have become more complicated to interpret than hydrogen σ-complexes. As depicted in Figure IV-2, and mentioned in a recent review by J. Corey,[103] at present, there is still no uniform agreement on the classification of non-classical silane complexes. In fact, Si-H interactions cover a spectrum of opportunities.[87, 103, 113-114, 308-309, 311, 313] There are several recognized forms of non-classical Si-H interactions, such as in σ-complexes, Si-H agostic, IHI (Interligand Hypervalent Interactions) and SISHA (secondary interactions between silicon and hydrogen).

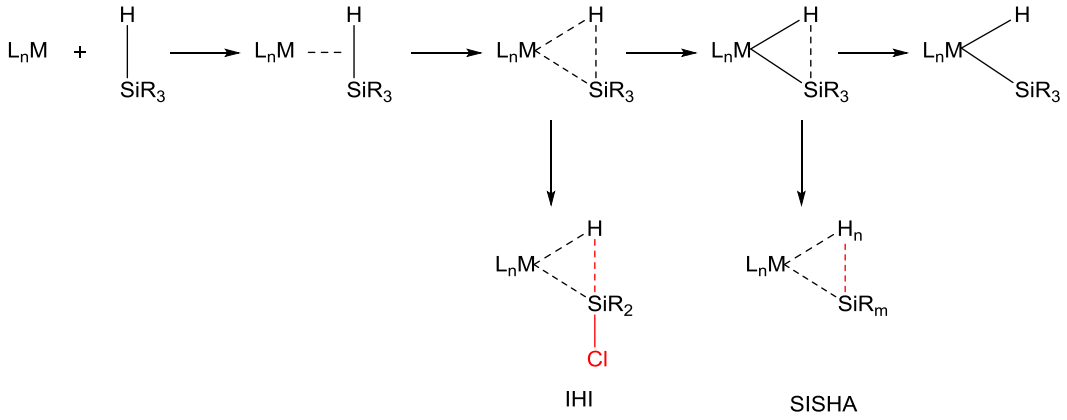

Figure IV- 2. Silane complexes and inter ligand interactions

First introduced by Nikonov in 1996, inter ligand hypervalent interactions (IHI) are described in terms of partial electron transfer from a metal-hydride bond to a nearby electrophilic silicon centre (usually to a halosilyl ligand).[314] One of the common features of complexes bearing this specific interaction is that the halide substituent at the silicon atom is oriented *trans* to the hydride, so that the silicon part of the σ*(Si-Hal) orbital can overlap with the M-H σ-bonding orbital, which brings about several distinct structural features: 1) the population of the antibonding orbital elongates the Si-X bond in comparison with averaged values found for tetrahedral silanes and related silyl complexes; 2) the M-Si bond shortens, likely as the result of increased silicon s-character in this bond; 3) the Si-H contacts (usually in the range 1.8-2.1 Å) are in the bonding range but are longer than those in σ-complexes (1.7-1.8 Å), and 4) the M-H bonds are slightly elongated.

The term SISHA was coined by the Sabo-Etienne group,[315] who used it to describe the MH· · · Si interactions between the η^2-SiH-coordinated silane ligand and metal-bound hydrides in several silane hydride complexes of ruthenium. The key features of SISHA are short Si-H distances falling in the range 1.9-2.4 Å. These

workers also proposed that the value of 1.7-1.8 Å for the Si-H bonds should be used as a distinctive feature for the formation of a σ-silane complex.

IV.1 Comments on X-ray, NMR studies for silane σ-complexes

The Si-H bond distance can be considered as an important parameter for the determination of the Si-H interaction with the metal centre. As stated in Corey's review,[103] the average bond length of Si-H bonds in different silanes can vary from 1.425 Å to 1.5 Å. Therefore, the presence of any Si-H distance longer than 1.5 Å in silane metal complexes could indicate the presence of a Si-H interaction with the metal centre. In a classical review on Si-H interactions, Schubert[316] set the upper limit for the shortest nonbonding Si-H contact, which is longer 2.0 Å and less than the radius sum of Si and H. Using Cp″L(OC)Mn(η^2-$HSiR_3$) (L: CO or a two-electron donor; Cp″ : Cp, Cp′, or Cp*) complexes, Nikonov et al. proposed shorter Si-H distances, ranging from 1.7 to 1.8 Å, as an indication of σ-coordination of these complexes.[314] Unfortunately, due to the strong influence of substituents on silicon, as well as the divergent effects of metal centres, this perspective is too narrow to develop a general picture of Si-H σ-interactions in other metal silane σ- complexes.

Another important parameter for silane σ-complexes is the M-H bond distance, which might be elongated (as suggested from the DCD model) due to inherent electron-deficiency of the metal centre. However, because of the scarcity of neutron diffraction studies and the inaccuracy of finding hydrides in the vicinity of heavy elements by X-ray diffraction, the application of M-H bond distances to interpret bonding situations and to draw reasonable conclusions about silane σ-complexes is less reliable. In fact, in a neutron diffraction study of the benchmark non-classical complex [Cp′$(OC)_2$Mn(η^2-$HSiFPh_2$] Scherer et al. did not observe any elongation of the Mn-H distance relative to the normal Mn-H bond observed in the related complex [Cp′$(OC)_2$Mn(η^2-$HSiHPh_2$)].[105] In addition, the number of neutron diffraction

studies of silyl hydrido complexes is not sufficient to establish a clear distinction between silane σ-complexes and silyl hydrido complexes. Even though, as mentioned in a recent review by Sabo-Etienne,[94, 113-114, 315] X-ray data can be now considered as more reliable for locating hydrogen positions, owing to the fact that X-ray measurements are now performed at low temperature with a higher-quality instrumentation and are aided by the DFT calculations, there is still some skepticism about the applicability of X-ray data for the characterization of silane σ- complexes.

The last crucial structural parameter, which can, in principle, convey information about the presence of silane σ-complexes, is the M-Si bond distance. Mostly established by X-ray crystallography, the M-Si bond distance can be measured with a much higher accuracy than the M-H or Si-H bond distances. However, there are still some complications brought about by the effects of substituents on the silicon atom and the metal on the M-Si bond. Regrettably, there is a very limited number of silane σ-complexes (Nb,[90] Ta,[317] Mo,[318] Mn[319]) which were characterized by neutron diffraction analysis, and most of them have different metal centres. A straightforward comparison of M–Si bonds in complexes with different metals and ligation is not possible and should be performed with caution.

While both X-ray and neutron diffraction measurements have certain drawbacks, NMR spectroscopy appears to offer a distinct advantage of being an inexpensive, fast, accessible and reliable method to identify Si–H interactions. NMR spectroscopy is very well-developed for characterization of σ-bond coordination,[315] especially for dihydrogen complexes, and has become a very powerful technique for the *in situ* detection of Si-H interactions in the coordination sphere of metals in solutions. The data acquired from the *J* coupling between silicon and hydrogen

nuclei and the T_{1min} measurements are great sources of information for non-classical Si–H bonding. As found by Corriu et al.,[320] the *J*(Si–H) coupling constant in a Mn silane σ-complex (65 Hz) is much higher than the typical *J*(Si–H) in hydrido silyl complexes (3–10 Hz), but significantly smaller than the *J*(Si–H) in free silanes, which fall in the range of 150-200 Hz (except for $HSiCl_3$ which has the value of 400 Hz). In 1990, Schubert[316] attempted to establish a borderline value for *J*(Si–H) to distinguish between a "significant" σ-Si-H interaction and a non-bonding situation, for which the coupling constant values of 10–20 Hz were suggested to be the highest possible values. Schubert suggested that the lowest value for non-classical Si-H interaction in a metal complex should be 20 Hz, with the typical values being around 40–70 Hz. In fact, as an indicator of the Si-H interaction, the value of the Si-H coupling constant should be used with caution, and the sign should be considered along with the magnitude of *J*(Si–H). When the complete oxidative addition of the Si-H to a metal takes place to give a hydrido silyl complex, the ^1J(Si-H) coupling constant must be zero, while the ^2J(Si-H) coupling constant can have still a non-zero value. At an intermediate stage of addition, for any non-classical Si-H interactions, the observed coupling constant J_{obs}(Si–H) should be the sum of both ^1J and ^2J coupling constants (Equation IV-2). Since the sign of these two coupling constants is usually opposite, then the observed coupling constant J_{obs}(Si–H) can vary quite significantly, and it is quite possible the negative ^1J(Si-H) value will cancel the positive ^2J(Si-H)[87]. This may actually result in the value of observed J_{obs}(Si–H) falling below the Schubert's 20 Hz threshold even in the case of significant non-classical interaction.

J_{obs} (Si-H)=^{1}J(Si-H) + ^{2}J(S-iH)

Equation IV- 1. J_{obs}

IV.2 Cationic silane σ- complexes

Unlike neutral silane σ-complexes, for which there are plenty of examples,[87, 103] cationic silane σ-species are very hard to isolate, which is reflected in the fact that the number of of "X-ray quality" crystals in this compound class are very limited.[321-322] This is due to their very poor stability and highly reactive nature. The main reason for this remarkable instability of cationic silane σ-complexes is the development of a highly electrophilic silicon centre, which strongly resembles the electron-deficient silicon centre in silylium ions R_3Si^+. The highly electrophilic silicon centre in cationic silane σ-complexes is very sensitive toward the presence of any nucleophilic substances, and therefore, even the usually noncoordinating (innocent) anions, such as PF_6^-, BF_4^-, and OTf^-, are not innocent enough to allow for their isolation. Therefore, their isolation is usually only possible with very robust borates and carboranes, such as $[BArF_4]^-$ (tetrakis(pentafluorophenyl)borate). Cationic silane σ-complexes are also very sensitive to the purity and the nature of solvents, which must be extremely dry and oxygen free. The presence of trace amounts of water or many other nucleophiles is very harmful to cationic silane σ- complexes. As a result, most cationic silane σ- complexes were characterized *in situ* at low temperature by NMR spectroscopy, and only a handful of cationic silane σ-complexes were studied by X-ray crystallography. Unfortunately, none of these crystals have yet been studied by neutron diffraction analysis.

IV.3 Selected examples of cationic silane σ-complexes from groups 8 and 9

Cationic iridium silane σ-complexes

In 1989, the first example of a cationic silane σ-complex was presented by Crabtree et al.[323] In this study, they succeeded in generating $[Ir(PPh_3)_2(H)_2(\eta^2\text{-}HSiEt_3)_2]SbF_6$ from the reaction of $[Ir(PPh_3)_2(H)_2(THF)_2]SbF_6$ and $HSiEt_3$ at a very low temperature, -80 °C. Due to the fact that this complex was only stable at low temperature, and easily decomposed to a known dimer iridium complex $[Ir_2(\mu\text{-}H_3)(H_2)(PPh_3)_4]SbF_6$, these authors used only low-temperature NMR spectroscopy to characterize this species. They observed two peaks in the hydride regions: one at -9.85 ppm (triplet) assigned to the *trans* Ir-H signal, and another at -12.75 ppm (multiplet) assigned to the Si-H-Ir signal with a *J*(Si-H) of 79 Hz. This complex was also found to be a very active catalyst for the alcoholysis of hydrosilanes, reaching a TON as high as 130,000 for the catalyzed reaction of isopropanol and $HSiEt_3$.

Cationic ruthenium silane σ-complexes

The first cationic ruthenium silane σ-complex, which was first characterized by NMR spectroscopy at low temperature in 1994,[324] and later by X-ray analysis in 2002,[321] was successfully isolated by the Lemke group. This complex, $[CpRu(PMe_3)_2(HSiCl_3)][BX_4]$ (X= 3,5-$(CF_3)_2$-C_6H_4), was obtained by protonation of $CpRu(PMe_3)_2(SiCl_3)$ with $[H(Et_2O)_2]$ $[B(3,5\text{-}(CF_3)_2C_6H_3)_4]$ in CH_2Cl_2. The hydride signal appeared as a triplet at -9.87 ppm, and the ^2J(Si-H) had a value of 49 Hz. This ^2J(Si-H) coupling constant was significantly smaller than that observed in free $HSiCl_3$, which was rationalized in terms of the presence of Si-H σ-interaction in this complex. This conclusion was later confirmed by the X-ray diffraction analysis.[325] The Si-H bond of this complex (1.77 Å) was found to be longer than the

normal Si-H bond in free silane (1.48 Å).[326] This was one of the rare examples of cationic ruthenium silane σ-complexes, and only the second example of a structurally characterised cationic ruthenium silane σ complex, with the first being [{Cp*Ru(μ-η^2:η^2-H_2($SiEt_2$)}$_2$-(μ-H)][BPh_4] reported by Takao et al.[327] The Si-H bonds in this complex are also longer than normal Si-H bonds. Interestingly, the *J*(Si-H) in this complex was only 18 Hz, which fell into the borderline zone for hydride silyl complexes. Therefore, there has still been a debate for the classification of this complex.

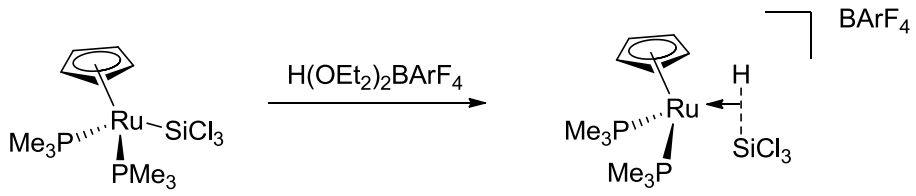

Figure IV- 3. The first cationic ruthenium silane σ-complex prepared by Lemke's group

Recently, our group reported the preparation of several new cationic ruthenium complexes bearing different Cp/PR_3 fragments (Figure IV-4, top), which were capable of forming the corresponding silane σ-complexes upon the addition of silanes at low temperature. The *J*(Si-H) coupling constants for these new complexes were in the range of 40-65 Hz, which indicated non-classical Si-H interactions. Remarkably, these silane σ-complexes were very stable thermally and tolerated chlorinated solvents, such as CH_2Cl_2 and chloroform. Moreover, Nikonov et al. also showed that these compounds are the key intermediates in the hydrosilylation of nitriles[108] and pyridines[125] (Figure IV-4, bottom).

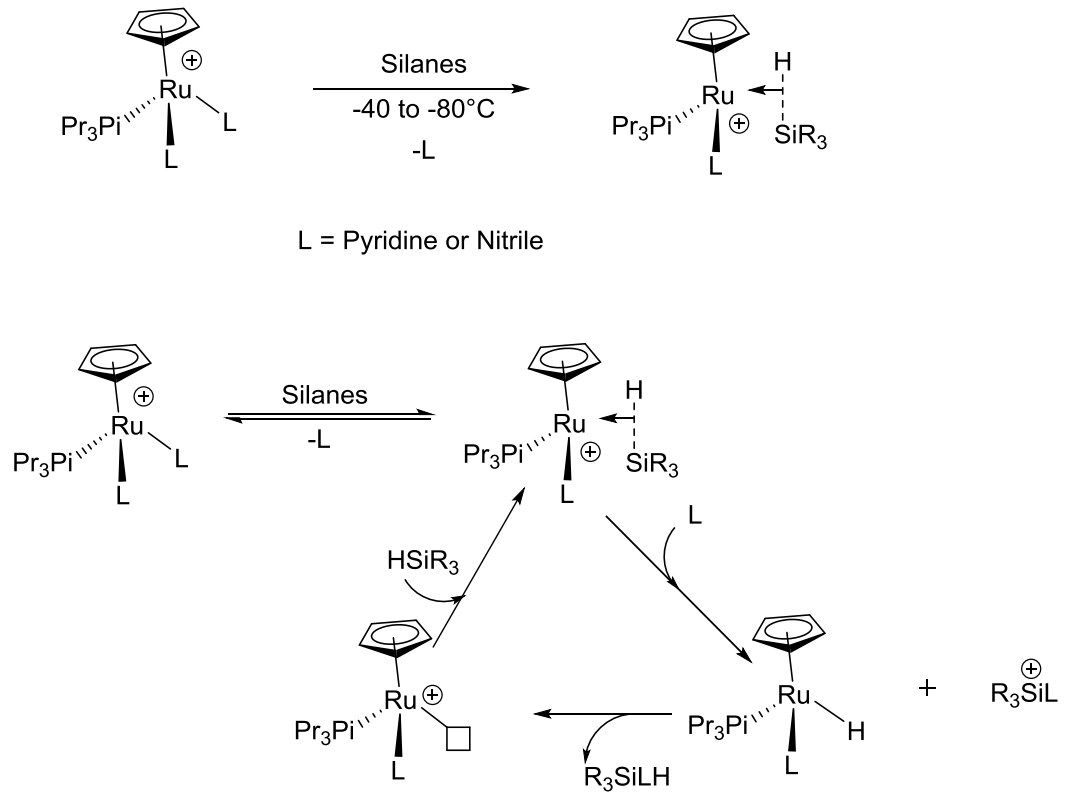

Figure IV- 4. Nikonov's ruthenium cationic σ-complexes for hydrosilylation

In the chapter VII, new silyl dihydride Ru complexes are prepared and characterized for the investigation of IHI interactions.

In the chapter VIII, new cationic and neutral Ru complexes are prepared and characterized for the investigation of Si---H interactions.

IV.4 H/D exchange

Deuterium labelled compounds find important application as solvents for NMR (nuclear magnetic resonance) spectroscopy, for characterization of protein structures, and for mechanistic investigations in catalysis.[328-333] Several methods for synthesizing D-labelled compounds are known and usually are based on the displacement of a proton bonded to carbon by deuterium. These methods can be classified as 1) pH-dependent H/D exchange[334-336] and 2) metal-catalyzed C-H activation for H/D exchange (both homogeneous and heterogeneous catalysis).[79, 331, 337-343] The former method is a traditional route, which has significant reverse exchange reactions. On the other hand, C-H activation has become an effective way for both academic and industrial chemists to achieve specific D-labelled molecules.[330, 344] Labelled pyridines and N-heteroaromatic compounds are very important in pharmaceutical applications; however, there are very few studies focused on H/D exchange of these specific substrates.[338, 343] Numerous studies employing various transition metal catalysts have been carried out for the last several decades to tackle this problem.[345-349] However, only a few catalyst systems can be listed as highly efficient and mild for deuteration of pyridine and its derivative. Moreover, none of them has shown a regioselective H/D exchange of N-heterocycles.

Of all transition metal catalysts studied, polyhydride species have been shown to have better capabilities in catalyzing H/D exchange.[332, 337, 342, 346, 349] Recently, Nikonov's group reported that half-sandwich tris(hydride) complexes of ruthenium are potent catalysts of the H/D exchange.[342] In particular, the complex $Cp(P^iPr_3)RuH_3$ was one of the first catalysts, that can catalyze H/D exchange in unactivated aliphatic C-H bonds (Figure IV-5, top). Interestingly, DFT calculations

suggested that the H/D reaction goes via dissociation of the phosphine ligand to form an unsaturated dihydrogen complex (Figure IV-5, bottom).

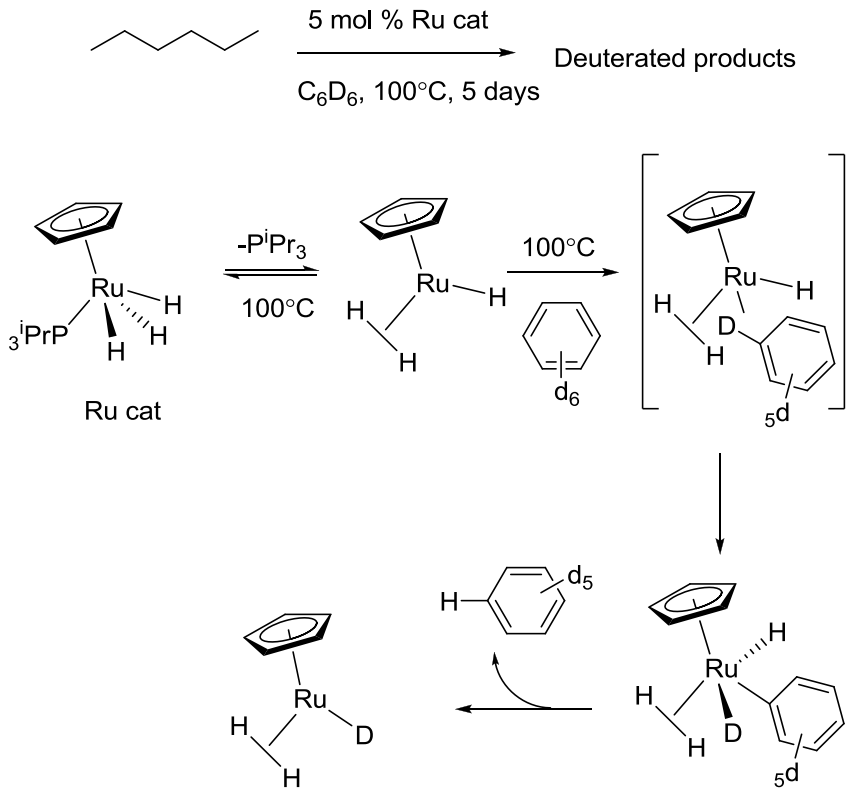

Figure IV- 5. H/D exchange reaction catalyzed by a phosphine trihydride ruthenium complex

In the chapter IX, various multi hydride ruthenium complexes are tested for the H/D exchange reactions.

Results and Discussion

V. Transfer hydrogenation

V.1 Catalyst synthesis

The preparation of complexes $[Cp(Pr^{i}_{3}P)Ru(NCCH_3)_2]^+[PF_6]^-$ (**V-1**) and $Cp(Pr^{i}_{3}P)RuH_3$ (**V-2**) has been previously achieved by a simple ligand exchange reaction with phosphines in the commercially available tris(nitrile) precursor $[CpRu(NCCH_3)_3]^+$ (**V-3**) to give the target Cp/phosphine derivatives.[124] Therefore, we thought that a similar approach would be applicable for the synthesis of isolobal Cp/NHC complexes of ruthenium. Supporting this notion was a previous report by Kirchner et al.[350] who described the preparation of a similar carbene complex by the direct reaction of **V-3** with 1,3-bis(2,6-diisopropylphenyl)imidazol-2-ylidene (IPr) in a 3: 2 mixture of THF and toluene. However, we failed to reproduce this synthesis. In our hands, the reaction consistently resulted only in a low yield of the target carbene complex $[Cp(IPr)Ru(NCCH_3)_2]^+[PF_6]^-$ (**V-4**) and formation of unidentified decomposition products. *In situ* NMR monitoring of the crude reaction mixture revealed a significant amount of the imidazolium salt $[HIPr]^+$ formed along with unknown products presumably derived from deprotonation of the acetonitrile ligand. These observations suggested that concurrently with our desired ligand exchange reaction, deprotonation of the coordinated acetonitrile in the starting tris(nitrile) complex could have taken place by the basic carbene IPr. Similar processes were observed for related systems,[351] due to the increased CH acidity of coordinated nitriles. By a careful analysis of the characteristic Cp region, we managed to identify another product, the compound $[CpRu(toluene)]PF_6$ (**V-5**), which was likely produced as a result of displacement of three nitrile ligands by one molecule of the

solvent, toluene. To avoid the problem of nitrile deprotonation, and because the formation of the compound [CpRu(toluene)]PF_6 is a thermodynamically preferable pathway, we decided to change our strategy and use a tris(pyridine) ruthenium complex instead of the tris(nitrile) as our starting material. We also chose to avoid the usage of toluene as a co-solvent. The preparation of the tris(pyridine) ruthenium complex $CpRu(pyr)_3]^+$ (**V-6**) was easily achieved by dissolving complex **V-3** in neat pyridine at room temperature for 24 h, followed by removal of volatiles under vacuum. The large excess of pyridine is required to shift the equilibrium to the right. The reverse formation of the tris(nitrile) from the tris(pyridine) complex can be accomplished by dissolving **V-6** in acetonitrile. Compound **V-6** was characterized by ^1H and ^{13}C NMR spectroscopy and elemental analysis.

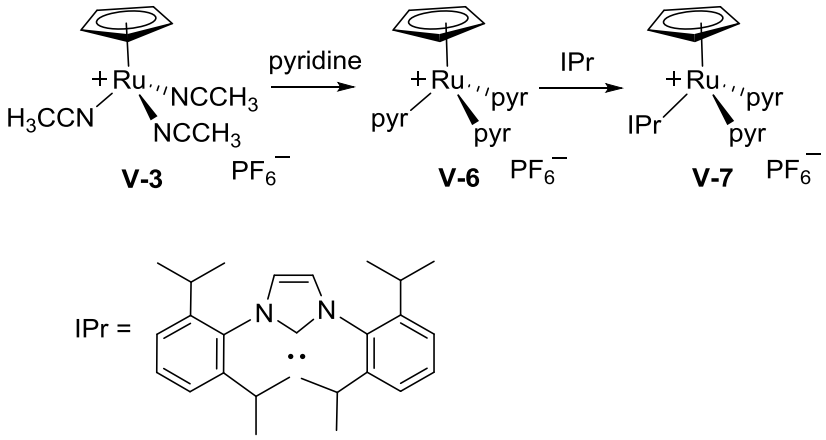

Scheme V- 1. Synthesis of complex **V-7**

Complex **V-6** reacts with IPr in THF or CH_2Cl_2 during 30 min at room temperature to give a new NHC carbene complex $[Cp(IPr)Ru(pyr)_2]^+$ (**V-7**) in 97% yield (Scheme V-1). The ^1H NMR signal of the Cp ligand in **V-7** is shifted upfield in comparison with the corresponding signal for the starting tris(pyridine) complex **V-6**: 3.77 ppm vs 4.19 ppm, respectively. ^1H NMR signals of the coordinated IPr in

V-7 appear to have the same pattern as those of the free IPr. X-ray quality crystals of a THF solvate of complex **V-7** were obtained from a THF/hexane mixture (3:2 v/v). The molecular structure of the cationic part is shown in Figure V-1. Complex **V-7** shows a typical tripodal piano-stool structure having one carbene and two pyridine legs. The Ru-C (pyridine) distances are 2.1481(17) and 2.1968(18) Å and the Ru–C bond to the IPr ligand is 2.1426(18) Å. We also succeeded in the synthesis of **V-4** by a ligand exchange reaction between **V-7** and an excess amount of acetonitrile.

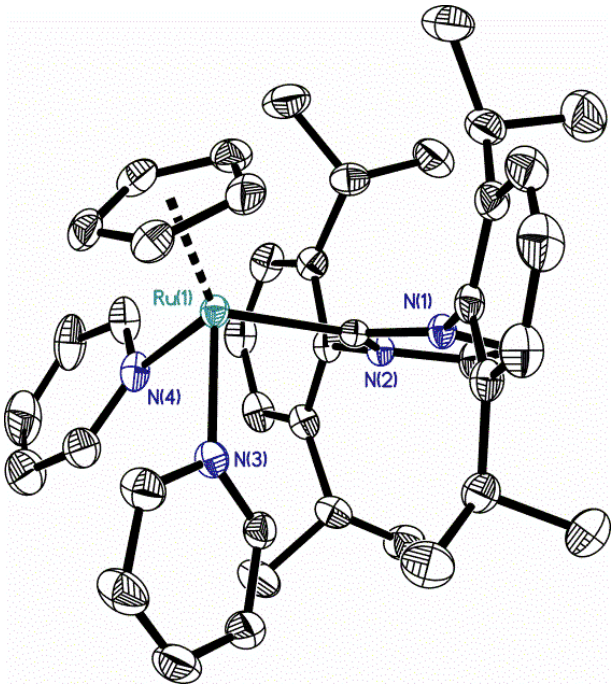

Figure V- 1. The molecular structure of complex $[Cp(IPr)Ru(pyr)_2][PF_6]$ (**V-7**). The counter-anion, the THF solvate, and hydrogen atoms are omitted for clarity.

V.2 Transfer hydrogenation of nitriles

Compounds bearing amine functional groups are important intermediates in the synthesis of dyes, agrochemicals, pharmaceuticals, polymers, surfactants, and different fine chemicals. Of various routes to prepare amines, the reduction of nitriles

is a less common pathway as it usually involves in the use of expensive and hazardous, reducing reagents, such as $LiAlH_4$ and $NaBH_4$. However, there has been recent progress in developing alternative methods for reduction of nitriles based on catalytic hydroboration and hydrosilylation[124]. Despite significant achievements in chemoselectivity and overall practicability, these transformations still have certain drawbacks, such as the use of expensive silanes and boranes, and production of large amounts of waste. On the other hand, the possibility of catalytic reduction of nitriles by alcohols is an attractive alternative because of the milder reaction conditions, low cost, and less wasteful co-products. But this approach has been little studied. In addition, the homogeneous catalytic transfer hydrogenation has recently emerged as a clean, green, and milder method to replace classical hydrogenation using heterogeneous catalysts, such as Ni/Raney and Pd/C, which normally yield low selectivities and various amine by-products. Unlike heterogeneous hydrogenation, homogenous transfer hydrogenation of nitriles is underdeveloped, with only a handful of examples, and these previous studies involved high catalyst loadings, high temperatures of operation, and/or expensive reducing reagents, such as Hantzsch esters.[23]

In 2014, our research group discovered that half-sandwich ruthenium complexes (Figure V-2) $[Cp(P^iPr_3)Ru(CH_3CN)_2][PF_6]$ (**V-1**; Cp=cyclopentadienyl) and $[Cp^*(phen)Ru(CH_3CN)][PF_6]$ (**V-8**; Cp*=pentamethylcyclopentadienyl, phen=phenanthroline) can catalyse the transfer hydrogenation of aromatic nitriles to imines under milder conditions (room temperature, < 3h).[21] This was one of the first examples of homogeneous catalytic transfer hydrogenation of nitriles; however, the catalyst load and amount of required base were quite high (5 mol % catalyst, 10 mol %

KOtBu). Wishing to develop a better catalytic system, we reckoned that the NHC-substituted complex $Cp(IPr)Ru(pyr)_2]PF_6$ (**V-7**), isolobally related to the phosphine catalyst $Cp(PR_3)Ru(CH_3CN)_2]PF_6$, may show a similar or even superior activity. Rewardingly, the latter complex has shown its capability in the catalytic TH of various unsaturated compounds, such as ketones, aldehydes, nitriles, N-heterocycles, imines, and olefins.[21] In this section, the optimization of catalytic conditions, screening of various nitriles, and kinetic studies will be discussed in detail.

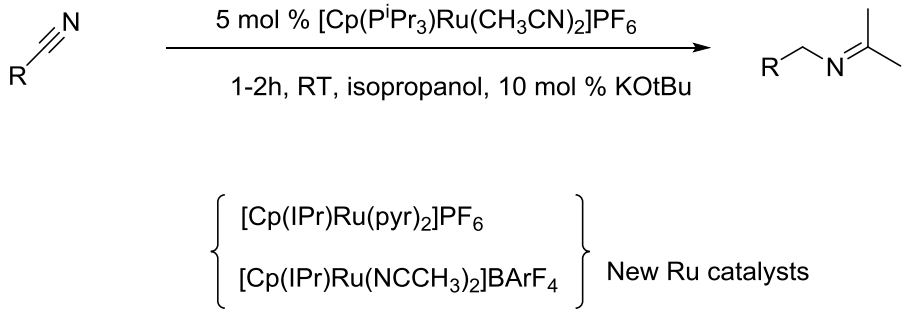

Figure V- 2. New ruthenium catalysts for the TH of benzonitrile

Catalytic optimization:

With our new complex in hand, we started screening the transfer hydrogenation of benzonitrile, as a benchmark system (Table V-1), in isopropanol used as a solvent and reducing agent and catalyzed by four different complexes, **V-3**, **V-4**, **V-6** and **V-7**, in the presence of KO^tBu (3:1 mol/mol base to catalysts). Under the same reaction conditions, catalyst **V-7** showed a greater activity than **V-3**, **V-4,** and **V-6**.

Table V- 1. Screening of different catalysts for the TH of benzonitrile

Entry	Cat [a]	Substrate	Product	Yield (%)	Time
1	**V-7**	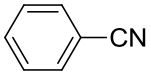	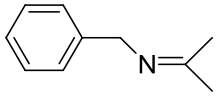	90	2h15min
2	**V-6**			71	3h13min
3	**V-3**			15	8h
4	**V-4**			34	8h

[a]0.5 mol % **cat**, 1.5 mol % of KO^{t}Bu in isopropanol at 70^{o}C

Screening different ratios of the base (B) and catalyst (C) (Table V-2) showed that the 3:1 molar ratio was the best for this reaction. Higher B/C ratios could inhibit and slow down the catalytic process. Decreasing the B/C ratio down to 0.5 led to an ineffective catalysis, which was later explained by the observation that at least two equivalents of a base should be used to activate the catalyst.

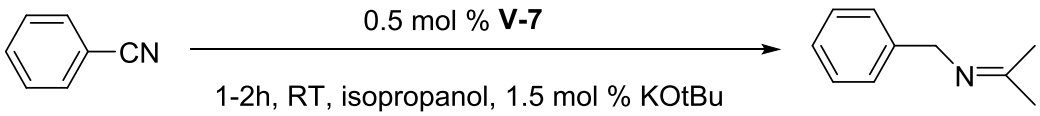

Scheme V- 2. Optimization of base to catalyst ratios

Table V- 2. Optimization of the base/catalyst ratio for the **V-7**-catalyzed transfer hydrogenation of benzonitrile

Entry	Time	Base: Catalyst	Yield [a] (%)
1	7h	0.5	50
2	8h43min	1	90
3	4h36min	2	90
4	1h50min	3	90
5	1h54min	4	90
6	2h29min	6	90
7	2h25min	8	90
8	2h15min	10	90
9	2h05min	20	90

[a]. NMR yield.

Varying the temperature of our catalytic reaction, we noticed that although the TH took place already at room temperature with a catalyst loading of 0.1 mol %, the yield was quite low (<10%). Stopping the reaction once the yield reached 90%, we showed that increasing the reaction temperature from 50°C to 80°C led to decrease

of the reaction time from 8h50m (entry 4) to less than 2h (entry 2). An attempt to decrease the catalyst load to 0.05 mol % at 70°C ended up with a lower yield of 63%. Considering that we had a reasonable time and yield at 70°C and 0.5 mol % catalyst, we decided to take the entry 6 as our optimized conditions.

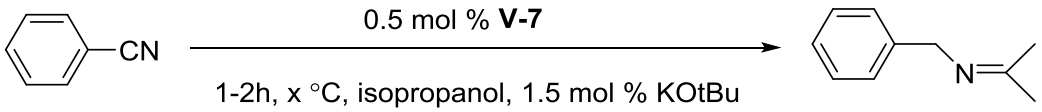

Scheme V- 3. Optimization of temperature and catalyst loadings

Table V- 3. Optimization of catalytic conditions for the **V-7**-catalyzed transfer hydrogenation of benzonitrile

Entry	%C[a]	Temp	Yield[b]	Time
1	0.05	70°C	63%	4h50min
2	0.1	80°C	99%	1h50min
3	0.1	RT	<10%	24h
4	0.5	50°C	87%	8h50min
5	0.5	60°C	93%	5h10min
6	0.5	70°C	94%	2h15min

[a] B = base KO^{t}Bu, C = catalyst. [b] NMR yield.

Having the optimized conditions (0.5 mol% catalyst, 1.5 mol% KO^{t}Bu, 70°C),

we screened the TH of various aliphatic and aromatic nitriles (Table V-4) in isopropanol. Hydroxyl, amino, ester, and methoxy para-substituted benzonitriles were reduced chemoselectively to form the corresponding imine derivatives in good to excellent yields (entries 1-4). Benzonitriles bearing such reactive C=O groups as acetyl and aldehyde were reduced nonselectively, in that the reduction of C=N happened after the TH of C=O bonds (entries 5-6). Para-cyano pyridine was also reduced successfully, without any sign of the reduction of the pyridine ring (entry 7). For aliphatic nitriles, which are usually more difficult to reduce, a higher temperature (90°C) and longer reaction time were employed to achieve complete reduction (entries 8-12). The nitro group appeared to poison the catalyst since its presence stopped this catalytic reaction at only 35% yield, even when a longer reaction time (48 h) was applied (entry 13). Surprisingly, the C=C bond remained untouched under these reaction conditions (entry 14).

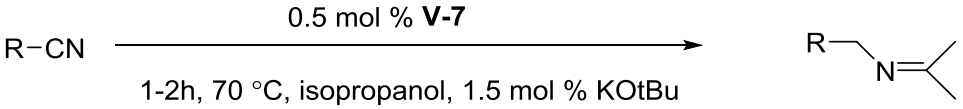

Scheme V- 4. **V-7**-catalyzed transfer hydrogenation of nitriles

Table V- 4. **V-7**-catalyzed transfer hydrogenation of nitriles

Entry	Product	Yield (%)[c]	Time
1	4-MeCH(OH)$C_6H_4CH_2N$=CMe_2	97	45min
2	4-(MeO)$C_6H_4CH_2N$=CMe_2	98	50min

		(57)	
3	4-$(H_2N)C_6H_4CH_2N=CMe_2$	87 (68)	90min
4	4-$(EtO_2C)C_6H_4CH_2N=CMe_2$	90	195min
5	4-$(HOCH_2)C_6H_4CH_2N=CMe_2$	97	120min
6	4-$(CH_3COHCH_2)C_6H_4CH_2N=CMe_2$	93	2h15min
7	4-$(H_2N)NC_5H_4$-3-$CH_2N=CMe_2$	95	165min
8	$Me(CH_2)_5CH_2N=CMe_2$	59	48h
9[a]	$Me_3CCH_2N=CMe_2$	32	48h
10[a]	$MeCH_2CH_2N=CMe_2$	98	48h
11[a]	$Me(CH_2)_2CH_2N=CMe_2$	99 (83)	48h
12[a]	$Me(CH_2)_3CH_2N=CMe_2$	87 (73)[d]	48h
13[b]	$C_6H_4CH_2N=CMe_2$	83	120min
14	3-NO_2-C_6H_4-$CH_2N=CMe_2$	35[e]	48h
15	$HC\equiv C-(CH_2)_4N=CMe_2$	24	48h

[a]At 90°C, [b] 1% **5** was used as a catalyst without added base, [c] NMR yield, isolated yield of ammonium salt after treatment with HCl in parentheses, [d] Isolated yield of amine after aqueous workup with NaOH. [e] Catalyst was deactivated upon the disappearance of tris-hydride peak and color of sample turned black.

V.3 Transfer hydrogenation of imines

After discovering the catalytic reactivity of **V-7** toward the TH of nitriles, we examined the TH of imines under the same catalytic conditions (0.5 mol% catalyst, 1.5 mol% KO^{t}Bu). Since the TH of nitriles stopped at the formation of imine products (coupled with acetone), we were interested in the capability of this catalyst to mediate the TH of other imines (Table V-5). Rewardingly, a tosyl protected imine was reduced completely to amine with only 0.5 mol % of catalyst within 2 h (entry 1), while it took 8 h to obtain 45% of the corresponding amine from the aldimine PhHC=NPh (entry 2). Ketimines (entries 3-5) were much harder to reduce even with a higher catalyst loading (5 mol %) and elevated temperature (90°C), so only < 5% yield was achieved. However, an activated ketimine was reduced more easily to 82% after16h (entry 6). Surprisingly, the reduction of diimines (entries 7-9) happened with 5 mol % of catalysts within a long period of reaction time (48 h) to gain moderate yields (up to 35 %).

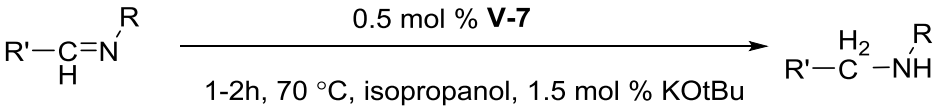

Scheme V- 5. **V-7**-catalyzed transfer hydrogenation of imines

Table V- 5. **V-7**-catalyzed transfer hydrogenation of imines

Entry	% mol cat	Substrates	Yield[a]	Time
1	5	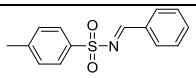	99(88)	2h
2	0.5	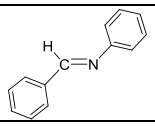	45	8h
3	5	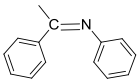	5[b]	48h
4	5	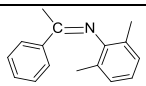	0[b]	48h
5	5	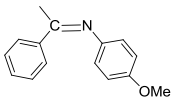	<5[b]	72h
6	0.5	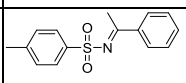	82[b]	16h
7	5	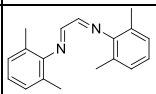	35[b]	48h
8	5	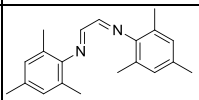	23[b]	48h
9	5	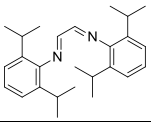	19	48h

[a] NMR yields, isolated yield of amine in parentheses; [b] At 90°, 5 mol % catalysts.

V.4 Transfer hydrogenation of N-heterocycles

The scope for the TH of C=N bonds by using this catalytic system was then expanded to include various N-heterocycles containing cyclic-imine frameworks (Table V-6). Much to our surprise and satisfaction, quinoline and 1,5-napthyridine were reduced in good yields (entries 1-2). Other substrates, such as 1,3,5-triazine, acridine, and phenanthridine, which are less aromatically stabilized than pyridine, were also hydrogenated within 8 h (entries 3-5). Substrates bearing bulky groups, such as 2-phenylquinoline, or more electron-rich substrates, such as 8-aminoquinoline, were inert under these catalytic conditions. Pyridine, isoquinoline, pyrimidine, pyrole, and imidazole were not reduced, even at elevated temperature (up to 120°C) and a higher catalyst loading (5 mol %).

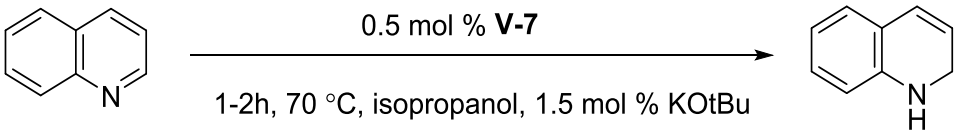

Scheme V- 6. **V-7**-catalyzed transfer hydrogenation of N-heterocycles

Table V- 6. **V-7**-catalyzed transfer hydrogenation of N-heterocycles

Entry	Substrate	Product	Yield[a]	Time
1	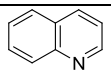	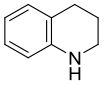	62 (45)	6h
2	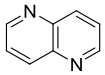	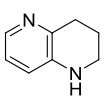	67	8h

3			60 (38)	75min
4	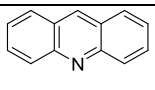	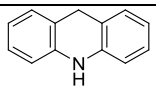	72	8h
5	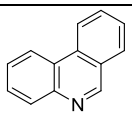	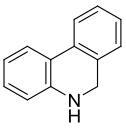	58 (43)	8h
6	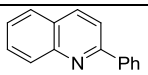	NR		8h
7	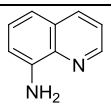	NR		8h

[a] NMR yields, isolated yield of amine in parentheses;

V.5 Transfer hydrogenation of esters

We were interested to extend the substrate scope of Ru-mediated reduction to esters because: (i) in our previous study, $[Cp(P^iPr_3)Ru(CH_3CN)_2][PF_6]$ was found to be active in the TH of several esters,[21] and (ii) the activity of this catalyst **V-7** in the TH of other challenging substrates: nitriles, imines and N-heterocycles.

As was expected, esters are harder-to-reduce substrates under the TH conditions using alcohol as the hydrogen donor,[352] and the process is further complicated by a concurrent transesterification (Table V-7). Most of our ester substrates remained untouched under these catalytic conditions, except 4-

methylphenyl benzoate, phenyl acetate, ethyl trifluoroacetate, which were partially hydrogenated. All of the screened esters were transesterified to form the corresponding isopropyl derivatives. Noteworthy, an ester-bearing acetophenone was reduced selectively on the acetyl group under the same conditions, and the reduction process for this acetyl group was very fast to achieve 99% yield in 5 m (entry 2, Table V-7).

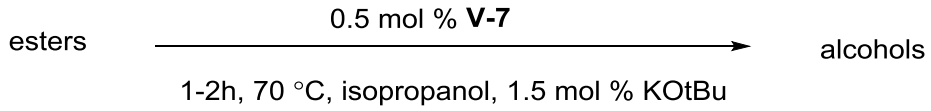

Scheme V- 7. **V-7**-catalyzed transfer hydrogenation of esters

Table V- 7. **V-7**-catalyzed transfer hydrogenation of esters

Entry	Substrate	Product	Conversion (%)[b]	Time	Note[c]
1	ethyl benzoate	$PhCO_2CH(CH_3)_2$	50	5 min	TE
2	ethyl 4-acetylbenzoate	$4\text{-}\{CH_3CH(OH)\}C_6H_4CO_2CH(CH_3)_2$	99 (16)	5 min	TE+TH
3	ethyl 4-aminobenzoate	$4\text{-}H_2NC_6H_4CO_2CH(CH_3)_2$)	99	10 min	TE
4	ethyl(dimethylamino)-benzoate	$4\text{-}(CH_3)_2NC_6H_4CO_2C(CH_3)_2$	89	20 min	TE
5	methyl 3-cyanobenzoate	$3\text{-}CH_3O_2CC_6H_4CH_2N{=}C(CH_3)_2$	99	2h35 min	TE
6	phenyl	$4\text{-}CH_3OC_6H_4CO_2C(CH_3)_2$	34	30	TE

	4-methoxybenzoate			min	
7	phenyl benzoate	$PhCO_2CH(CH_3)_2$, and $PhCH_2OH$	40	11h30 min	TE
8	4-methylphenyl benzoate	$4\text{-}CH_3C_6H_4CO_2CH(CH_3)_2$ + $4\text{-}CH_3C_6H_4CH_2OH$	68 (11)	9h	TE+TH
9	ethyl 4-nitrobenzoate	$4\text{-}H_2NC_6H_4CO_2CH(CH_3)_2$	99(<5)	5 min	TE+TH
10	vinyl benzoate	$PhCO_2CH(CH_3)_2$	<10	11h30 min	TE
11	4-chlorobenzoyl benzoate	$4\text{-}ClC_6H_4CO_2C(CH_3)_2$	20	4h	TE
12	phenyl acetate	$PhCO_2C(CH_3)_2$+$PhCH_2OH$	50 (10)	2h	TE+TH
13	ethyl trifluoroacetate	CF_3CH_2OH, CH_3CH_2OH	86 (8)	1h45 min	TE+TH
14	phenyl trifluoroacetate	PhOH and CF_3CH_2OH	68 (<5)	2h40 min	TE+TH
15	dimethyl phthalate	NR	-	2h	TE

[a] 1 mol % **3**, 3 mol % of KO^tBu in isopropanol at 70ºC**;** [b] Conversion to the transfer-hydrogenated (TH) products in parentheses; conversions determined by NMR spectroscopy.; [c] TH=transfer-hydrogenation, TE=trans-esterification.

V.6 Transfer hydrogenation of olefins

Given the success of the TH of C=N and C=O bonds by this catalytic system,

we next explored the catalytic reactivity of **V-7** toward the reduction of C=C bonds. The result of attempted hydrogenation of non-activated olefins is shown in Table V-8. The reduction of 1-hexene was achieved in high yield (95 %) in 48 h with 0.5 mol % of catalyst and 1.5 mol % of KOtBu (entry 1). Di-substituted cyclic olefins, such as 1-methyl-cyclopentene, were harder to reduce (entry 5) (12%, 48h), while 1-cyclohexene (entry 3) was hydrogenated in moderate yield (82 %). 1-Cyclohexene was also chosen as a test substrate for the screening of the catalytic activity of $Cp(IPr)RuH_3$ (**V-9**). As shown in entry 4, **V-9** can catalyze the TH of 1-cyclohexene to cyclohexane under base-free conditions. For a noncyclic tri-substituted olefin, 2-methyl-2-butene, the yield dropped significantly (entry 6) as only 8% of the hydrogenated product was observed. No activity was found for a tetra substituted olefin (entry 7). Interestingly, attempts to reduce styrene yielded an unknown gum-like product, which could be a polymerized form of styrene (entry 8). There was no reactivity in attempts to reduce alkynes under the same catalytic conditions (entries 9 and 10).

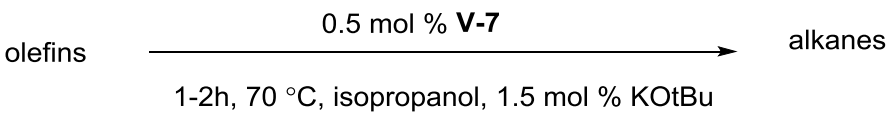

Scheme V- 8. **V-7**-catalyzed transfer hydrogenation of olefins

Table V- 8. **V-7**-catalyzed transfer hydrogenation of olefins

Entry	Substrate	Product	Yield (%)	Time
1			95	48h
2			78	48h
3[a]			82	48h
4[b]			82	48h
5[b]			12	48h
6			8[c]	48h
7		NR		48h
8		Polystyrene gum[e]		48h
9	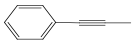	NR		48h
10	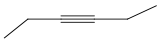	NR		48h

[a] $Cp(IPr)RuH_3/^tBuOK$ was used as a catalyst. [b] $Cp(IPr)RuH_3$ was used as a catalyst without added base. [c] 80°C [d] NMR yields. [e] Styrene polymerized.

To verify the reactivity of our catalysts, we evaluated different catalytic

conditions with methyl acrylate as a benchmark substrate (Table V-9). Our results showed that the catalyst **V-7** was superior to analogs without a supporting donor ligand, such as $[CpRu(pyr)_3][PF_6]$ (**V-6**) and $[CpRu(NCCH_3)_3][PF_6]$ (**V-1**) (entries 1-3). $Cp(IPr)RuH_3$ showed interesting results in that it could catalyze the TH of methyl acrylate under base-free conditions (entry 4), and the selectivity of hydrogenation (yield up to 98 %) increased significantly in the presence of a base (0.5 % mol) (entry 5); while excess base led to increased formation of the Michael product (entry 6). In the presence of a base and 0 % catalyst loading (entry 7), only Michael addition products were observed (Scheme V-4). A blank experiment returned no activity (entry 8).

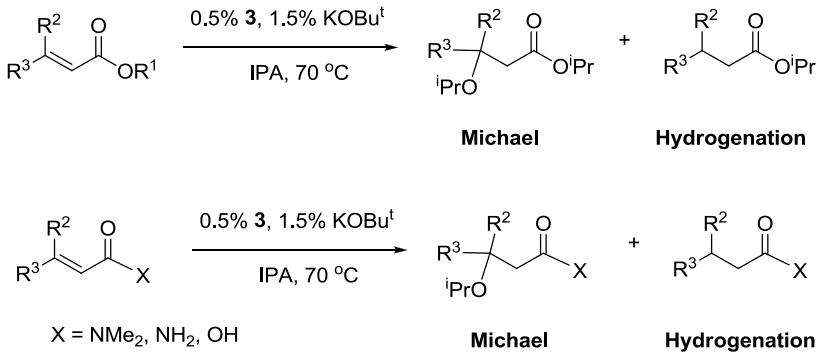

Scheme V- 9. Michael addition vs Hydrogenated products

Table V- 9. Control and blank experiments

Entry	Conditions	Yield[a]	Time
1	**V-7** + 3KO^{t}Bu	15%M, 85% H	72h

2	**V-6** + 3KO^{t}Bu	85%M, 15% H	72h
3	**V-1** + 3KO^{t}Bu	17%M, 83%H	16h
4	**V-9**	18% H	24h
5	**V-9** + KO^{t}Bu	98% H	24h
6	**V-9** + 3KO^{t}Bu	11%M, 89% H	8h
7	KO^{t}Bu	99%M, 0% H	20min
8	No catalyst + No base	0%M, 0% H	24h

[a] NMR yield, 0.5 mol % of cat, Michael (M) vs Hydrogenated (H) products

The reactivity of catalyst **V-7** was also studied in the transfer hydrogenation of activated olefins (Table V-10), which are important precursors for the synthesis of fine chemicals, pharmaceuticals, and perfume products. In the presence of a base only (entry 7, Table V-9), the reaction of an α,β-unsaturated ester (methyl acrylate) with isopropanol yielded only the Michael addition product, a β-isopropoxy-substituted ester, which was formed very fast under these catalytic conditions (<20m) (entry 7, Table V-9). Further examining α,β-unsaturated esters showed that all of these reactions yield Michael addition products (entries 1-5, Table V-10). These

Michael products can be considered as kinetic products due to the fact that upon further heating the reaction mixture, hydrogenated products $RH_2C\text{-}O\text{-}^{i}Pr$ were obtained by means of reduction of the ether moiety. Simultaneously, the transesterification process also takes place, which converts the starting material to different ester derivatives. Therefore, upon heating, the final products were mixtures of two esters, one with the original alcohol part, and another one with the isopropyl alcohol moiety. Generally, the yields of the hydrogenation of different conjugated esters (entries 1-5) were moderate to high (up to 95 % NMR yield, and 82% isolated yield). A conjugated ester with an additional N-coordinating site (entry 6) was reduced in an excellent hydrogenation yield (98 %), albeit at a long reaction time (48 h). Trisubstituted olefins with α,β-unsaturated ester or acid groups were also hydrogenated in good yields in 16 h (entries 7 and 8). Surprisingly, the TH of crotonic acid showed no reactivity, however, after being esterified by isopropanol, the resulting isopropyl ester was reduced effectively to yield isopropyl isobutyrate (entry 9). To our delight, conjugated amides (entries 10-12) were also transfer-hydrogenated in good yields (45-98 %).

Table V- 10. **V-7**-catalyzed transfer hydrogenation of activated olefins

Entry	Substrate	Yield[a]	Time
1	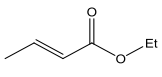	20% M, 80% H ethyl butyrate (78%)[b]	8h
2	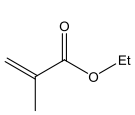	5% M, 95%H ethyl isobutyrate (82%)[b]	8h

3	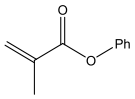	15%M , 85%H	8h
4	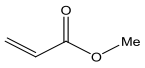	11% M, 89% H methyl propionate (64%)[b]	8h
5	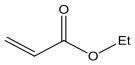	11% M, 89% H ethyl propionate (74%)[b]	16h
6	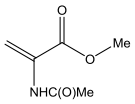	98%H	48h
7	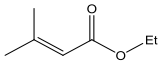	7% M, 93% H	16h
8[c]	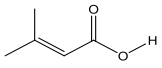	99% H isopropyl isovaleriate[d]	72h
9	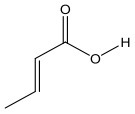	NR[e]	24h
10	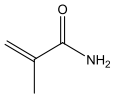	15% M, 85% H isobutyramide (58%)	48h

11	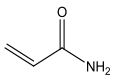	55% M, 45% H propionamide (43%)	48h
12	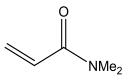	98% H	8h

[a] NMR yields, isolated yields in parentheses; [b] Isolated yields for ester obtained after transesterification with ethanol or methanol; [c] The catalyst was premixed with base in IPA prior to addition of the substrate; [d] After the TH, the isovaleric acid was converted to ester by acid catalyzed esterification; [e] However, prior conversion of crotonic acid into isopropyl ester resulted in 65% isolated yield of isopropyl isobutyrate. Michael addition (M) vs Hydrogenated (H) products.

V.7 Transfer hydrogenation of ketones and aldehydes

We have also briefly screened the reactivity of **V-7** toward the TH of ketones and aldehydes (Table V-11), and the results were very promising. As can be seen from entry 1, acetophenone was reduced quickly and effectively with only 0.05 mol % catalyst loading (82 %, 70°C, 1h 20m) to yield 1-phenylethanol. In comparison with **V-7**, other catalysts (entries 2-4) took longer times (up to 8h) to achieve lower yields (up to 75 %) even with a higher catalyst loading (up to 1 mol %) at the same temperature (70°C). Further examining a series of aldehydes and ketones, we found that our catalyst **V-7** also showed an excellent activity (entries 5-9) with high yields. However, compared to the best ruthenium-based catalytic systems, such as the Baratta's catalyst [RuCl(κ^3-CNN)-(dppb)] (5 min at 0.005 mol%)[353], and the Stradiotto's catalyst [(η^6-cymene)Ru(κ^2-P,N)(Cl)] (5 min at 0.05 mol%)[354], which showed reactivity approaching the performance of enzymes, our system reached only a decent reactivity.

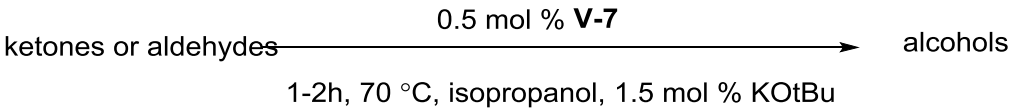

Scheme V- 10. **V-7**-catalyzed transfer hydrogenation of ketones and aldehydes

Table V- 11. **V-7**-catalyzed transfer hydrogenation of ketones and aldehydes

Entry	Cat [a,b]	Substrate	Product	Yield (%)	Time
1	**V-7**[a]	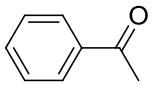	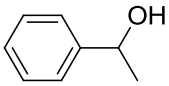	82	1h20m
2	**V-5** [a]			75	4h20m
3	**V-3** [a]			29	8h
4	**V-8** [a]			37	8h
5	**V-7**[b]	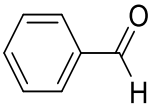	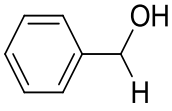	86	35m
6	**V-7** [b]	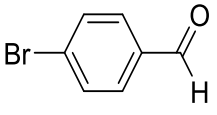	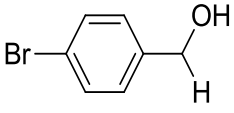	74	50m
7	**V-7** [b]	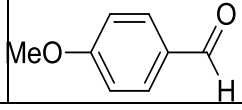	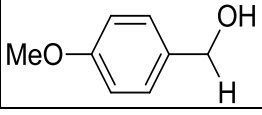	78	25m

8	**V-7** [b]	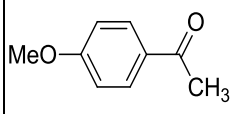	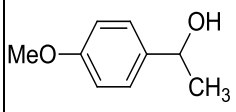	62	30m
9	**V-7** [b]	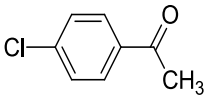	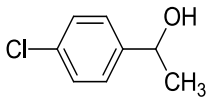	55	35m

[a]0.05 mol % cat, 0.15 mol % KO[t]Bu. [b] 0.1% mol cat, 0.3 mol % KOtBu

V.8 Kinetic studies

Careful observation of ^{1}H NMR spectra for the catalytic samples of the TH reaction revealed the occurrence of a new hydride species at about -10 ppm. Intrigued by this hydride signal, we reckoned that our catalytic cycle could involve the formation of a ruthenium hydride(s). To further verify this conjecture, we conducted several stoichiometric experiments (Scheme V-11).

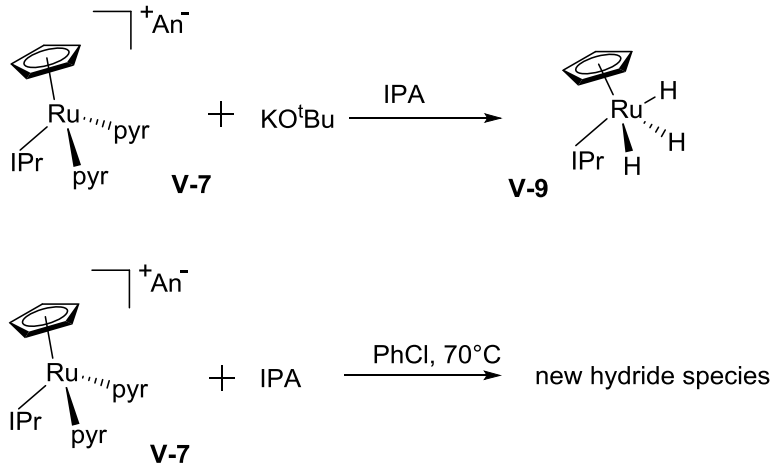

Scheme V- 11. Stoichiometric reactions.

A stoichiometric reaction between $[Cp(IPr)Ru(pyr)_2][PF_6]$ (**V-7**) and KO[t]Bu

in isopropanol yielded a ruthenium trihydride Cp(IPr)RuH_3 (**V-9**). Indeed, when employed as a catalyst in the TH of benzonitrile and acetophenone, **V-9** was able to catalyze the TH of these substrates in the absence of an external base. Based on these observations, we suggested that the role of the external base in our catalytic system could be only to convert the pre-catalyst [Cp(IPr)$Ru(pyr)_2$][PF_6] (**V-7**) into Cp(IPr)RuH_3 (**V-9**).

Intrigued by the fact that Cp(IPr)RuH_3 was the resting state of this catalytic system and that this compound could catalyze the reaction in the absence of a base, we conducted kinetic studies using Cp(IPr)RuH_3 as the catalyst. Methoxybenzonitrile was chosen as the substrate for these studies since its MeO proton signal is easy to observe and interpret by ^{1}H NMR spectroscopy, and because the complete reduction of this substrate could be done in a reasonable period of time for kinetic analysis. As our catalytic condition involved the use of three equivalents of an external base (in the equivalents of the catalyst), we decided to add additional amounts of a base to match the real catalytic conditions developed for **V-7**.

To measure the dependence of the reaction on the concentration of isopropanol, a series of NMR samples was prepared in such a way that the amount of isopropanol would vary in the range of 10 - 40 equivalents to the substrate to keep the pseudo-first order conditions toward IPA. The reaction rates were obtained from the slopes of kinetic plots, linearized in the coordinates $-\ln([MePhCN]_t/[MePhCN]_0)$ versus time (Figures XII-1-7, Appendix). Further plotting these reaction rates versus the amount of IPA revealed that there was a saturation behavior at large concentrations of IPA (Figure V-3).

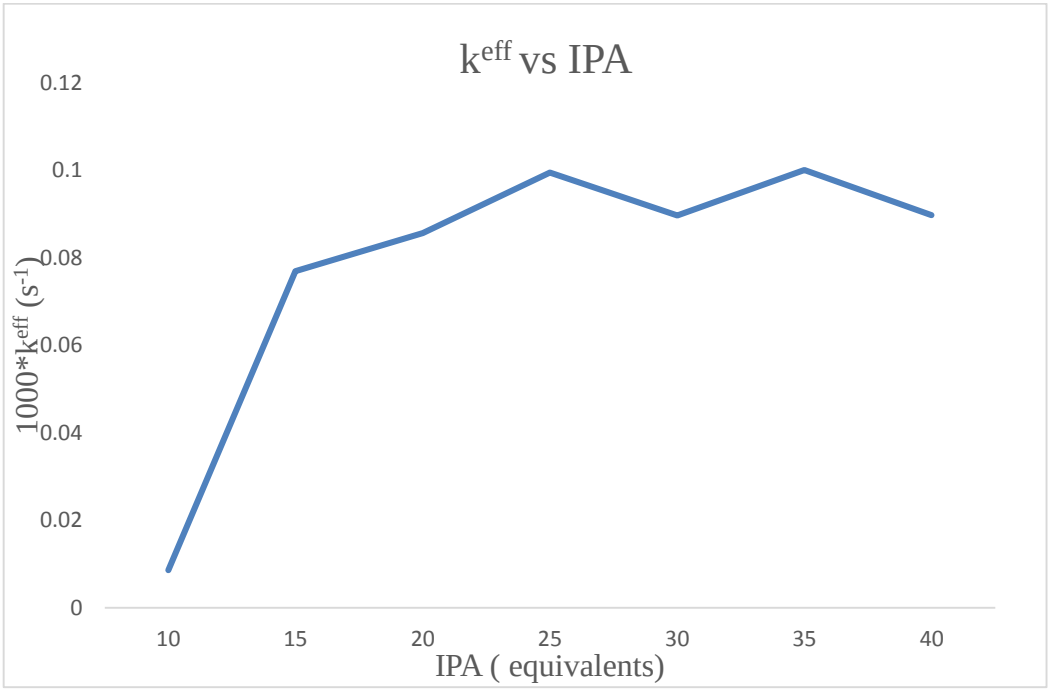

Figure V- 3. Dependence of the **V-9** catalyzed TH on the amount of IPA

This saturation kinetics can be interpreted in terms of a pre-equilibrium involving the substrate and the catalyst **V-9**. To clarify the role and effect of an external base on the catalytic cycle, we performed additional kinetic experiments. To ensure the pseudo-first-order conditions, we used a large but fixed amount of IPA (15 equivalents to the substrate) and varied the amount of external base (KO^tBu, 0.5 to 4 equivalents to the catalyst). The amounts of the pre-catalyst and the substrate were also fixed. Reaction progress was monitored by ^1H NMR spectroscopy, and the reaction rates were obtained as in previous experiments (Figure XII-8-13, Appendix). Plotting the reaction rates versus the amount of base revealed that increasing the amount of base had a detrimental effect on catalysis (Figure V-4), which agrees with our previous hypothesis that the main role of the external base in this transformation is to convert the pre-catalyst ($[Cp(IPr)Ru(pyr)_2][PF_6]$) into the active form,

$Cp(IPr)RuH_3$.

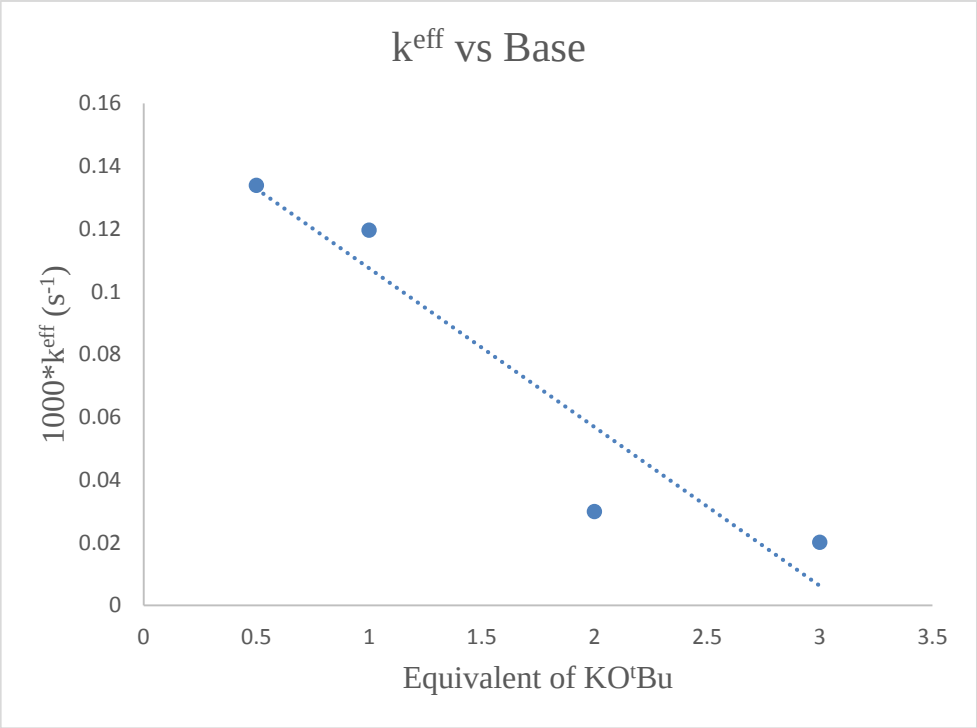

Figure V- 4. The dependence of the reaction rate on the amount of $KOBu^t$.

All of these kinetic experiments suggest that our catalytic cycle likely follows a classical hydride mechanism, which can be illustrated in Scheme V-12. Firstly, the pre-catalyst $[Cp(IPr)Ru(pyr)_2][PF_6]$ is converted into $Cp(IPr)RuH_3$. Upon heating, H_2 dissociates from $Cp(IPr)RuH_3$ to yield an unsaturated intermediate (**V-10**) which then coordinates the substrate to give **V-11**. Subsequent hydride transfer to the coordinated substrate generates intermediate **V-12**. **V-12** undergoes metathesis with alcohol to furnish the alcoholate **V-13**. β-Hydride from the latter yields a η^2-acetone hydride complex (**V-14**), which after dissociation of acetone regenerates the catalyst

V-10 and closes the cycle.

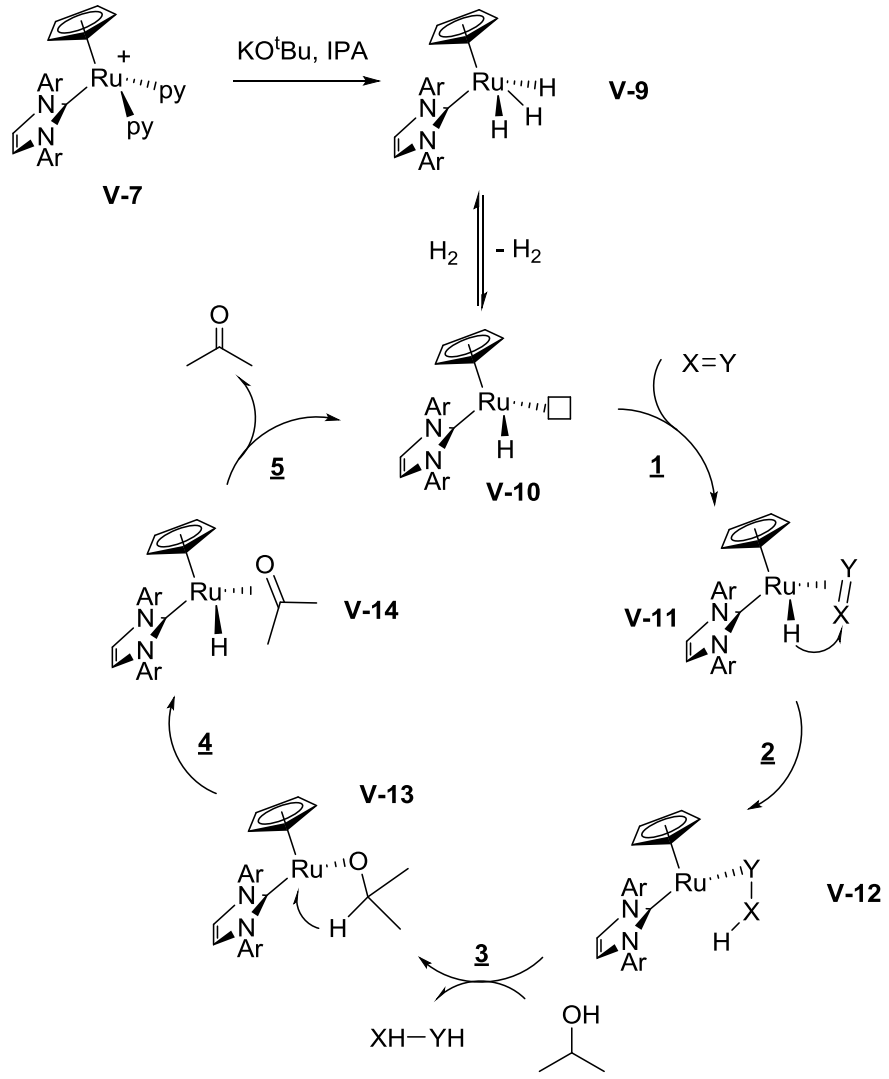

Scheme V- 12. Proposed mechanism for the TH using **V-7** as catalyst

One of the interesting features of this catalytic system is that the resting state of the catalyst is Cp(IPr)RuH_3, which is totally different from what was observed in the catalytic cycles of our previous studies, where the analogous ruthenium catalyst [Cp(P^iPr_3)Ru($NCCH_3$)$_2$][PF_6] was used as a pre-catalyst and complex Cp(P^iPr_3)Ru($NCCH_3$)H played the role of the active species in catalytic cycles. Another interesting feature to note is that the TH of nitriles with

[Cp(IPr)Ru(pyr)$_2$][PF$_6$] as pre-catalyst obeys the classical hydride mechanism, whereas in the TH of nitriles catalyzed by the analogous complex [Cp(P^{i}Pr$_3$)Ru(NCCH$_3$)$_2$][PF$_6$] an MVP-like (MVP = Meerwein–Ponndorf–Verley) mechanism was favoured (Scheme V-13).

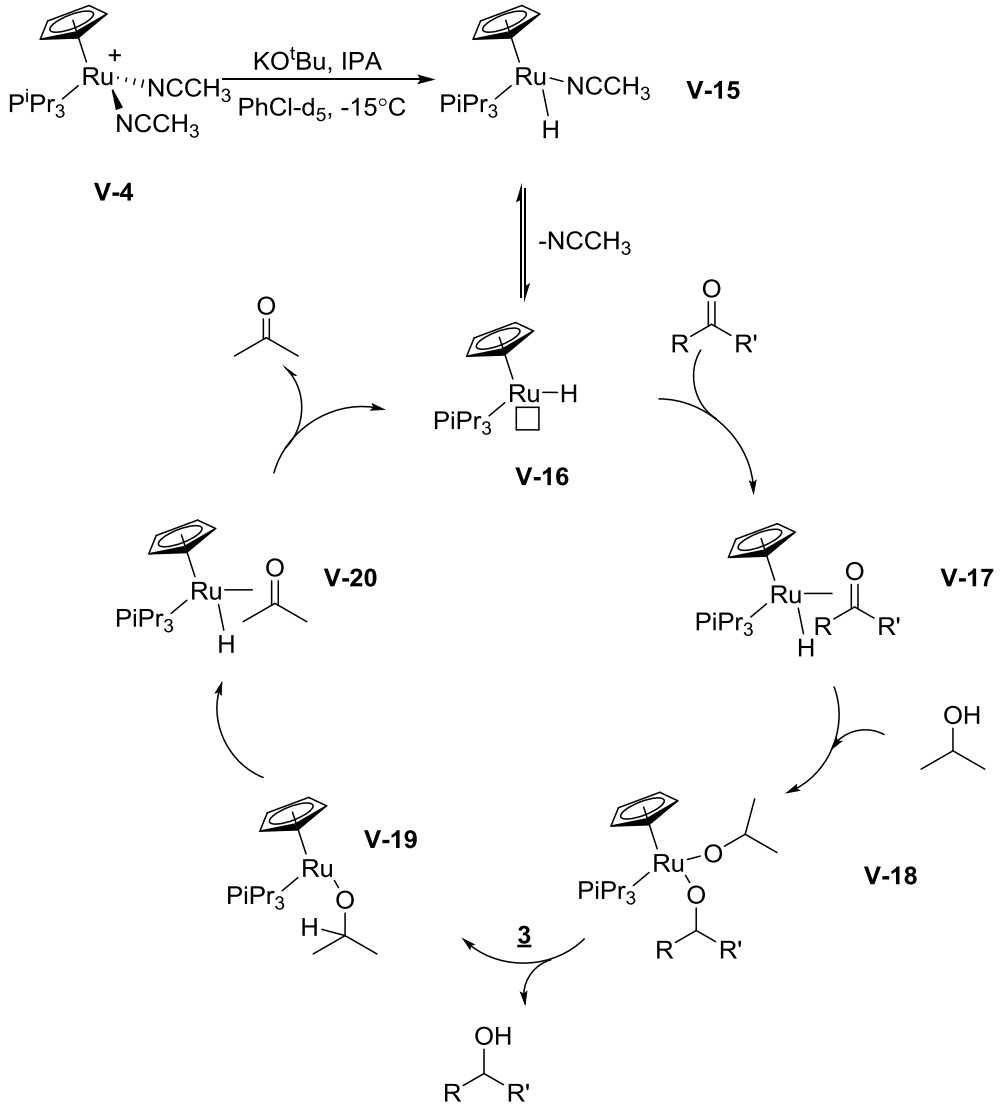

Scheme V- 13. Proposed mechanism for TH catalyzed by pre-catalyst [Cp(P^{i}Pr$_3$)Ru(NCCH$_3$)$_2$][PF$_6$]

VI. HDF of perfluorinated compounds

VI.1 Catalyst syntheses

The preparation of complexes $Cp(IPr)RuH_3$ (**VI-1**, Cp = cyclopentadienyl, IPr = 1,3-bis(2,6-diisopropylphenyl)-imidazol-2-ylidene), $[Cp(IPr)Ru(pyr)_2][BArF_4]$ (**VI-2**, pyr = pyridine), $[Cp(IPr)Ru(NCCH_3)_2][BArF_4]$ (**VI-3**, $BArF_4$ = tetrakis(pentafluorophenyl)borate) and $[CpRu(pyr)_3][PF_6]$ (**VI-4**) was reported in the previous chapter on the catalytic transfer hydrogention. The preparation of new cationic Cp and Cp* ruthenium complexes supported by IPr or IMes carbene ligands $[Cp'(IPr)Ru(NCCH_3)_2][Anion]$ (Cp' = Cp*, Pentamethylcyclopentadienyl, or Cp Cyclopentadienyl, Anion = PF_6^-, hexafluorophosphate, or $BArF_4^-$ tetrakis(pentafluorophenyl)borate) is shown in Scheme **VI-1**.

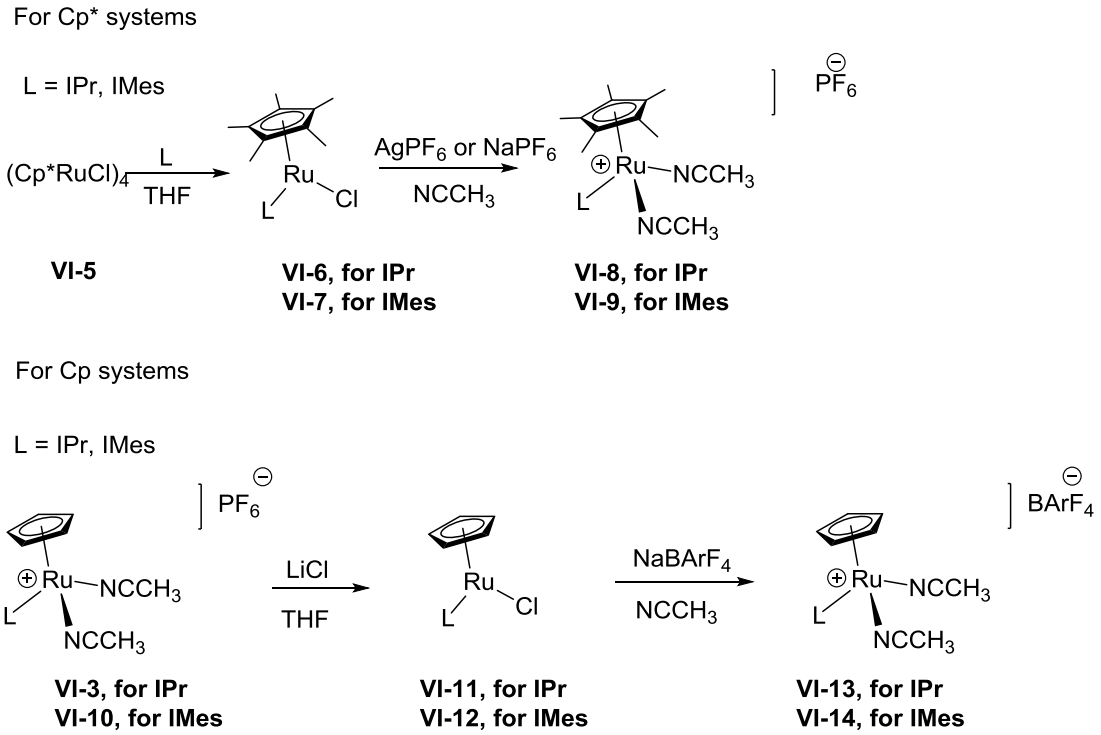

Scheme VI- 1. Preparation of Cp and Cp* ruthenium complexes supported by NHC carbenes.

Cp ruthenium complexes supported by IPr or IMes carbene ligands*

Complexes Cp*(L)RuCl (L = IPr, **VI-6**, or IMes, **VI-7**) were prepared according to a literature procedure reported by Nolan et al.[355] The corresponding cationic ruthenium complexes were obtained upon the addition of one equivalent of $AgPF_6$ (or $NaBArF_4$) To a solution of Cp*(L)RuCl (L = IPr, of IMes) in acetonitrile. The crude product was then recrystallized from a mixture of ether and hexane (5:1 v/v) to yield $[Cp^*(L)Ru(NCCH_3)_2]^+$ (L = IPr (**VI-8**) or L=IMes (**VI-9**)). Complex **VI-8** are shown in Figure VI-1 and Figure VI-2. These complexes were used in subsequent preparations and in catalysis without further purification.

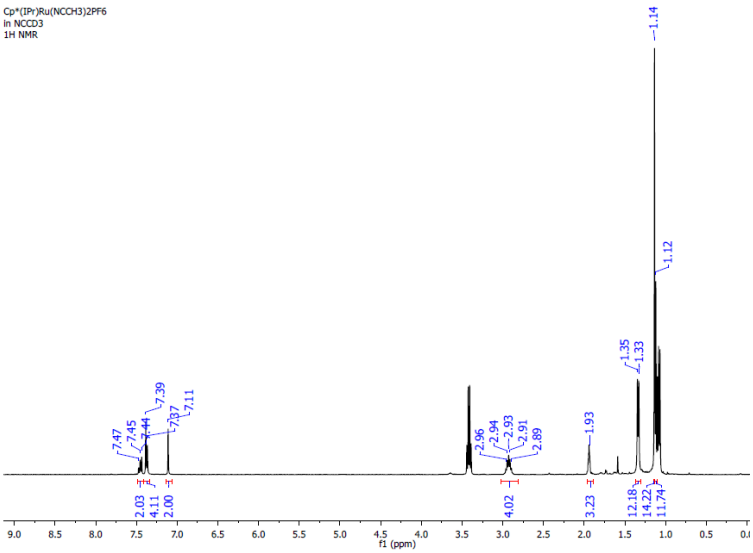

Figure VI- 1. ^1H NMR (600 MHz, $NCCD_3$) spectrum of $[Cp^*(IPr)Ru(NCCH_3)_2][PF_6]$

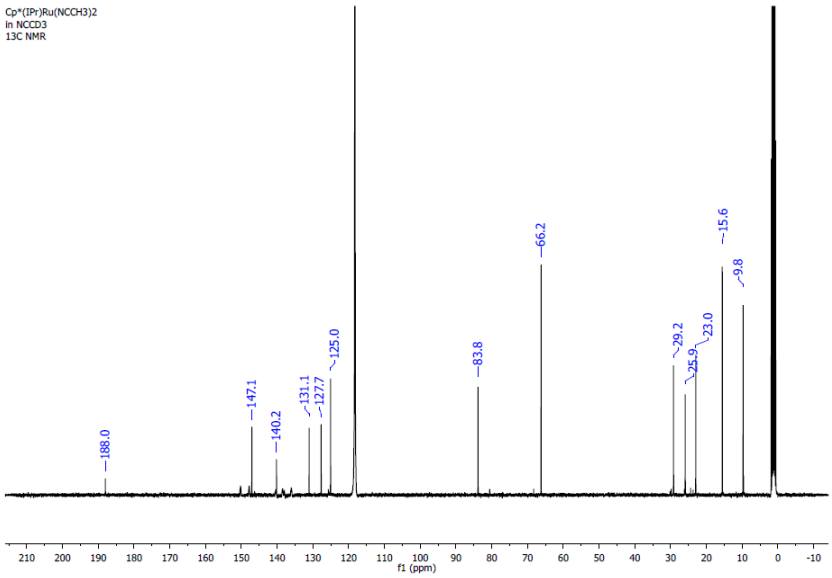

Figure VI- 2. ^{13}C NMR (600 MHz, $NCCD_3$) spectrum of $[Cp^*(IPr)Ru(NCCH_3)_2][PF_6]$

Cp ruthenium complexes supported by IPr or IMes carbene ligands

Preparations of complexes $[Cp(L)Ru(NCCH_3)_2][PF_6]$, L = IPr (**VI-3**) or L=IMes (**VI-10**)) were outlined in the previous section about transfer hydrogenation. The treatment of $[Cp(L)Ru(NCCH_3)_2][PF_6]$ with one equivalent of LiCl in THF yielded blue complexes Cp(L)RuCl (L = IPr (**VI-11**) or L=IMes (**VI-12**)) which were extracted into toluene and recrystallized from a mixture of toluene and hexane (3/2, v/v) to afford clean products (The NMR spectra of **VI-11** were showed as an example in Figures VI-3 and VI-4). Cp(IPr)RuCl was also characterized by an X-ray study, which will be discussed in the next section VIII.

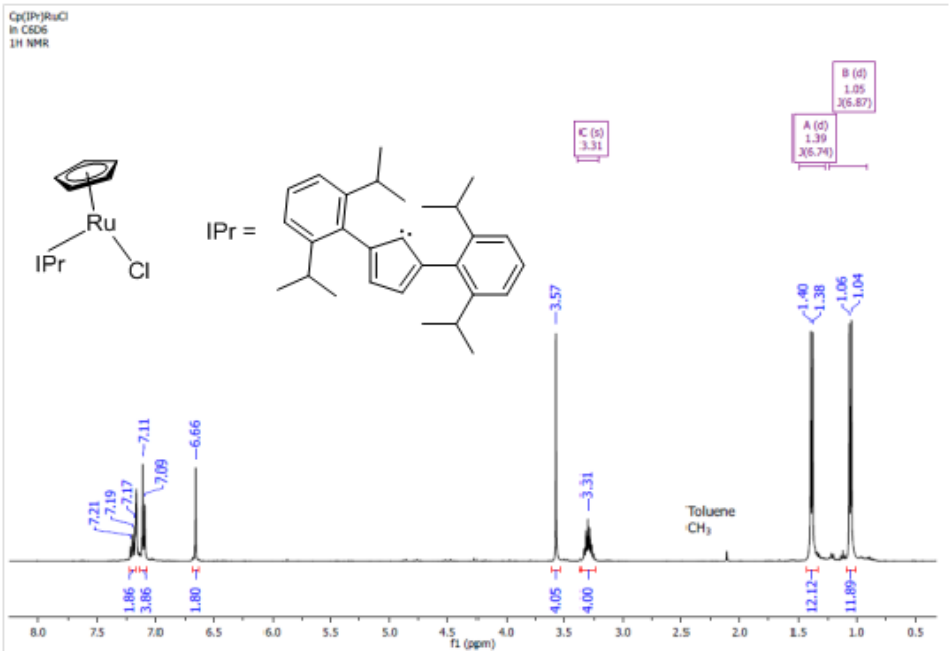

Figure VI- 3. ^{1}H NMR (400 MHz, 22°C, C_6D_6) of Cp(IPr)RuCl (**VI-11**).

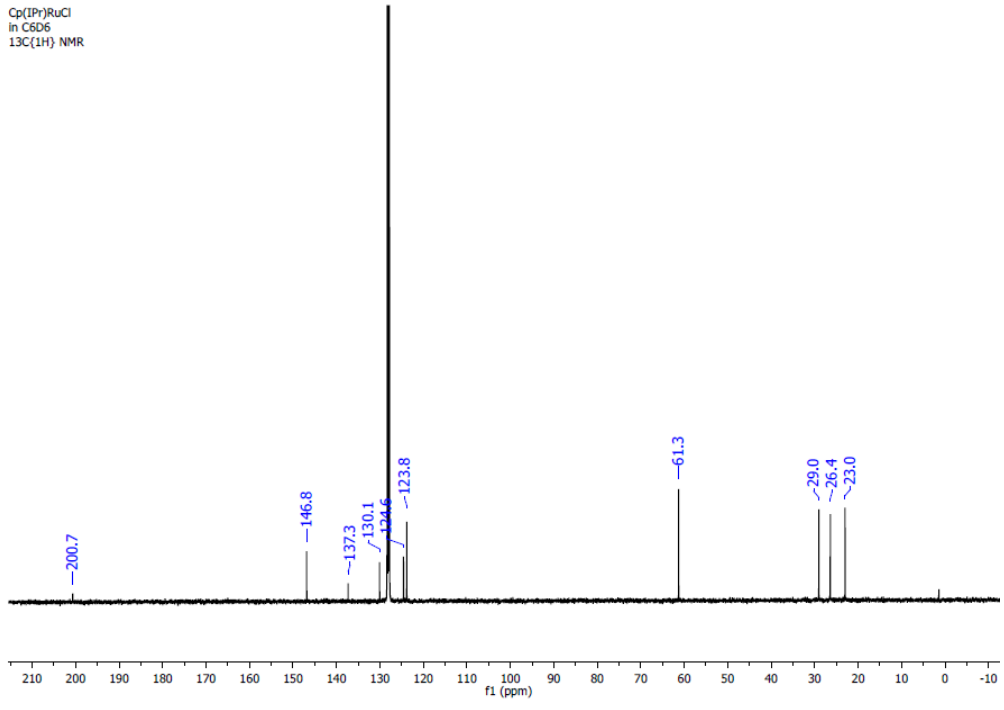

Figure VI- 4. ^{13}C NMR spectrum (100.6 MHz, 22°C, C_6D_6) of Cp(IPr)RuCl (**VI-11**).

Tris(hydride) ruthenium catalysts

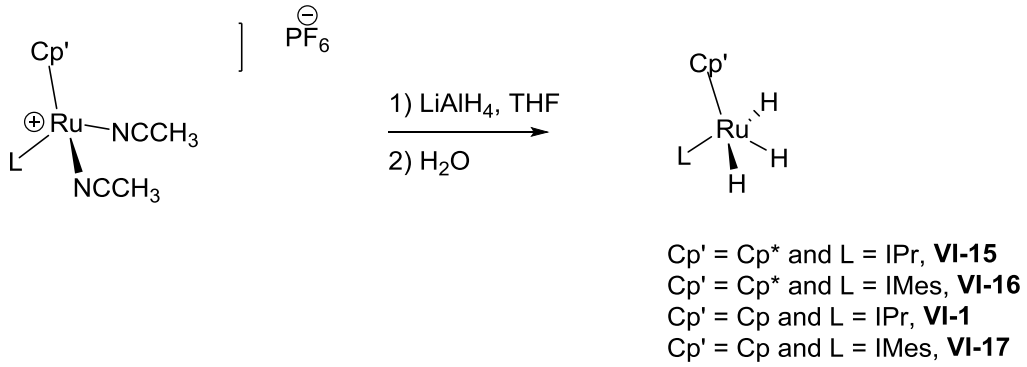

Scheme VI- 2. The synthesis of tris(hydride) ruthenium complexes

The reaction of cationic ruthenium complexes supported by NHC ligands with $LiAlH_4$ in THF, followed by hydrolysis yielded the corresponding tris(hydride) ruthenium complexes (Scheme VI-2). Complexes **VI-15-VI-17** were isolated by extraction with hexane and recrystallized from a mixture of toluene/hexane (3/2, v/v) to afford products clean by NMR spectroscopy (The NMR spectra of complex **VI-17** were shown as an example in Figures VI-5 and VI-6). The discussion of these NMR spectra will be provided in the section V-IX about H/D exchange reactions.

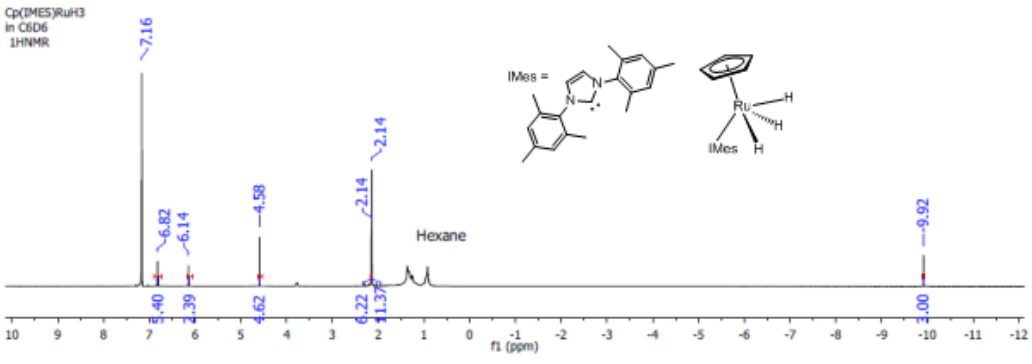

Figure VI- 5. ^1H NMR (600 MHz, C_6D_6) spectrum of $Cp(IMes)RuH_3$.

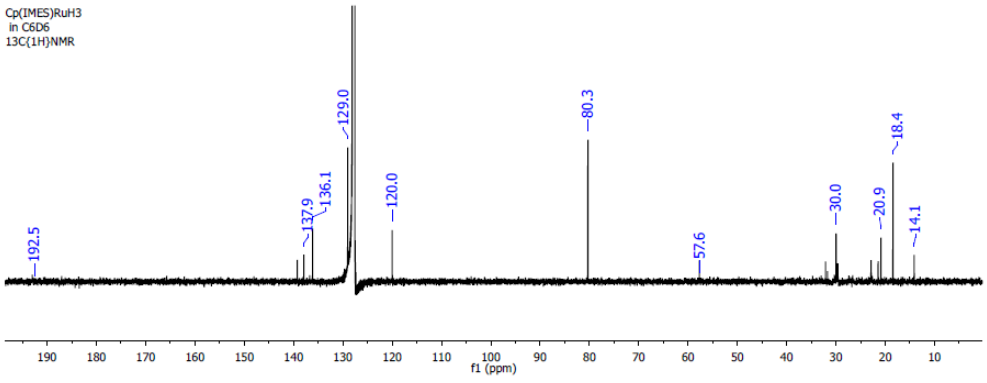

Figure VI- 6. ^{13}C NMR (600 MHz, C_6D_6) spectrum of Cp(IMes)RuH_3.

VI.2 Catalyst screening and optimization

During our studies on transfer hydrogenation of heteroaromatic compounds (Section V), we observed that subjecting 6-fluoro-2-methyl quinoline to catalytic conditions resulted in smooth defluorination of the heterocycle. This interesting discovery prompted us to screen our ruthenium catalysts in the hydrodefluorination (HDF) of various fluorinated substrates. At first, the activity of **VI-1**, **VI-2**, **VI-3**, **VI-4**, **VI-8** and that of the commercially available compound [CpRu(NCCH$_3$)$_3$][PF$_6$] (**VI-18**) was tested in the HDF of pentafluorobenzene in isopropanol (IPA) at 70 °C in the presence of a base (KO^{t}Bu or Na_2CO_3). Pentafluorobenzene was used as the standard substrate (Table VI-1) with 0.5% of catalyst, 1.5% of KO^{t}Bu in 0.7mL of IPA at 70°C; the parameters were chosen to mimic the conditions for the HDF of 6-fluoro-2-methyl quinoline. Gratifyingly, under these conditions, catalyst **VI-1** showed catalytic activity with the test substrate, affording 50% total conversion after 4 hours at 70°C (entry 2). We even observed some catalytic activity of **VI-1** at room temperature (entry 13, Table VI-1) reaching 15% conversion after 24 hours. As described above, in our other TH studies, we demonstrated that the role of a base

was only to generate the active catalyst **VI-1** from the pre-catalyst **VI-2**. Surprisingly, under the same catalytic conditions in the absence of a base, catalyst **VI-1** still showed activity (entry 1 of Table VI-1) toward the hydrodefluorination of pentafluorobenzene to yield 1,2,4 trifluorobenzene in 35% yield; however, the yield was lower than in the presence of a base (entry 2 Table VI-1). We, therefore, reckoned that basic conditions were required in this case, likely to consume the HF co-product and thus stabilize the catalyst.

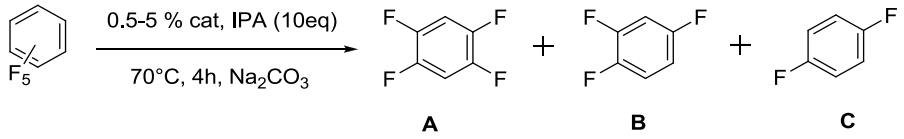

Scheme VI- 3. Screening catalysts for the HDF of pentafluorobenzene.

Table VI- 1. Screening of different catalysts for the HDF of pentafluorobenzene as standard substrate.

Entry	Catalyst	% cat	% base	Yields, % **A** / **B** / **C**
1	$Cp(IPr)RuH_3$ (**VI-1**)	0.5	0	35/0/0
2	$Cp(IPr)RuH_3$ (**VI-1**)	0.5	1.5[b]	45/<5/0
3	$Cp(IPr)RuH_3$ (**VI-1**)	0.5	120	58/16/0
4	$[Cp(IPr)Ru(pyr)_2][PF_6]$ (**VI-2**)	0.5	1.5[b]	12/0/0
5	$[Cp(IPr)Ru(NCCH_3)_2][BArF_4]$(**VI-3**)	0.5	120	18/0/0
6	$[Cp^*(IPr)Ru(NCCH_3)_2][PF_6]$ (**VI-8**)	0.5	1.5[b]	29/13/<5

7	[CpRu(pyr)$_3$][PF$_6$](**VI-4**)	5	120	<5
8	[CpRu(NCCH$_3$)$_3$][PF$_6$](**VI-18**)	5	120	0
9	[Cp(IPr)Ru(pyr)$_2$][PF$_6$] (**VI-2**)	0.5	120	16/0/0
10	IPr only as catalyst	2.0	0	0
11	no catalyst, no base	0	0	0
12	no catalyst	0	120	0
13	Cp(IPr)RuH$_3$ (**VI-1**)	0.5	1.5[c]	15/<5/0
14	[Cp(IPr)Ru(pyr)$_2$][PF$_6$] (**VI-2**)	0.5	1.5[c]	7/0/0
15	[Cp(IPr)Ru(NCCH$_3$)$_2$][BArF$_4$](**VI-3**)	0.5	1.5[b]	8/0/0
16	[CpRu(pyr)$_3$][PF$_6$](**VI-4**)	5	1.5[c]	0/0/0
17	[CpRu(NCCH$_3$)$_3$][PF$_6$](**VI-18**)	5	1.5[c]	0/0/0

[a] Standard conditions: Na_2CO_3 used as a base, 70°C, pentafluorobenzene as a substrate, 0.7 mL IPA, 24 h.[b] KO^{t}Bu was used as a base, 4h. [c] Room temperature, 24h. Yields are determined by ^{19}F NMR or ^{1}H NMR. **A** tetra-fluorobenzene, **B**, tri-fluorobenzene, **C**, di-fluorobenzene.

At this point, it was not clear how this reaction proceeded and whether HF was generated as a by-product or not. Therefore, we performed the reaction with a large quantity of Na_2CO_3 as the external base. The main reasons for using Na_2CO_3 are: 1) it is cheaper compared to KO^{t}Bu; 2) it can act as a base as well as a sacrificial reagent to absorb HF, 3) it is less soluble in IPA at low temperature, and therefore, the separation of Na_2CO_3 from the reaction mixture is simple. Under the same base loading conditions (entries 3, 5, 7, 8 and 9, Table VI-1), catalyst **VI-1** (entry 3)

showed superior catalytic activity in comparison with its cationic derivatives **VI-2** (entry 9) and **VI-3** (entry 5), as well as NHC free derivatives **VI-4** (entry 7) and **VI-18** (entry 8) and increased quantity of a base (entry 2) actually increased the yield of reactions. This fact was not surprising because in our previous studies we found out that **VI-2** was converted into the active form **VI-1** in the TH of unsaturated substrates. In entries 4, 6 and 15, complexes **VI-3** (entry 15) and **VI-8** (entry 6) isolobal with the catalyst **VI-2** (entry 4) were screened under the same conditions. Unsurprisingly, catalyst **VI-8** showed a greater activity compared to catalyst **VI-2** and **VI-3**, which could be accounted for by the stronger donating ability of the Cp* ligand compared to the Cp ligand in **VI-2** and **VI-3**. One more interesting observation could be made from entries 7, 8, 16 and 17 that the cationic complexes **VI-4** and **VI-18** showed reduced catalytic activity in comparison to the IPr supported complexes **VI-1**, **VI-1-2**, **VI-1-3**, and **VI-1-8**. This enhanced activity of NHC-substituted complexes could be attributed to the stronger σ donor ability of IPr compared to that of acetonitrile and pyridine. Entries 10 to 12 were blank experiments which confirmed that the reaction does not proceed in the absence of a catalyst and that the base or the IPr ligand themselves do not act as catalysts. Based on these preliminary trials, we concluded that neutral ruthenium tris(hydrides) are more active than their cationic precursors and that modifying the ligand environment around the ruthenium centre has a significant effect on the catalytic activity of the resulting complexes. In order to examine the impact of ligand modification, we systematically studied several neutral ruthenium complexes with different steric and electronic properties.

VI.3 Finding the optimal ruthenium hydride for catalytic HDF

With a selection of tris(hydride) ruthenium complexes in hand, we screened

their activity in the HDF of pentafluorobenzene, using the same catalyst loading (0.5%), and the amount of base (1.2 eq of Na_2CO_3) in 0.7 mL of IPA. To compare the reactivity of these new complexes, the total conversion of the standard substrate was chosen as the indicator of activity (Table VI-2). As seen from entries 1-6, Table VI-2. The comparison of the Cp/NHC and Cp/PR_3 system revealed a significant increase in HDF activity of the carbene ligated complexes compared to the phosphine ligated complexes. This phenomenon could be attributed to the stronger σ donation ability of the carbene ligand and also by the difference in the steric bulk between the NHC carbenes and phosphines. Catalyst **VI-15** showed the best catalytic activity in comparison with the other tris(hydride) ruthenium complexes. The striking activity of catalyst **VI-15** is due to the presence of both Cp* and IPr ligands, both of which have a stronger σ donation ability than Cp and IMes or phosphines, respectively. Catalyst **VI-16** is a good example of a mismatch in the steric profile of the catalyst, as Cp* and IMes are both strong donor ligands; however, catalyst **VI-16** displayed the lowest activity in the series. Variation of the catalyst load for **VI-15** showed that a decrease to 0.1 and 0.25 mol % results in a noticeable decrease in efficacy (entries 7 and 8), whereas an increase in the catalyst load up to 5% brings about only a marginal increase of activity. Therefore, we determined that complex **VI-15** at 0.5 mol % loading is the optimal choice of catalyst and conditions.

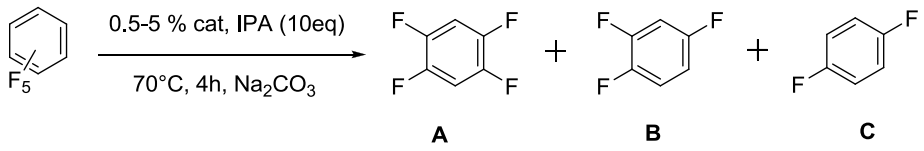

Scheme VI- 4. Screening various tris(hydride) ruthenium catalysts in the HDF of pentafluorobenzene.

Table VI- 2. Screening of different tris(hydride) ruthenium catalysts in the HDF of pentafluorobenzene.

Entry	Catalyst	% catal	% base	Yield, % **A** / **B** / **C**
1	Cp(IPr)RuH_3 (VI-**1**)	0.5	120	45/<5/0
2	Cp*(IPr)RuH_3 (VI-**15**)	0.5	120	60/21/7
3	Cp(IMes)RuH_3 (VI-**17**)	0.5	120	19/28/0
4	Cp*(IMes)RuH_3(VI-**16**)	0.5	120	23/7/0
5	Cp(Ph_3P)RuH_3(VI-**19**)	0.5	120	18/9/<5
6	Cp($^iPr_3P$)RuH_3 (**VI-20**)	0.5	120	27/11/0
7	**VI-15**	0.1	120	22/9/0
8	**VI-15**	0.25	120	34/13/<5
9	**VI-15**	1	120	64/16/<5
10	**VI-15**	2	120	52/28/9
11	**VI-15**	5	120	54/26/11

[a] Standard conditions: Na_2CO_3 used as base, 70°C, pentafluorobenzene as substrate, 0.7 mL IPA, 24

h. Yields are determined by ^{19}F NMR or ^{1}H NMR. **A**, tetra-fluorobenzene, **B**, tri-fluorobenzene, **C**, di-fluorobenzene.

In an attempt to test our complexes in the HDF catalysis with other hydrogen donors, such as silanes and boranes, the same loading 0.5 mol % of catalyst, pentafluorobenzene as a substrate, and 3 equivalents of a silane (or 5 equivalents of a borane) in 0.7 mL of benzene were applied. The results were not promising (Table VI-3), giving <30 % yield for all cases, however, they were unsurprising. As observed in our studies discussed below, reactions of silanes and Cp(IPr)RuH_3 (in 1:1 mol ratio) in benzene at 50°C yield the dihydrosilane complexes, which are stable at high temperatures, suggesting that they may be the resting state of the catalyst under these reaction conditions. In addition, our studies revealed that the addition of excess silane to the Cp(IPr)Ru fragments also produces bis-silyl complexes along with the decomposition of IPr to the imidazolium salt derivative (see below). Therefore, silanes and boranes are not good hydrogen sources for the HDF reactions using tris(hydride) ruthenium catalysts. The formation of dihydrido silyl complexes in the silane test reactions was confirmed by the appearance of the diagnostic dihydride signals at about −7 to −8 ppm in the ^{1}H NMR spectrum.

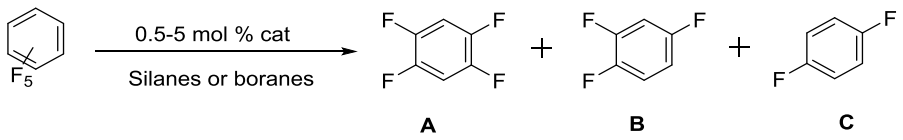

Scheme VI-5. Screening different hydrogen donors with catalyst **VI-15** for the HDF of pentafluorobenzene.

Table VI- 3. Screening different hydrogen donors for the HDF of pentafluorobenzene using catalyst **VI-15**

Entry	Hydrogen donors[a]	mol % catalysts	Yields (**A**) + (**B**) + (**C**)
1	$PhSiH_3$	0.5	14% of **A**
2	Et_3SiH	0.5	19% of **A**
3	$Me(EtO)_2SiH$	0.5	<5% of **A**
4	$MePhSiH_2$	0.5	21% of **A**
5	Me_2PhSiH	0.5	19 % of **A**
6	Me_2SiClH	0.5	<5% of **A**
7	$MeCl_2SiH$	0.5	<5% of **A**
8	Cl_3SiH	0.5	<5% of **A**
9	Et_2SiH_2	0.5	<5% of **A**
10	$Me_2(EtO)SiH$	0.5	<5% of **A**
11	$(EtO)_3SiH$	0.5	<5% of **A**
12	PMHS	0.5	<5% of **A**
13	HBpin	0.5[b]	<5% of **A**
14	HBcat	0.5[b]	15% of **A**
15	9BBN	0.5[b]	21% of **A**

[a] Standard conditions: benzene 0.8mL, 70°C, pentafluorobenzene as substrate, 24 h.

[b] 5 equivalents of boranes, 90°C, 24h. Yields are determined by ^{19}F NMR or ^{1}H NMR spectroscopy. **A**, tetra-fluorobenzene.

VI.4 Substrate scope in the HDF reaction

Using these optimized conditions, we explored the scope of the tris(hydride) ruthenium-catalyzed HDF using different fluoroarenes and fluorinated aliphatics. As shown in Table VI-4, the HDF of fluoroaromatic compounds with different degrees of fluorination (entries 1-9) was achieved in moderate to good yields. For example, using hexafluorobenzene (entry 1), the total conversion was about 90%, producing 2 products (80 % C_6F_5H + 11 % $C_6F_4H_2$) in 2h, while C_6F_5H was further hydrodefluorinated to a mixture of tetrafluoro-, trifluoro-, and difluoro-substituted products (entry 2), as observed in the preliminary catalytic runs. In entries 3 and 4, the HDF of 1,2,3,4- and 1,2,4,5-tetrafluorobenzene was also accomplished with good selectivity and yield within 6 h. For other substrates, such as 1,2,3- and 1,3,5-trifluorobenzene (entries 5 and 6), it took longer times (6 h and 12 h, respectively) to give moderate yields (32 and 28 %). For difluoro substrates (entries 5 and 6), 1,2-difluorobenzene was easier to activate than 1,4-difluorobenzene under the same reaction time (48 h). Surprisingly, the HDF of fluorobenzene, one of the hardest substrates to activate, was also observed, albeit with a higher loading of the catalyst (5 mol %), to give 16 % in 48 h.

Scheme VI- 6. **VI-15**-catalyzed HDF of fluorinated aromatic and aliphatic compounds.

Table VI- 4. **VI-15**-catalyzed HDF of fluorinated aromatic and aliphatic compounds.

Entry	Substrate	Product	Time	Yield(s)
1	C_6F_6	C_6F_5H + $C_6F_4H_2$	2h	80 / 11
2	C_6F_5H	**A** + **B** + **C**	4h	60 **A** / 21 **B** / 7 **C**
3	1,2,3,4-$C_6F_4H_2$	1,2,4-$C_6F_3H_3$	6h	63
4	1,2,4,5-$C_6F_4H_2$	1,2,4-$C_6F_3H_3$	6h	48
5	1,2,3-$C_6F_3H_3$	1,3-$C_6F_2H_4$	12h	27
6	1,3,5-$C_6F_3H_3$	1,3-$C_6F_3H_3$	24h	38
7	1,2-$C_6F_2H_4$	$C_6F_1H_5$	48h	32
8	1,4-$C_6F_2H_4$	$C_6F_1H_5$	48h	28
9	C_6FH_5	C_6H_6	48h	16[b]
10	1-fluoronaphthalene	naphthalene	96h	96
11	6-fluoro-2-methyl quinoline	quinaldine	6h	73
12	C_5F_5N	2,3,5,6-C_5F_4HN (**E**) and 2,3,4,6-C_5F_4HN (**F**)	24h[c]	56 (**E**) / 24 (**F**)
13	4-fluorophenol	phenol	7days	26
14	4-fluoro-benzaldehyde	benzyl alcohol	48 h	51
15	fluoro-cyclohexane	cyclohexane	96h	<5[b]

16	1-fluoropentane	pentane	96h	<5[b]
17	$C_6H_5CF_3$	$C_6H_5CF_2H$	48h	<5[b]
18	3-trifluoromethylanisole	3-difluoromethyl anisole	7days	10
19[e]	ethyl-trifluoro acetate	transesterification in 2h, 64%; No HDF	48h	-
20[e]	phenyl-trifluoro acetate	trans esterification in 2h, 58%; No HDF	48h	-
21	perfluoromethylcyclohexane	NR[d]	48h	-
22	perfluorohexane	NR[d]	96h	-
23[e]	ethylpentafluoropropionate	$XCF_2CF_2C(=O)X$, X=O^{i}Pr	96h	47

[a] Conditions unless specified otherwise: 70 °C, 0.5 mol % of the catalyst. [b] Conditions: 70 °C, 5 mol % of the catalyst. [c] Conditions: 0.1 mol % of the catalyst. [d] Substrate not miscible with IPA. [e] 80 °C. **A,** tetra-fluorobenzene, **B**, tri-fluorobenzene, **C**, di-fluorobenzene.

However, we found that substrates bearing other functional groups, such as OH (entry 13) and CHO (entry 14), were more challenging (requiring 7 and 2 days, respectively), which we still cannot rationalize. As expected, transfer hydrogenation of the CHO group was also observed (entry 14). The HDF of fluorinated N-heterocycles was also performed with surprising results. For examples, the HDF of pentafluoropyridine was achieved with 0.1 mol % catalyst within 24 h to give

conversion of about 80 % to two products, 2,3,5,6- (56 %) and 2,3,4,6-tetrafluoropyridine (24 %, entry 12). Moreover, 6-fluoro-2-methyl quinoline was also reduced to quinaldine (73 %) within 6 hours with a catalyst loading of 5 mol % (entry 11). For 1-fluoronaphthalene, an extended reaction time (96 h) was needed to give an excellent yield (96 %). In general, fluorinated N-heterocycles were easier to activate than other fluorinated aromatics. These results can be attributed to the basic nature of N-heterocycles in comparison to arenes. We also attempted to effect the HDF of the C(sp^3)-F bonds in the aliphatic branch of several substrates (entries 15-20). For the HDF of substrates bearing C(sp^3)-F bonds in the aliphatic fluoroalkyls, such as 1-fluoro-cyclohexane (entry 15) and 1-fluoropentane (entry 16), the reactions were quite sluggish, requiring 96 h to have less than a 5% yield, even with a higher catalyst loading of 5 mol %. For heavily fluorinated aliphatics, such as perfluoromethylcyclohexane (entry 21) and perfluorohexane (entry 22), the miscibility between IPA and the substrates was very poor resulting in the separation of the reaction mixture into three layers (IPA, the substrate and a layer of Na_2CO_3). The immiscibility of these components of the reaction mixture could account for the low degree of HDF. Interestingly, when ethyl pentafluoropropionate was used as a substrate, under the same catalytic conditions, there was 52% conversion after 48h; one of the products appeared to be a new species identified by signals at -138 ppm (m, 2F), -163 ppm (m, 2F) and -155ppm (t, *J*(F-F) = 20Hz, 1F) in the ^{19}F NMR. ^{19}F-^{19}F COSY showed that there were two CF_2 groups, which were vicinally coupled, concurrently with an additional coupling between the triplet at 141 ppm and the CF_2 signal at 157 ppm. Since ^{1}H-^{19}F HSQC spectrum did not show any correlation between these ^{19}F signals and nearby protons, we suspected that the newly formed species was not the product of hydrodefluorination, CHF_2. After 96 h the reaction

proceeds further, resulting in the formation of another species exhibiting a CF_2-CF_2 pattern in the ^{19}F NMR spectrum. A blank experiment carried out for this substrate in the absence of a Ru catalyst resulted in no reaction. We interpret these results in terms of Ru-catalyzed formation of $ROCF_2CF_2C(=O)F$, where R= Me or ^{i}Pr, followed by esterification into $ROCF_2CF_2C(=O)O^{i}Pr$. At the moment we cannot offer any explanation how this rearrangement into the fluoro-anhydride occurs.

VI.5 Kinetic studies

To elucidate the nature of this catalytic system, kinetic studies using the initial rate analysis were carried out. 1,2,3,4-Tetrafluorobenzene was chosen as the substrate because it allows for easy monitoring of the fluorine signals by ^{19}F NMR spectroscopy. Stock solutions of the catalyst **VI-15** in benzene were prepared in advance. The amount of base, Na_2CO_3, was also kept the same in the kinetic studies to mimic catalytic conditions. The reaction rates were obtained by monitoring the disappearance of 1,2,3,4-tetrafluorobenzene's ^{19}F NMR signals under pseudo-first order conditions, with the excess amount of IPA ranging from 8 to 35 equivalents. The reaction rate was found to have the first-order dependence on the concentration of substrate (Figures XII-19-26, Appendix). Plotting the reaction rate versus the equivalents of IPA revealed saturation behavior at large concentrations of the alcohol (>20 eq). A pre-equilibrium involving the substrate could account for this kinetic behaviour. As observed in our previous studies, the formation of the IPr imidazolium salt suggested that the dissociation of IPr could be involved in the mechanism of this HDF reaction.

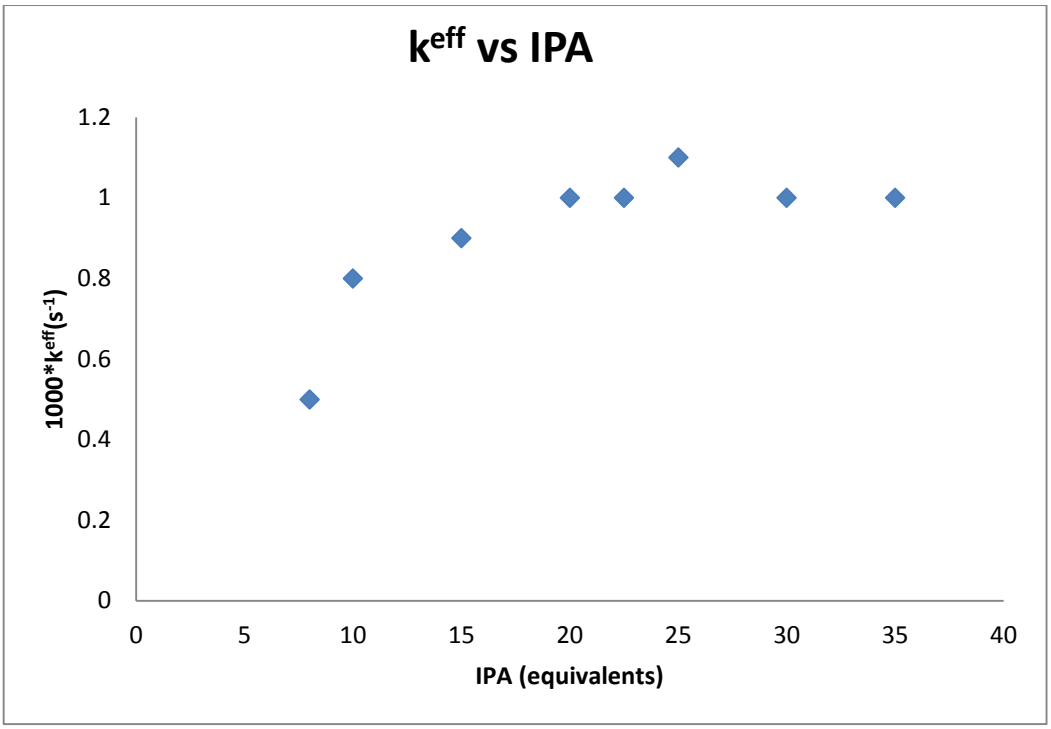

Figure VI- 7. Dependence of the effective reaction rate constant k^{eff} on the amount of isopropyl alcohol

We then evaluated the stability of IPr in IPA, and we were surprised to observe that IPr does not decompose into the imidazolium salt in IPA solutions. In fact, unreacted IPr was isolated upon removal of alcohol, and its spectrum compares well with that of freshly prepared IPr. This result is consistent with our hypothesis that IPr could reversible dissociate from the tris(hydride) species. Intrigued by this fact, we took a closer look at the hydride region of several HDF reaction mixtures and observed a second hydride species (which appeared at −8.58 ppm) compared to the tris(hydride) signal at −9.53 ppm. These observations prompted us to study the rate of the reaction with varying amounts of IPr.

To gain insight into the role of IPr in the reaction, kinetic measurements were performed under pseudo-first-order conditions (30 equivalents of IPA relative to the

substrate) with varying amounts of IPr. In contrast to what we expected, 2 equivalents of IPr relative to the catalyst hindered the rate of reaction. Subsequent experiments with 1, 3, 4, and 5 of extra equivalents of IPr further confirmed the inhibition effect (Figures XII-28-33, Appendix). As shown in Figure VI-8, the plot of $1/(1000*k^{eff})$ versus the number of added equivalents of IPr is linear, which establishes the inverse relationship between IPr and k^{eff}. This was an unexpected result because we initially believed that an additional base (in this case the free IPr) would increase the reaction rate. Based on these observations and by applying the steady-state approximation, we could derive a rate law of this reaction and propose a mechanism that agrees with the kinetic data (Scheme VI-7).

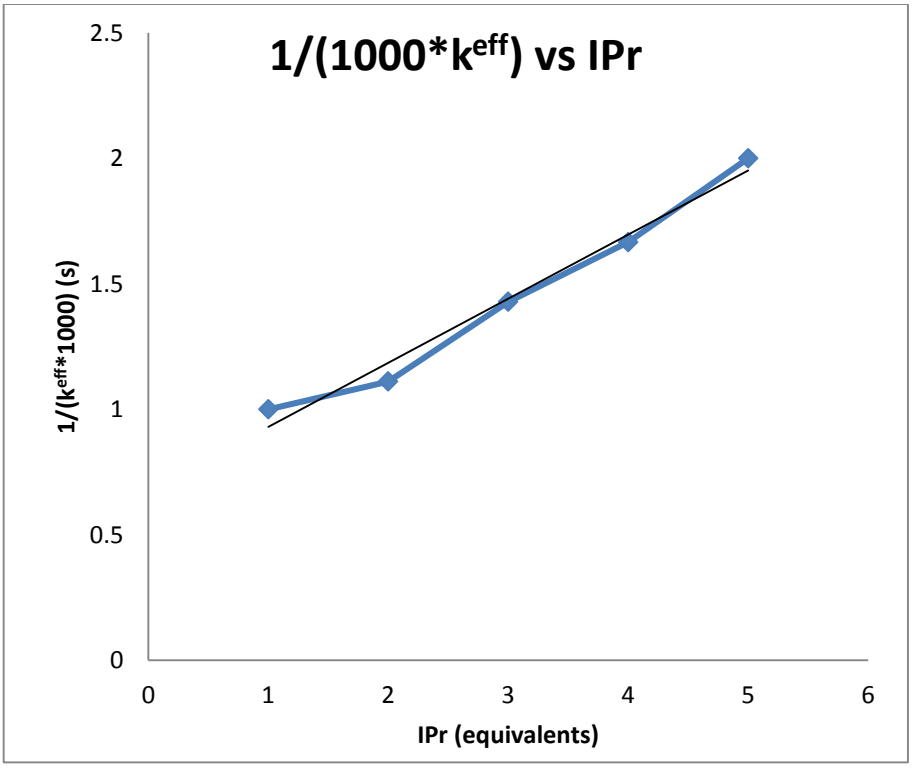

Figure VI- 8. Dependence of $1/k^{eff}$ on the amount of added IPr (in equivalents of catalyst **VI-15**)

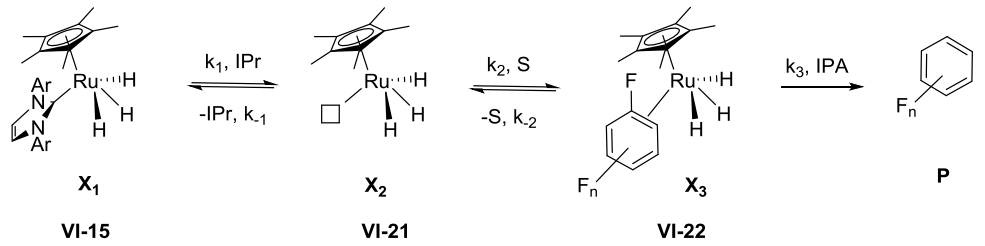

Scheme VI- 7. Suggested dissociation pathway for the **VI-15** catalyzed hydrodefluorination.

Derivation of the reaction rate law based on the steady state approximation

$$\text{rate} = -\frac{\text{d[R]}}{\text{dt}} = \text{k}_3[\text{IPA}][\text{x}_3]$$

Equation VI- 1

$$\frac{d[\text{x}_3]}{dt} = -k_{-2}[\text{x}_3] - k_3\,[\text{x}_3][IPA] + k_2[S][\text{x}_2] = 0$$

Equation VI- 2

$$\frac{d[\text{x}_2]}{dt} = k_1\,[\text{x}_1] + k_{-2}[\text{x}_3] - k_{-1}[\text{x}_2][IPr] - k_2[S][\text{x}_2] = 0$$

Equation VI- 3

Since x_2 and x_3 are reactive intermediates, we can apply the steady state approximation.

Therefore,

$\frac{d[\text{x}_3]}{dt} = 0$ and $\frac{d[\text{x}_3]}{dt} = 0$.

From eq 2 we obtain:

$$[x_3] = \frac{k_2[S][x_2]}{k_3[IPA] + k_{-2}}$$

Equation VI- 4

From eq 3 and eq 4, one derives:

$$k_1\ [\mathrm{x_1}] + k_{-2}\frac{k_2[S][x_2]}{k_3[IPA]\ + k_{-2}} - k_{-1}[\mathrm{x_2}][IPr] - k_2 = 0$$

Equation VI- 5

Rearrangement of eq 5 gives:

$$k_1\ [\mathrm{x_1}] = [\mathrm{x_2}]\frac{k_2k_3[S][IPA] + (k_{-1}k_{-2} + k_{-1}k_3[IPA])[\mathrm{IPr}]}{k_3[IPA]\ + k_{-2}}$$

Equation VI- 6

Finally, from eq 1, eq 3, and eq 6, we obtain:

$$\mathrm{rate} = -\frac{\mathrm{d[R]}}{\mathrm{dt}} = k_3[\mathrm{IPA}][\mathrm{x_3}] = k_3[\mathrm{IPA}]\frac{k_2[S][x_2]}{k_3[IPA]\ + k_{-2}}$$

$$= k_2k_3[\mathrm{IPA}][S]\frac{k_1\ [\mathrm{x_1}]}{k_2k_3[S][IPA] + (k_{-1}k_{-2} + k_{-1}k_3[IPA])[\mathrm{IPr}]}$$

$$= k^{eff}[\mathrm{x_1}][S]$$

where

$$k^{eff} = \frac{k_1\ k_2k_3[\mathrm{IPA}]}{k_2k_3[S][IPA] + (k_{-1}k_{-2} + k_{-1}k_3[IPA])[\mathrm{IPr}]}$$

Given the fact that Cp*(IPr)RuH_3 is the resting state, k_{-1} is large. Then, at large concentration of IPA, we obtain the saturation behavior in IPA observed in

Figure VI-7 and the inverse relationship between k^{eff} and IPr (as in Figure V-8).

$$k^{eff} \sim \frac{k_1\ k_2 \mathrm{k}_3}{k_{-1} k_3 [\mathrm{IPr}]}$$

Crossover experiments:

To verify our hypothesis about the dissociation of carbene, we conducted two further experiments. The first one was designed to test the possibility of NHC dissociation from Cp*(IPr)RuH_3. To this end, we prepared an NMR sample, which contained Cp*(IPr)RuH_3 in the protio-benzene to avoid the H/D exchange process (Figure VI-9), and heated this sample at 90°C for 8h. Analyzing the ^{1}H-NMR spectrum of this sample (Figure VI-10), we obtained the direct evidence for the dissociation of IPr. In the IPr backbone region of the spectrum, we observed two proton signals, which were assigned to the free IPr and coordinated IPr. Similarly, signals in the methylene region were assigned to the free and coordinated IPr species. Carefully looking at the hydride region, we also noticed a new hydride species at -12.53 ppm, which was likely generated from the decomposition of Cp*(IPr)RuH_3. As observed in the ^{1}H-NMR spectrum of Cp*(IPr)RuH_3 in C_6D_6 after 2h at 50°C (Figure VI- 9), we found that the singlet peak (-9.55 pm) of hydride signals was completely replaced by a multiplet (-9.58 ppm) of deuteride labelled Cp*(IPr)$RuH_{3-x}D_x$. This incidence indicated that it would be problematic to interpret the results of the crossover experiments if they were carried out in C_6D_6 solvent.

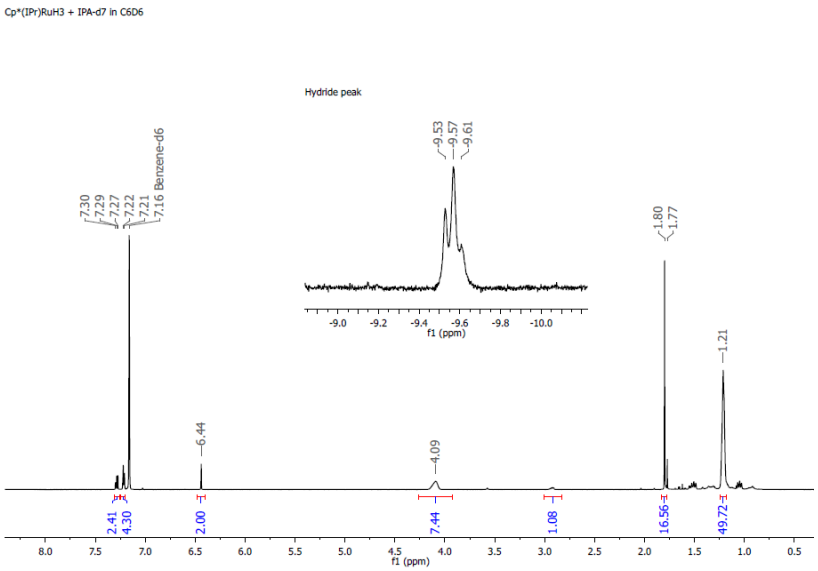

Figure VI- 10. ^{1}H NMR spectrum of D-labelled Cp*(IPr)Ru(H_x/D_{3-x})

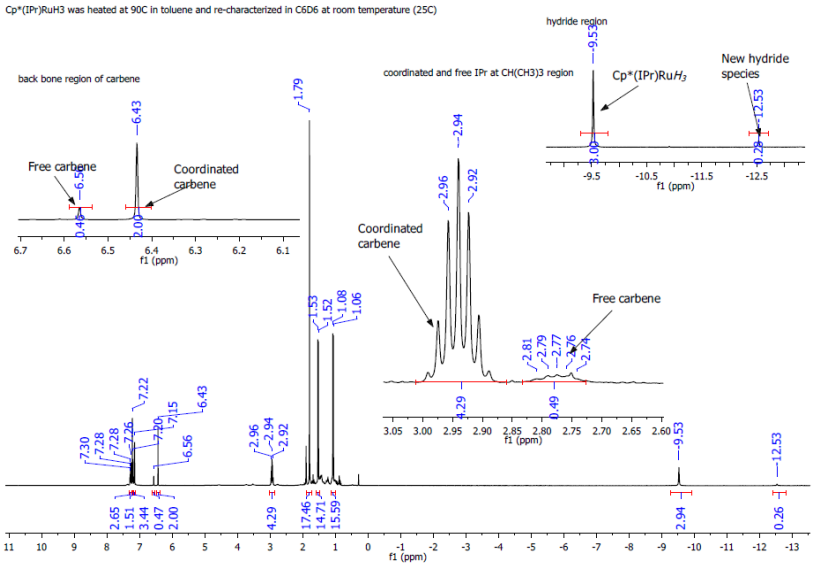

Figure VI- 11. ^{1}H-NMR spectrum for Cp*(IPr)RuH_3 at 23 °C after being heated at 90 °C for 8h in protio-benzene and then redissolved in C_6D_6.

The second experiment was designed to examine whether there is a re-association of NHC to the previous new hydride species. Therefore, we carried out

an NMR experiment, in which IMes and Cp*(IPr)RuH_3 were mixed in an NMR tube and heated to 70°C for 8h (Figure VI-11). Gratifyingly, we saw the formation of the exchange product Cp*(IMes)RuH_3, and the absence of the addition product Cp*(IPr)(Mes)Ru, which might be indicative of a H_2 dissociation pathway. This experiment supports our suggestion of the dissociation of NHC.

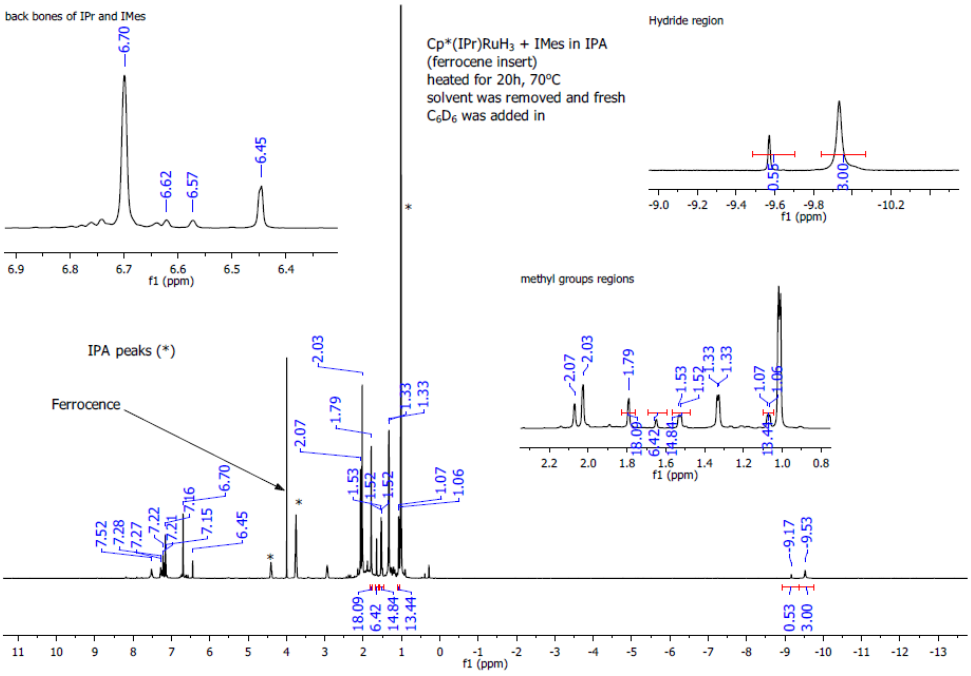

Figure VI- 12. ^{1}H-NMR spectrum for Cp*(IPr)RuH_3 + IMes in IPA after heated at 70°C for 20h, IPA was removed and fresh C_6D_6 was added.

On the basis of these stoichiometric reactions, kinetic studies, and crossover experiments, we proposed the mechanism below (Figure VI-12). Upon heating, the dissociation of IPr from **VI-15** occurs to yield the unsaturated species **VI-21**, which then reversibly coordinates the fluorinated substrate by η^2(C=C) coordination. A hydride transfer and the displacement of the fluorine take place to facilitate the

formation of the reduced substrate. With the aid of IPA and its solvation abilities, the fluoride is abstracted from the intermediate **VI-24** and dissolves in the solution mixture in the form of very stable HF (or as NaF). Later steps are typical with the formation of alkoxide complex (**VI-25**).

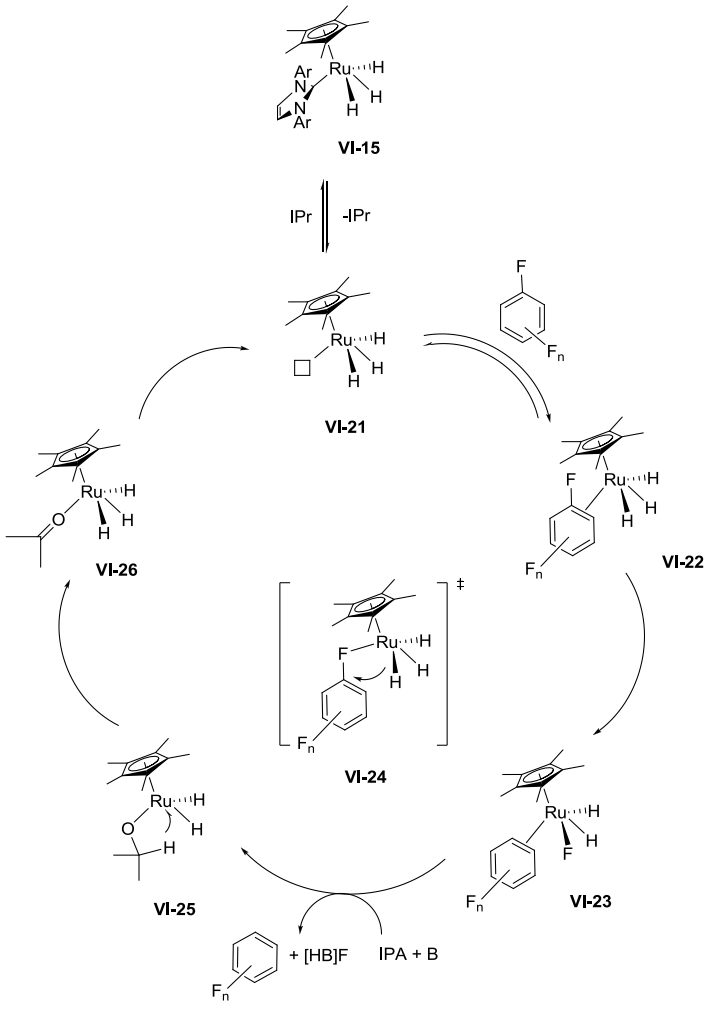

Figure VI- 13. Proposed mechanism for the VI-15-catalyzed HDF.

VII. Silyl hydride ruthenium complexes

The Nikonov group has a long-standing interest in catalytic hydrosilylation of unsaturated molecules, such as nitriles, pyridines, N-heterocycles, and olefins.[108, 124-126, 159] Previous mechanistic studies of half-sandwich phosphine complexes of ruthenium suggested that the catalytic hydrosilylation of these above substrates correlates strongly with the formation of nonclassical silane complexes.[85, 89, 117, 122, 314, 356] Due to the fact that our previous catalysts bearing the Cp(^{i}Pr$_3$P)Ru fragments showed good activity toward the hydrosilylation of nitriles and N-heterocycles, and based on the isolobal relationship between phosphines and NHC carbenes, we elected to investigate the new hydride silyl ruthenium complexes containing the NHC and Cp' ligands. We also attempted to illustrate the effect of the strong donor ability of NHC to support inter ligand hypervalent interaction (IHI) between the silyl and hydride ligands (Scheme VII-1).

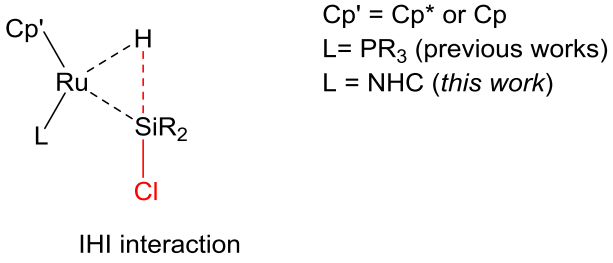

Scheme VII- 1. Our IHI studies on silyl hydride ruthenium complexes

VII.1 Silyl hydride ruthenium complexes synthesis

Reactions of Cp(IPr)RuH$_3$ (**VII-1**) with silanes in toluene at 50°C for 12 h yield complexes Cp(IPr)RuH$_2$SiR$_3$ [**VII-2**, R$_3$ = Cl$_3$ (**a**), Cl$_2$Me (**b**), ClMe$_2$ (**c**), H$_2$Ph

(**d**), HMePh (**e**) Me_2Ph (**f**)]. The reaction is completed within 2h if the reaction mixture is heated to 50°C. Meanwhile, reactions of the analogous trihydride compounds $Cp(R_3P)RuH_3$ with silanes took place at a higher temperature (>70°C), took longer times and usually generated many unwanted decomposition products.[88] In the special case, when the most acidic silane ($HSiCl_3$) was used, we observed only $Cp(IPr)RuH_2SiCl_3$ as the product of a complete Si-H addition. In contrast, in our previous studies, using a similar starting material $Cp^*(PR_3)RuH_3$ (**VII-3**), we saw the formation of different products, such as $Cp^*(PR_3)Ru(Cl)(SiCl_3)(H)$ (**VII-4**) and $Cp^*(Pri_3P)RuH_2(SiHCl_2)$ (**VII-5**) but not $Cp^*(Pri_3P)RuH_2(SiCl_3)$ (**VII-6**). The new silyl hydride ruthenium complexes **VII-2** were characterized by NMR, and IR spectroscopy, elemental analysis, and X-ray studies.

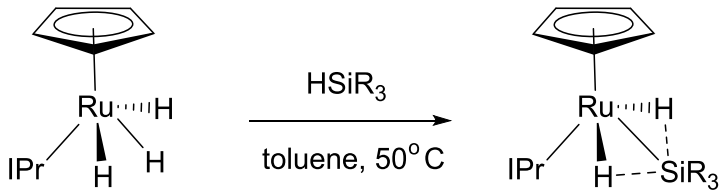

VII-1 **VII-2**

R_3 = Cl_3 (Cl_2Me) ($ClMe_2$) (H_2Ph) (HMePh) (Me_2Ph)

a **b** **c** **d** **e** **f**

Scheme VII- 2. Preparation of dihydride silyl complexes.

NMR studies

Hydride signals of these silyl ruthenium complexes appeared in the range −9.59 to −11.25 ppm in the NMR spectrum, which are typical values. Interestingly, complex $Cp(IPr)RuH_2SiHMePh$ (**VII-2e**) showed two different signals at −10.92 and −11.63 ppm due to diastereotopic hydrides formed because of the chiral silicon

centre. And indeed, only one silicon signal was observed in ^{29}Si-NMR. The ^{29}Si–^{1}H coupling constants were collected from ^{29}Si–^{1}H HSQC for these silyl ruthenium complexes, giving the values of 12.0–13.6 Hz, which are similar to what was observed in the related compounds Cp′(Pri$_3$P)RuH$_2$SiR$_3$.

IR studies

In the IR spectrum, the RuH hydrides showed characteristic bands at 1985–2032 cm^{-1}, which are known for the metal-hydride bond stretch. The substituents on the silicon centre also have an impact on IR and NMR signals, as complex, Cp(IPr)RuH$_2$SiCl$_3$ (**VII-2a**) bearing three chlorine groups exhibits a more red-shifted stretch in the IR and a more low-field shift for the NMR signals than what are observed for Cp(IPr)RuH$_2$SiMe$_2$Ph (**VII-2f**).

VII.2 X-ray studies of silyl hydride ruthenium complexes

Previously, our group reported the incidence of Interligand Hypervalent Interactions (IHI) between the silyl and hydride ligands in several new families of compounds,[89, 115, 118, 121, 159, 314, 357] which exhibit Si-H bonding features different from what was normally observed in silane σ-complexes. In our recent reports, we discussed X-ray studies of several complexes Cp′LRuH$_2$SiR$_3$ (Cp′ = cyclopentadienyl ligand or pentamethylcyclopentadienyl ligand; L = a two-electron donor, phosphine ligand, PR$_3$), which were rationalized by the presence of an inter ligand interaction between the silyl ligand and the *trans* hydride on the metal centre. These interactions were also indirectly supported by the appearance of the upfield shift of the central hydride ^{1}H NMR signal relative to the original hydride of

$Cp'LRuH_3$. In fact, as stated in recent reviews about the Si-H interactions,[103, 358] complexes bearing IHI interactions should be classified in a subclass of complexes with multiple inter ligand Si–H interactions, which can be also described as complexes of silicate ligands (Scheme VII-3). The analysis of X-ray structures of ruthenium compounds $Cp'LRuH_2SiR_3$ (L= PR_3) showed several characteristic structural features: (i) the electron-withdrawing groups at silicon (i.e. chlorides) are usually located *trans* to the hydride ligands, (ii) the Ru-silyl bond lengths are shorter than expected; and (iii) the Si–Cl bonds are longer than expected which can be explained by a donation of the M-H bond to the σ*(Si-Cl) antibonding orbital.

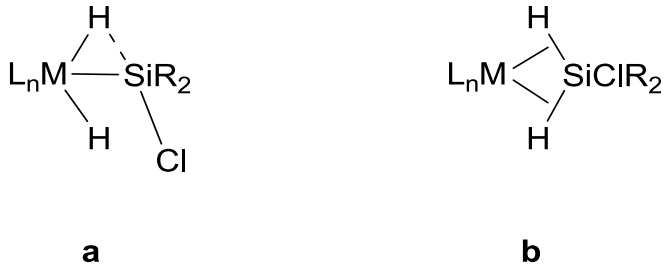

Scheme VII- 3. The description of inter ligand interactions in chlorosilyl complexes (a) in terms of IHI and (b) in terms of $[SiH_2ClR_2]^-$ silicate coordination.

Combined X-ray studies and DFT calculations of ruthenium compounds with different phosphine ligands, cyclopentadienyl groups, and substituents at silicon revealed that: (i) the presence of electron-withdrawing groups at silicon, such as chlorides, enhances the Si···H interactions through their ability to stabilize the hypervalent silicon centre; (ii) stronger donating properties of phosphine ligands actually increase the basicity of the hydrides, and thus indirectly intensify the strength of Si–H interactions, and (iii), the favourable *trans* orientation of the

chloride group relative to the hydride ligand is inhibited by the presence of substituents in the cyclopentadienyl ligand due to its bulkiness, such as in Cp* complexes, resulting in the weakening of the Si-H interaction.

The interrelationship between these ligands triggered our curiosity about the outcome of the displacement of phosphine in Cp′LRuH$_2$SiR$_3$ by a stronger σ donating NHC on the Si-H interaction. With these ideas in mind, we prepared systematically a series of complexes **VII-2** with different silyl moieties. These new complexes were isolated successfully, and studied by X-ray diffraction analysis. The molecular structure of complex **VII-2b** is shown in Fig. VII-1 as an example.

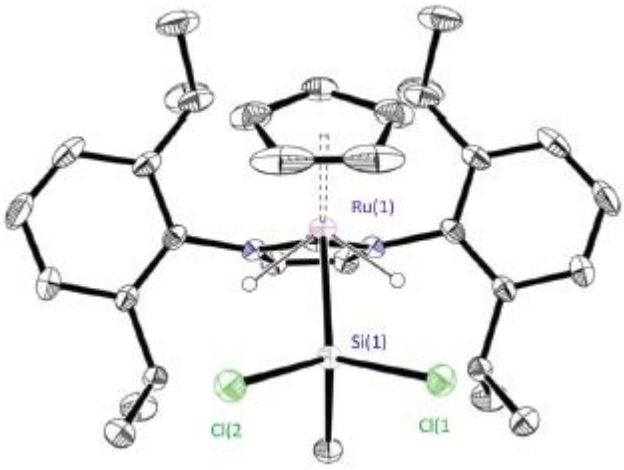

Figure VII- 1. The molecular structure of complex Cp(IPr)RuH$_2$SiMeCl$_2$ (**VII-2b**). Hydrogen atoms, except the hydrides on ruthenium atom, are omitted for clarity.

The similarity of these silyl hydride complexes suggested that we could present them in a table consisting of characteristic bond lengths and angles. Therefore, selected molecular parameters for these complexes **VII-2a–f** are given in Table VII-1.

Table VII- 1. Selected molecular parameters (distances in Å, angles in°) for complexes **VII-2a-f**

	VII-2a[a]	**-b**	**-c**	**-d** [c]	**-e**	**-f**[d]
Ru-Si	2.250(1)	2.2951(8)	2.315(1)	2.3276(14)	2.3355(5)	2.354(3)
Si-Cl(trans)	2.100(2)[b]	2.1350(7)	2.174(1)	-	-	-
Ru-H1	1.47(4)	1.51(3)	1.53(3)	1.39(4)	1.63	-
Ru-H2	1.50(6)	1.51(3)	1.55(3)	1.46(5)	1.52	-
Ru-C(IPr)	2.055(4)	2.065(3)	2.043(3)	2.026(4)	2.027(2)	2.053(9)
Si···H	2.02(4) 2.12(6)	2.03(3)	2.03(3) 2.05(4)	1.76(4) 1.96(5)	2.12 2.00	-
H1-Ru-H2	110(2)	106.5(9)	106.9(18)	86(2)	105	-
RuH-Si-X(*trans*)	157.2(12) 152.4(17)	152.2(7) 152.2(7)	151.3(10)	144(2)	-	-

[a] The structure contains two independent molecules, mean values of geometric parameters are given for them; [b] Average of two bonds (2.104(2) and 2.098(2) Å). The third chloride atom is *trans* to the Cp group and gets distance from the Si atom by 2.072(2) Å; [c] X=H; [d] The hydride atoms were placed at calculated positions but

not refined (see Appendix for details).

Similar to what has been observed in related complexes $Cp'(R_3P)RuH_2SiMe_{3-n}Cl_n$ (n = 1–3), the orientation of the chloro group in complexes **VII-2a–f** is *trans* to the Ru-bound hydride. The (Ru)H···Si–Cl angles for two independent molecules of the trichloride **VII-2a** are 152(2)° and 157(1)° and, unsurprisingly, the (Ru)H···Si–Cl angle of the dichloride **VII-2b** very close (152.2(7)°). And finally, in the monochloride **VII-2c** the open (Ru)H···Si–Cl bond angle is 151.3(10)°. The presence of more electron-donating groups at silicon atoms induces an increase of the Ru–Si bond lengths from 2.250(1) Å (average for two independent molecules) in **VII-2a** to 2.354(3) Å in **VII-2f**. Noteworthy, the lengths of two Si–Cl bonds in **VII-2a** that are *trans* to hydrides are slightly longer than the Si–Cl bond that lies *trans* to the Cp ligand: 2.104(2) and 2.098(2) Å vs 2.072(2) Å. This incidence is consistent with the proposal that the former two Si–Cl bonds are engaged in hypervalent interactions with the hydride ligand. The RuH···Si contacts in most complexes of the type $Cp(IPr)RuH_2SiR_3$ (**VII-2**) complexes are close to 2 Å and the H–Ru–H bond angles fall in the range 105(1)–110(2)°, except for **VII-2d**, which has a significantly smaller H–Ru–H bond angle of 86(2)° leading to much shorter RuH···Si distances, 1.76(4) and 1.96(5)°. We attribute this discrepancy to the presence of a much smaller SiH_2Ph group in **VII-2d** that has a better ability to stabilize a formally six-coordinate silicate centre. The successful isolation of the monochloride complex **VII-2c** is very important, as it allows for a systematic comparison with analogous phosphine complexes $Cp(Pr^i_3P)RuH_2SiMe_2Cl$ and $Cp^*(Pr^i_3P)RuH_2SiMe_2Cl$ previously studied by X-ray analyses (Table VII-2).

Table VII- 2. Selected molecular parameters in complex **VII-2c** and its phosphine analogs.

Parameter	Cp/IPr	Cp/Pr^i_3P	Cp*/ Pr^i_3P
Ru-Si	2.315(1)	2.3277(7)	2.332(1)
Si-Cl	2.174(1)	2.153(2) [a]	2.126(7)

[a] This Si-Cl distance can be compromised by the rotation disorder of the $SiMe_2Cl$ ligand. In the related Cp/Pr^i_2PhP complex, the Si-Cl bond is 2.164(1) Å.

The shorter Ru–Si and longer Si–Cl bond lengths of Cp/IPr and Cp/Pr^i_3P complexes than are found in the Cp*/Pr^i_3P complexes are consistent with stronger Si–H interactions in the Cp derivatives. This may be explained by the presence of a less bulky Cp ligand, which allows for the favorable *trans* disposition of the hydride and chloride groups in these complexes.

The comparison of complexes Cp(Pr^i_3P)RuH_2SiMe_2Cl and Cp(IPr)RuH_2SiMe_2Cl (**VII-2c**) reveals the decrease of the Ru–Si distance from 2.3377(7) Å to 2.315(1) Å, respectively. This shortening of the Ru-Si bond and the concurrent lengthening of the Si–Cl bond from 2.153(2) Å to 2.174(1) Å suggests a better donor ability of the IPr ligand, which results in stronger H···Si interactions. The Si–Cl bond length of Cp(IPr) complex **VII-2c** falls in the range observed for other hydrido chlorosilyl complexes with Interligand Hypervalent Interactions. These structural trends are in accord with the fact that in both the silicate complexes Cp(L)RuH_2SiMe_2Cl and in compounds with IHI, the silicon centre is hypervalent.

VIII. Ruthenium σ-complexes

Over the last three decades, complexation of the Si-H bond of silanes to metal centers has remained a hot research topic.[87, 103, 312, 359] This interest is driven primarily by the understanding that transition metal silane complexes are important intermediates in such important transformations as metal-catalyzed hydrosilylation, alcoholysis, and coupling reactions.[108, 124-126] However, the direct involvement of these σ-species into catalytic reactions has been documented only in a few cases[108, 322, 360] because of their instability and difficult isolation. The sub-class of cationic silane σ-complexes is particularly challenging to synthesize and isolate due to the very high electrophilicity of the silylium centre. Not surprisingly, there have been only two examples which were fully characterized by X-ray studies.[321-322] Recently, by adding silanes to cationic complexes $[Cp(PR_3)Ru(NCCH_3)_2]^+$ (**VIII-1**) Nikonov's group succeeded in the preparation of a series of surprisingly stable cationic complexes $[Cp(^iPr_3P)Ru(\eta^2\text{-}HSiR_3)(NCCH_3)]^+$ (**VIII-2**), which displayed very interesting catalytic activities in hydrosilylation reactions.[108, 124-125] On the other hand, our group was also interested in the study of related neutral silane complexes $Cp'(^iPr_3P)Ru(\eta^2\text{-}HSiR_3)Cl$ (Cp′ = Cp (**VIII-3**) or Cp* (**VIII-4**)), which display additional inter ligand interactions between the ruthenium-bound chloride and the silicon centre[85, 361]. Given the isolobal relationship between phosphines and NHC carbenes, we were curious about the feasibility of preparing NHC-supported analogs of complexes **VIII-2** and **VIII-3** and their potential reactivity in catalysis.

Herein we describe the preparation and X-ray studies of some new neutral and cationic silane σ-complexes supported by the IPr carbene (IPr = 1,3-bis(2,6-diisopropylphenyl)imidazol-2-ylidene), namely the compounds $Cp(IPr)Ru(\eta^2\text{-}$

HSiR$_3$)Cl (**VIII-5**) and [Cp(IPr)Ru(η^2-HSiR$_3$)(NCCH$_3$)]$^+$(**VIII-6**).

VIII.1 Neutral and cationic ruthenium σ-complexes

Neutral sigma ruthenium complexes

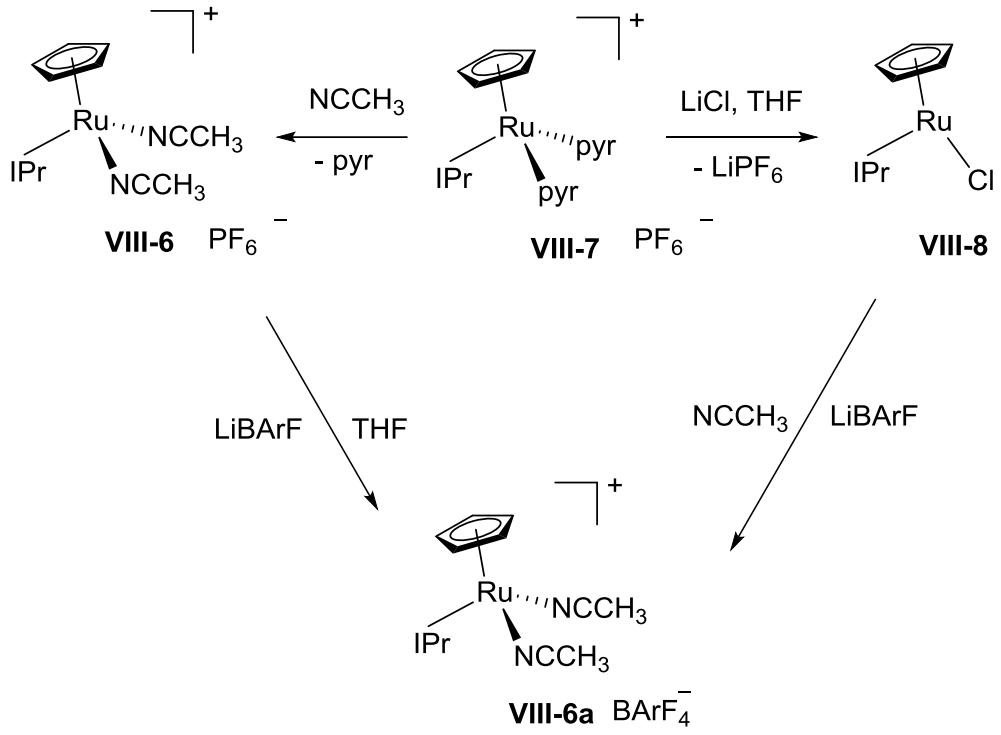

Scheme VIII- 1. The synthesis of cationic precursor **VIII-6a** and neutral 16e complex **VIII-8**

The preparation of the cationic carbene complex [Cp(IPr)Ru(pyr)$_2$][PF$_6$] (**VIII-7**) (pyr =pyridine) was described in the previous section VII. This parent complex is a very convenient precursor for the synthesis of [Cp(IPr)Ru(NCCH$_3$)$_2$][PF$_6$] (**VIII-6**) by a ligand exchange reaction and for the synthesis of the unsaturated 16e complex Cp(IPr)RuCl (**VIII-8**) by the addition of chloride (Scheme VIII-1). The latter complex (**VIII-8**) was isolated with a good yield (80%) after recrystallization from hexane as a deep blue crystalline material, and its structure was determined by NMR spectroscopy, EA, and X-ray analysis.

Similar procedures to generate 16e species Cp′LRuCl (L = phosphine or carbene), had been previously reported by Tilley et al.[107, 362-363] and Nolan et al.[355] Complex $[Cp(IPr)Ru(NCCH_3)_2][BArF_4]$ (**VIII-6a**) was prepared by two pathways: 1) the counteranion exchange between complex **VIII-6** and $LiBArF_4$ ($BArF_4$ = tetrakis(pentafluorophenyl)borate) in THF; and 2) by treatment of complex **VIII-8** with $LiBArF_4$ in an excess amount of acetonitrile. Both methods can cleanly generate the related complex $[Cp(IPr)Ru(NCCH_3)_2][BArF_4]$ (**VIII-6a**), characterized by NMR and IR spectroscopies.

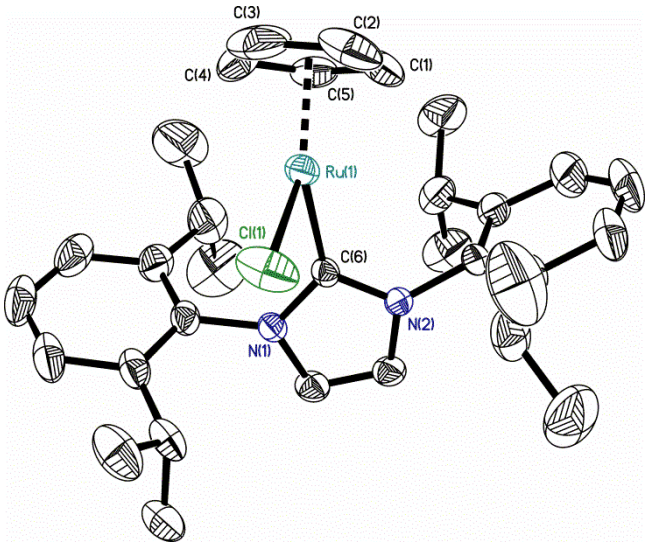

Figure VIII- 1. The molecular structure of compound **VIII-8**. Hydrogen atoms are omitted for clarity.

The X-ray crystal structure compound **VIII-8** is presented in Figure **VIII-1**. The Cp ligand occupies three coordination sites, which agrees with the L2X nature of this ligand, while the chlorine and IPr ligands occupy one coordination site each. The Ru-C(IPr) distance of 2.068(2) Å falls in the range of distances 2.068-2.074 Å

for related Cp*(NHC)RuCl complexes bearing *N*-aryl substituted NHC ligands,[355] but is noticeably shortened compared to the Ru-C(IAd) distance of 2.153 Å of a derivative bearing bulkier adamantyl groups on the nitrogen atoms of NHC. The reduced steric demand of the Cp ligand in complex **VIII-8** in comparison with the Cp* ring in complex Cp*(IPr)RuCl results in a much shorter Ru-Cl bond (2.3346(8) Å) in **VIII-8** than in Cp*(IPr)RuCl (2.524 Å).[355] While the Cp(cent)-Ru-C(IPr) angle of 136.5° falls in the range 129.3-142.7° found for the Cp* congeners, the Cp(cent)-Ru-Cl angle of 135.8° is surprisingly larger than the corresponding values in Cp* complexes (125.5-132.8°).

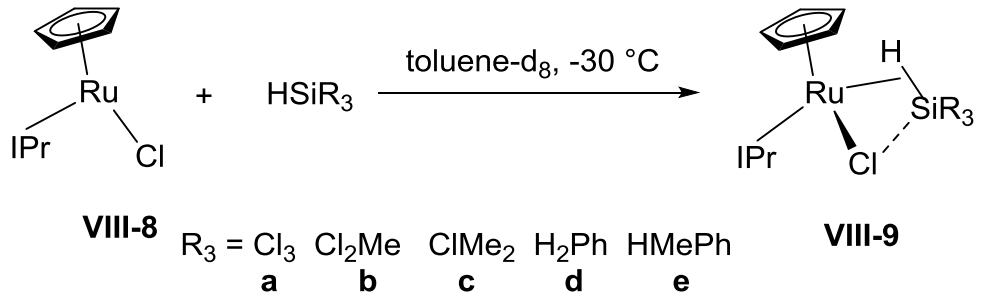

Scheme VIII- 2. The preparation of **VIII-9a-e** neutral silane σ- complexes

Neutral sigma ruthenium complexes

The addition of hydrosilanes to the blue solution of complex VIII-**8** in toluene at low temperatures (-5 to -40ºC) results in the formation of the corresponding silane σ-complexes **VIII-9a-f**, which normally show the yellow color of the final mixture. Single crystals of **VIII-9a-f** were grown by slow vapor diffusion of hexane into a saturated solution of toluene (Scheme VIII-2). Compounds **VIII-9** were characterized by NMR, and IR spectroscopy, and elemental analyses; and the

molecular structures of **VIII-9b** and **9d** were also confirmed by X-ray studies. Since the coupling constant *J*(H-Si) is the key parameter for the structural assignment of silane σ-complexes, we carried out special NMR experiments (INEPT) to measure these values of compounds **VIII-9**. The values of *J*(H-Si) of complexes **VIII-9** are summarized in Table VIII-1, which also provides a comparison with related phosphine-supported complexes.

Table VIII- 1. H-Si coupling constants *J*(H-Si) (Hz) in complexes **VIII-9a-e** and related phosphine complexes ($Cp(^iPr_3P)Ru(\eta^2\text{-}HSiR_3)Cl$) **VIII-10a-e** and ($Cp^*(^iPr_3P)Ru(\eta^2\text{-}HSiR_3)Cl$) **VIII-11a-e**.

	$SiCl_3$ (**a**)	$SiMeCl_2$ (**b**)	$SiMe_2Cl$ (**c**)	SiH_2Ph (**d**)	SiHMePh (**e**)
VIII-9	63.8	56.4	43.6	43.2	40.5
VIII-10	33	45	50	39	46
VIII-11	<6	19	34	-	32

All H-Si coupling constants of **VIII-9a-e** are bigger than 40 Hz, which indicates the formation of silane σ-complexes (Table VIII-1). One can see that the magnitude of *J*(H-Si) in series **VIII-9** decreases from the more chlorinated

compound **VIII-9a** (64.4 Hz) to the chlorine-free compounds **VIII-9d** and **VIII-9e** (43.2 and 40.5 Hz). This trend is different from what is observed in the phosphine-supported complexes **VIII-10**. In fact, previous studies of complexes with nonclassical H-Si interactions showed both increasing and decreasing trends in *J*(H-Si) coupling constants. The decreasing trend is normally observed for silanes having more electron-withdrawing groups at the silicon atom (e.g. complexes **VIII-10a-c** and **VIII 11a-c**, Table VIII-1), which reflects the increasing back-donation to the σ*(Si-H) orbital from the metal[87] due to the increased electronegativity of substituents at silicon. In this regard, complexes **VIII-9** showed an unusual trend of increasing *J*(H-Si). However, due to the fact that the magnitude of *J*(H-Si) is dictated by the combination of metal-to-Si-H back-donation and the change of hybridization of the silicon centre, the increased values of Si-H coupling in complexes **VIII-9a-c** can be explained by the much increased 3s character of silicon in the residual Si-H bond.

In their previous studies,[89] the Nikonov group observed simultaneous Si···H and Si···Cl interactions of complexes Cp'(R_3P)Ru(η^2-$HSiR_3$)Cl (Cp' = Cp or Cp*). We became curious whether the replacement of phosphine by its isolobal NHC ligand would show any significant change in the extent of these inter ligand interactions in complexes **VIII-9a-e** and their relation to the unusual trend in the hydrogen-silicon coupling constants. For that purpose, the X-ray structures of complexes **VIII-9b** and -**9d** were examined. The molecular structure of **VIII9b** is presented in **Figure VIII-2**.

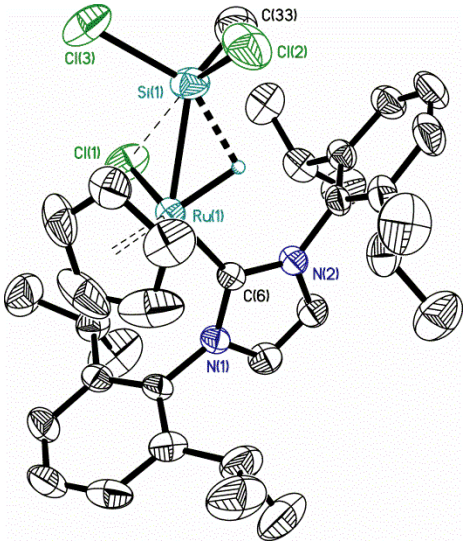

Figure VIII- 2. The molecular structure of compound **VIII-9b**. Hydrogen atoms, except the hydride on Ru, are omitted for clarity.

The Ru-Cl bond length of Cp(IPr)Ru(η^2-HSiMeCl$_2$)Cl) (**VIII-9b**) is very short as compared to the sum of van der Waals radii of Si and Cl (3.85Å), and in fact, this bond distance is the shortest in the family of related complexes Cp'(L)Ru((η^2-HSiR$_3$)Cl (L = phosphine or carbene) (range 2.873−3.111(2) Å).[85, 89] Because of the additional inter ligand interaction RuCl···Si and because of the hypervalent nature of the silicon centre, the geometry at silicon in this complex is better described as a trigonal bipyramid, in which one of the Si bound-chlorides occupies the equatorial position, while the other is apical and *trans* to the Ru-bound chloride, with the Cl-Si···Cl angle being 164.9°. Interestingly, the *trans* chloride Cl2 displays an elongated Si-Cl bond length (2.1199(17) Å) compared to the Si-Cl(eq) distance (2.1134(16) Å), which reveals the involvement of the Cl(*trans*)-Si···ClRu unit in the hypervalent interaction. Complex **VIII-9b** can be compared to the phosphine derivative Cp(^{i}Pr$_3$P)Ru(η^2-HSiMeCl$_2$)Cl) (**VIII-10b**) which features the same silyl groupSiMeCl$_2$. The Si-Cl(*trans*) distance of **VIII-9b** (2.1199(17) Å) is slightly

longer than that of **VIII-10b** (2.1104(9) Å), whereas the Ru-Cl bond is shorter, 2.3984(9) and 2.4199(6) Å, respectively, which correlates with the shorter Cl···Si inter ligand distance of 2.851 Å in **VIII-9b** (*cf.* 2.8965(9) Å in **VIII-10b**). Since the Ru-Si distances in both **VIII-9b** and **VIII-10b** are the same within three sigmas, 2.3587(11) and 2.3564(7) Å, respectively, we can conclude that both the phosphine P^iPr_3 and the carbene IPr have a similar impact on the inter ligand interactions, but stronger silane/chloride inter ligand interactions in the latter lead to slightly in the latter stage of Si-H addition to the metal. Supporting this conclusion, albeit less reliably established by X-ray, is the shorter Si-H distance in **VIII-9b** (1.750 Å) than in **VIII-10b** (1.855 Å), which correlates with the increase of *J*(H-Si) in these compounds (Table VIII-1). However, because of the well-known inaccuracy of finding hydrogen atoms by X-ray crystallography in a heavy element environment, one should be careful in interpreting these structural data. The minor difference between **VIII-9b** and **VIII-10b** is likely caused by sterics: the bulkier NHC ligand hampers silane approach to metal so that the decreased back-donation to silicon is compensated by increased transfer of electron density from the chloride lone pair.

The molecular structure of complex **VIII-9d** is presented in **Figure VIII-3**. This structure is similar to **VIII-9b**, except that the apical position is now occupied by a less electron withdrawing phenyl group (the Ph-Si···Cl angle is 165.5°). Interestingly, the Si···Cl distance in **VIII-9d** is elongated to 2.889 Å, due to the weakening of inter ligand hypervalent interaction. Unfortunately, since the crystallization of analogous phosphine complex turned to be difficult, the direct structural comparison between **VIII-9d** and **VIII-10d** cannot be done.

In the presence of excess silane, complex **VIII-9a** showed an unexpected

reactivity, in that it reacted with another equivalent of silane to generate a new silyl complex. Careful reproduction of this reaction by the addition of two equivalents of $HSiCl_3$ to a solution of **VIII-8** and toluene at -30 °C led to the formation of an imidazolium salt of the ruthenate complex $[CpRuClH(SiCl_3)_2]^-$ (**VIII-12**). The presence of the imidazolium salt and the ruthenate complex in the resulting reaction mixture proves the possibility of carbene dissociation from ruthenium. We think that IPr dissociates in the first step to generate an electron-deficient species $CpRuCl(H)(SiCl_3)$ (**VIII-13**), which then reacts with another equivalent of $HSiCl_3$ to form the silane complex **VIII-14** (Scheme VIII-3). The subsequent deprotonation of **VIII-14** by the basic carbene can give the final product **VIII-12**. This reaction sequence accounts for the fact that the imidazolium ion only forms in the presence of excess silane. Compound **VIII-12** was characterized by NMR spectroscopy and its molecular structure was confirmed by X-ray diffraction and elemental analysis.

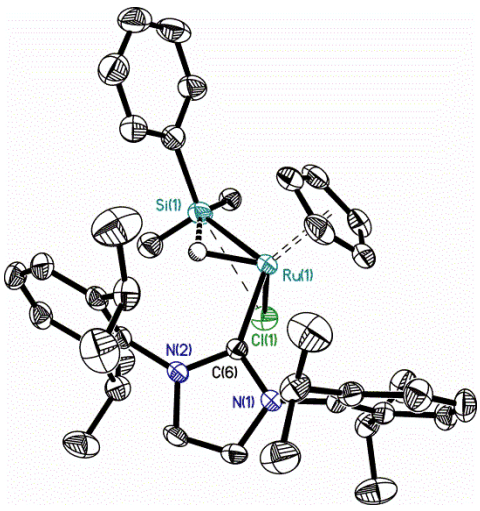

Figure VIII- 3. The molecular structure of compound **VIII-9d**. Hydrogen atoms, except the hydride on Ru, are omitted for clarity.

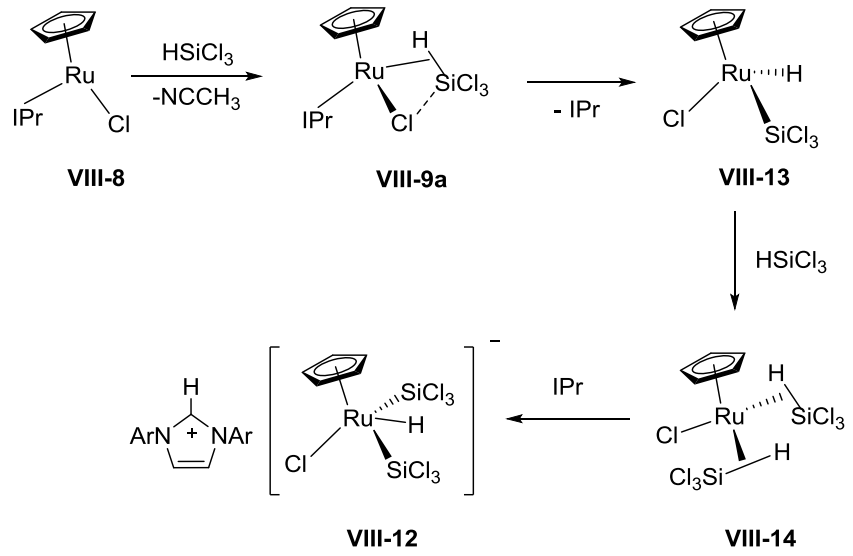

Scheme VIII- 3. A possible mechanism of the formation of complex **VIII-12**.

In the ^{1}H NMR spectrum of complex **VIII-12** in $CDCl_3$ (Figure XII-24, Appendix), the hydride signal at −10.59 ppm is shifted to a higher field compared to its parent hydride **VIII-9a** (−7.57 ppm). The presence of this Ru-H hydride bond in **VIII-12** is further confirmed by the observation of an IR stretch at 2012 cm^{-1}. The silicon atoms give rise to an upfield ^{29}Si NMR signal at −10.7 ppm (Figure XII-26, Appendix) displaying a moderate H-Si coupling of 14.5 Hz. The formation of compound **VIII-12** highlights a possible decomposition pathway for other NHC-supported silane σ-complexes, which will be discussed further in the following section.

The molecular structure of complex **VIII-12** is presented in Figure VIII-4, in which only the ruthenate part is highlighted. As can be seen from the Figure, this ruthenate part displays a typical four-legged piano-stool geometry, as the two silyl ligands are in the *trans* position to each other, while the hydride and chloride ligands reside on two other coordination sites. The Ru-Si distances (2.3055(9) and 2.3094(11)

Å) are longer than in the neutral three-legged compound $Cp^*(Me_3P)_2RuSiCl_3$ (2.265(2) Å), likely because of the more encumbered coordination sphere of ruthenium in **VIII-12**, but are shorter than in the cationic silane σ-complexes $[Cp^*(Me_3P)_2Ru(\eta^2\text{-}HSiCl_3)]^+$ (2.329(1) Å), $Cp^*(Pr^i{}_2MeP)Ru(\eta^2\text{-}HSiCl_3)Cl$ (2.3152(8) Å) and $Cp^*(Pr^iMe_2P)Ru(\eta^2\text{-}HSiCl_3)Cl$ (2.3111(5) Å). On the other hand, the Ru-Cl bond of 2.3988(9) Å in **VIII-12** is comparable to those in complexes **VIII-9b** and **VIII-9d** (2.3984(9) and 2.4279(8) Å, respectively). The H---Si distances in complex **VIII-12** are 2.129 and 2.156 Å. Previous DFT studies of isoelectronic half-sandwich silyl rhodium complexes $Cp^*Rh(SiR_3)_2H_2$, $CpRh(SiR_3)_3H$, $[Cp^*(Me_3P)Rh(SiR_3)_2H]^+$ and $[Cp^*(Me_3P)Rh(SiR_3)H_2]^+$ showed that these compounds have highly delocalized inter ligand interactions $R_3Si\cdots H\cdots SiR_3$ and $H\cdots SiR_3\cdots H$. By analogy, we can assume that similar multicentre interactions may be present in the compound **VIII-12**.

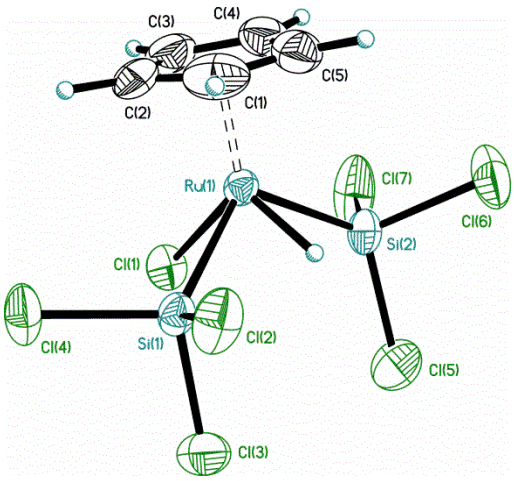

Figure VIII- 4. Molecular structure of compound **VIII-12**

Cationic silane σ-complexes:

The formation of cationic silane σ-complexes $[Cp(IPr)Ru(\eta^2\text{-}HSiR_3)(NCCH_3)]^+$ (**VIII-13**, Scheme VIII-4) was observed by NMR spectra at low temperature (-30 to -40 °C) upon addition of silanes to CD_2Cl_2 solutions of the cation **VIII-6a**. The resulting solutions contain equilibrium mixtures of silane σ-complexes **VIII-13** and the parent complex **VIII-6a.**

Unlike the related compounds **VIII-1**, complexes **VIII-13** are very labile and thus defied isolation in crystalline form. Therefore, they were characterized only by low-temperature NMR spectroscopy in solutions. Noteworthy, unlike the chemistry of the neutral silane σ-complex **VIII-9a**, this cationic silane σ-complex does not undergo addition of a second equivalent of silane to give cationic bis(silyl) derivatives, even when large excess (10 equivs) of silane was added.

An interesting feature of compounds **VIII-13** is that, unlike the neutral analogs **VIII-9**, their *J*(H-Si) values correlate well with the H-Si coupling in the P^iPr_3 congeners **VIII-1** (Table VIII-2). At the moment we do not have a clear-cut explanation for the divergent trends in the related series of compounds **VIII-9** and **VIII-13**.

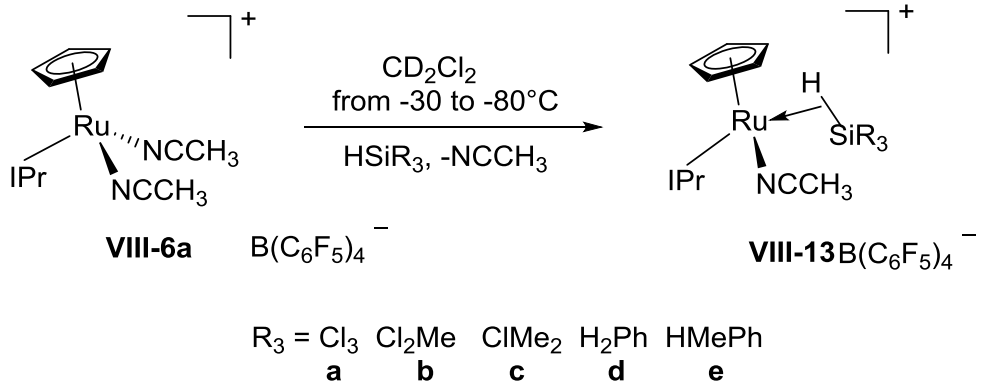

Scheme VIII- 4. Preparation of complexes **VIII-13 a-e**.

Table VIII- 2. H-Si coupling constants *J*(H-Si) (Hz) in complexes **VIII-13 a-e** and related phosphine complexes **VIII-1a-e**

	$SiCl_3$ (**a**)	$SiMeCl_2$ (**b**)	$SiMe_2Cl$ (**c**)	SiH_2Ph (**d**)	SiHMePh (**e**)
5	60.8	47.3	-	50.6	45.6
1	53	45	45	48	48

Since the addition of $HSiCl_3$ to the unsaturated complex **VIII-8** yields the neutral silane complex **VIII-9a**, we became curious about the reactivity of **VIII-6a** under the same conditions. The addition of an equivalent of $HSiCl_3$ to a CD_2Cl_2 solution of **VIII-6a** at -78°C followed by a slow warming to -30°C resulted in the formation of $[Cp(IPr)Ru(\eta^2\text{-}HSiCl_3)(NCCH_3)]^+$ (**VIII-13a**) in the course of 11 hours. This new species shows a hydride signal at – 7.61 ppm, concurrent with the appearance of ^{29}Si satellites with a large *J*(H-Si) of 60.8 Hz. The Cp and $NCCH_3$ ligands give rise to singlets at 4.95 ppm (5 H) and at 1.94 ppm (3 H), respectively.

The isopropyl moieties of the NHC carbene display eight doublets for nonequivalent methyl groups, consistent with the C_1 symmetry. Once warmed up to room temperature, the NMR spectrum showed a new set of signals, including the hydride signal at -9.65 ppm and the Cp signal at 5.30 ppm. These were accompanied by the formation of an equivalent of imidazolium ion $[IPrH]^+$ and a mixture of hydride compounds. Interestingly, the ^{29}Si satellites of this new hydride peak are integrated as 9.4% to the main signal (90.6%), suggesting the presence of two equivalent silicon atoms coupled to the central hydride atom (the natural abundance of the ^{29}Si isotope is 4.7%). The value of the *J*(H-Si) constant in this species found from the ^{29}Si satellites and from a 1D ^{1}H-^{29}Si HSQC experiment was 24.9 Hz (the ^{29}Si NMR signal was observed at 39.0 ppm). These features are similar to what was observed for the ruthenate complex **VIII-12** but the larger value of the *J*(H-Si) shows the formation of a different compound. The observation of a coordinated nitrile peak at 2.28 ppm allows us to formulate tentatively this compound as a neutral bis(silyl) hydride complex $CpRu(NCCH_3)(H)(SiCl_3)_2$ (**VIII-14**).

As demonstrated in the previous studies,[124-125] $HSiMe_2Ph$ was the best choice of silane in the catalytic hydrosilylation mediated by complex **VIII-1**. Therefore, we became curious about the performance of this silane in the hydrosilylation catalyzed by the analogous complex **VIII-6a**, and we wanted to understand if this complex could coordinate and activate this electron-rich silane. Upon monitoring an NMR sample containing **VIII-6a** and $HSiMe_2Ph$ (taken in excess) at -80°C, we noticed the appearance of additional products, as there was a new Ru*H* signal at -7.79 ppm in the ^{1}H NMR. Unfortunately, the peaks in the NMR spectra were too broad at this temperature to allow for a more in-depth analysis of this compound. This addition

of silane is reversible because an increase of temperature or removal of volatiles under vacuum regenerates the starting compound **VIII-6a**. Similar reactions of **VIII-6a** with silanes $HSi(OEt)_2Me$, $HSi(OEt)_3$, and $HSiEt_3$ in CD_2Cl_2 at -40°C did not yield the corresponding silane σ-complexes.

VIII.2 Catalytic activities of ruthenium σ-complexes

Given the fact that **VIII-2** displayed interesting reactivities in hydrosilylation of various substrates and on the basis of the isolobal relationship between **VIII-6a** and **VIII-2**, we decided to study the potency of **VIII-9** in catalytic hydrosilylation. Benzaldehyde, benzonitrile, and pyridine were chosen as the test substrates and the results are summarized in Table VIII-3. Unfortunately, the catalytic activity of **VIII-9** is significantly lower than that of **VIII-2**, For example, heating was required for benzonitrile and pyridine, whereas analogous reactions catalyzed by **VIII-1** occur at room temperature and are complete in less than one hour. Four silanes were screened in these reactions, but none of them showed good reactivity. Our explanation is that catalyst **VIII-9** may degrade under these reaction conditions. This assertion was then confirmed by ^1H NMR spectra of the reaction mixtures, which displayed the appearance of signals belonging to the imidazolium ion $[IPrH]^+$. This observation, combined with the formation of compound **VIII-12** described above, strongly suggests that the main decomposition pathway in hydrosilylation includes the dissociation of IPr from the catalytically active species followed by proton abstraction from the cationic ruthenium hydride.

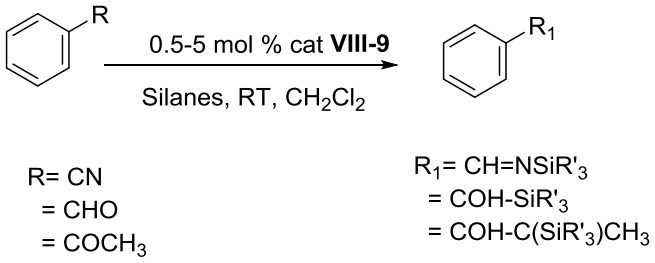

Scheme VIII- 5 Hydrosilylation catalyzed by complex **VIII-9**

Table VIII- 3. Hydrosilylation catalyzed by complex **VIII-9**

	H_3SiPh	$H_2SiMePh$	$HSiMe_2Ph$	$HSiMeCl_2$
PhC(O)H	47 %[b], 1h, 25ºC	36 %, 1h, 25ºC	18 %, 1h, 25ºC	23 %, 1h, 25ºC
PhCN	26 %, 3h, 50ºC	21 %, 3h, 50ºC	11 %, 3h, 50ºC	18 %, 3h, 50ºC
C_5H_5N	12 %, 2h, 50ºC	17 %, 2h, 50ºC	9 %, 2h, 50ºC	N/A

[a] 0.14 mmol of silane, 0.1 mmol of substrates, 0.6ml of CD_2Cl_2, 5 mol % catalyst; [b]NMR yield

IX. H/D exchange

Deuterium-labeled organic compounds and N-heterocycles labelled in specific positions are important classes of isotopically labelled chemicals, which find applications in the monitoring of drug metabolism, spectroscopic analyses (and most importantly in NMR), and investigations of mechanisms of catalytic reactions.[328, 333] Preparation of D-labelled precursors normally relies on two strategies: 1) the application of CH-acidic organic molecules, such as chloroform or acetone, and 2) metal catalyzed H/D exchange. The former approach is limited to acidic substrates and may suffer from low chemoselectivity. In contrast, the latter method has become the preferable pathway to efficiently obtain D-labelled molecules. Although catalytic H/D exchange in aromatics has been known since the early 60s,[364] to the best of our knowledge, up to now there has been no example of a metal-catalyzed regioselective H/D exchange reaction in N-heterocycle substrates, which would be also mild, green, and atom-efficient. In this section, we disclose the first example of such a catalytic system. Also, fascinated by the electronic analogy between N-heterocycles carbene (NHC) and phosphines, we tried to examine a series of newly synthesized Cp'(NHC)RuH_3 species (Cp' = Cp or Cp*,) toward the H/D exchange reaction and attempted to establish a possible correlation between T_1 min, $J(H^a\text{-}H^b)$ values of Cp'(NHC)RuH_3 species and their H/D exchange capabilities by employing pyridine as the standard substrate.

IX.1 Catalytic optimization for H/D exchange reaction

In our previous project (transfer hydrogenation, Section V), attempts to prepare one of the active catalysts, Cp(IPr)Ru(pyr)H (**IX-1**), led to a surprising observation that signals due to the pyridine decrease in intensity in the ^1H NMR

spectrum at room temperature when Cp(IPr)RuH_3 (**IX-2**) is mixed with pyridine in C_6D_6. In addition to this observation, during kinetic studies of the HDF reaction (section VI), we also observed that the hydrides of Cp*(IPr)RuH_3 (**IX-3**) were very quickly exchanged with deuterium coming from NMR solvents, and this process was very fast already at room temperature. Given these observations and our previous work on the Ru-catalyzed H/D exchange[342], we became curious about the possibility that our NHC supported tris(hydride) complexes of ruthenium should be active toward the H/D exchange reaction. We were additionally motivated to delineate the effect of supporting ligands on this H/D exchange. Because our other projects generated a library of tris(hydride) half-sandwich complexes of Ru, we started to screen them in the H/D exchange reaction with pyridine as the standard substrate.

Pyridine was chosen for this purpose, because it is one of the hardest substrates to activate and because we were so lucky to observe its reactivity as discussed above. By carefully reproducing the experiments with different loadings of **IX-2** (5, 0.5 and 0.1 mol%, Table IX-1, entries 1-3), we found that **IX-2** can efficiently catalyze H/D exchange of pyridine with C_6D_6 as the deuterium source with only 0.1 mol % of the catalyst to yield about 76 %, 79% and 80% deuteration for the ortho, para and meta positions of pyridine, respectively, after 24h at room temperature. To speed up the H/D process, the exchange was also attempted at 50°C (entry 3), and after only 2 h the degree of deuteration of pyridine was 82% (o), 87% (p), 79% (m).

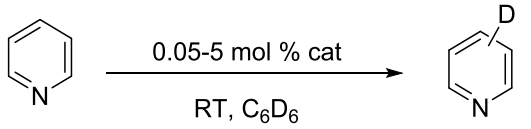

Scheme IX- 1. Catalyst screening for H/D exchange reaction

Table IX- 1. Catalyst screening and optimization for the H/D exchange reaction

Entry	mol % C	Catalyst	Degree of deuteration[a]
1	5	**IX-2**	12h, *o*(92%), *p*(92%), *m*(84%)
2	0.5	**IX-2**	24h, *o*(71 %), *p*(65%), *m*(69%)
3	0.1	**IX-2**	24h, *o*(76%), *p*(79%), *m*(80%) 2h, *o*(82%), *p*(87%), *m*(79%) [b]
4	0.1	**IX-6**	24h, *o*(<5%), *p*(<5%), *m*(<5%) No significant exchange after 12h.[b]
5	0.1	**IX-7**	24h, *o*(<5%), p(<5%), *m*(<5%) 24h, *o*(26%), *p*(32%), *m*(27%) [d] 24h, *o*(84%), *p*(81%), *m*(82%) [e]
6	0.1	**IX-8**	24h, *o*(<5%), *p*(<5%), *m*(<5%)
7	0.1	**IX-9**	24h, *o*(<5%), *p*(<5%), *m*(<5%)
8	0.1	**IX-10**	24h, *o*(<5%), *p*(<5%), *m*(<5%)
9	0.1	**IX-3**	24h, *o*(69%), *p*(79%), *m*(71%) 2h, *o*(85%), *p*(82%), *m*(83%) [b]

10	0.1	**IX-4**	24h, *o*(84%), *p*(81%), *m*(86%) 2h, *o*(92%), *p*(90%), *m*(91%) [b]
11	0.1	**IX-5**	24h, *o*(48%), *p*(49%), *m*(50%) 2h, *o*(84%), *p*(86%), *m*(87%) [b]
12	0	blank	No significant exchange after 12h[c]

[a] Rt, [b] 50ºC, [c] 70ºC, [d] 100ºC. [e] 100ºC, 5%, D_2O as deuterium source[342]. $Cp(IPr)RuH_3$ (**IX-2**), $Cp^*(IPr)RuH_3$ (**IX-3**), $Cp(IMes)RuH_3$ (**IX-4**) and $Cp^*(IMes)RuH_3$ (**IX-5**), $Cp(PPh_3)RuH_3$ (**IX-6**), $Cp(P^iPr_3)RuH_3$ (**IX-7**), $Cp(IPr)RuH_2SiH_2Ph$ (**IX-8**), $Cp(IPr)RuH_2SiHMePh$ (**IX-9**), $Cp(IPr)RuH_2SiMeCl_2$ (**IX-10**). *o*-ortho position, *p*-para position, *m*-meta position relative to N atom of pyridine

Intrigued by these initial results with catalyst **IX-2**, we aimed to screen a family of tris(hydride) and related di- and monohydride ruthenium species (catalysts **IX-2-10**, Table **IX-1**) to find out which catalyst is the best for this reaction. Cp/PR_3 catalysts (**IX-6** and **IX-7**) were also tested under conditions similar to those used for the catalyst **IX-2** (Entries 4 and 5), however, these trials returned much inferior results. In a recent report from our group[342], the compound **IX-7** was found to catalyze efficiently (o(84%), p(81%), m(82%) after 24 h) the H/D exchange of pyridine with 5 mol % at 100ºC, using D_2O as the deuterium source. However, at the best conditions found for catalyst **IX-2**, i.e, at a much lower catalyst load (0.1 mol %) and milder temperature (23ºC), **IX-7** could reach only 25-28% extent of deuteration. Several silyl dihydride ruthenium complexes, **IX-8**, **-9**, **-10**, were also

examined under the same conditions (entries 6-8). None of them was active in the H/D exchange of pyridine. This phenomenon could be related to the decreased hydride lability in these more thermodynamically more stable species, which appears to be an important feature of related tris(hydride) compounds. Catalysts **IX-3**, **-4**, **-5** were also evaluated under the conditions of the **IX-2**-catalyzed reactions, both at room temperature and at 50°C (entries 9-11), and the results were very encouraging for **IX-4**. A degree of deuteration of 92%, 90%, 91% for the *ortho*, *meta*, and *para* positions of pyridine, respectively, could be achieved after 2h at 50°C, which was the best activity among all tris(hydride) complexes we tested. At this point, we reasoned that the superb performance of catalyst **IX-4** compared to other tris(hydride) complexes could be attributed to three factors: 1) IMes has less bulky arms (the mesityl groups compared to the 2,6-bis(isopropyl)phenyl in IPr); 2) IMes has a stronger σ-donor ability than phosphines and $PiPr_3$ and PPh_3;[355, 365] 3) Cp* has a stronger donor ability than Cp, but is also bulkier. As a result, the Cp/IMes couple becomes "well-matched" in terms of the electronic and steric properties to ligate to the Ru centre. As a compromise between the reaction time, catalyst load, and temperature, we chose the loading of 0.1 mol % catalyst **IX-4** at 50°C as the optimized conditions for the H/D exchange reactions of other subtrates.

IX.2 H/D exchange of N-heterocycles

With this optimized system in hand, we started to examine other substrates. As depicted in Table IX-2, pyridine and its derivatives were deuterated qualitatively with catalyst **IX-4** after less than 5 h (entries 1-6). For the 3-chloropyridine (entry 2), only about 70% incorporation of deuterium occurred after 4.5h, and the catalyst deactivation was also observed in the course of the reaction, resulting in a slow

disappearance of the peaks due to tris(hydride) upon heating for a long period of time. Our explanation for this result is that the ruthenium hydride can be deactivated by an H/Cl exchange with the substrate. This assertion is supported by the fact that this is a known phenomenon for Cp/PR_3 ruthenium catalysts.[21] The usually reactive benzylic positions of substituted pyridines remain intact under these catalytic conditions; the acidic acetyl groups were also unreactive (entry 3). A longer reaction time is required for 2,2' bipyridyl, which might be caused by its chelate nature and strong complexation to the active form of the catalyst. The higher incorporation of deuterium found for the 3,5-dimethyl pyridine (entry 5) compared to 2,6-dimethyl pyridine (entry 6) could be assigned to reduced steric and hence stronger coordinating ability of the former substrate. A variety of other N-heterocycles were then examined in the catalytic H/D exchange with C_6D_6 mediated by catalyst **IX-4** (Table IX-2, entries 7-18). In general, most of the examined substrates were deuterated effectively (> 60%) under very mild conditions, within 10h at 50°C.

To elucidate the effect of different groups in the H/D exchange, a careful analysis of each substrate was done. For the case of quinoline, after 2.75 h, a higher deuteration of the 2-position (88%) and 3-position (82%) was observed (entry 11), whereas other positions were deuterated to about the same extent. However, in the case of quinaldine (entry 10), a longer reaction time (3h45m) is required to have a similar amount of deuterium incorporation, which could be explained simply by the increased steric hindrance caused by the methyl group of quinaldine. Like the methyl groups of lutidine, the methyl group of quinaldine was not much deuterated, which indicates that the hydrogen bound to a sp^3 carbon is not sensitive to this tris-hydride catalyst. The increase in the steric bulkiness of substituents at the aromatic ring has

a big impact on the H/D exchange. For example, phenyl quinoline required a longer time to be deuterated (entry 17). The exchange is regioselective as more deuteration is observed for the heteroarene ring (>60%) in comparison with the phenyl ring (<15%). One possible explanation is that this is the result of proximity to the coordination site of the substrate (nitrogen atom). For isoquinoline and phenanthridine (entries 7 and 8), it took longer times (>7h) to have the even moderate extent of deuteration (about 50-70%), which indicates the position of the coordination site may also dictate the activity. For bi-dentate substrates such as phenanthroline and 2,2' bipyridyl (entries 4 and 16), quite surprisingly, we also observed good activity, even though these substrates are expected to poison the catalyst due to their strong chelating ability. Acridine (entry 12) can be deuterated efficiently in under 3h to achieve a good degree of deuteration (>75%) in most hydrogen positions. For other N-aromatic compounds, such as triazine, imidazole, pyrrole (entries 13, 14, and 15), it was very hard to analyze the degree of H/D exchange for the protons directly bonded to nitrogen atoms, due to the broadness of their ^{1}H NMR signals. However, a trend could be seen for those compounds, which is that it took a longer time to activate the 5-membered rings (4-5h) than the 6-membered rings (2h15 min) for the same degree of deuteration (about 70%).

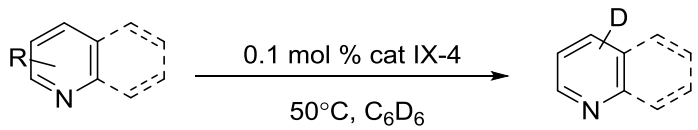

Scheme IX- 2. **IX-4** catalyzed H/D exchange of N-heterocycles

Table IX- 2. **IX-4** catalyzed H/D exchange of N-heterocycles

Entry	Degree of deuteration [a]	Time	Entry	Degree of deuteration	Time
1	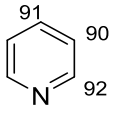	2h	10	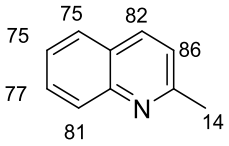	3h45 min
2	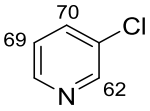	4.5h [b]	11	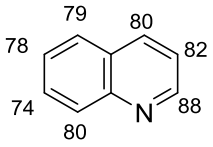	2h45 min
3	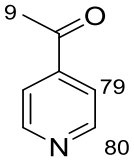	3h15 min	12	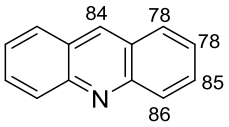	2h45 min
4	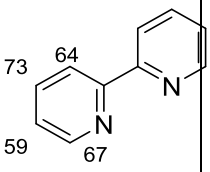	5h15 min	13	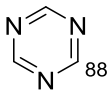	2h15 min
5	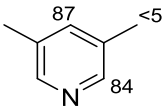	3h20 min	14	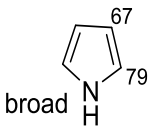	4h
6	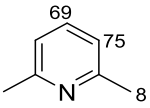	3h20 min	15	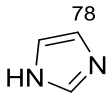	5h15 min
7	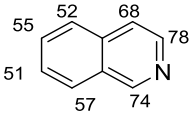	7h20 min	16	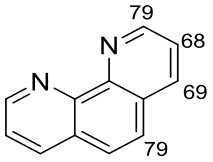	6h30 min

8	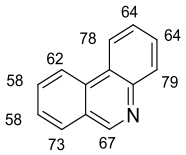	8h30 min	17	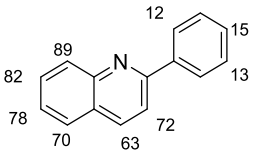	10h30min
9	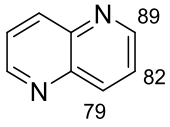	6h30 min	18	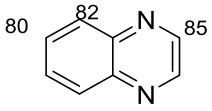	4h20 min

[a] 50ºC, 0.1mol % cat. Cp(IMes)RuH_3 (**IX-4**). [b] catalyst was deactivated after 2h due to the possible chloride poisoning of to ruthenium catalyst.

IX.3 H/D exchange in other substrates

After the success of deuteration of a series of pyridine derivatives and other N-heterocycles, we decided to extend the substrate scope to several other substrates to gain a better understanding of this unusually mild H/D exchange reaction (Table IX-3). In entry 1, the deuteration of toluene under the same conditions used for pyridine (0.1mol % of cat **IX-4**, at 50°C) revealed several interesting aspects: 1) toluene could be deuterated, which means that the presence of a coordinating atom is not a decisive factor; 2) the para-position of toluene had a higher degree of deuteration than ortho and meta positions, which could be explained by the steric impact of the methyl group. An attempt to deuterate benzonitrile (entry 2) further revealed that the H/D exchange tolerates the presence of coordinating sites on a side arm. In the case of naphthalene, the deuteration preferably goes to the less hindered 2-position (90% vs 74%). In entry 4, it took a longer time to activate trifluorotoluene, which implies that the electronic effect is important for this type of C-H bond activation. To test the hypothesis that Cp(IMes)RuH_3 can only activate the C-H

bonds at the sp^2-carbon of aromatics, we tested 1-hexene and 1-hexyne (entries 6 and 5). Even though a longer time is required for these two substrates (4 days), our experiments showed that the C-H bonds at the sp- and sp^2-carbons of aliphatic compounds also can be activated. Moreover, experiments with these two substrates again confirmed that the C-H at the sp^3-hybridized carbon remains untouched. In entry 7, the reactivity of catalyst **IX-4** was tested with cyclohexene, which again showed that exchange at the sp^2-position is easier than at sp^3 (21 %) vs <10 %). In entries 8, 9 and 10, tetrahydrofuran (THF), furan, and thiophene were examined. There was no deuterium incorporation in THF and thiophene. For THF, this happens because it has only sp^3-hybridized carbons. And for thiophene, it poisoned the catalyst, which was confirmed by the disappearance of signals due to the tris(hydride) complex in the ^{1}H NMR spectrum. For furan, it took 4 days to be deuterated to only about 10%. Nevertheless, aliphatic positions of isopropanol and ethanol were deuterated up to 65%, albeit at a time longer than 2 days (entries 11 and 12). It is not clear if this increased reactivity is due to the electronic effect of the accepting OH group or because it can coordinate to the ruthenium via its oxygen lone pairs.

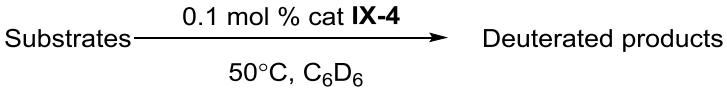

Scheme IX- 3. **IX-4** catalyzed H/D exchange of others substrates

Table IX- 3. **IX-4** catalyzed H/D exchange of others substrates

Entry	Degree of deuteration[a]	Time	Entry	Degree of deuteration	Time

1	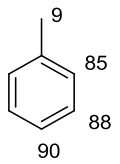	5h40 min	7	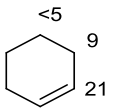	4 days
2	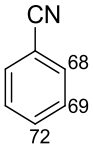	5h40 min	8		NR
3	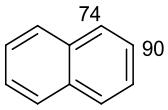	5h40 min	9	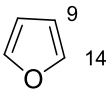	4 days
4	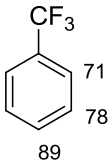	24h	10		NR[b]
5	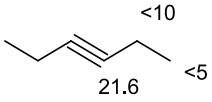	4 days	11[c]	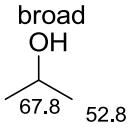	2 days
6	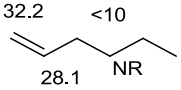	4 days	12	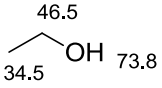	4days

[a] 50ºC, 0.1mol % cat. Cp(IMes)RuH_3 (**IX-4**). [b] catalyst was deactivated after 24h, the signal of tris-hydride totally disappeared. [c] 70ºC, 0.5mol % cat.

X. Conclusions and Future Work

As part of our interest in the chemistry of ruthenium catalysts, we prepared a series of new half-sandwich complexes of ruthenium supported by NHC carbene ligands. Several catalytic transformations mediated by these species, such as H/D exchange, transfer hydrogenation, hydrodefluorination, hydrosilylation, and borylation catalyzed reactions, were then explored. Another focus of our interest was the investigation of non-classical Si···H inter ligand interactions in some new NHC-supported dihydride silyl ruthenium complexes.

In our first project, we examined the ability of complex $[Cp(IPr)Ru(NCCH_3)_2][PF_6]$ (IPr = 1,3-bis(2,6-disopropylphenyl)imidazol-2-ylidene) to catalyze transfer hydrogenation (TH) of nitriles, activated N-heterocycles, olefins, and conjugated olefins in isopropanol. Significant activity was observed at the catalyst loading of 0.5% in the presence of KO^tBu. A good chemoselectivity in the reduction of nitriles to imines formed as a result of coupling between the initially formed amines with acetone (produced from isopropanol). This catalytic system also worked well for several activated N-heterocycles, which could be reduced with decent yields (40 to 70%). Due to the chelate effect, diimines could not be reduced efficiently; however, the reduction of activated imines could be done with high yield (99%) and in a short period of time (<2h). In addition, activated olefins also can be reduced and isolated with high yields. However, non-activated olefins, especially tri- or tetra-substituded olefins, were not reduced or little reduced under the same catalytic conditions. From a mechanistic study of this catalytic system, we concluded that the resting state of this catalytic cycle is the trihydride $Cp(IPr)RuH_3$, which could catalyze the reduction of nitriles without any additional base, and that the

external base actually had a detrimental effect on catalysis.

Accidentally, hydrodefluorination (HDF) of fluorinated compounds became the interesting second project for us. During our study of the transfer hydrogenation of N-heterocycles using isopropanol, we found that 6-fluoro-2-methyl quinoline was partially hydrodefluorinated under the same catalytic conditions. We also observed that NHC-supported tris(hydride) complexes Cp'(NHC)RuH_3 are efficient catalysts for hydrodefluorination of aromatic fluorides by using isopropanol as a reductant. The best catalyst from a family of tris(hydride) ruthenium complexes, both newly prepared and known compounds, is Cp*(IPr)RuH_3, which is the bulkiest one. Highly fluorinated compounds (hexa-, penta-, and tetra-fluoro) were easily reduced by our catalytic systems (<6h), but it took a longer time to reduce substrates having three and fewer fluorines (>24h). However, due to their reduced aromaticity, compared to benzene, reductions of polycyclic compounds, such as 1-fluoronaphthalene and 6-fluoro-2-methyl quinoline, were faster. Mechanistic studies revealed that the HDF reaction is first order in the substrate but shows saturation behaviour for isopropanol. The addition of an external carbene (IPr) had a deactivating effect on catalysis. These mechanistic patterns were rationalized in terms of sterically promoted dissociation of carbene from Cp*(IPr)RuH_3 and reversible coordination of substrate to the intermediate Cp*RuH_3. The substitution of fluoride for hydride is believed to be an inner-sphere process.

In the third project of this thesis, we reported the synthesis of a novel NHC supported trihydride complex of ruthenium and its reactions with silanes to give new monosilyl dihydride derivatives. We then conducted a systematic analysis of their X-ray structures and the effect that NHC-for-phosphine substitution has on the

extent of Si–H inter ligand interactions. These silyl dihydride complexes $Cp(IPr)RuH_2SiR_3$ were also characterized by NMR and IR spectroscopy. The magnitude of *J*(Si-H) in the range of 12.0–13.6 Hz was consistent with the expected values for silicon - hydride coupling of other silyl hydrido complexes. Moreover, their RuH resonances at −9.59 to −11.25 ppm suggested the formation of equivalent hydrides of these complexes. The orientation of chlorosilyl ligands in $Cp(IPr)RuH_2SiMe_{3-n}Cl_n$ (n = 1–3) are such that the chloride is in the *trans* position to a Ru-bound hydride, which is similar to the geometry observed in related complexes $Cp'(R_3P)RuH_2SiMe_{3-n}Cl_n$ (n = 1–3) and other compounds with inter ligand hypervalent interactions (IHI). In addition, the elongated distances in these hydrido chlorosilyl complexes also agree with the IHI theory. Compared to phosphine analogs, the strengthening of the RuH···Si interactions in $Cp(IPr)RuH_2SiR_3$, confirmed by X-ray data, could be attributed to the replacement of the phosphine ligand in the fragment Cp(L)Ru for a more electron releasing NHC carbene.

The fourth project of this thesis was focused on synthesizing new neutral and cationic silane σ-complexes supported by the NHC ligand, and examining their catalytic activities toward the hydrosilylation of N-heterocycles and nitriles. Another goal of this project was to investigate whether additional inter ligand interactions were present between the ruthenium - bound chloride and the silicon centre. The formation of silane σ-complexes was confirmed by characteristically high *J*(Si-H) coupling constants >40 Hz for all complexes $Cp(IPr)Ru(\eta^2\text{-}HSiR_3)Cl$. Furthermore, the magnitude of the *J*(H-Si) decreases from the most chlorinated compound $Cp(IPr)Ru(\eta^2\text{-}HSiCl_3)Cl$ (64.4 Hz) to the electron-rich compound $Cp(IPr)Ru(\eta^2\text{-}$

$HSiR_3$)Cl (40.5 Hz), which is very typical for silane σ-complexes. This trend could be explained by the predominant 3s character of silicon in the residual Si···H bond. X-ray diffraction studies of complexes Cp(IPr)Ru(η^2-$HSiMeCl_2$)Cl showed a short Si···Cl distance of 2.851 Å, which is the shortest in the series of complexes Cp'(L)Ru((η^2-$HSiR_3$)Cl (L = phosphine or carbene). The additional inter ligand RuCl···Si interaction gives rise to a hypercoordinated geometry around the silicon centre, with one Si-bond chloride being equatorial and the other in the apical position, trans to the Ru-bound chloride (the Cl-Si···Cl angle is 164.9°).

We also found that [Cp(IPr)Ru($NCCH_3$)$_2$][BArF] was less active for hydrosilylation of N-heterocycles and nitriles compared to its related compounds [Cp(^{i}Pr_3P)Ru($NCCH_3$)$_2$]$^+$. This was attributed to the ease of dissociation of IPr from the ruthenium centre. This conclusion was further supported by the isolation and characterization of the ruthenate complex [IPrH]$^+$[CpRuCl(H)($SiCl_3$)$_2$]$^-$ formed upon the reaction of Cp(IPr)RuCl with two equivalents of $HSiCl_3$.

The fifth project emerged also accidentally, as we found that one of our tris(hydride) complexes catalyzed efficiently H/D exchange of pyridine in the presence of C_6D_6 at room temperature. The least sterically hindered complex Cp(IMes)RuH_3 was found to be the best catalyst for the H/D exchange of a series of N-heterocycle derivatives. The addition of excess NHC led to decrease of the degree of deuteration. This occurrence is similar to what we observed in our HDF reactions, suggesting a similar mechanism.

For the future work, there is a possibility of using our ruthenium catalysts for the hydrogenation of unsaturated substrates with pressurized hydrogen gas. Alternative hydrogen donors, such as ammonium formate or the HCOOH/NEt_3

azeotropic mixture, should also be investigated. Furthermore, new reactions of these new complexes, such as borylation, silylation, acceptorless dehydrogenation, should be screened. Isolobal ligands with phosphine and NHC, should be considered as new directions for the future catalyst design. Importantly, the utility of chiral ligands for asymmetric synthesis should be the potential direction for the design of new ruthenium catalysts.

XI. Experimental section

XI.1 General methods and instrumentation

All manipulations were carried out using conventional atmosphere glove-box or nitrogen-line Schlenk techniques. All solvents were pre-dried using Grubbs-type purification columns or appropriate drying agents and stored in ampoules equipped with Teflon valve. NMR spectra were obtained with a Bruker DPX-300 (^{1}H 300 MHz, ^{13}C 75.5 MHz, ^{29}Si 59.6 MHz, ^{31}P 121.5 MHz) and/or Bruker DPX-600 (^{1}H 600 MHz, ^{13}C 151 MHz, ^{29}Si 119.2 MHz, ^{31}P 243 MHz) and/or Bruker DPX-400 (^{1}H 400 MHz, ^{13}C100.6 MHz, ^{29}Si 79.5 MHz, ^{31}P 162.0 MHz) spectrometers at room temperature, unless otherwise stated. Chemical shifts are quoted in δ (ppm) and coupling constants in Hertz. IR data were obtained on Perkin-Elmer 1600 FT-IR spectrometer. All IR data are quoted in wavenumbers (cm^{-1}). All organic substrates were purchased from Sigma-Aldrich and Alfa Aesar. These reagents were used without further purification. Deuterated solvents were dried over sodium, potassium, or CaH_2 as appropriate, distilled under reduced pressure and stored in Teflon valve ampoules. The silanes were purchased from Gelest.

XI.2 The synthesis of Cp' (Cp or Cp*) ruthenium (II) complexes ligated with NHC carbenes

XI.2.1 Ligand synthesis

IPr (1,3 -bis(2,6 -diisopropylphenyl) imidazol-2 -ylidene):

Synthesis of bis(2,6 -diisopropylphenyl)diazabutadiene

A 250 ml round-bottom flask was charged with 12 g (0.0672 mol) of 2,6-

diisopropylaniline, 3.795 ml (0.28 mol, 40% in water) of glyoxal and 100 ml of absolute ethanol. A few drops of formic acid were added as a catalyst. The color of the reaction mixture turned from colorless to yellow immediately, and a yellow precipitate appeared after a few hours. The reaction mixture was stirred for two days and the yellow solid was collected by filtration and washed with cold methanol to afford the analytically pure compound. Yield 7.93 g (77.5%) ^{1}H NMR (400 MHz, $CDCl_3$): δ 1.28 (d, *J*(H–H) = 7.6 Hz, 24H, CH(C*H*$_3$)$_2$, 3.03 (sep, *J*(H–H) = 6.4 Hz, 4H, C*H*(C*H*$_3$)$_2$), 7.27 (m, 6H, (CH(C*H*$_3$)$_2$)$_2$_C$_6$*H*$_3$), 8.19 (s, 2H, NC*H*).

Synthesis of IPrHCl

To a solution of bis (2,6-diisopropylphenyl)diazabutadiene (7.83 g, 20.67 mmol) in toluene (100 ml) was added 0.6344 g (20.67 mmol) of paraformaldehyde in solid form. The reaction mixture was heated to 100°C untill most of the paraformaldehyde was dissolved. It was then cooled to 40°C and 10.3 ml of HCl (20.67 mmol, 2 M in diethyl ether) was syringed in. The reaction mixture was heated to 70°C for 5 h during which time the color of the reaction mixture turned brown and a white precipitate appeared. It was then allowed to stir at r.t. for 36 h. The off-white precipitate was collected by filtration and washed with THF. Yield 3.1 g (35%) ^{1}H NMR (400 MHz, CD_2Cl_2): d 1.24 (d, *J*(H–H) = 7.2 Hz, 12 H, CH(C*H*$_3$)$_2$), 1.27 (d, *J*(H–H) = 7.2 Hz, 12 H, CH(C*H*$_3$)$_2$), 2.42 (sep, *J*(H–H) = 6.8 Hz, 4 H, C*H*(C*H*$_3$)$_2$), 7.18 (t, *J*(H–H) = 7.2 Hz, 2 H, *p*-C$_6$H$_3$), 7.4 (m, 4 H, *m*- C$_6$H$_3$), 7.80 (s, 2 H, NC*H*), 11.00 (s, 1 H, NC(*H*Cl)N).

Synthesis of IPr

To a mixture of **IPrHCl** (3.1 g, 7.3 mmol) and KOtBu (0.81g, 7.3 mmol) was

added THF (60 ml) at r.t. The color turned brown immediately and a white precipitate was formed. The reaction mixture was stirred for 4 h, the solvent was removed in vacuo and the residue was taken up in hot toluene (70°C). The reaction mixture was then filtered through Celite. Evaporation of the volatiles afforded a brown solid. Yield 2.04 g (70%). ^{1}H NMR (400 MHz, C_6D_6): δ 1.18 (d, 12 H, CH(CH_3)$_2$), 1.27 (d, 12 H, CH(CH_3)$_2$), 2.96 (sep, 4 H, CH(CH_3)$_2$), 6.61 (s, 2 H, NCH), 7.19 (m, 4 H, *m*-C$_6H_3$), 7.29 (m, 2 H, *p*-C$_6H_3$).

IMes (1,3 -bis(2,4,6 -trimethylphenyl) imidazol-2 -ylidene):

Synthesis of bis(2,4,6 -trimethylphenyl)diazabutadiene

A 250 ml round-bottom flask was charged with 34.5 g (0.28 mol) of 2,6-dimethylaniline, 15.6 ml (0.14 mol, 40% in water) of glyoxal and 100 ml of absolute ethanol. A few drops of formic acid were added as a catalyst. The color of the reaction mixture turned from colorless to yellow immediately, and a yellow precipitate appeared after a few hours. The reaction mixture was stirred for two days and the yellow solid was collected by filtration and washed with cold methanol to afford the analytically pure compound. Yield 7.93 g (77.5%). ^{1}H NMR (400 MHz, CD_2Cl_2): δ 2.18 (s, 12H, (*o*(CH_3)$_2$_C$_6H_3$), 2.32 (s, 6H, (*p*(CH_3)_C$_6H_3$), 7.06 (s, 4H, ((CH_3)$_2$_ C$_6H_3$), 8.06 (s, 2H, N=CH).

Synthesis of IMesHCl

To a solution of bis (2,4,6-trimethylphenyl)diazabutadiene (7.83 g, 20.67 mmol) in toluene (100 ml) was added 0.6344g (20.67 mmol) of paraformaldehyde in solid form. The reaction mixture was heated to 100°C untill most of the

paraformaldehyde was dissolved. It was then cooled to 40°C and 10.3 ml of HCl (20.67 mmol, 2 M in diethyl ether) was syringed in. The reaction mixture was heated to 70°C for 5 h during which time the color of the reaction mixture turned brown and a white precipitate appeared. It was then allowed to stir at r.t. for 36 h. The off-white precipitate was collected by filtration and washed with THF. Yield 3.1 g (35%). ^{1}H NMR (400 MHz, CD_2Cl_2): 2.18 (s, 12H, (*o*(CH_3)$_2$-C_6H_2), 2.37 (s, 6H, (*p*(CH_3)-C_6H_3), 7.1 (s, 4H, ((CH_3)$_2$-C_6H_2), 7.58 (s, 2H, NC*H*), 8.73 (s, 1H, NC(*H*Cl)N).

Synthesis of IMes

To a mixture of **IMesHCl** (3.1 g, 7.3 mmol) and KOtBu (0.81 g, 7.3 mmol) was added THF (60 ml) at r.t. The color turned brown immediately and a white precipitate was formed. The reaction mixture was stirred for 4 h, the solvent was removed in vacuo and the residue was taken up in hot toluene (70°C). The reaction mixture was then filtered through Celite. Evaporation of the volatiles afforded a brown solid. Yield 2.04 g (70%). ^{1}H NMR (400 MHz, C_6D_6): 2.15 (s, 12H, *o*(CH_3)$_2$-C_6H_2), 2.17 (s, 6H, *p*(CH_3)$_2$-C_6H_2), 6.82 (s, 4H, C_6H_2), 6.45 (s, 2H, NC*H*).

<u>ItBu (1,3-di-tert-butylimidazol-2-ylidene-1):</u>

Synthesis of 1,3-di-tert-butylimidazolium tetrafluoroborate (ItBuHBF$_4$)

To a stirring solution of toluene (15 mL) and paraformaldehyde(0.5 g, 16 mmol) at 0 °C was added dropwise *tert*-butylamine (3.5 ml, 32 mmol), under argon, over a 20 min period. The reaction mixture was stirred for a further 5min, and then 4 mL of HCl (4 N in dioxane) was added slowly. After the reaction reached completion (no longer exothermic), the mixture was allowed to warm to room

temperature, and glyoxal (40 wt %,1.8 g, 32 mmol) was slowly added. The resulting mixture was stirred at 25 °C for 12 h. The solvent volume was concentrated almost to dryness via slow distillation by heating the reaction mixture at 105 °C for 4 h. The reaction mixture was cooled to 50 °C, and the remaining solvent was removed under vacuum. The resulting brown solid (ItBuHCl) was dissolved in water (12.5 mL) with 1.2 equivs of KBF_4. The resulting white precipitate (**ItBuHBF$_4$**) was filtered, and dried under vacuum. Yield: 2.17g (50%). ^{1}H NMR (400 MHz, $CDCl_3$): δ 8.83 (s, *J*(H-C) = 219.6 Hz, 1H, NC(*H*BF_4)N), 7.46 (s, 2H,N=C*H*), 1.72 (s, 18H, *t*Bu). $^{13}C\{^1H\}$ NMR (100.6MHz, $CDCl_3$) : δ 131.8 (N*C*HN), 119.8 (N=*C*H), 60.6 (*C*$(CH_3)_3$), 29.5 (*C*H_3).

Synthesis of (ItBu)

In a dry box, tetrahydrofuran (15 mL) was added to a mixture of **ItBuHBF$_4$** (1 g, 3.7 mmol), NaH (0.178 g, 7.4 mmol), and a catalytic amount of KO*t*Bu (10mg). The resulting mixture was stirred for 12 h and the solvent was then removed under vacuum. **ItBu** was extracted into toluene, and after that, all volatiles were removed under vacuum to get a gel-like crude product. This solid was transferred to a sublimation apparatus where **ItBu** was sublimed under static vacuum with slight heating to afford a white crystalline product. Yield: 0.495 g, (90%). ^{1}H NMR (400 MHz, C_6D_6): δ 7.56 (s, 2H, N=C*H*), 1.89 (s, 18H, *t*Bu). $^{13}C\{^1H\}$ NMR (100.6MHz, C_6D_6): δ 212.8 (N*C*N carbene), 115.2 (N=*C*H), 56.1 (*Ct*Bu), 31.62 (*C*H_3).

<u>IiPr (1,3-Diisopropylimidazol-2-ylidene):</u>

1,3-Diisopropylimidazolium hexafluorophosphate (IiPrHPF$_6$):

A modified procedure was used for the synthesis of the imidazolium salt. Isopropylamine (15.45 mL, 0.18 mol) was added dropwise to a suspension of formaldehyde (5.4 g, 0.18 mol) in toluene (120 mL). The temperature of the reaction mixture was kept below 40°C during the addition. Afterward, the reaction mixture was stirred for ten minutes and then cooled to 0°C. Another equivalent of isopropylamine (15.45 mL, 0.18 mol) and 12M HCl (15 mL, 0.18 mol) were then added slowly. The temperature of the solution was raised to 25°C and glyoxal (20.7mL, 0.18 mol; 40% in H_2O) was added dropwise. The mixture was stirred overnight to give a dark solution. All volatile material was then removed in vacuo. The brown solid was treated with KPF_6 in H_2O to yield **IiPrHPF$_6$** which precipitated from the aqueous solution. The brown residue was vigorously dried in vacuo at 150°C for 6 h to yield a brown solid (24.8 g, 78%). ^{1}H NMR (400 MHz, D_2O): δ 1.43 (d, 12H, C*H*$_3$), 4.52 (m, 2H, ^{i}Pr-C*H*), 7.47 (s, 2H, NC*H*C*H*N), 8.76 ppm (s, 1H, NC*H*N); ^{13}C{^{1}H} NMR (100.6 MHz, D_2O): δ 22.07 (*C*H$_3$), 53.04 (^{i}Pr-*C*H), 120.47 (N*C*CN), 132.47 ppm (N*C*N).

Synthesis of IiPr:

THF (200 mL) was added at room temperature to a mixture of **IiPrHPF$_6$** (26.8 g, 0.16 mol), sodium hydride (4.1 g, 0.17 mol), and potassium tert-butoxide (0.82 g, 7.35 mmol). The mixture was stirred overnight to give a dark suspension. All volatile material was then removed in vacuo and the resulting brown oil was distilled at 150°C into a trap cooled with liquid nitrogen to afford 1,3-diisopropylimidazol-2-ylidene (15.6g, 64%) as a colorless liquid (melting point approximately 20°C). The carbene is thermally labile and forms a dark oil at room temperature, but it can be stored for a longer period of time at -40°C without decomposition. ^{1}H NMR (400

MHz, C_6D_6): δ 1.27 (d, 12H, C*H*$_3$), 4.40 (m, 2H, ^{i}Pr-CH), 6.63 ppm (s, 2H, NC*H*C*H*N); $^{13}C\{^1H\}$ NMR (100.6 MHz, C_6D_6): δ 24.27 (^{i}Pr-*C*H$_3$), 52.12 (^{i}Pr-*C*H), 115.74 (N*CC*N), 211.86 ppm (N*C*N).

IX.2.2 Precursor ruthenium complexes synthesis.

Cp$_2$Ru:

Ruthenium trichloride (5.26 g, 20.0 mmol) was dissolved in degassed ethanol (80 mL) in a 200 mL Schlenk tube. Freshly distilled cyclopentadiene (25 mL, 300 mmol, 15 eq.) was added to the dark red-black solution followed by the slow addition of finely powdered zinc (13 g, 200 mmol, 10 eq.). During this process, the reaction was cooled by an ice/water bath. The reaction mixture was stirred for 2 h at r.t., then filtered over Celite, (rinsed with toluene (120 mL)). The filtrate was evaporated to dryness, then redissolved in toluene (400 mL), passed through a pad of silica gel (rinsed with toluene). The resulting clear yellow solution was evaporated to dryness and dried under vacuum to afford ruthenocene (4.46 g, 96%) as yellow crystalline solid. 1H NMR (600 MHz, $CDCl_3$): δ 4.55 (s). $^{13}C\{^1H\}$ NMR (151 MHz, $CDCl_3$): δ 70.1

[CpRu(Naphthalene)]PF$_6$:

To a 100 mL Schlenk tube equipped with a magnetic stirring bar were added: ruthenocene 7 (2.31 g, 10 mmol), naphthalene (2.56 g, 20 mmol, 2.0 eq), Al (fine powder, 135 mg, 5 mmol, 50 mol%), and $AlCl_3$ (2.70 g, 20 mmol, 2.0 eq). Then the Schlenk flask tube was sealed, degassed, and purged with N_2. Degassed decalin (15 mL) was added followed by $TiCl_4$ (550 μL, 5 mmol, 50 mol%) was added. The

temperature of the dark reaction mixture was then raised to 140°C and the mixture stirred at this temperature for 3 days. After cooling to r.t., the reaction mixture was poured into a mixture of ice and water (80 mL), 32% HCl (20 mL), 30% H_2O_2 (20 mL) and stirred vigorously for 10 min. The resulting solution was extracted with pentane (3 × 200 mL). The combined organic phases were extracted with water (2 × 100 mL). To the combined aqueous phases was added KPF_6 (2.76 g, 15 mmol, 1.5 eq.) to give a yellow precipitate and the resulting mixture was stirred for 10 min. The aqueous solution was extracted with CH_2Cl_2 (4 × 200 mL), and then the combined organic phases were dried over $MgSO_4$, filtered, concentrated under vacuum to afford 4.1 g of an orange solid. The crude product was dissolved in 60 mL of CH_2Cl_2 and filtered through a short plug of Celite (4 x 5 cm). The Celite was washed with CH_2Cl_2 until washings become colorless. The CH_2Cl_2 solution was concentrated to c.a. 10 mL and then poured into vigorously stirred diethyl ether (100 mL) to yield a light-colored precipitate which was filtered off on a Büchner filter and washed with pentane (3 × 20 mL). The light cream-colored solid was dried in air and stored in a dark glass vial (3.7 g, 85%). mp: 155-160°C (dec.). ^{1}H NMR (600 MHz, CD_3COCD_3): δ 5.15 (s, 5H), 6.47-6.48 (m, 2H), 7.24-725 (m, 2H), 7.70-7.73 (m, 2H), 7.89-7.92 (m, 2H). $^{13}C\{^1H\}$ NMR (151 MHz, CD_3COCD_3): 79.7, 83.9, 85.9, 97.2, 129.3, 131.5. ^{31}P NMR (243 MHz, CD_3COCD_3): δ -144.1 (sept, J = 708 Hz).

[CpRu(NCCH$_3$)$_3$]PF$_6$:

The naphthalene complex [CpRu(Naphthalene)]PF_6 (1.25 g, 2.85 mmol) was placed in a Schlenk tube equipped with a magnetic stirring bar. Dry, N_2-saturated acetonitrile (13 mL) was added under N_2 atmosphere. The yellow solution was stirred for 24 h at r.t. The resulting solution was washed with degassed hexane (3 ×

18 mL) under N_2 atmosphere (naphthalene extraction). Then the acetonitrile solution was stirred for a further 24 h at r.t. followed by a second extraction by degassed hexane (4 × 18 mL) to $[CpRu(NCCH_3)_3]PF_6$ (1.2g) as a yellow air-sensitive solid. ^1H NMR (400 MHz, CD3COCD3): δ 2.44 (s, 9 H), 4.25 (s, 5H). $^{13}C\{^1H\}$ NMR (600 MHz, CD_3COCD_3): δ 2.4, 68.6, 125.9.

[CpRu(pyr)$_3$]PF$_6$:

$[CpRu(NCCH_3)_3][PF_6]$ (0.250 g, 0.576 mmol) was placed in a Schlenk tube equipped with a magnetic stirring bar. Dry pyridine (20 mL) pre-saturated with N_2 was added. The yellow solution was stirred at room temperature for 24 h. Volatiles were removed under vacuum to give 0.310 g of $[CpRu(pyr)_3]PF_6$ as a dark yellow, air sensitive

solid. Yield 98%. ^1H NMR (600 MHz, CD_2Cl_2): δ 4.19 (s, 5 H, Cp), 7.38 (t, *J*(H–H) = 7.0 Hz, 6H, py), 7.82 (t, *J*(H–H) = 7.8 Hz, 3H, py), 8.52 (t, *J(*H–H) = 7.0 Hz, 6H, py). $^{13}C\{^1H\}$ NMR (600 MHz, CD_2Cl_2): δ 53.4 (s, Cp), 125.7 (s, NC*C*C), 137.3 (s, NCC*C*), 154.5 (s, N*C*CC). Anal. Cal. for $C_{20}H_{20}RuN_3PF_6$ (548.43): C, 43.80; H, 3.68; N: 7.66. Found: C, 43.61, H, 4.13; N: 7.54.

Ru(PPh$_3$)$_3$Cl$_2$:

To a 500mL Schlenk flask was added $RuCl_3.3H_2O$ (2 g) and ethanol (200 mL). The complex dissolved and a sixfold excess (12 g) of triphenylphosphine was added. After vigorous stirring under nitrogen at room temperature for 24h, the solution was recrystallized and filtered at -30°C. The resulting dark brown crystals of the complex were then washed with methanol and diethyl ether and dried under *vacuum* (60 °C) for several hours (yield 88 %).

(Cp*RuCl)$_4$:

Synthesis of [Cp*RuCl$_2$]$_n$

The synthesis of [Cp*RuCl$_2$]$_n$ was performed based on a previously reported procedure under N_2 atmosphere. Pentamethylcyclopentadiene (20 mL, 143.7 mmol) was added to a solution of $RuCl_3 \cdot nH_2O$ (13 g, 57.5 mmol) in CH_3OH (600 mL). The resulting solution was refluxed for 7 h until the color reaction mixture changed from green to brown-red. The brown-red solution was kept for 12 h at -80 °C. The solution was then filtered, and the residue was washed with hexane to remove Cp$^*_2$Ru. The residue was dried under vacuum to afford [Cp*RuCl$_2$]$_n$ as a brown solid. Yield 11.3 g (62 %).

Synthesis of [Cp*RuCl]$_4$

To a 100 mL Schlenk tube equipped with a magnetic stirring bar was added: 11.3g [Cp*RuCl$_2$]$_n$, 2.6g (0.04 mol) of Zn, and 500mL of methanol. The mixture was stirred at 50 °C for 24h. All volatiles was then removed under vacuo. The crude solid was extracted with benzene, and the resulting brown solution was dried under high vacuum to yield 9.5 g (87.%) of **[Cp*RuCl]$_4$**.

IX.3 The syntheses of ruthenium (II) complexes supported by NHC carbene ligands.

[Cp(IPr)Ru(pyr)$_2$]PF$_6$ (VI-2):

To [CpRu(pyr)$_3$][PF$_6$] (0.250 g, 0.456 mmol) in 20 mL dichloromethane solution was added IPr NHC (0.174 g, 0.456 mmol). After stirring at room

temperature for 1 day, the resulting solution was dried to yield 4 as a brownish-yellow, air sensitive solid (0.380 g, 97%). This new compound was recrystallised from a THF/hexane (4 : 1 v/v) mixture to give a THF solvate of [Cp(IPr)Ru(pyr)$_2$]PF$_6$. ^{1}H NMR (300 MHz, CD_2Cl_2): δ 1.13 (d, *J*(H–H) = 6.9 Hz, 12H, C*H*$_3$), 1.30 (d, *J*(H–H) = 7.0 Hz, 12H, C*H*$_3$), 2.82 (sept, *J*(H–H) = 7.0 Hz, 4H, C*H* in ^{i}Pr), 3.77 (s, 5H, Cp), 7.11 (s, 2H, NC*H*), 7.32–7.46 (m, 6H, C$_6$*H*$_3$), 7.5 (t, *J*(H–H) = 6.8 Hz, 4H, m-pyr), 7.9 (t, *J*(H–H) = 6.8 Hz, 2H, *p*-pyr), 8.5 (d, J(H–H) = 6.8 Hz, 4H, *o*-pyr). ^{31}P NMR: −145.6 (sept, *J*(P–F) = 709 Hz, PF_6). Anal. Cal. for $C_{50}H_{67}RuN_4O_2PF_6$ (1002.13) C, 59.93; H, 6.74; N: 5.59. Found: C, 60.74, H, 6.76; N: 5.24.

Cp(IPr)RuCl (VI-11):

Addition of 0.012 g (0.29 mmol) of LiCl to a THF solution of 0.250 g (0.29 mmol) of [Cp(IPr)Ru(pyr)$_2$][PF_6] gave a deep blue solution of Cp(IPr)RuCl. All volatiles were removed under vacuum, and the residue was extracted by toluene, filtered, and dried to give 0.138 g (0.23 mmol) of Cp(IPr)RuCl. This product was further recrystallized from a mixture of toluene and hexane (2:3) at −30 °C. Isolated yield: 80%. The compound is highly moisture sensitive. ^{1}H NMR (C_6D_6): δ 1.16 (d, ^{3}*J*(H−H) = 6.8 Hz, 12H, C*H*$_3$ of ^{i}Pr), 1.49 (d, ^{3}*J*(H−H) = 6.8 Hz,12H, C*H*$_3$ of ^{i}Pr), 3.43 (sept, ^{3}*J*(H−H) = 6.8 Hz, 4H, C*H* of ^{i}Pr), 3.68 (s, 5H, Cp), 6.68 (s, 2H, NC*H*), 7.19−7.27 (m, 6H, C$_6$*H*$_3$). ^{13}C NMR (C_6D_6): δ 26.4 (s, *C*H$_3$ of ^{i}Pr), 22.9 (s, *C*H$_3$ of ^{i}Pr), 28.7 (s, *C*H of ^{i}Pr), 61.9 (Cp), 124.4 (N*C*H), 123.7 (s, *m*-*C*$_6$H$_3$), 129.8 (s, *p*-*C*$_6$H$_3$), 198.7 (Ru-*C*N2). Anal. Calcd for $C_{32}H_{41}RuN_2Cl$·0.5toluene (636.274): C, 67.01; H, 7.13; N, 4.40. Found: C, 67.34; H, 6.94; N, 4.81.

[Cp(IPr)Ru(NCCH$_3$)$_2$]BArF$_4$ (VI-3):

Reaction of 0.200 g (0.34 mmol) of Cp(IPr)RuCl with 0.296 g (0.34 mmol) of LiBArF$_4$ in acetonitrile at room temperature yields a solution of [Cp(IPr)Ru(NCCH$_3$)$_2$]BArF$_4$ and a precipitate. The precipitate was filtered off, and the filtrate was dried under vacuum to yield 0.420 g of [Cp(IPr)Ru(NCCH$_3$)$_2$]BArF$_4$. Yield: 93% (0.420 g). ^{1}H NMR (CD$_3$CN): δ 1.14 (d, ^3J(H−H) = 7.0 Hz, 12H, CH_3 of ^{i}Pr), 1.28 (d, ^3J(H−H) = 7.0 Hz, 12H, CH_3 of ^{i}Pr), 1,96 (s, 6H, CH_3CN), 2.81 (sep, J(H−H) = 7.0 Hz, 4H, CH of ^{i}Pr), 3.77 (s, 5H, Cp), 7.29 (s, 2H, NCH), 7.36−7.5 (m, 6H, C$_6$H$_3$). ^{13}C NMR (CD$_3$CN): δ 0.8 (NCCH_3), 25.0 (CH_3 of ^{i}Pr), 21.9 (CH_3 of ^{i}Pr), 28.5 (CH of ^{i}Pr), 73.2 (Cp), 125.9 (NCH), 123.8 (*mC*-C$_6$H$_3$), 130.4 (*pC*-C$_6$H$_3$), 137.0 (NCCH_3), 185.4 (Ru-*C*N2). ^{11}B NMR (CD$_3$CN): δ −16.69. ^{19}F NMR (CD$_3$CN): δ −169.3, −163.8 (t, ^3J(F−F) = 20.4 Hz), −133.7 (t, ^3J(F−F) = 20.4 Hz). Anal. Calcd for C$_{60}$H$_{47}$RuBF$_{20}$N$_4$ (1315.891): C, 54.76; H, 3.60; N, 4.26. Found: C, 54.54; H, 3.84; N, 4.55.

[Cp(IMes)Ru(pyr)$_2$][PF$_6$] (VI-10):

To [CpRu(pyr)$_3$][PF$_6$] (0.200 g, 0.36 mmol) in 20 mL dichloromethane solution was added IMes (0.137 g, 0.456 mmol). After stirring at room temperature for 1 day, the resulting solution was dried to yield [Cp(IMes)Ru(pyr)$_2$][PF$_6$] as a brownish-yellow, air sensitive solid. This new compound was recrystallised from a 5mL THF/hexane (4 : 1 v/v) mixture to give a THF solvate of 0.18 g (64%) [Cp(IMes)Ru(pyr)$_2$]PF$_6$. ^{1}H NMR (400 MHz, CD$_2$Cl$_2$): δ 1.13 (s, 12H, CH_3), 1.30 (s, 12H, CH_3), 23.77 (s, 5H, Cp), 7.11 (s, 2H, NCH), 7.38 (s, 4H, C$_6H_3$), 7.52 (t, J(H–H) = 6.8 Hz, 4H, m-pyr), 7.88 (t, J(H–H) = 6.8 Hz, 2H, *p*-pyr), 8.49 (d, J(H–H)

= 6.8 Hz, 4H, *o*-pyr). ^{31}P NMR: −144.3 (sept, *J*(P–F) = 710 Hz, PF_6).

Cp*(IPr)RuCl (VI-6):

To the brown solution of 0.5 g (1.8 mmol) $[Cp^*RuCl]_4$ in 100 mL THF was added 0.687g (1.8 mmol) IPr. After stirring at room temperature for 24h, the resulting purple solution was dried to yield corresponding unsaturated 16e Cp*(NHC)RuCl as a brownish-yellow, air sensitive solid. Then the crude product was recrystallized from a 50 mL mixture of benzene and hexane (4:1 v/v) at -30 °C to yield analytically pure Cp*(IPr)RuCl.^{1}H and $^{13}C\{^1H\}$ NMR spectra of the compound matched those from Nolan's procedure.[355]

[Cp*(IPr)Ru(NCCH$_3$)$_2$]PF$_6$ (VI-8):

The reaction of 0.2 g (0.3 mmol) of Cp*(IPr)RuCl with 0.26 g (0.3 mmol) of $AgPF_6$ in acetonitrile at room temperature yields a solution of $[Cp(IPr)Ru(NCCH_3)_2]PF_6$ and a precipitate. The precipitate was filtered off, and the filtrate was dried under vacuum to afford the crude $[Cp^*(IPr)Ru(NCCH_3)_2]PF_6$. The crude product was recrystallized from a 12 mL mixture of ether and hexane (5:1) to yield 0.2 g (78%) $[Cp^*(IPr)Ru(NCCH_3)_2]PF_6$. ^{1}H NMR ($CD_3CN$): δ 1.12 (d, ^3J(H−H) = 6.7 Hz, 12H, C*H*$_3$ of ^{i}Pr), 1.14 (s, 15H, C*H*$_3$ of Cp*) 1.34 (d, ^3J(H−H) = 6.7 Hz, 12H, C*H*$_3$ of ^{i}Pr), 1,93 (s, 6H, C*H*$_3$CN), 2.93 (sep, *J*(H−H) = 6.7 Hz, 4H, C*H* of ^{i}Pr), 7.11 (s, 2H, NC*H*), 7.37−7.47 (m, 6H, C_6H_3). ^{13}C NMR (101 MHz, CD_3CN): δ 1.3 (NC*C*H$_3$), 9.75 (*C*H$_3$ of Cp*), 23.0 (*C*H$_3$ of ^{i}Pr), 25.9 (*C*H$_3$ of ^{i}Pr), 29.2 (*C*H of ^{i}Pr), 83.8 (Cp*), 125.0 (N*C*H), 127.7 (*pC*-C_6H_3), 131.1 (*oC*-C_6H_3), 140.2 (*mC*-C_6H_3), 140.2 (CH_3-*C*C2 of C_6H_3), 188.0 (Ru-*C*N2). ^{31}P NMR (162.0 MHz, CD_3CN): −144.7

(sept, J(P–F) = 712 Hz, PF_6). Anal. Calcd for $C_{41}H_{58}F_6N_4PRu$ (852.96): C, 57.73; H, 6.85; N, 6.57. Found: C, 56.38; H, 6.96; N, 6.39.

Cp*(IMes)RuCl (VI-7):

To the brown solution of 0.5 g (1.8 mmol) $[Cp^*RuCl]_4$ in 100 mL THF was added 0.54 g (1.8 mmol) IMes. After stirring at room temperature for 24h, the resulting purple solution was dried to yield corresponding unsaturated 16e Cp*(NHC)RuCl as a brownish-yellow, air sensitive solid. Then the crude product was recrystallized from a 50 mL mixture of benzene and hexane (4:1 v/v) at -30 °C to yield analytically pure 0.67 g (65%) Cp*(IPr)RuCl. ^1H and $^{13}C\{^1H\}$ NMR spectra of the compounds matched with Nolan's procedure.[355]

[Cp*(IMes)Ru(NCCH$_3$)$_2$]PF$_6$:

The reaction of 0.5 g (0.87 mmol) of Cp*(IMes)RuCl with 0.75 g (0.87 mmol) of $AgPF_6$ in acetonitrile at room temperature yields a solution of $[Cp(IMes)Ru(NCCH_3)_2]PF_6$ and a AgCl precipitate. The precipitate was filtered off, and the filtrate was dried under vacuum to afford the crude $[Cp^*(IMes)Ru(NCCH_3)_2]PF_6$. The crude product was recrystallized from a12 mL mixture of ether and hexane (5:1) to yield 0.6 g (90%) $[Cp^*(IMes)Ru(NCCH_3)_2]PF_6$. ^1H NMR (CD_3CN): δ 1.10 (d, ^3J(H−H) = 6.7 Hz, 12H, CH_3 of ^{i}Pr), 1.12 (s, 15H, CH_3 of Cp*) 1.34 (d, ^3J(H−H) = 6.7 Hz, 12H, CH_3 of ^{i}Pr), 1,93 (s, 6H, CH_3CN), 2.93 (sep, J(H−H) = 6.7 Hz, 4H, CH of ^{i}Pr), 7.11 (s, 2H, NCH), 7.37−7.47 (m, 6H, C_6H_3). ^{13}C NMR (101 MHz, CD_3CN): δ 1.3 (NCCH_3), 9.75 (CH_3 of Cp*), 23.0 (CH_3 of ^{i}Pr), 25.9 (CH_3 of ^{i}Pr), 29.2 (CH of ^{i}Pr), 83.8 (Cp*), 125.0 (NCH), 127.7 (*pC*-C_6H_3), 131.1 (*oC*-C_6H_3), 140.2 (*mC*-C_6H_3), 140.2 (CH_3-*C*C2 of C_6H_3), 188.0 (Ru-*C*N2). ^{31}P

NMR (162.0 MHz, CD_3CN): −144.7 (sept, *J*(P–F) = 712 Hz, PF_6).

IX.3.1 Tris(hydride) ruthenium complexes.

Cp(IPr)RuH$_3$ (VI-1)

To a solution of [Cp(IPr)Ru(pyr)$_2$]PF_6 (0.200 g, 0.36 mmol) in 2 ml of THF was added $LiAlH_4$ (0.034 g, 0.9 mmol). The resulting mixture was left overnight at ambient temperature and then was slowly hydrolysed with degassed water. After evaporation of the solvent, the yellow residue was extracted with hexane (3×10 mL). Removal of volatiles and recrystallization at −30 °C from hexane solution afforded 0.117 g of 5 in the form of white crystals. Yield: 85% (0.117 g). IR (Nujol): ν(Ru–H) = 1982 cm^{-1}. ^{1}H NMR (600 MHz, C_6D_6): δ −10.67 (s, 3H, Ru*H*$_3$), 1.11 (d, *J*(H–H) = 7.0 Hz, 12 H, C*H*$_3$), 1.39 (d, J(H–H) = 7.0 Hz, 12 H, C*H*$_3$), 2.72 (sept, J(H–H) = 7.0 Hz, 4H, C*H* in ^{i}Pr), 4.30 (s, 5 H, Cp), 6.91 (s, 2 H, NC*H*), 7.32–7.46 (m, 6H, C_6H_3). ^{13}C NMR (600 MHz, C_6D_6): δ 25.7 (s, *C*H$_3$), 23.1 (s, *C*H$_3$), 28.8 (s, *C*H(CH$_3$)$_2$), 80 (s, Cp), 122.1 (s, N*C*H), 123.8 (*m*-*C*, C_6H_3), 129 (*p*-*C*, C_6H_3), 146.0 (Ru–*C*N2). Anal. Cal. for $C_{32}H_{44}RuN_2$ (557.78): C, 68.91; H, 7.95; N: 5.02. Found: C, 68.03, H, 7.81; N: 5.01.

Cp(IMes)RuH$_3$ (VI-17):

To 0.230 g (0.30 mmol) of [Cp(IMes)Ru(pyr)$_2$][PF_6] in 20 mL of isopropanol was added 0.040 g (0.36 mmol) of KO^{t}Bu. After stirring at room temperature for 3h, the solution was dried, extracted by hexane, and then recrystalized at room temperature from a 5mL mixture of toluene/hexane (2 : 3 v/v) by slow evaporation to give Cp(IMes)RuH_3 as a hexane solvate. Yield: 0.146 g (87%). IR (Nujol): ν(Ru–

H) = 2016 cm^{-1}. ^{1}H NMR (600 MHz, C_6D_6): δ -9.92 (s, 3H, Ru*H*), 2.12 (s, 12H, *o*-CH_3 of mesityl), 2.13 (s, 6H, *p*-CH_3 of mesityl), 4.57 (s, 5H, Cp), 6.12 (s, 2H, NC*H*), 6.8 (s, 4H, C_6H_2). ^{13}C NMR (151 MHz, C_6D_6): δ 18.44 (s, *o*-CH_3 of mesityl), 20.89 (*p*-CH_3 of mesityl), 81.0 (*C* ring of Cp), 120.2 (NCH), 129.2 (s, *m*-C_6H_2), 136.25 (s, *p*-C_6H_2), 193.4 (Ru-CN_2). Anal. Cal. for Cp(IMes)RuH_3*hexane, $C_{32}H_{46}RuN_2$ (559.8): C, 68.66; H, 8.28; N, 5.00. Found: C, 68.60, H, 8.55; N, 4.99.

Cp*(IPr)RuH_3 (VI-15):

To a solution of 0.26 g (0.40 mmol) of Cp*(IPr)RuCl in 20 mL ethanol was added 1.2 equivalent of NaH (0.012g, 0.48 mmol). After stirring at room temperature for 12h, the resulting solution was dried, extracted by hexane, and then recrystalized at room temperature from 8 mL mixture of toluene/hexane (3:1) by slow evaporation to yield 0.15 g (60%) of Cp*(IPr)RuH_3. IR (Nujol): ν(Ru–H) = 2030 cm^{-1}. ^{1}H NMR (600 MHz, C_6D_6): δ -9.53 (s, 3H, RuH_3), 1.07 (d, ^{3}J(H-H)=6.7 Hz, 12 H, CH_3 of ^{i}Pr), 1.52 (d, ^{3}J(H-H)=6.7 Hz, 12 H, CH_3 of ^{i}Pr), 1.8 (s, 15 H, CH_3 of Cp*), 2.93 (sept, ^{3}J(H-H)=6.7Hz, 4H, C*H* of ^{i}Pr), 6.44 (s, 2 H, NC*H*), 7.21-7.31 (m, 6H, C_6H_3). ^{13}C NMR (151 MHz, C_6D_6): 12.6 (s, *C*H_3 of Cp*), δ 28.5 (s, *C*H_3), 28.8 (s, *C*H(CH_3)$_2$), 93.4 (s, *C* ring of Cp*), 122.6 (s, NCH), 124.2 (*m*-C, C_6H_3), 129.2 (*p*-C, C_6H_3), 197.13 (Ru-CN_2). Anal. Cal. for $C_{37}H_{55}RuN_2$ (628.92): C, 70.66; H, 8.81; N: 4.45. Anal. Cal. for $C_{37}H_{55}RuN_2$ (628.92): C, 70.66; H, 8.81; N: 4.45. Found: C, 70.27, H, 8.71; N, 4.06.

Cp*(IMes)RuH_3 (VI-16):

To Cp*(IMes)RuCl (0.4 mmol) in 20 mL ethanol solution was added 1.2 equivalent of NaH (0.48 mmol). After stirring at room temperature for 12h, the

resulting solution was dried, extracted with hexane, and then recrystalized in hexane a mixture of toluene/hexane (1:3) to give the corresponding Cp*(IMes)RuH_3. This compound was characterized by NMR and IR. IR (Nujol): ν(Ru–H) =2023 cm^{-1}. ^1H NMR (600 MHz, C_6D_6): δ -9.39 (s, 3H, Ru*H*), 1.84 (s, 15H, CH_3 of Cp*), 2.13 (s, 12H, 2 ortho CH_3 of mesityl), 2.19 (s, 6H, 1 para CH_3 of mesityl), 6.12 (s, 2H, NC*H*), 6.88 (s, 4H, C_6H_2). ^{13}C NMR (151 MHz, C_6D_6): δ 12.5 (s, *C*H_3 of Cp*), 18.9 (s, *oC*H_3 of mesityl), 20.9 (*pC*H_3 of mesityl), 78.9 (*C* ring of Cp*), 120.5 (N*C*H), 129.2 (s, *m*-C_6H_2), 135.9 (s, *p*-C_6H_2), 194.3 (Ru-*C*N_2).

XI.2.2 Silyl-dihydride ruthenium complexes.

<u>Cp(IPr)$RuH_2(SiCl_3)$ (VI-2a)</u>

To a solution 0.050 g of Cp(IPr)RuH_3 in C_6D_6 was added an equivalent of (0.012 g) $HSiCl_3$. The mixture was heated to 50 °C overnight. The ^1H NMR spectrum showed that Cp(IPr)$RuH_2(SiCl_3)$ was formed in 82% yield. All solvents were removed under vacuum. Then the product was extracted by hexanes and recrystallized from a mixture of hexane and ether (1 : 1 v/v ratio). Isolated yield: 57% (0.035 g). IR (Nujol): ν(Ru–H) = 1985 cm^{-1}. 1H NMR (600 MHz, C_6D_6): δ −9.59 (s, 2H, RuH_2), 0.92 (d, *J*(H–H) = 6.6 Hz, 12H, CH_3), 1.45 (d, *J*(H–H) = 6.6 Hz, 12H, CH_3), 2.82 (sept, *J*(H–H) = 6.6 Hz, 4H, C*H* in ^{i}Pr), 4.57 (s, 5H, Cp), 6.51 (s, 2H, NC*H*), 7.15–7.24 (m, 6H, C_6H_3). ^{13}C NMR (600 MHz, C_6D_6): δ 26.3 (s, *C*H_3), 22.9 (s, *C*H_3), 28.6 (*C*H(CH_3)$_2$), 84.5 (s, Cp), 124.7 (NCH), 124.1 (*m*-*C*, C_6H_3), 128.4 (*p*-*C*, C_6H_3), 184.0 (Ru-*C*N2). ^{29}Si NMR (^1H–^{29}Si HSQC): 33.6 ($SiCl_3$). Anal. Cal. for $C_{32}H_{43}RuN_2$ $SiCl_3$ (691.21): C, 55.4; H, 6.27; N: 4.05. Found: C, 53.57, H, 5.98; N: 3.27.

Cp(IPr)RuH$_2$(SiCl$_2$Me) (VI-2b)

To a solution of 0.050 g Cp(IPr)RuH$_3$ in C_6D_6 was added an equivalent of (0.010 g) HSiCl$_2$Me. The mixture was heated to 70 °C for 2 h. The ^{1}H NMR spectrum showed quantitative formation of Cp(IPr)RuH$_2$(SiCl$_2$Me). All volatiles were removed under vacuum. The product was extracted by hexanes and recrystallized from a mixture of hexane and ether (1 : 1 ratio). Isolated yield: 88% (0.053 g). IR (Nujol): ν(Ru–H) = 1970 cm^{-1}. ^{1}H NMR (600 MHz, C_6D_6): δ −10.17 (s, 2H, Ru*H*$_2$), 1.04 (d, *J*(H–H) = 6.9 Hz, 12H, C*H*$_3$ of ^{i}Pr), 1.53 (d, *J*(H–H) = 6.9 Hz,12H, of ^{i}Pr), 1.34 (s, 3H, SiC*H*$_3$), 2.97 (sept, *J*(H–H) = 6.9 Hz, 4H, C*H* in ^{i}Pr), 4.63 (s, 5H, Cp), 6.64 (s, 2H, NC*H*), 7.25–7.36 (m, 6H, C_6H_3). ^{13}C NMR (600 MHz, C_6D_6): δ 26.3 (s, *C*H$_3$), 22.9 (s, *C*H$_3$), 24.8 (Si*C*H$_3$), 28.7 (s, *C*H(CH$_3$)$_2$)2), 83.3 (Cp), 124.3 (NCH), 123.9 (*m*-*C*, C_6H_3), 128.4 (*p*-*C*, C_6H_3), 187.3 (Ru–*C*N2). ^{29}Si NMR (^{1}H–^{29}Si HSQC): 66.7 (SiCl$_2$Me), J (Si–H) = 12.5 Hz. Anal. Cal. for $C_{33}H_{46}RuN_2SiCl_2$ (670.79): C, 59.09; H, 6.91; N: 4.18. Found: C, 58.94, H, 7.09; N: 4.09.

Cp(IPr)RuH$_2$(SiClMe$_2$) (VI-2c)

To a solution of 0.050 g of Cp(IPr)RuH$_3$ in C_6D_6 was added an equivalent of (0.0084 g) HSiClMe$_2$. The mixture was heated to 70 °C for 2 h. The ^{1}H NMR spectrum showed quantitative formation of Cp(IPr)RuH$_2$(SiClMe$_2$). All volatiles were removed under vacuum. The product was extracted by hexanes and recrystallized from a mixture of hexane and ether (1 : 1 ratio). Isolated yield: 90% (0.053 g). IR (Nujol): ν(Ru–H) = 1981 cm^{-1}. ^{1}H NMR (600 MHz, C_6D_6): δ −10.88 (s, 2H, Ru*H*$_2$), 1.05 (d, *J*(H–H) = 7.0 Hz, 12H, C*H*$_3$ of ^{i}Pr), 1.51 (d, *J*(H–H) = 7.0

Hz, 12H, C*H*$_3$ of ^{i}Pr), 1.02 (s, 6H, Si(CH_3)$_2$, 2.98 (sept, *J*(H–H) = 7.0 Hz, 4H, CH of ^{i}Pr), 4.63 (s, 5H, Cp), 6.64 (s, 2H, NC*H*), 7.26–7.37 (m, 6H, C$_6$H$_3$). ^{13}C NMR (600 MHz, C$_6$D$_6$): δ 26.3 (s, *C*H$_3$), 22.7 (s, *C*H$_3$), 18.63 (s, SiCH$_3$), 28.8 (s, *C*H(CH$_3$)$_2$)$_2$), 82.4 (Cp), 124.1 (NCH), 123.78 (*m-C*, C$_6$H$_3$), 129.8 (*p-C*, C$_6$H$_3$), 191.3 (Ru–*C*N2). ^{29}Si NMR (^{1}H–^{29}Si HSQC): 66.7 (SiClMe$_2$), J (Si–H) = 11.6 Hz. Anal. Cal. for C$_{34}$H$_{49}$RuN$_2$SiCl (650.37): C, 62.79; H, 7.59; N: 4.31. Found: C, 61.76, H, 7.54; N: 4.18.

Cp(IPr)RuH$_2$(SiH$_2$Ph) (VI-2d)

To a solution of 0.050 g Cp(IPr)RuH$_3$ in C$_6$D$_6$ was added an equivalent of (0.0097 g) H$_3$SiPh. The mixture was heated to 70 °C for 2 h. The ^{1}H NMR spectrum showed that Cp(IPr)RuH$_2$(H$_2$SiPh) was formed in 99% yield. All solvents were removed under vacuum. Then the product was extracted by hexanes and recrystallized from a mixture of hexane and ether (1 : 1 v/v ratio). Isolated yield: 95% (0.057 g). IR (Nujol): ν(Ru–H) = 1992 cm^{-1}. ^{1}H NMR (600 MHz, C$_6$D$_6$): δ −9.59 (s, 2H, Ru*H*$_2$), 0.99 (d, *J*(H–H) = 7.0 Hz, 12H, C*H*$_3$ of ^{i}Pr), 1.37 (d, 12H, C*H*$_3$ of ^{i}Pr), 2.89 (sept, *J*(H–H) = 7.0 Hz, 4H, C*H* of ^{i}Pr), 4.44 (s, 5H, Cp), 5.22 (s, 2H, Si*H*$_2$), 6.56 (s, 2H, NC*H*), 7.15–7.24 (m, 6H, C$_6$H$_3$), 7.40 (t, *J*(H–H) = 7.3 Hz, ortho H of SiC$_6$H$_5$), 7.42 (t, *J*(H–H) = 7.3 Hz, meta H of SiC$_6$H$_5$), 7.82 (t, *J*(H–H) = 7.3 Hz, para H of SiC$_6$*H*$_5$). ^{13}C NMR (600 MHz, C$_6$D$_6$): δ 26.1 (s, *C*H$_3$), 22.5(s, *C*H$_3$), 29.3 (s, CH of ^{i}Pr), 81.9 (Cp), 124.1 (N*C*H), 127.2 (*m-C*, C$_6$H$_3$), 136.1 (*p-C*, C$_6$H$_3$), 192.4 (Ru–*C*N2). ^{29}Si NMR (^{1}H–^{29}Si HSQC): −18.8 (*Si*H$_2$Ph). Anal. Cal. for C$_{38}$H$_{50}$RuN$_2$Si (663.97): C, 68.74; H, 7.59; N: 4.22. Found: C, 67.8, H, 7.46; N: 4.10.

Cp(IPr)RuH_2(SiHMePh) (VI-2e)

To a solution of 0.050 g Cp(IPr)RuH_3 in C_6D_6 was added an equivalent of (0.011 g) H_2SiMePh. The mixture was heated to 70 °C for 2 h. ^{1}H NMR spectrum showed that Cp(IPr)RuH_2(SiHMePh) was formed in 99% yield. All solvents were removed under vacuum. Then the product was extracted by hexanes and recrystallized from a mixture of hexane and ether (1 : 1 v/v ratio). Isolated yield: 78% (0.047 g). IR (Nujol): ν(Ru–H) = 2032 cm^{-1}. ^{1}H NMR (600 MHz, C_6D_6): δ −11.25 (s, 1H, RuH_2), −10.81 (s, 1H, RuH_2), 1.11 (d, *J*(H–H) = 7.0 Hz, 12H, C*H*$_3$ of ^{i}Pr), 1.37 (d, *J*(H–H) = 7.0 Hz, 6H, C*H*$_3$ of ^{i}Pr), 1.53 (d, *J*(H–H) = 7.0 Hz, 6H, C*H*$_3$ of ^{i}Pr), 0.86 (d, *J*(H–H) = 3.6 Hz, 3H, Si(C*H*$_3$), 2.98 (sept, *J*(H–H) = 7.0 Hz, 2H, C*H* of ^{i}Pr), 3.10 (sept, *J*(H–H) = 7.0 Hz, 2H, C*H* of ^{i}Pr), 4.52 (s, 5H, Cp), 5.38 (q, 1H, Si*H*MePh), 6.67 (s, 2H, NC*H*), 7.22–7.40 (m, 6H, C_6H_3), 7.36–7.42 (3H, *m*- and *p*- of SiC_6H_5), 7.75 (d, *J*(H–H) = 3.8 Hz 2H, o- SiC_6H_5). ^{13}C NMR (600 MHz, C_6D_6): δ 25.7 (s, *C*H$_3$ of iPr), 22.6 (s, *C*H$_3$ of iPr), 7.2 (Si*C*H$_3$), 28.9 (CH of iPr), 81.6 (Cp), 123.7 (N*C*H), 124.05 (*m-C*, C_6H_3), 129.6 (*p-C*, C_6H_3), 124.43 (*p-C* of SiC_6H_5), 126.8 (*m-C* of SiC_6H_5), 135.1 (*o-C* of SiC_6H_5), 193.4 (Ru–*C*N2). ^{29}Si NMR (^{1}H–^{29}Si HSQC): −0.8 (*Si*HMePh). Anal. Cal. for $C_{39}H_{52}RuN_2Si$ (678.00): C, 69.09; H, 7.73; N: 4.13. Found: C, 71.58, H, 7.55; N: 4.1.

Cp(IPr)RuH_2(SiMe$_2$Ph) (VI-2f)

To a solution of 0.050 g Cp(IPr)RuH_3 in C_6D_6 was added an equivalent of (0.012 g) HSiMe$_2$Ph. The mixture was heated to 70 °C for 2 h. The ^{1}H NMR spectrum showed that Cp(IPr)RuH_2(SiMe$_2$Ph) was formed in 99% yield. All solvents were removed under vacuum. Then the product was extracted by hexanes

and recrystallized from a mixture of hexane and ether (1 : 1 v/v ratio). Isolated yield: 67% (0.042 g). IR (Nujol): ν(Ru–H) = 2030 cm^{-1}. ^{1}H NMR (600 MHz, C_6D_6): δ −11.25 (s, 2H, RuH_2), 1.07 (d, *J*(H–H) = 7.0 Hz, 12H, CH_3 of ^{i}Pr), 1.41 (d, *J*(H–H) = 7.0 Hz, 12H, CH_3 of ^{i}Pr), 0.80 (s, 6H, Si(CH_3)$_2$, 3.00 (sept, *J*(H–H) = 7.0 Hz, 4H, CH_3 of ^{i}Pr), 4.53 (s, 5H, Cp), 6.69 (s, 2H, NC*H*), 7.28–7.42 (m, 6H, C_6H_3), 7.36–7.42 (3H, *m*- and *p* of SiC_6H_5), 7.82 (d, 2H, *o*- of SiC_6H_5). ^{13}C NMR (600 MHz, C_6D_6): δ 26.3 (s, *C*H_3 of ^{i}Pr), 22.6 (s, *C*H_3 of ^{i}Pr), 11.7 (s, Si*C*H_3) 28.8 (s, *C*H_3 of ^{i}Pr), 81.7 (Cp), 123.7 (s, N*C*H), 123.9 (s, *m*-*C*, C_6H_3), 129.46 (s, *p*-*C*, C_6H_3), 126.4 (s, *p*-*C* of SiC_6H_5), 126.7 (s, *m*-*C* of SiC_6H_5), 134.9 (s, *o*-C of SiC_6H_5), 194.7 (s, Ru–*C*N2). ^{29}Si NMR (^{1}H–^{29}Si HSQC): 15.2 (*Si*Cl_2Me), J(Si–H) = 13.23 Hz. Anal. Cal. for $C_{40}H_{54}RuN_2Si$ (692.03): C, 69.42; H, 7.87; N: 4.05. Found: C, 68.9, H, 7.46; N: 4.04.

XI.2.3 Neutral and cationic silane σ-complexes.

Cp(IPr)RuCl(η^2-H SiCl_3) (VIII-9a)

Addition of (0.011 g) H$SiCl_3$ to a blue solution of Cp(IPr)RuCl (0.050 g, 0.085 mmol) in 5 mL of toluene at −30 °C results in the immediate color change to yellow. Hexane was added and the product was recrystallized at −30 °C from a mixture of toluene/hexane (4:1 v/v), resulting in crystallization of 4a. The product was filtered and dried under vacuum. Yield: 62% (0.038 g). IR (Nujol): ν(Ru−H) = 2030 cm^{-1}. ^{1}H NMR (−23 °C, toluene-d_8): δ −7.57 (s, 1H, RuH), 0.85 (br, 6H, CH_3 of ^{i}Pr), 0.96 (br, 6H, CH_3 of ^{i}Pr), 1.03 (d, ^{3}J(H−H) = 6.4 Hz, 3H, CH_3 of ^{i}Pr), 1.16 (d, ^{3}J(H−H) = 6.4 Hz, 3H, CH_3 of ^{i}Pr), 1.32 (d, ^{3}J(H−H) = 6.4 Hz, 6H, CH_3 of ^{i}Pr), 2.87 (br, 2H, CH of iPr), 3.41 (br, 2H, C*H* of ^{i}Pr), 4.38 (s, 5H, Cp), 6.41 (s, 2H, NC*H*), 7.03−7.23 (m, 6H, C_6H_3). ^{13}C NMR (−23 °C, toluene-d_8): δ 25.3 (*C*H_3 of ^{i}Pr), 26.3 (*C*H_3 of ^{i}Pr),

23.4 (*C*H$_3$ of ^{i}Pr), 23.5 (*C*H$_3$ of ^{i}Pr), 28.4 (*C*H of ^{i}Pr), 86.0 (Cp), 125.5 (N*C*H), 122.9 (s, *m*- C$_6$H$_3$), 130.9 (s, *p*- C$_6$H$_3$), 179.0 (Ru-*C*N2). ^{29}Si NMR (^{1}H–^{29}Si HSQC): δ 13.6 (^{1}J(Si−H) = 64.3 Hz, SiCl$_3$). Anal. Calcd for $C_{32}H_{42}RuN_2SiCl_4$ (725.658): C, 52.89; H, 5.96; N, 3.86. Found: C, 52.46; H, 5.67; N, 3.73.

Cp(IPr)RuCl(η^2-HSiCl$_2$Me) (VIII-9b)

Addition of (0.0096 g) HSiCl$_2$Me to a blue solution of 0.050 g (0.085 mmol) of Cp(IPr)RuCl in 5 mL of toluene at −30 °C results in the immediate color change to yellow. The product was recrystallized from a mixture of toluene and hexane (4:1) at −30 °C. Isolated yield: 84% (0.050 g). IR (Nujol): ν(Ru−H) = 2054 cm^{-1}. ^{1}H NMR (−5 °C, toluene-d$_8$): δ −8.10 (1H, Ru*H*), 0.87 (d, ^{3}J(H−H) = 6.7 Hz, 6H, C*H*$_3$ of ^{i}Pr), 0.97 (d, ^{3}J(H−H) = 6.7 Hz, 6H, C*H*$_3$ of ^{i}Pr), 1.22 (br, 6H, C*H*$_3$ of ^{i}Pr), 1.36 (d, ^{3}J(H−H) = 6.7 Hz, 6H, C*H*$_3$ of ^{i}Pr), 0.54 (s, 3H, SiC*H*$_3$), 2.49 (br, 2H, C*H* of ^{i}Pr), 3.33 (br, 2H, C*H* of ^{i}Pr), 4.48 (s, 5H, Cp), 6.49 (s, 2H, NC*H*), 6.99- 7.20 (m, 6H, C$_6$H$_3$). ^{13}C NMR (−5 °C, toluene-d$_8$): δ 15.8 (Si*C*H$_3$), 25.2 (s, *C*H$_3$ of ^{i}Pr), 26.4 (s, *C*H$_3$ of ^{i}Pr), 22.7 (s, *C*H$_3$ of ^{i}Pr), 21.6 (s, *C*H$_3$ of ^{i}Pr), 28.4 (s, *C*H of ^{i}Pr), 85.0 (Cp), 125.2 (NCH), 124.8 (m- C$_6$H$_3$), 130.3 (p- C$_6$H$_3$), 184.9 (Ru-*C*N2). ^{29}Si NMR (^{1}H–^{29}Si HSQC): δ 39.1 (^{1}J(Si−H, = 43.6 Hz). Anal. Calcd for $C_{33}H_{45}RuN_2SiCl_3$ (705.240): C, 56.20; H, 6.43; N, 3.97. Found: C, 55.95; H, 6.81; N, 3.84.

Cp(IPr)RuCl(η^2-HSiClMe$_2$) (VIII-9c)

Addition of (0.008 g) HSiClMe$_2$ to a blue solution of 0.050 g (0.085 mmol) of Cp(IPr)RuCl in 5 mL of toluene at −30 °C results in the immediate color change to yellow. Hexane was added, and the product was recrystallized from a mixture of toluene and hexane (4:1) at −30 °C. Isolated yield: 79% (0.046 g). IR (Nujol):

ν(Ru−H) = 1993 cm^{-1}. ^{1}H NMR (−23 °C, toluene-d_8): δ −7.80 (1H, Ru*H*), 0.92 (br, 6H, C*H*$_3$ of ^{i}Pr), 1.01 (br, 6H, C*H*$_3$ of ^{i}Pr), 1.14 (br, 6H, C*H*$_3$ of ^{i}Pr), 1.45 (d, ^{3}J(H−H) = 6.8 Hz, 6H, C*H*$_3$ of ^{i}Pr), 0.18 (s, 3H, C*H*$_3$ of Si(C*H*$_3$)$_2$, 1.26 (s, 3H, C*H*$_3$ of Si(C*H*$_3$)$_2$), 2.55 (br, 2H, C*H* of ^{i}Pr), 3.42 (br, 2H, C*H* of ^{i}Pr), 4.31 (s, 5H, Cp), 6.46 (s, 2H, NC*H*), 7.06−7.23 (m, 6H, C_6H_3). ^{13}C NMR (−23 °C, toluene-d_8): δ 10.2 (Si(*C*H$_3$)$_2$), 23.6 (Si(*C*H$_3$)$_2$), 24.5 (*C*H$_3$ of ^{i}Pr), 26.6 (*C*H$_3$ of ^{i}Pr), 23.4 (*C*H$_3$ of ^{i}Pr), 22.7 (*C*H$_3$ of ^{i}Pr), 28.4 (*C*H of ^{i}Pr), 85.0 (Cp), 125.1 (N*C*H), 128.4 (s, *m*- C_6H_3), 130.4 (s, *p*- C_6H_3), 185.9 (Ru-*C*N2). ^{29}Si NMR (^{1}H–^{29}Si HSQC): δ 29.5 (^{1}J(Si−H) = 56.4 Hz, *Si*ClMe$_2$). Anal. Calcd for $C_{34}H_{48}RuN_2SiCl_2$ (684.821): C, 59.63; H, 7.06; N, 4.08. Found: C, 60.06; H, 7.06; N, 3.57.

Cp(IPr)RuCl(η^2-H$_3$SiPh) (VIII-9d)

Addition of (0.009 g) H_3SiPh to a blue solution of 0.050 g (0.085 mmol) of Cp(IPr)RuCl in 5 mL of toluene at −40 °C results in the immediate color change to yellow. Cp(IPr)RuCl(η^2-H_3SiPh) was recrystallized from a mixture of toluene and hexane (4:1 v/v) at −30 °C. Yield: 76% (0.045 g). IR (Nujol): ν(Ru−H) = 1980 cm^{-1}. ^{1}H NMR (−30 °C, toluene-d_8): δ −8.96 (br s, 1H, Ru*H*), 0.90−1.57 (br, 24H, *C*H$_3$ of ^{i}Pr), 2.41, 2.77, 3.28, 3.79 (br, 4H, C*H* of ^{i}Pr), 3.41 (br, 2H, C*H* of ^{i}Pr), 3.94 (s, 5H, Cp), 4.4 (d, ^{2}J(H−H) = 9.5 Hz, 1H, Si*H*$_2$), 5.39 (d, ^{2}J(H−H) = 9.5 Hz, 1H, Si*H*$_2$). 6.52 (s, 2H, NC*H*), 7.18−7.26 (m, C_6H_3+Ph), 7.65 (d, ^{3}J(H−H) = 6.9 Hz 2H, ortho of SiH_2Ph). ^{13}C NMR (−58 °C, toluene-d_8): δ 22.1 (*C*H$_3$ of ^{i}Pr), 23.7 (*C*H$_3$ of ^{i}Pr), 26.7 (*C*H$_3$ of ^{i}Pr), 28.6 (*C*H$_3$ of ^{i}Pr), 25.4, 26.3, 28.0, 29.6 (*C*H of ^{i}Pr), 81.7 (Cp), 125.5 (N*C*H), 138.6 (*m*- C_6H_3), 135.4 (*p*- C_6H_3), 147.9 (meta of SiPh), 145.9 (para *C* of SiPh), 148.6 (ortho *C* of SiPh), 186.8 (Ru- *C*N2). ^{1}H–^{29}Si HSQC (−58 °C, toluene-d_8): δ −22.7 (SiH_2Ph). 1D ^{29}Si INEPT+ (−58 °C, toluene-d_8): δ −22.7

(^{1}J(Si−H(Ru)) = 43.2 Hz, ^{1}J(Si−H of SiH_2) = 218.2 Hz, SiH_2Ph). Anal. Calcd for $C_{38}H_{49}RuN_2SiCl$: (698.42) C, 65.35; H, 7.07; N, 4.01. Found: C, 65.01, H, 6.35; N, 4.07.

Cp(IPr)RuCl(η^2-H_2SiMePh) (VIII-9e)

The addition of (0.010 g) H_2SiMePh to a blue solution of 0.050 g (0.085 mmol) of Cp(IPr)RuCl in 5 mL of toluene at −30 °C results in the immediate formation of a yellow silane σ-complex, Cp(IPr)RuCl(η^2-HSiHMePh). ^{1}H NMR spectra showed the presence two isomers of Cp(IPr)RuCl(η^2-HSiHMePh). Attempted scale-up of this reaction failed because of the thermal instability of the product. ^{1}H NMR (toluene-d_8, −40 °C): δ −8.89 (RuH, major isomer), −8.57 (RuH of minor isomer), 0.93−1.63 (br, CH_3 of ^{i}Pr of both isomers), 2.33−3.41 (br, C*H* of ^{i}Pr of both isomers), 4.41 (H, SiH(CH_3)Ph major isomer), 4.47 (H, SiH(CH_3)Ph minor isomer), 1.14 (H, SiH(CH_3)Ph major isomer), 0.49 (H, SiH(CH_3)Ph minor isomer), 3.93 (s, H, Cp of major isomer), 4.03 (s, H, Cp of minor isomer), 6.46−6.48 (br, H, NCH of both isomers), 6.92−7.27 (m, 6H, C_6H_3), 7.31 (H, ortho of SiHMePh of major isomers. ^{13}C NMR (toluene-d_8, −40 °C): δ 25.3−26.8 (*C*H_3 of ^{i}Pr of both isomers), 28.5 (*C*H of ^{i}Pr of both isomers), 81.2 (Cp of major isomer), 81.8 (Cp of minor isomer), 124.08 and 124.56 (NCH of both isomers), 122.9−130.5 (C_6H_3), 187.3 (Ru-*C*N2 of major isomer), 187.8 (Ru-*C*N2 of minor isomer). ^{29}Si NMR (^{1}H–^{29}Si HSQC, −40 °C): δ −4.2 (SiHMePh major isomer, ^1J(Si−H)Ru)) = 40.5 Hz, ^1J(Si−H of $SiHCH_3$) = 212.4 Hz), −7.38 (SiHMePh minor isomer).

[Cp(IPr)Ru(NCCH$_3$)(η^2-HSiCl$_3$)]BArF$_4$(VIII-13a) and CpRu(NCCH$_3$)(H)(SiCl$_3$)$_2$ (VIII-14)

Addition of $HSiCl_3$ (5.6 mg, 42 μmol) to 0.050 g (38 μmol) of $[Cp(IPr)Ru(NCCH_3)_2]BArF_4$ in 0.5 mL of CD_2Cl_2 at −78 °C followed by warming to −30 °C resulted in clean formation of $[Cp(IPr)Ru(NCCH_3)(\eta^2\text{-}HSiCl_3)]BArF_4$. Warming this sample to room temperature generated a mixture of three hydride species, the main of which is tentatively assigned the structure $CpRu(NCCH_3)(H)(SiCl_3)_2$. Significant dissociation of the imidazolium ion characterized by the imidazole proton peak at 8.58 ppm in the ^1H NMR spectra was also noticed. 5a: ^1H NMR (−40 °C, CD_2Cl_2): δ −7.81 (s + satelite, ^1J(Si−H) = 64.4 Hz, RuH), 0.97 (d, ^3J(H−H) = 6.7 Hz, 3H, C*H*$_3$ of ^{i}Pr), 1.09 (d, ^3J(H−H) = 7.5 Hz, 3H, C*H*$_3$ of ^{i}Pr), 1.10 (d, ^3J(H−H) = 7.5 Hz, 3H, C*H*$_3$ of ^{i}Pr), 1.21 (d, ^3J(H−H) = 6.7 Hz, 3H, C*H*$_3$ of ^{i}Pr), 1.22 (d, ^3J(H−H) = 6.7 Hz, 3H, C*H*$_3$ of ^{i}Pr), 1.38 (d, ^3J(H−H) = 6.8 Hz, 3H, C*H*$_3$ of ^{i}Pr), 1.47 (d, ^3J(H−H) = 6.8 Hz, 3H, C*H*$_3$ of ^{i}Pr), 1.49 (d, ^3J(H−H) = 7.5 Hz, 3H, C*H*$_3$ of ^{i}Pr), 1.90 (s, NCCH3), 2.75 (m, 2H, C*H* of ^{i}Pr), 4.92 (s, 5H, Cp).

$CpRu(NCCH_3)(H)(SiCl_3)_2$ (VIII-14)

^1H NMR (−40 °C, CD_2Cl_2): δ −9.79 (s + satt, ^1J(Si−H) = 24.8 Hz, 1H, RuH), 2.30 (s, 3H, NCC*H*$_3$), 5.26 (s, 5H, Cp). ^1H NMR (23 °C, CD_2Cl_2): δ −9.65 (s, 1H, RuH), 2.37 (s, 3H, NCC*H*$_3$), 5.27 (s, 5H, Cp). ^{13}C NMR (23 °C, CD_2Cl_2): δ 4.5 ($NCCH_3$), 89.6 (s, Cp). ^{29}Si NMR (^1H−^{29}Si HSQC, 23 °C): δ 39.3 (^1J(Si−H) = 24.9 Hz).

Generation of $[Cp(IPr)Ru(NCCH_3)(\eta^2\text{-}HSiMeCl_2)]BArF_4$ (VIII-13b):

Reaction of 0.050 g (38 μmol) of $[Cp(IPr)Ru(NCCH_3)_2]BArF_4$ in 5 mL of CD_2Cl_2 at −40 °C with 4.7 mg (42 μmol) of $HSiMeCl_2$ yielded an equilibrium mixture of $[Cp(IPr)Ru(NCCH_3)(\eta^2\text{-}HSiMeCl_2)]BArF_4$,

[Cp(IPr)Ru(NCCH$_3$)$_2$]BArF$_4$, and another, yet unknown, hydride species formed in a 1:0.37:0.14 mol ratio. Addition of nine more equivalents of silane changed the ratio of [Cp(IPr)Ru(NCCH$_3$)(η^2-HSiMeCl$_2$)]BArF$_4$ and [Cp(IPr)Ru(NCCH$_3$)$_2$]BArF$_4$ to 1:0.39. The formation of imidazolium salt [HIPr]BArF$_4$ in 16% yield was also noticed.

[Cp(IPr)Ru(NCCH$_3$)(η^2-HSiMeCl$_2$)]BArF$_4$ (VIII-13c):

^{1}H NMR (−30 °C, CD_2Cl_2): δ −7.94 (1H, RuH), 0.85 (s, 3H, SiC*H*$_3$), 0.99 (br, 3H, C*H*$_3$ of ^{i}Pr), 1.07 (br, 3H, C*H*$_3$ of ^{i}Pr), 1.18 (br d, ^3J(H−H) = 7.2 Hz, 6H, C*H*$_3$ of ^{i}Pr), 1.26 (br d, ^3J(H−H) = 7.2 Hz, 6H, C*H*$_3$ of ^{i}Pr), 1.35 (br, 3H, C*H*$_3$ of ^{i}Pr), 1.38 (br, 3H, C*H*$_3$ of ^{i}Pr), 2.65 (br s, 1H, C*H* of ^{i}Pr), 2.37 (br s, 1H, C*H* of ^{i}Pr), 2.30 (br s, 2H, C*H* of ^{i}Pr), 4.74 (s, 5H, Cp), 7.41 (br, 4H, m- C_6H_3), 7.54 (br t, 3J(H− H) = 7.8 Hz, 2H, p- C_6H_3). ^{13}C NMR (−30 °C, CD_2Cl_2): δ 2.24 (NC*C*H$_3$), 4.63 (Si*C*H$_3$), 21.4 (*C*H$_3$ of ^{i}Pr), 22.2 (*C*H$_3$ of ^{i}Pr), 28.6 (*C*H of ^{i}Pr), 86.5 (Cp), 125.2 (N*C*H), 127.8 (m- C_6H_3), 130.0 (p- C_6H_3), 177.9 (N*C*CH$_3$), 207.7 (Ru-*C*N2). ^{29}Si NMR (^{1}H–^{29}Si HSQC): δ 56.6 ($SiMeCl_2$), ^1J(Si−H(Ru), 1D ^{29}Si INEPT+) = 49.9 Hz, ^1J(Si−H of SiH, 1D ^{29}Si INEPT+) = 206.6 Hz. The minor hydride species: ^{1}H NMR (−30 °C, CD_2Cl_2): δ −8.40 (1H, RuH), 0.03 (s, 3H, SiC*H*$_3$). 29Si NMR (^{1}H–^{29}Si HSQC): δ 41.1 ($SiMeCl_2$, coupling constant cannot be measured).

Generation of [Cp(IPr)Ru(NCCH$_3$)(η^2-HSiH$_2$Ph)] BArF$_4$ (VIII-13d):

Reaction of 0.050 g (38 μmol) of [Cp(IPr)Ru(NCCH$_3$)$_2$]BArF$_4$ in CD_2Cl_2 at −40 °C with 4.7 mg (42 μmol) of $PhSiH_3$ yielded a mixture of [Cp(IPr)Ru(NCCH$_3$)$_2$]BArF$_4$ and [Cp(IPr)Ru(NCCH$_3$)(η^2-HSiH$_2$Ph)]BArF$_4$ in a 1.15:1 mol ratio. Less than 10% of imidazolium salt was also formed. ^{1}H NMR

(−30 °C, CD_2Cl_2): δ −8.28 (1H, RuH), 1.06−1.27 (br m, 24H, C*H*$_3$ of ^{i}Pr), 2.09 (s, 3H, C*H*$_3$CN), 2.45 (br, C*H* of ^{i}Pr), 4.18 (s, 5H, Cp), 4.05 (d, ^{2}J(H−H) = 9.0 Hz, 1H, SiH_2), 4.33 (d, ^{2}J(H−H) = 9.0 Hz, 1H, SiH_2), 7.35 (s, 2H, NC*H* in ^{i}Pr). ^{13}C NMR (−30 °C, CD_2Cl_2): δ 4.8 (NC*C*H$_3$), 22.6 (*C*H$_3$ of ^{i}Pr), 25.9 (*C*H$_3$ of ^{i}Pr), 29.0 (*C*H of ^{i}Pr), 83.6 (Cp), 117.8 (N*C*CH$_3$), 126.0 (N*C*H), 125.6, 130.6, 135.2 (ortho, meta, and para C of SiH_2Ph). ^{29}Si NMR (^{1}H–^{29}Si HSQC): δ −23.4 (SiH_2Ph), ^{1}J(Si−H(Ru), 1D ^{29}Si INEPT+) = 50.9 Hz, ^{1}J(Si−H of SiH, 1D ^{29}Si INEPT+) = 208.4 and 211.0 Hz.

Generation of [Cp(IPr)Ru(NCCH$_3$)(η^2-HSiHMePh)]BArF$_4$ (VIII-13e)

Reaction of 0.050 g (38 μmol) of [Cp(IPr)Ru(NCCH$_3$)$_2$]BArF$_4$ with 5.7 mg (42 μmol) of H_2SiMePh in CD_2Cl_2 at −40 °C resulted in an equilibrium between the starting compound, silane, and two isomers of [Cp(IPr)Ru(NCCH$_3$)(η^2-HSiHMePh)]BArF$_4$ (formed in a 1:2 ratio). At −40 °C, the ratio of [Cp(IPr)Ru(NCCH$_3$)$_2$]BArF$_4$ to [Cp(IPr)Ru(NCCH$_3$)(η^2-HSiHMePh)]BArF$_4$ was 10:1. Major isomer. ^{1}H NMR (−30 °C, CD_2Cl_2): δ −8.39 (1H, RuH), 0.36 (SiC*H*$_3$), 3.83 (Si*H*), 4.30 (s, 5H, Cp). ^{29}Si NMR (^{1}H–^{29}Si HSQC): δ 0.4 (^{1}J(Si−H(Ru), 1D ^{29}Si INEPT+) = 46.2 Hz, ^{1}J(Si−H of SiH, 1D ^{29}Si HSQC 1D JC) = 207.4 Hz. Minor isomer. ^{1}H NMR (−30 °C, CD_2Cl_2): δ −8.15 (1H, RuH), 0.61 (SiC*H*$_3$), 4.14 (Si*H*), 4.16 (s, 5H, Cp). ^{29}Si NMR (^{1}H–^{29}Si HSQC): δ −2.5 (^{1}J(Si−H (Ru), 1D ^{29}Si INEPT+) = 46.1 Hz, ^{1}J(Si−H of SiH, 1D ^{29}Si HSQC 1D JC) = 195.2 Hz.

[IPrH][CpRuCl(H)(SiCl$_3$)$_2$] (VIII-12):

Two equivalents of $HSiCl_3$ were added by syringe to a precooled (−30 °C) solution of 0.050 g (0.085 mmol) of Cp(IPr)RuCl in 5 mL of toluene. The mixture was charged with hexanes and kept at −30 °C to result in crystallization of compound

10. Yield: 0.057 g (0.067 mmol, 82%). IR (Nujol): ν(Ru−H) = 2012 cm^{-1}. NMR spectra were taken on a Bruker DPX-400 spectrometer: ^{1}H NMR (400 MHz, $CDCl_3$): δ −10.59 (1H, RuH), 5.20 (s, 5H, Cp). ^{13}C NMR (100.1 MHz, $CDCl_3$): δ 88.7 (Cp). ^{29}Si NMR (H−Si HSQC): δ −10.7 (Si*H*), ^{1}J(Si−H(Ru), 1D ^{29}Si INEPT+)) = 14.5 Hz. Anal. Calcd for $C_{32}H_{45}RuN_2Cl_7Si$ (825.35): C, 46.53; H, 5.25; N, 3.39. Found: C, 46.44; H, 5.86; N, 3.23.

XI.3 Syntheses of ruthenium (II) complexes supported by thiourea ligands.

[CpRu(IPr=S)]PF_6:

To a solution of 0.5 g (1.15mmol) of [CpRu($NCCH_3$)$_3$]PF_6 in 10mL of dichloromethane was added 0.45 g (1.15 mmol) IPr=S ligand. The mixture was stirred at room temperature for 30m. All volatiles were removed under high vacuum to yield the yellow [CpRu(IPr=S)]PF_6 crude product. This product was then recrystallized from a mixture of dichloromethane and hexane (4:1 v/v) to yield analytically pure CpRu(IPr=S)PF_6, which is characterized by NMR, IR and EA.

^{1}H NMR (600 MHz, CD_2Cl_2): δ 1.17 (s, 6H, C*H*$_3$ of ^{i}Pr), 1.27 (s, 18H, C*H*$_3$ of ^{i}Pr), 2.52 (s, 2H, C*H* of ^{i}Pr), 2.70 (s, 2H, C*H* of ^{i}Pr), 5.53 (s, 5H, Cp), 7.32 (d, 2H, NC*H*), 6.27 (d, 3H, η^3 of C_6H_3), 7.32 (d, 2H, C_6H_3), 7.51 (s, 1H, C_6H_3). ^{13}C NMR (151 MHz, CD_2Cl_2): 23.3 (*C*H$_3$ of ^{i}Pr), 23.6 (*C*H$_3$ of ^{i}Pr), 24.4 (*C*H$_3$ of ^{i}Pr), 24.5 (*C*H$_3$ of ^{i}Pr), 28.5 (*C*H$_3$ of ^{i}Pr), 29.5 (*C*H of ^{i}Pr), 82.1 (Cp), 84.3 (Cp), 109.7 (*pC*- η^3-C_6H_3), 112.4 (*mC*- η^3-C_6H_3), 120.2 (*oC*- η^3-C_6H_3), 124.9 (N*C*H), 130.9 (*mC*-C_6H_3), 133.9 (*pC*-C_6H_3), 146.8 (*oC*-C_6H_3), 167.0 (Ru-S*C*N2). Anal. Calcd for $C_{32}H_{41}RuSPF_6N_2$ (731.78): C, 52.52; H, 5.65; N, 3.83. Found: C, 52.40; H, 5.67; N, 3.73.

[CpRu(IMes=S)]PF_6

To a solution of 0.75 g (1.73mmol) of [CpRu($NCCH_3$)$_3$]PF_6 in 10mL of dichloromethane was added 0.58 g (1.15 mmol) IMes=S ligand. The mixture was stirred at room temperature for 24h. All volatiles were removed under high vacuum to yield the yellow CpRu(IMes=S)PF_6 crude product. Then the product was then recrystallized from a mixture of dichloromethane and hexane (4:1 v/v) to yield the analytically pure CpRu(IMes=S)PF_6, which is characterized by NMR, IR, and EA. Anal. Calcd for $C_{26}H_{29}RuSPF_6N_2$ (647.62): C, 48.22; H, 4.51; N, 4.33.

CpRu(IMes(-1)=S)PF_6

To a solution of 0.75 g (1.73mmol) of [CpRu($NCCH_3$)$_3$]PF_6 in 10mL of dichloromethane was added 0.35 g (1.15 mmol) IMes(-1)=S ligand. The mixture was stirred at room temperature for 24h. All volatiles were removed under high vacuum to yield the yellow crude product. Then the product was then recrystallized from a mixture of dichloromethane and hexane (4:1 v/v) to yield analytically pure CpRu(IMes(-1)=S)PF_6, which is characterized by NMR. Anal. Calcd for $C_{24}H_{25}RuSPF_6N_2$ (620.04): C, 46.53; H, 4.07; N, 4.52.

CpRu(ItBu=S)($NCCH_3$)$_2$$PF_6$

To a solution of 0.75 g (1.73mmol) of [CpRu($NCCH_3$)$_3$]PF_6 in 10mL of dichloromethane was added 0.24 g (1.15 mmol) ItBu=S ligand. The mixture was stirred at room temperature for 24h. All volatiles were removed under high vacuum to yield a yellow crude mixture of several products. Attempts to isolate the product failed, and the NMR characterization of the crude in CD_2Cl_2 showed a mixture of

several products which may be sulfur-bridged dimeric complexes. Further investigations need to be done to clarify the structures of the resulting complexes.

CpRu(IiPr=S)$(NCCH_3)_2PF_6$

To a solution of 0.75 g (1.73mmol) of $[CpRu(NCCH_3)_3]PF_6$ in 10mL of dichloromethane was added 0.21 g (1.15 mmol) IiPr=S ligand. The mixture was stirred at room temperature for 24 h. All volatiles were removed under high vacuum to yield a yellow crude mixture of several products. Several attempts to isolate the product failed, and the NMR characterization of the crude in CD_2Cl_2 showed the mixture of several products which may be sulfur-bridged dimeric complexes. Further investigations need to be done to clarify the structures of the resulting complexes.

CpRu(IPr=S)$(pyr)_2PF_6$

To a solution of 1.0 g (1.8 mmol) of $[CpRu(pyr)_3]PF_6$ in 10mL of dichloromethane was added 0.7 g (1.15 mmol) IPr=S ligand. The mixture was stirred at room temperature for 24h. All volatiles were removed under high vacuum to yield the yellow $[CpRu(IPr=S)(pyr)_2]PF_6$ crude product. This product was then recrystallized from a mixture of dichloromethane and hexane (4:1 v/v) to yield the analytically pure $[CpRu(IPr=S)(pyr)_2]PF_6$, which is characterized by NMR, IR.

XI.4 Catalytic reactions mediated by ruthenium complexes bearing Cp'/L fragments.

XI.4.1 General Procedure

General procedure for the reduction of nitriles, N-heterocycles, ketones by hydrosilylation process

Stock solutions of catalysts in CH_2Cl_2 were prepared separately before use. In a glovebox, a NMR tube equipped with D_2O insert was charged with cat (5 mol%), 0.1 mmol of substrates and (0.14 mol) of silane in CH_2Cl_2 (0.6 mL in total). The progress of the reaction was monitored by ^1H NMR.

General procedure for the reduction of nitriles by transfer hydrogenation using IPA

Stock solutions of catalysts in IPA and KOBut in IPA were prepared separately before use. In a glovebox, a 10 mL, flame-dried Schlenk tube equipped with a magnetic stirring bar was charged with 3 (0.5 mol %), nitrile (0.8 mmol) and KOBut (1.5 mol%) in IPA (4 mL). The Schlenk flask was brought out of the glovebox and equipped with a condenser under N_2 atmosphere. The progress of the reaction was monitored by NMR spectroscopy at 70 °C. The imine $RCH_2N\text{-}C(CH_3)_2$ was obtained as the major product. After the reaction was completed, the resulting solution was treated with aqueous HCl (1 M, 1.8 mL). Then the mixture was stirred for 1 h at room temperature to ensure the complete hydrolysis of imine. After the removal of volatiles under vacuum, 5 mL fresh water was added into solid residue to extract ammonium salts. The water solution of ammonium salts was then recrystallized with

(1 mL) addition of hexane (5:1 v/v) to yield corresponding ammonium microcrystal salts, which are analytically clean, as confirmed by NMR. The ammonium salt $[RCH_2NH_3]Cl$ was obtained as a pale yellow or brownish solid, depending on the nitrile used. The ammonium salt was converted to an amine by treatment with a 3 M NaOH solution (3 mL) in a 2 × 10 mL mixture of diethyl ether and water (2:1 v/v). The organic phase was separated and dried over $MgSO_4$.

General procedure for the reduction of N-heterocycles by transfer hydrogenation using IPA

In a glovebox, a 10 mL flame-dried Schlenk tube equipped with a magnetic stirring bar was charged with 3 (0.5 mol %), N-heterocycle (0.8 mmol), and KOBut (1.5 mol%) in IPA (4 mL). The Schlenk flask was brought out of the glovebox, equipped with a condenser under N_2 atmosphere and heated to 70 °C. The progress of the reaction was monitored by NMR spectroscopy and TLC. The reaction was stopped when the highest amount of the partially hydrogenated product was observed. After the removal of volatiles under vacuum, hexane was used to extract the product and the remaining substrate from the solid residue. The product was then isolated by chromatography on silica gel, using a mixture of hexane and ethyl acetate (4:1 v/v).

General Procedure for the Reduction of Olefins by transfer hydrogenation using IPA

In a glovebox, a 10 mL flame-dried Schlenk tube equipped with a magnetic stirring bar was charged with 3 (0.5 mol %), olefin (0.8 mmol), and KOBut (1.5 mol %) in IPA (4 mL). The Schlenk flask was brought out of the glovebox, equipped

with a condenser under N_2 atmosphere and heated to 70 °C. The progress of the reaction was monitored by NMR spectroscopy and TLC. The reaction was stopped when the highest amount of the hydrogenated products was observed. Then the reaction mixture was treated by two portions of a 10 mL mixture of diethyl ether and water (2:1 v/v). The organic phase was separated and dried over $MgSO_4$. In the case of ester substrates, the initially formed mixture of the starting ester (methyl or ethyl), reduced ester, and their isopropyl analogs, formed by the transesterification in IPA, was converted into the ethyl or methyl ester by transesterification with corresponding alcohol. For example, to convert a mixture of isopropyl butyrate and ethyl butyrate into ethyl butyrate, an excess amount of ethanol was added with a drop of H_2SO_4, and the mixture was refluxed for 2 h, followed by a standard workup.

General Procedure for H/D exchange reaction of N-heterocycles using C_6D_6 as deuterium source

Stock solutions of catalysts were prepared in C_6D_6 before use. In a glovebox, a NMR tube (with ferrocene insert in C_6D_6 as standard) was charged with 0.1 mol% cat, 0.1 mmol of substrates in C_6D_6 (0.5 mL in total). Deuteration degree was monitored by ^1H NMR at 50ºC. The deuterated solid substrate was simply isolated by the removal of volatiles under vacuum. If the substrates are liquid, then the deuterated substrates can be separated from the benzene-based mixture by liquid/ liquid distillation.

General procedure for HDF reaction of fluorinated aromatic and aliphatic compounds using IPA

A stock solution of catalyst was prepared in IPA before use. In a glovebox, a

NMR tube (with ferrocene insert in C_6D_6 as a standard) was charged with 0.5 mol % catalyst, 0.36 mmol of the substrate, 1.2 eq (0.43 mmol or 45.7 mg) of Na_2CO_3, in IPA with a total solvent volume of 0.7 mL. The yield and conversion of reaction were monitored by both ^1H and ^{19}F NMR spectroscopy.

XI.4.2 Hydrosilylation of C=O, C=N bonds.

Hydrosilylation of benzaldehyde:

A stock solution of $[Cp(IPr)Ru(NCCH_3)_2]BArF_4$ was prepared in CD_2Cl_2 before use. In a NMR tube with the sealed cap and a ferrocene insert, 0.14 mmol of silane, 0.1 mmol (10 μL) of benzaldehyde, 100μL of catalyst stock solution (5 mol %) and 0.5 mL of CD_2Cl_2 was added. After 2h at room temperature, the reaction yield was determined by ^1H NMR at room temperature.

Hydrosilylation of benzonitrile:

A stock solution of $[Cp(IPr)Ru(NCCH_3)_2]BArF_4$ was prepared in CD_2Cl_2 before use. In a NMR tubes with the sealed cap and a ferrocene insert, 0.14 mmol of silane, 0.1 mmol of (10 μL) benzonitrile, 100μL of catalyst stock solution (5 mol %) and 0.5 mL of CD_2Cl_2 was added. The reaction mixture was heated at 50°C for 3h, and the yield was determined by ^1H NMR spectroscopy.

Hydrosilylation of pyridine:

A stock solution of $[Cp(IPr)Ru(NCCH_3)_2]BArF_4$ was prepared in CD_2Cl_2 before use. In a NMR tube with the sealed cap and a ferrocene insert, 0.14 mmol of silane, 0.1 mmol of pyridine (8 μL), 100μL of catalyst stock solution (5 mol %) and 0.5 mL of CD_2Cl_2 was added. The reaction mixture was heated at 50°C for 2h, and

the yield was determined by ^{1}H NMR spectroscopy.

XI.4.3 Transfer hydrogenation of C=O bonds

Transfer hydrogenation of acetophenone:

Stock solutions of [Cp(IPr)Ru(pyr)$_2$]PF$_6$ and KO^{t}Bu were prepared in IPA before use. In a NMR tube equipped with the sealed cap and an ferrocene insert was charged 0.1 mmol (11.7 μL) acetophenone, 5 μL (up to 100 μL depended on the catalyst loading) of catalyst stock solution (to have 0.05 to 1 mol %), 5 μL (up to 50 μL depended on mol/mol ratios between KO^{t}Bu and cat) of KO^{t}Bu stock, and an additional fresh IPA with the total amount of IPA equal to 0.7 mL. The reaction mixture in NMR tube was placed inside a Bruker DPX- 600 NMR spectrometer preheated to a certain temperature; and the yield was determined by ^{1}H NMR spectroscopy.

Transfer hydrogenation of imines and ketimines:

NMR scale: Stock solutions of cats and KO^{t}Bu were prepared in IPA before use. In a NMR tube equipped with the sealed cap and an D_2O insert was charged 0.1 mmol imine (or ketimine), 50 μL of catalyst stock solution (to have 0.5 mol %), 150 μL (KOtBu/cat equal to 3:1 mol/mol ratio) of KO^{t}Bu stock, and an additional fresh IPA with the total amount of IPA equal to 0.7 mL. The reaction mixture in NMR tube was placed inside a Bruker DPX- 600 NMR spectrometer preheated to a certain temperature; and the yield was determined by ^{1}H NMR spectroscopy.

Large scale: mentioned in the general procedure.

No large scale synthesis for imines and ketimines was performed due to the low

yields of the reactions.

Transfer hydrogenation of N-heterocycles:

NMR scale: Stock solutions of cats and KO^{t}Bu were prepared in IPA before use. In a NMR tube equipped with the sealed cap and a D_2O insert was charged 0.1 mmol N-heterocycle, 50 μL of catalyst stock solution (to have 0.5 mol %), 150 μL (KOtBu/ cat equal to 3:1 mol/mol ratio) of KO^{t}Bu stock, and an additional fresh IPA with the total amount of IPA equal to 0.7 mL. The reaction mixture in NMR tube was placed inside a Bruker DPX- 600 NMR spectrometer preheated to a certain temperature; and the yield was determined by ^{1}H NMR spectroscopy.

Large scale and work up: mentioned in the general procedure.

Spectra of several isolated products from the TH of N-heterocycle was showed in the Appendix

XI.4.4 Transfer hydrogenation of C≡N bonds.

Transfer hydrogenation of benzonitrile:

Stock solutions of cats and KO^{t}Bu were prepared in IPA before use. In a NMR tube equipped with the sealed cap and a ferrocene insert was charged 0.1 mmol (10.3 μL) benzonitrile, 5 μL (up to 50 μL depending on the catalyst loading) of catalyst stock solution (to have 0.05 to 0.5 mol %), 5 μL (up to 25 μL depending on mol/mol ratios between KO^{t}Bu and cat) of KO^{t}Bu stock, and an additional fresh IPA with the total amount of IPA equal to 0.7 mL. The reaction mixture in NMR tube was placed inside a Bruker DPX- 600 NMR spectrometer preheated to a certain temperature; and the yield was determined by ^{1}H NMR spectroscopy.

Transfer hydrogenation of nitriles:

NMR scale: Stock solutions of $[Cp(IPr)Ru(pyr)_2]PF_6$ and KO^tBu were prepared in IPA before use. In a NMR tube equipped with the sealed cap and a ferrocene, insert was charged 0.1 mmol nitrile, 50 μL of catalyst stock solution (0.5 mol %), 15 μL of KO^tBu stock, and an additional fresh IPA with the total amount of IPA equal to 0.7 mL. The reaction mixture in NMR tube was heated in an oil bath at a certain temperature; and after a certain period of time, the yield was determined by ^1H NMR spectroscopy.

Large scale: mentioned in the general procedure.

Spectra of several isolated products from the TH of nitriles are included in the Appendix.

Transfer hydrogenation of olefins:

NMR scale: Stock solutions of $[Cp(IPr)Ru(pyr)_2]PF_6$ and KO^tBu were prepared in IPA before use. In a NMR tube equipped with the sealed cap and a ferrocene insert was charged 0.1 mmol olefins, 50 μL of catalyst stock solution (0.5 mol %), 15 μL of KO^tBu stock, and an additional fresh IPA with the total amount of IPA equal to 0.7 mL. The reaction mixture in NMR tube was heated in an oil bath at a certain temperature; and after a certain period of time, the yield was determined by ^1H NMR spectroscopy.

No large scale synthesis was performed for non-activated olefins

Transfer hydrogenation of conjugated olefins:

NMR scale: Stock solutions of $[Cp(IPr)Ru(pyr)_2]PF_6$ and KO^tBu were prepared in

IPA before use. In a NMR tube equipped with the sealed cap and a ferrocene insert was charged 0.1 mmol olefins, 50 μL of catalyst stock solution (0.5 mol %), 15 μL of KO^{t}Bu stock, and an additional fresh IPA with the total amount of IPA equal to 0.7 mL. The reaction mixture in NMR tube was heated in an oil bath at a certain temperature; and after a certain period of time, the yield was determined by ^{1}H NMR spectroscopy.

Large scale: mentioned in the general procedure.

Spectra of several isolated products from the TH of conjugated olefins are included in the Appendix

XI.4.5 H/D exchange

NMR scale: Stock solutions of trihydride cats were prepared in C_6D_6 before use. In a NMR tube equipped with the sealed cap and a ferrocene insert was charged 0.1 mmol substrate, 100 μL of catalyst stock solution (0.1 mol %), and an additional fresh C_6D_6 with the total amount of C_6D_6 equal to 0.5 mL. The reaction mixture in NMR tube was heated in an oil bath at a certain temperature; and after a certain period of time, the degree of deuteration was determined by ^{1}H NMR spectroscopy.

The progress of deuteration for some substrates is included in the Appendix.

XI.4.6 HDF of fluorinated compounds.

NMR scale: Stock solutions of cats were prepared in IPA before use. In a NMR tube equipped with the sealed cap and a ferrocene insert was charged 0.36 mmol substrate, 100 μL of catalyst stock solution (0.5 mol %), 1.2 eq (0.43 mmol or 45.7 mg) of Na_2CO_3 and an additional fresh IPAwith the total amount of IPA equal to 0.5 mL. The reaction mixture in NMR tube was heated in an oil bath at a certain temperature;

and after a certain period of time, the yield of the HDF reaction was monitored by both ^{1}H and ^{19}F NMR spectroscopy.

The progress of the HDF reaction for several substrates is included in the Appendix.

XI.4.7 TH with ammonium formate as hydrogen donor.

NMR scale: Stock solutions of catalysts and ammonium formate were prepared in methanol before use. In a NMR tube equipped with the sealed cap and a ferrocene insert was charged 0.05 mmol substrate, 100 μL of catalyst stock solution (1 mol %), 4 eq (0.2 mmol or 25μL of stock solution) of NH_4CO_2H and additional fresh methanol with the total amount of methanol equal to 0.7 mL. The reaction mixture in NMR tube was heated in an oil bath at a certain temperature; and after a certain period of time, the yield of the reaction was monitored by both ^{1}H and ^{19}F NMR spectroscopy for the fluorine-containing substrates.

The progress of the reaction for some substrates is included in the Appendix.

XI.5 Kinetic studies

XI.5.1 Kinetic studies of transfer hydrogenation.

Dependence of the Reaction Rate on Isopropanol.

In a glovebox, seven NMR samples were prepared each containing 0.5 mol % (0.527 mmol) of $Cp(IPr)RuH_3$ (from a stock solution in IPA), 1.5 mol% of KOBut (1.577 mmol, from a stock solution in PhCl), p-methoxy benzonitrile (105.1 mmol), and an additional amount of IPA with the total amount of IPA in the range of 10−40 equiv with respect to p-methoxy benzonitrile (250 μL, 105.1 mmol). For each sample, a timer was started when the sample was placed inside a Bruker DPX- 600 NMR spectrometer preheated to 70 °C, and ^{1}H NMR spectra were obtained every 5 min

for 1.5 h. The rate of the reaction was determined from the decrease of the MeO signal of p-methoxy benzonitrile in the ^{1}H NMR spectra as the reaction progressed. Under the pseudo-first-order conditions, the linearity of the plot of −ln-($[MePhCN]_t/[MePhCNe]_0$) versus time reveals that the reaction rate is first-order with respect to the substrate (Figures XII-1-XII-7). The slopes of the regression lines (k^{eff}) were then plotted versus the equivalents of IPA (Figure VI- 14). The reaction showed saturation behavior at high concentrations of IPA.

Dependence of the Reaction Rate on Base.

In a glovebox, five NMR samples were prepared, each containing 0.5 mol% of $Cp(IPr)RuH_3$ (1.577 mmol, from a stock solution in IPA), an additional amount of IPA up to the total amount of IPA of 112.5 μL (mmol), p-methoxybenzonitrile (105.1 mmol), and a variable amount of KOBut (from a stock solution in IPA) in the range 1.25−4 equiv with respect to catalyst . For each sample, a timer was started when the sample was placed inside a Bruker DPX-600 NMR spectrometer preheated to 70 °C, and ^{1}H NMR spectra were obtained every 5 min for 1.5 h. The rate of the reaction under the pseudo-first-order conditions was determined from the decrease of the MeO signal of pmethoxybenzonitrile in the ^{1}H NMR spectra as the reaction progressed (Figures XII-8- XII-13). The slopes of the regression lines (k^{eff}) were then plotted versus the equivalents of KOBut (Figure VIII-2).

XI.5.2 Kinetic studies of HDF reactions.

General procedure for kinetic study with the variation of IPA

A stock solution of catalyst was prepared in benzene before use. In a glovebox,

a series of 9 samples were prepared each containing 0.1 mol % (2.8 μmol) of catalyst **9** (from a stock solution in benzene), 1,2,3,4-tetrafluorobenzene (30μL, 0.28mmol), 1-fluorocyclohexane (10 μL as an internal standard for ^{19}F NMR spectra), 1.2 eq of Na_2CO_3 (0.34 mmol, 36 mg) and an additional amount of IPA with the total amount of IPA in the range of 10−40 equiv with respect to 1,2,3,4-tetrafluorobenzene (30μL, 0.28mmol), followed by the addition of more until a total volume of the sample is 1.2 mL. For each sample, a timer was started when the sample was placed inside the NMR spectrometer preheated to 75 °C and ^{19}F NMR spectra were obtained every 20 min for 7h. The rate of the reaction was determined by monitoring the decrease of the fluorine signal of 1,2,3,4-tetrafluorobenzene in the ^{19}F NMR spectra as the reaction progressed. Under pseudo-first-order conditions, the linearity of the plot of $-\ln([1,2,3,4C_6F_4H_2]_t/[1,2,3,4C_6F_4H_2]_0)$ versus time reveals that the reaction rate is first-order with respect to the substrate (Figure XII-19-XII-27, Appendix). The slopes of the regression lines (K^{eff}) were then plotted versus the equivalents of IPA (Figure IX-2), revealing saturation behavior at high concentrations (> 20 eq) of IPA.

General procedure for kinetic study with the variation of IPr

Stock solutions of catalyst and stock solution of IPr were prepared in benzene before use. In a glovebox, a series of 5 samples were prepared each containing 0.1 mol % (2.8 μmol) of catalyst **9** (from a stock solution in benzene), 1,2,3,4-tetrafluorobenzene (30 μL, 0.28 mmol), 1-fluorocyclohexane (10 μL as internal standard for ^{19}F NMR spectra), 1.2 equivalents of Na_2CO_3 (0.34 mmol, 36 mg), and IPA with the amount fixed at 30 equivalents with respect to 1,2,3,4-tetrafluorobenzene (30μL, 0.28mmol), and IPr (from the stock solution in benzene) with the amount of IPr in the range of 1 to 5 equiv with respect to catalyst **9**, followed

by the addition of more until a total volume of the sample is 1.2 mL. For each sample, a timer was started when the sample was placed inside the NMR spectrometer preheated to 75 °C and ^{19}F NMR spectra were obtained every 20 min for 7h. The rate of the reaction was determined from the decrease of the fluorine signal of 1,2,3,4-tetrafluorobenzene in the ^{19}F NMR spectra as the reaction progressed. Under the pseudo-first-order conditions, the linearity of the plot of $-\ln([1,2,3,4\text{-}C_6F_4H_2]_t/[1,2,3,4\text{-}C_6F_4H_2]_0)$ versus time reveals that the reaction rate is first-order with respect to the substrate (Figures XII-28- XII-32). The slopes of the regression lines ($1/1000*K^{eff}$) were then plotted versus the equivalents of IPA (Figure VI-8). The reaction showed the inversely proportional relationship between the amount of IPr and k^{eff}.

XII. Appendix.

XII.1 Kinetic studies

Kinetic sample preparation for TH of methoxy benzonitrile

Table XII- 1. Sample preparation for variation of isopropanol

Sample number	1	2	3	4	5	6	7
IPA ratios to substrate	10	15	20	25	30	35	40
IPA amount (µL)	75	112.5	150	187.5	225	262.5	300
Catalyst stock solution (µL)	100	100	100	100	100	100	100
Substrate stock (µL)	250	250	250	250	250	250	250
KOtBu stock in PhCl (µL)	5	5	5	5	5	5	5
Adding more PhCl fresh (µL)	225	187.5	150	112.5	75	42.5	5
Total (µL)	660	660	660	660	660	660	660

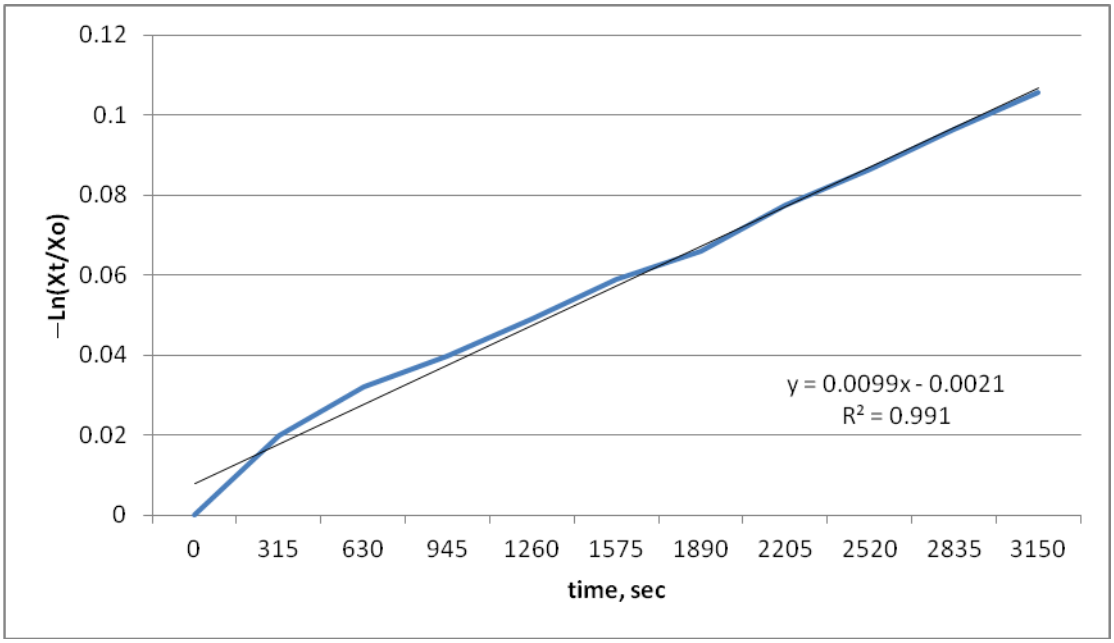

Figure XII- 1. Plot $-\ln([MePhCN]_t/[MePhCNe]_0)$ versus time under pseudo-first order conditions (10 equivs of IPA).

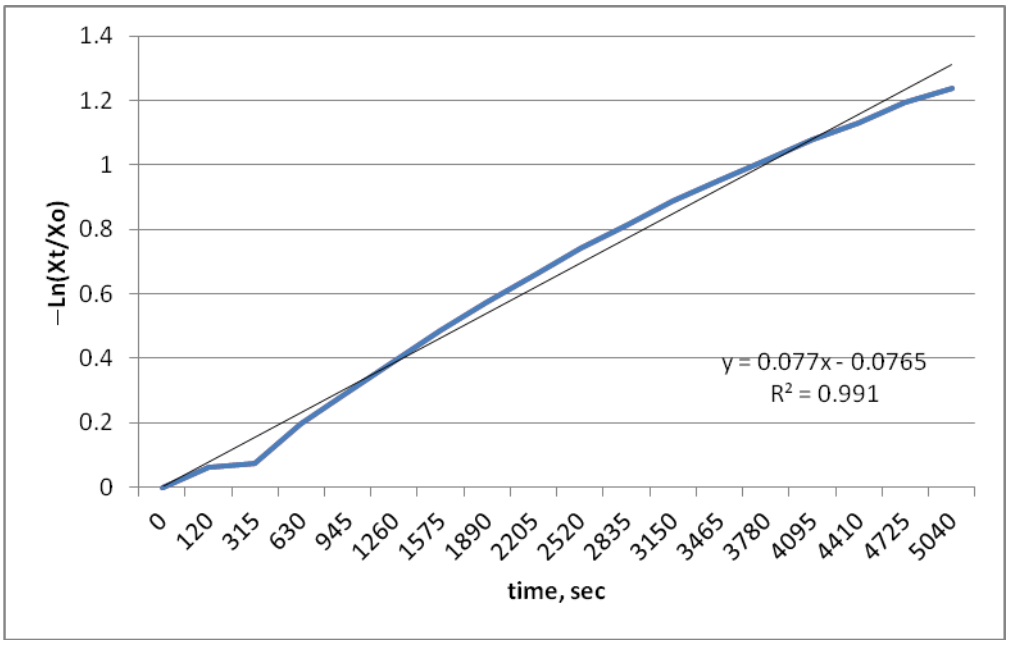

Figure XII- 2. Plot $-\ln([MePhCN]_t/[MePhCNe]_0)$ versus time under pseudo-first order conditions (15 equivs of IPA).

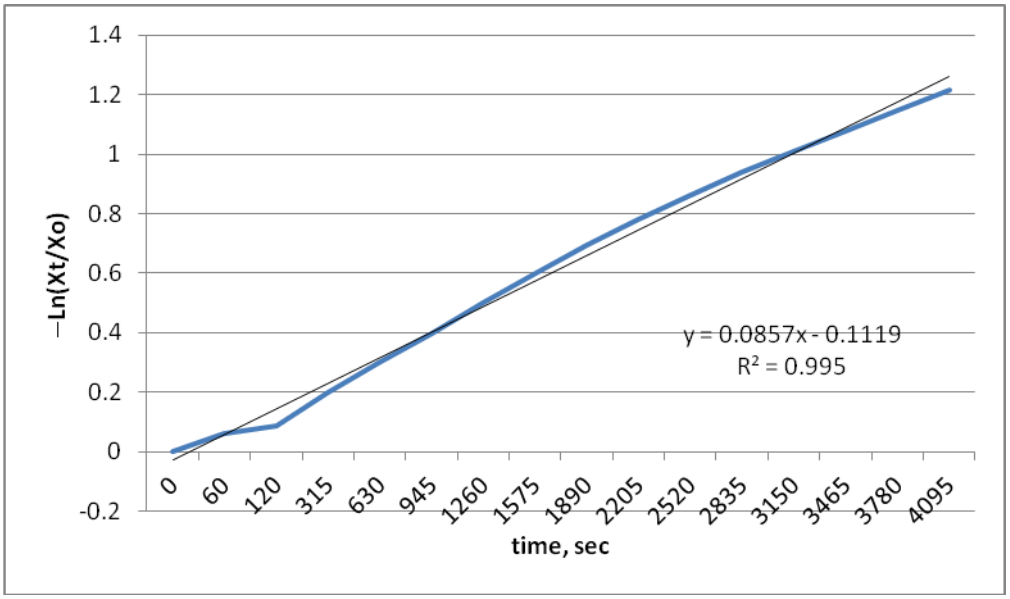

Figure XII- 3. Plot $-\ln([MePhCN]_t/[MePhCNe]_0)$ versus time under pseudo-first order conditions (20 equivs of IPA).

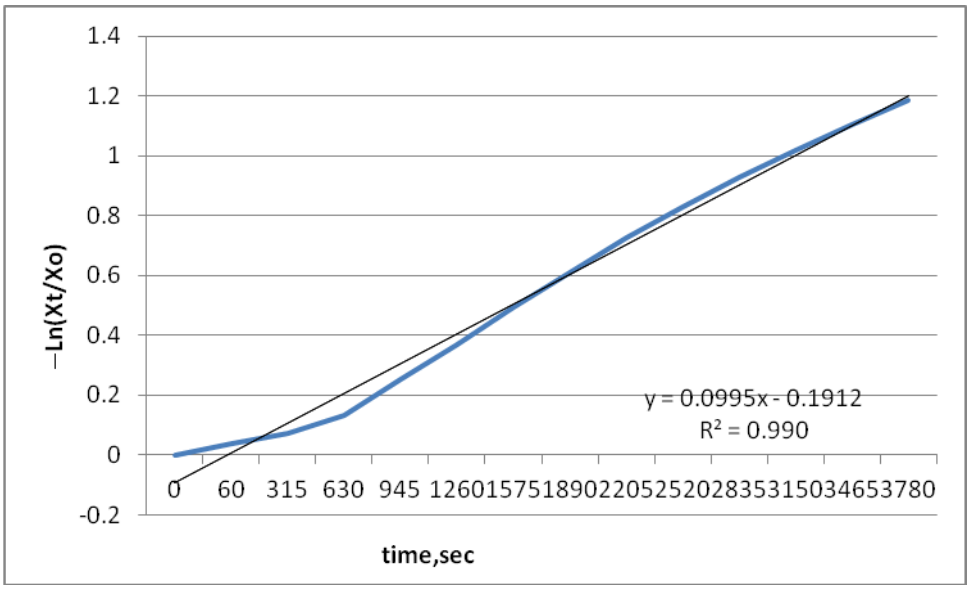

Figure XII- 4. Plot $-\ln([MePhCN]_t/[MePhCNe]_0)$ versus time under pseudo-first order conditions (25 equivs of IPA).

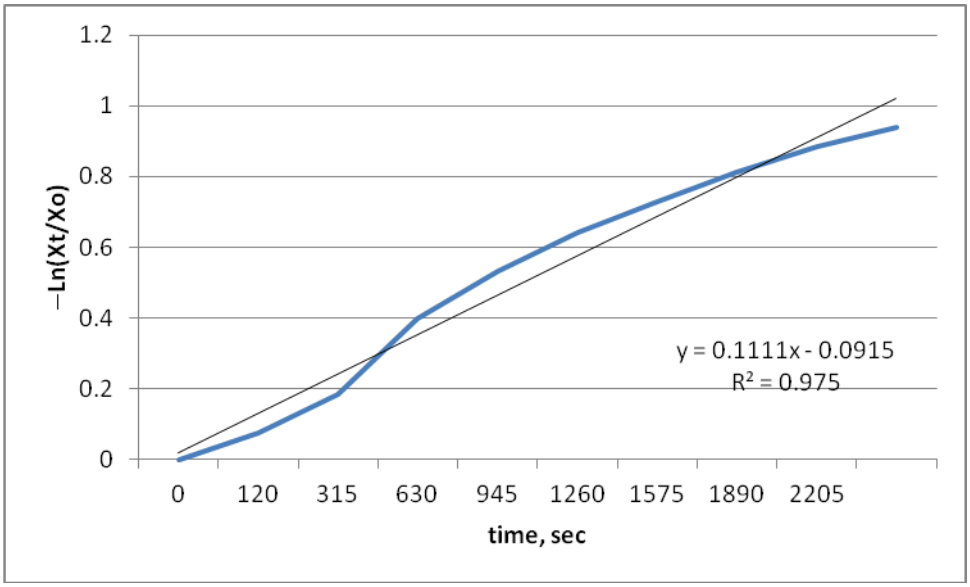

Figure XII- 5. Plot $-\ln([MePhCN]_t/[MePhCNe]_0)$ versus time under pseudo-first order conditions (30 equivs of IPA).

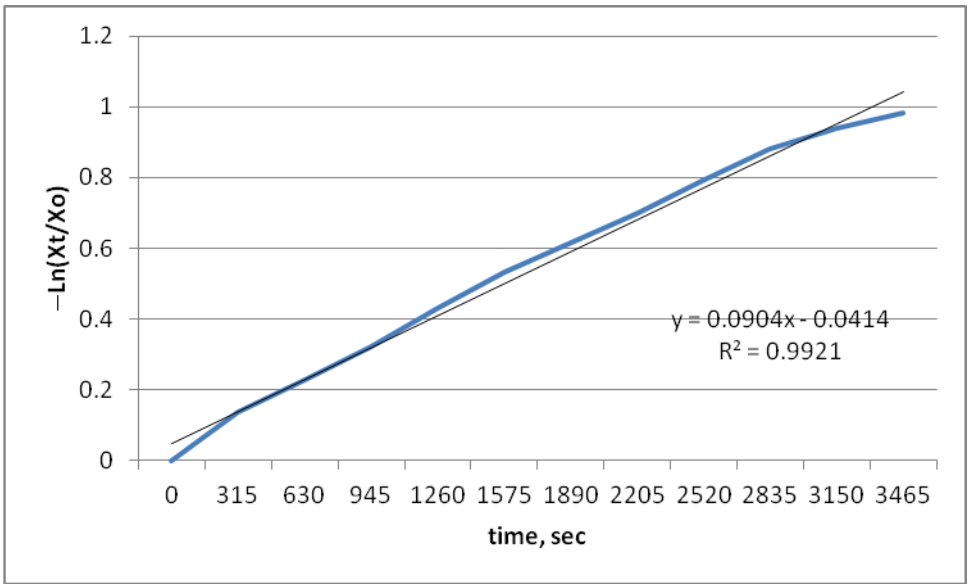

Figure XII- 6. Plot $-\ln([MePhCN]_t/[MePhCNe]_0)$ versus time under pseudo-first order conditions (35 equivs of IPA).

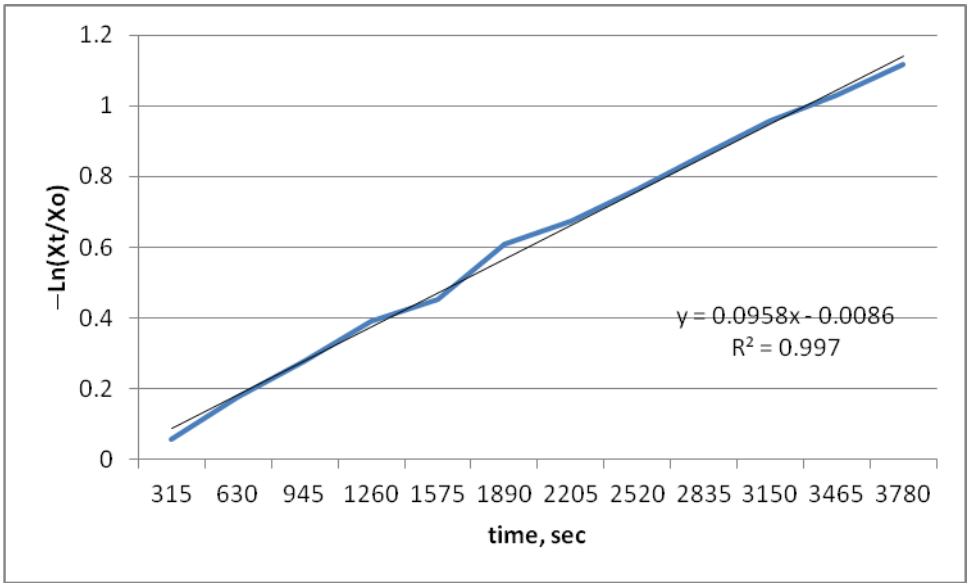

Figure XII- 7. Plot $-\ln([MePhCN]_t/[MePhCNe]_0)$ versus time under pseudo-first order conditions (40 equivs of IPA).

Table XII- 2. Sample preparation for variation of base

Sample number	1	2	3	4
Base ratio B:C	0.5	1.00	2.00	3.00
Catalyst stock solution (µL)	100	100	100	100
Substrate stock (µL)	250	250	250	250
$KOBu^t$ stock in IPA (µL)	5	10	20	30
Fresh IPA add more (µL)	107.5	102.5	92.5	82.5
PhCl added more (µL)	197.5	197.5	197.5	197.5
Total (µL)	660	660	660	660

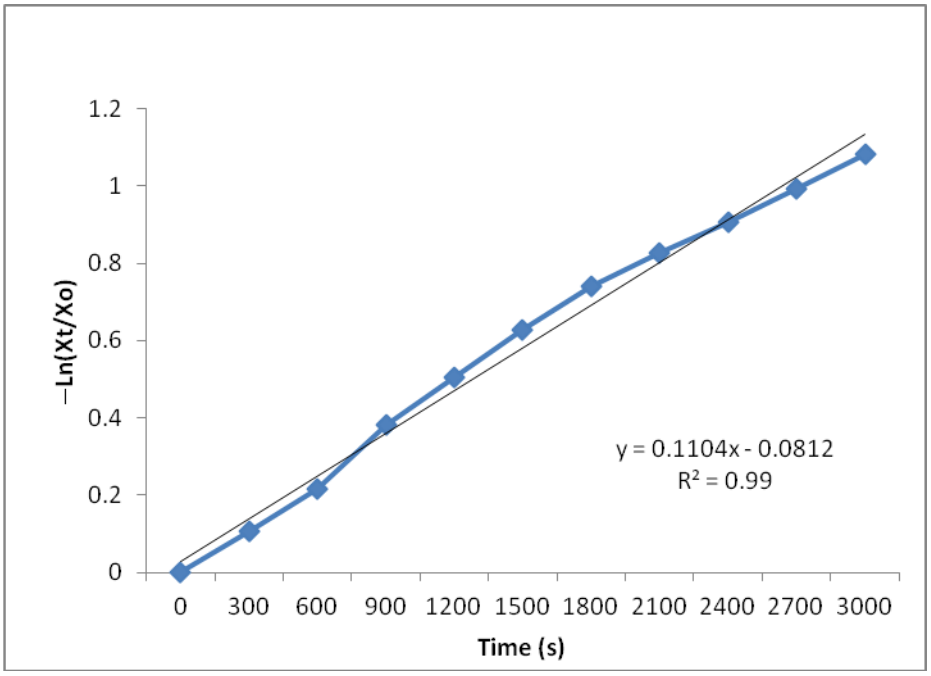

Figure XII- 8. Plot $-\ln([MePhCN]_t/[MePhCNe]_0)$ versus time under pseudo-first order conditions without added $KOBu^t$.

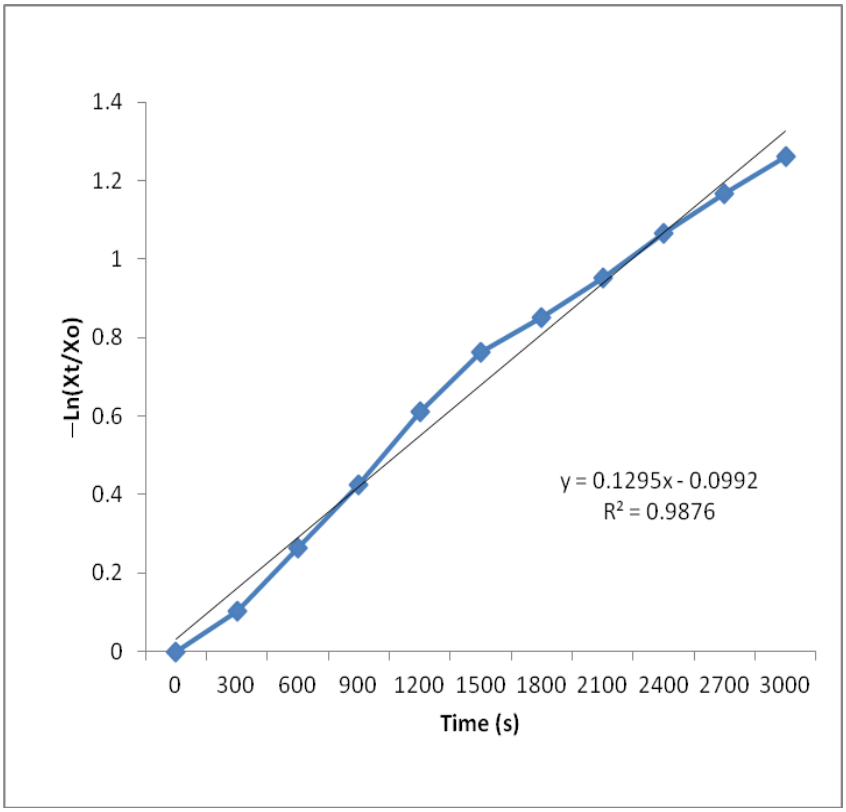

Figure XII- 9. Plot $-\ln([MePhCN]_t/[MePhCNe]_0)$ versus time under pseudo-first order conditions with 0.5 equiv of $KOBu^t$.

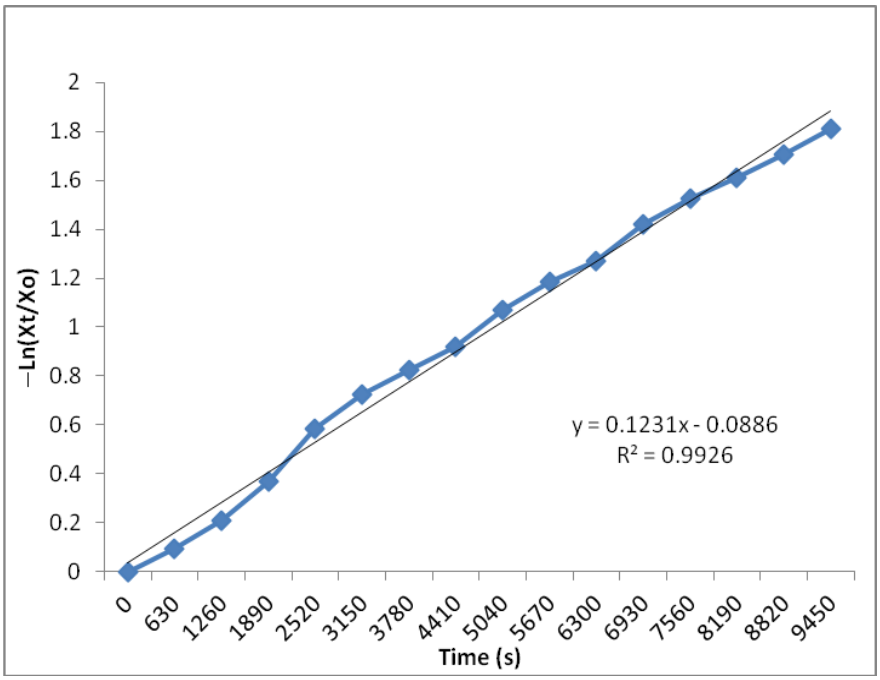

Figure XII- 10. Plot $-\ln([MePhCN]_t/[MePhCNe]_0)$ versus time under pseudo-first order conditions with 1 equiv of $KOBu^t$.

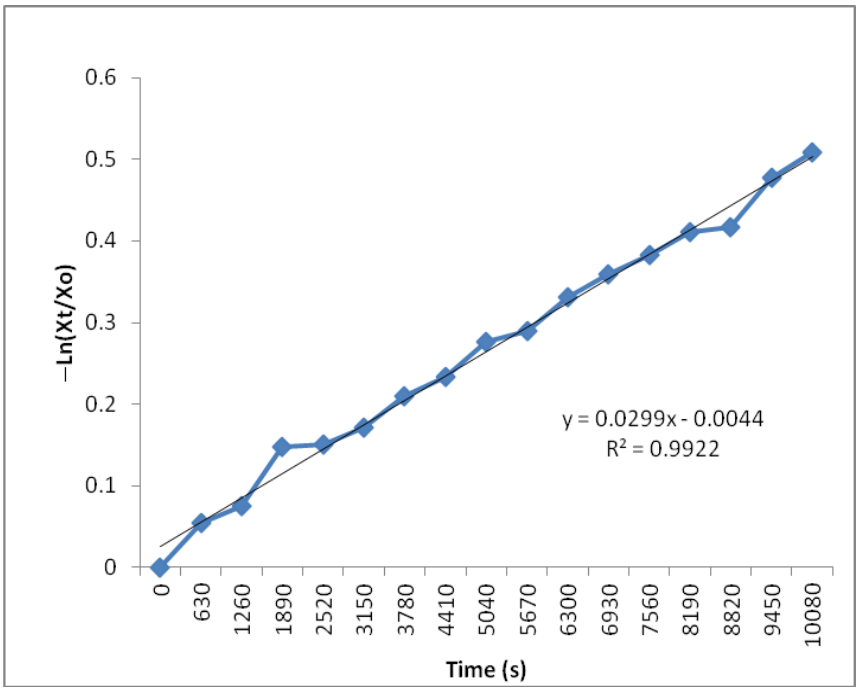

Figure XII- 11. Plot $-\ln([MePhCN]_t/[MePhCNe]_0)$ versus time under pseudo-first order conditions with 2 equiv of $KOBu^t$.

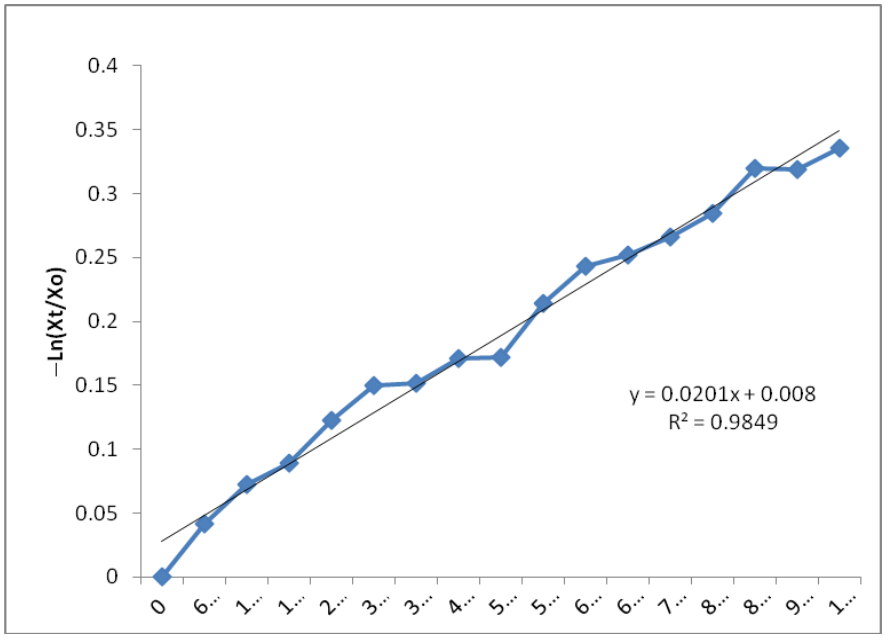

Figure XII- 12. Plot $-\ln([MePhCN]_t/[MePhCNe]_0)$ versus time under pseudo-first order conditions with 3 equiv of $KOBu^t$.

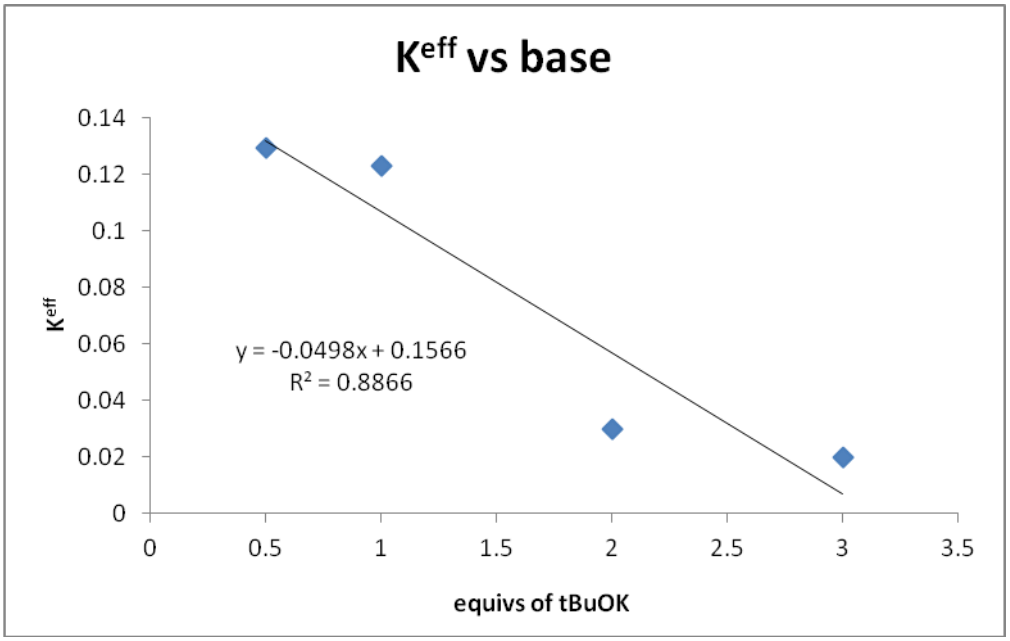

Figure XII- 13. The dependence of reaction rate on the amount of $KOBu^t$.

Kinetic sample preparation for HDF of 1,2,3,4 tetrafluorobenzene with IPA varations

Table XII- 3. IPA variations

IPA equi	10	15	20	25	30	35	40	8	22.5
Sample number (µL)	1	2	3	4	5	6	7	8	9
Stock of cat in benzene (µL)	100	100	100	100	100	100	100	100	100
IPA fresh (µL)	214 .16	321 .24	428 .32	535 .41	642 .49	749 .57	856 .65	171 .33	481 .87
Subtrate (µL)	30	30	30	30	30	30	30	30	30

Cyclohexane (µL)	10	10	10	10	10	10	10	10	10
benzen fresh(µL)	845.84	738.76	631.68	524.59	417.51	310.43	203.35	888.67	578.13
Total (µL)	1200	1200	1200	1200	1200	1200	1200	1200	1200
$NaCO_3$(mg)	29.66	29.66	29.66	29.66	29.66	29.66	29.66	29.66	29.66

K_{eff} vs IPA

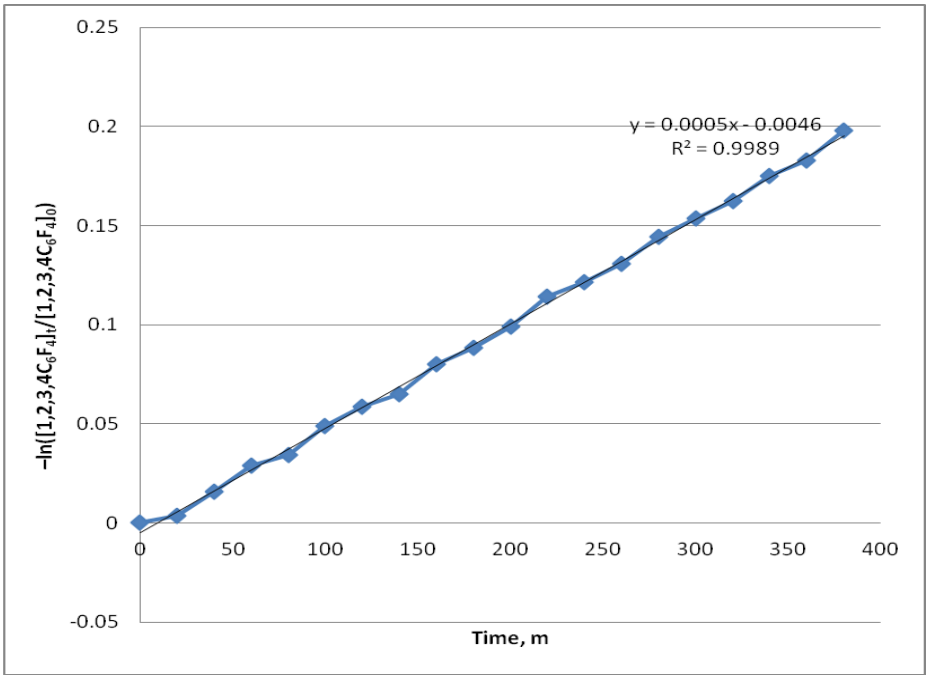

Figure XII- 14. Plot $-\ln([1,2,3,4C_6F_4]_t/[1,2,3,4C_6F_4]_0)$ versus time under pseudo-first order conditions (8 equivs of IPA)

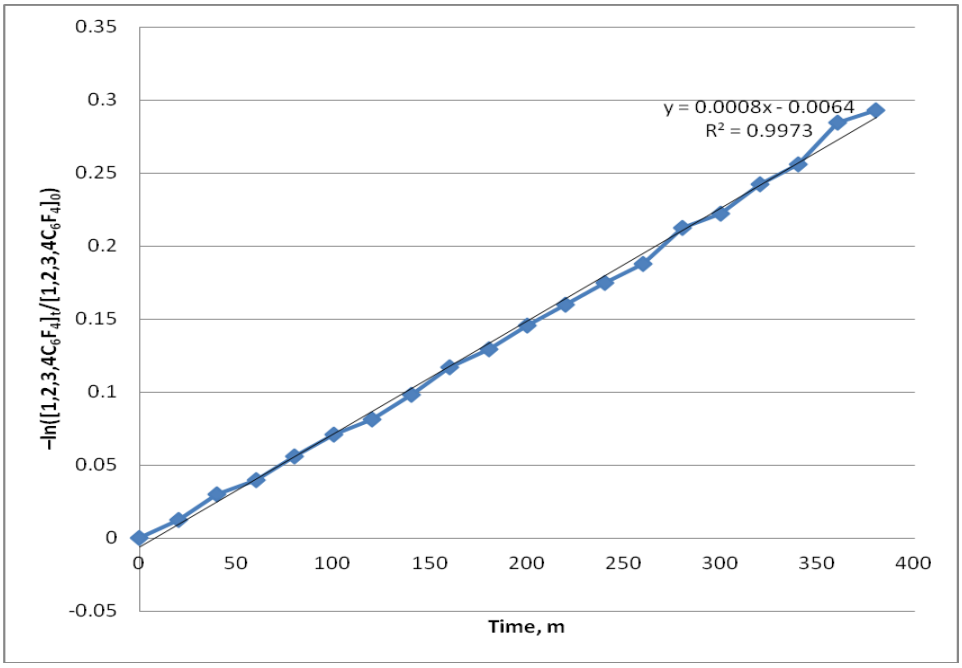

Figure XII- 15. Plot $-\ln([1,2,3,4C_6F_4]_t/[1,2,3,4C_6F_4]_0)$ versus time under pseudo-first order conditions (10 equivs of IPA)

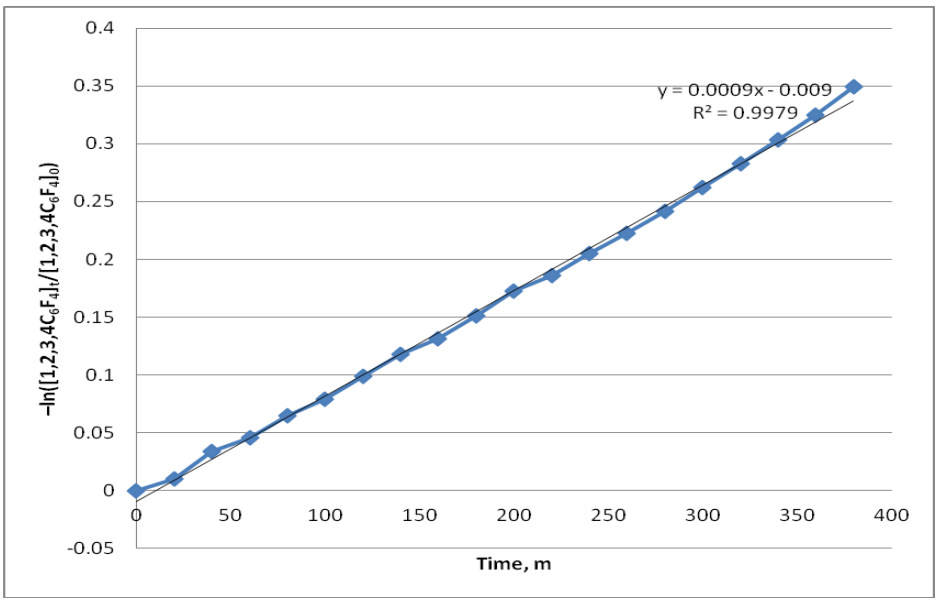

Figure XII- 16. Plot $-\ln([1,2,3,4C_6F_4]_t/[1,2,3,4C_6F_4]_0)$ versus time under pseudo-first order conditions (15 equivs of IPA)

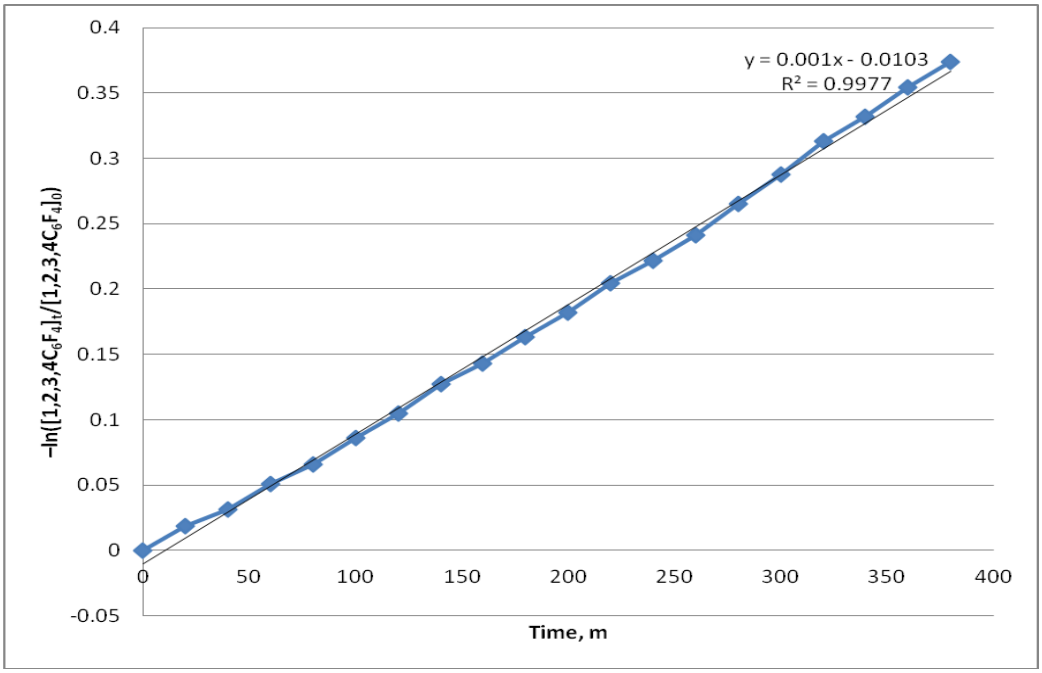

Figure XII- 17. Plot $-\ln([1,2,3,4C_6F_4]_t/[1,2,3,4C_6F_4]_0)$ versus time under pseudo-first order conditions (20 equivs of IPA)

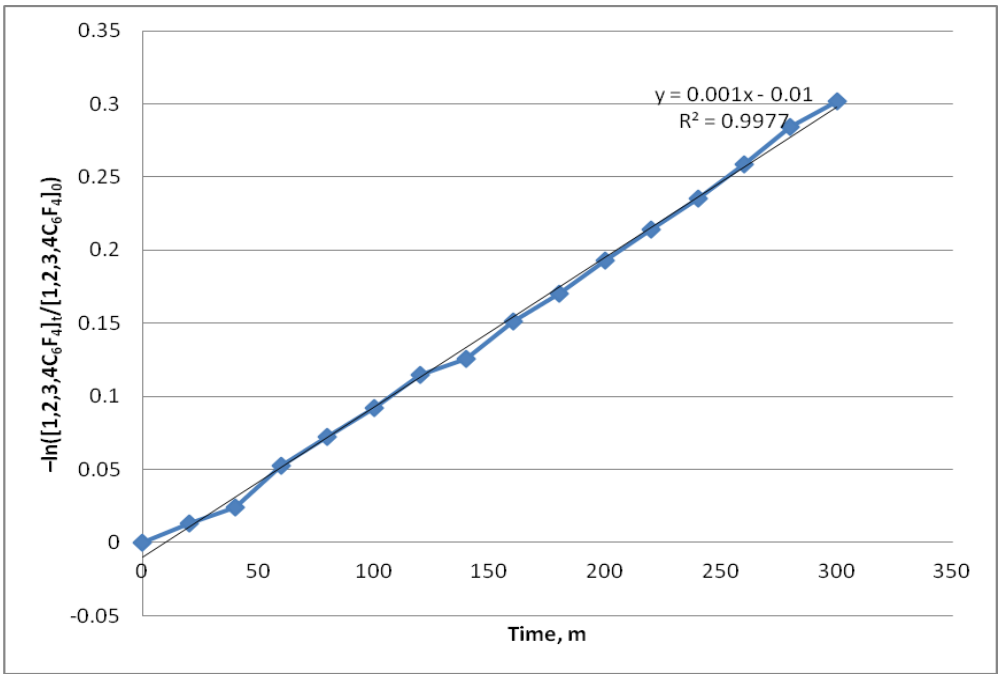

Figure XII- 18. Plot $-\ln([1,2,3,4C_6F_4]_t/[1,2,3,4C_6F_4]_0)$ versus time under pseudo-first order conditions (22.5equivs of IPA)

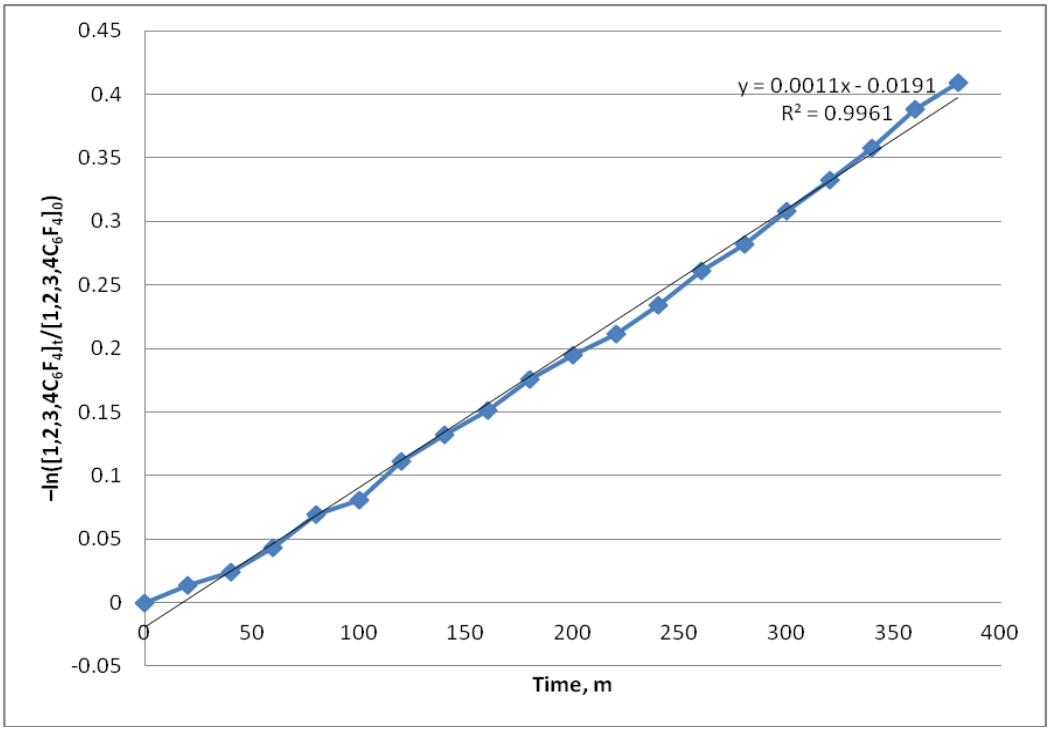

Figure XII- 19. Plot $-\ln([1,2,3,4C_6F_4]_t/[1,2,3,4C_6F_4]_0)$ versus time under pseudo-first order conditions (25 equivs of IPA)

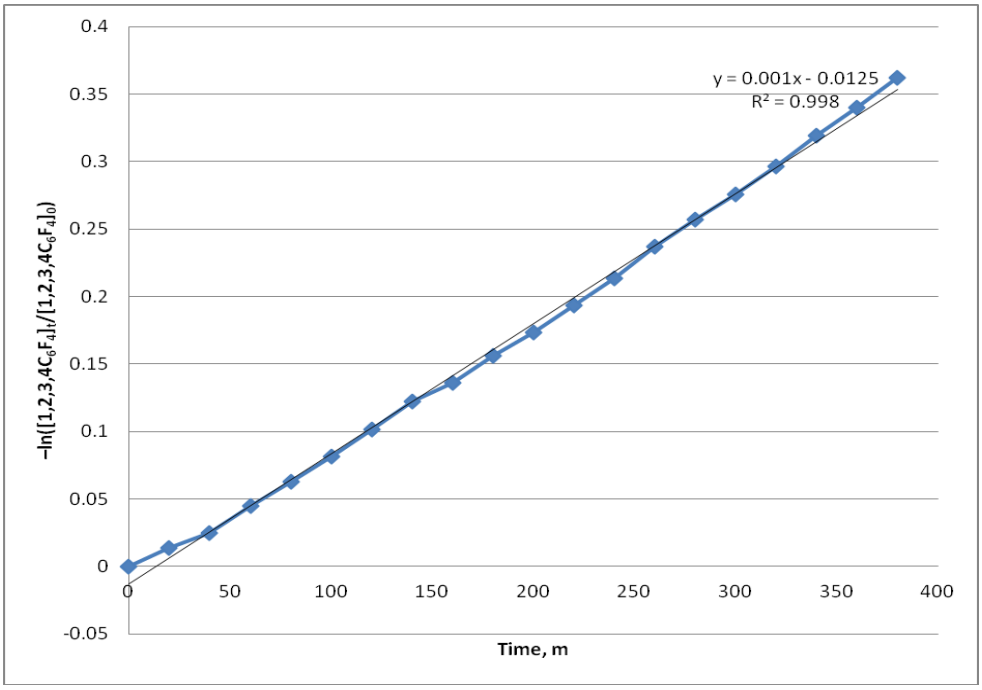

Figure XII- 20. Plot $-\ln([1,2,3,4C_6F_4]_t/[1,2,3,4C_6F_4]_0)$ versus time under pseudo-first order conditions (30 equivs of IPA)

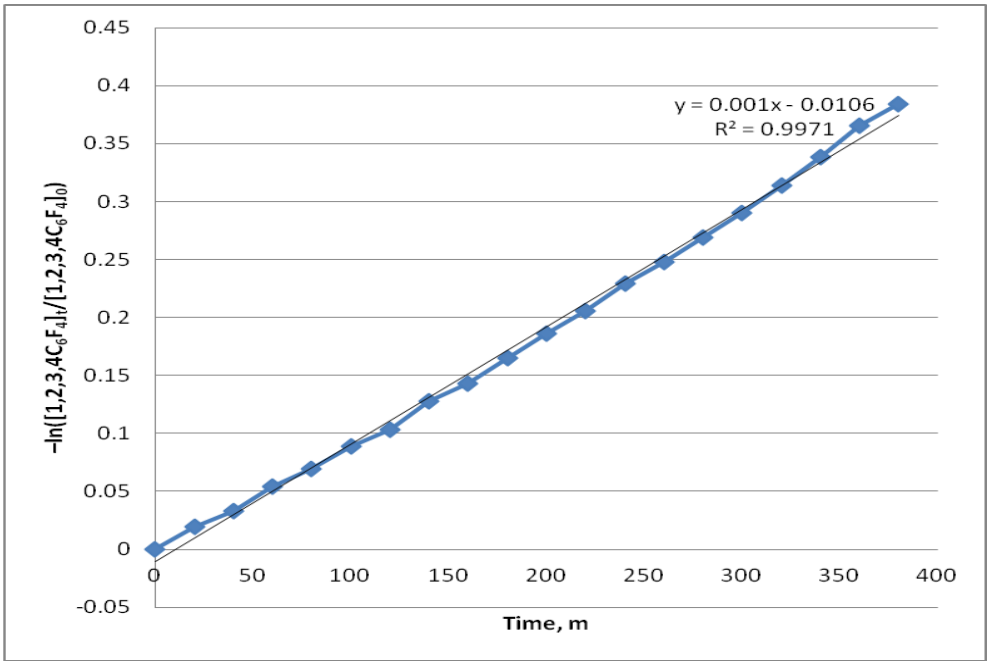

Figure XII- 21. Plot $-\ln([1,2,3,4C_6F_4]_t/[1,2,3,4C_6F_4]_0)$ versus time under pseudo-first order conditions (35 equivs of IPA)

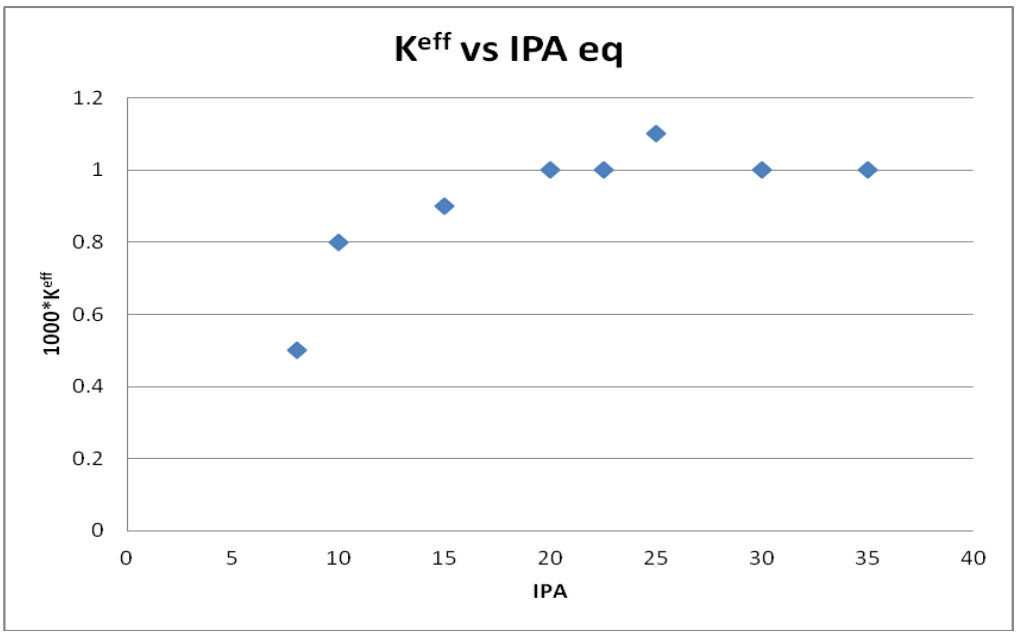

Figure XII- 22. Dependence of the HDF of 1,2,3,4- tetrafluorobenzene on the amount of IPA.

K^{eff} vs IPr

Kinetic sample preparation for HDF of 1,2,3,4 tetrafluorobenzene with IPr

varations

Table XII- 4. IPr variations

IPr equi	0	1	2	3	4	5
Sample number	5	1a	2a	3a	4a	5a
Stock of cat in benzene(µL)	100	100	100	100	100	100
IPA fresh (µL)	642.49	642.49	642.49	642.49	642.49	642.49
Subtrate (µL)	30	30	30	30	30	30
Cyclohexane (µL)	10	10	10	10	10	10
Benzen fresh (µL)	417.51	407.51	397.51	387.51	377.51	367.51
$NaCO_3$(mg)	29.66	29.66	29.66	29.66	29.66	29.66
IPr from stock solution in benzene (µL)	0	10	20	30	40	50
total	1200	1200	1200	1200	1200	1200

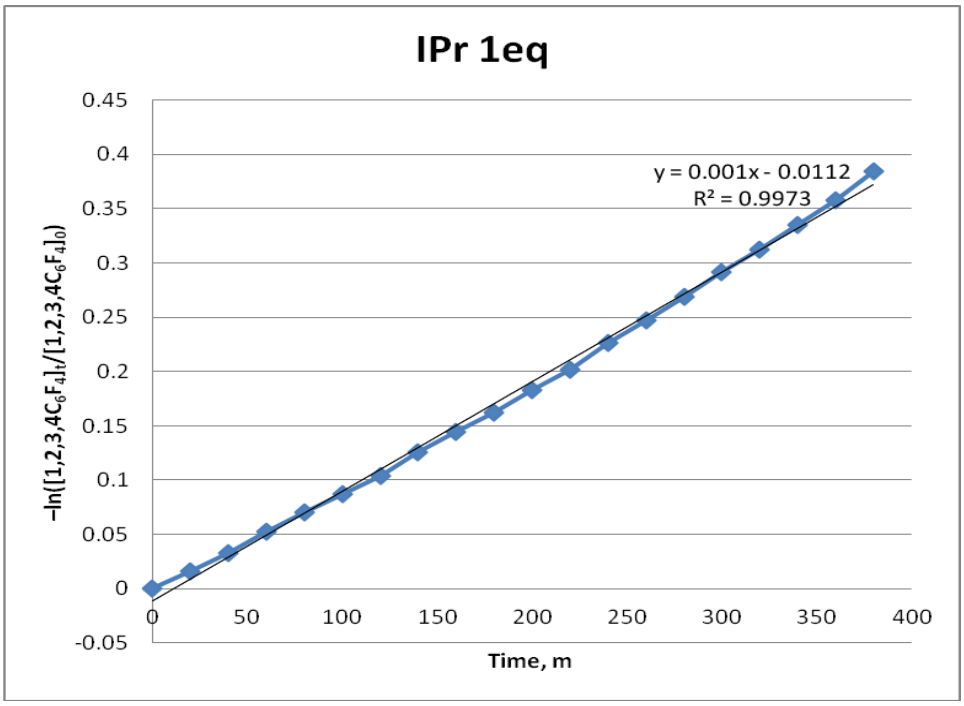

Figure XII- 23. Plot $-\ln([1,2,3,4C_6F_4]_t/[1,2,3,4C_6F_4]_0)$ versus time under pseudo-

first order conditions (30 equivs of IPA, 1eq of IPr)

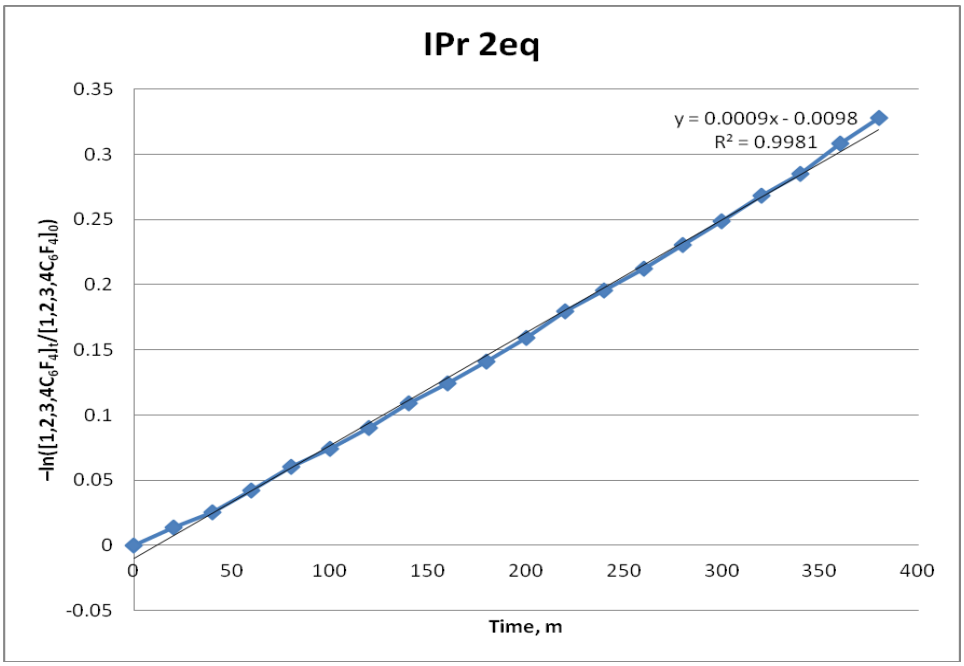

Figure XII- 24. Plot $-\ln([1,2,3,4C_6F_4]_t/[1,2,3,4C_6F_4]_0)$ versus time under pseudo-first order conditions (30 equivs of IPA, 2eq of IPr)

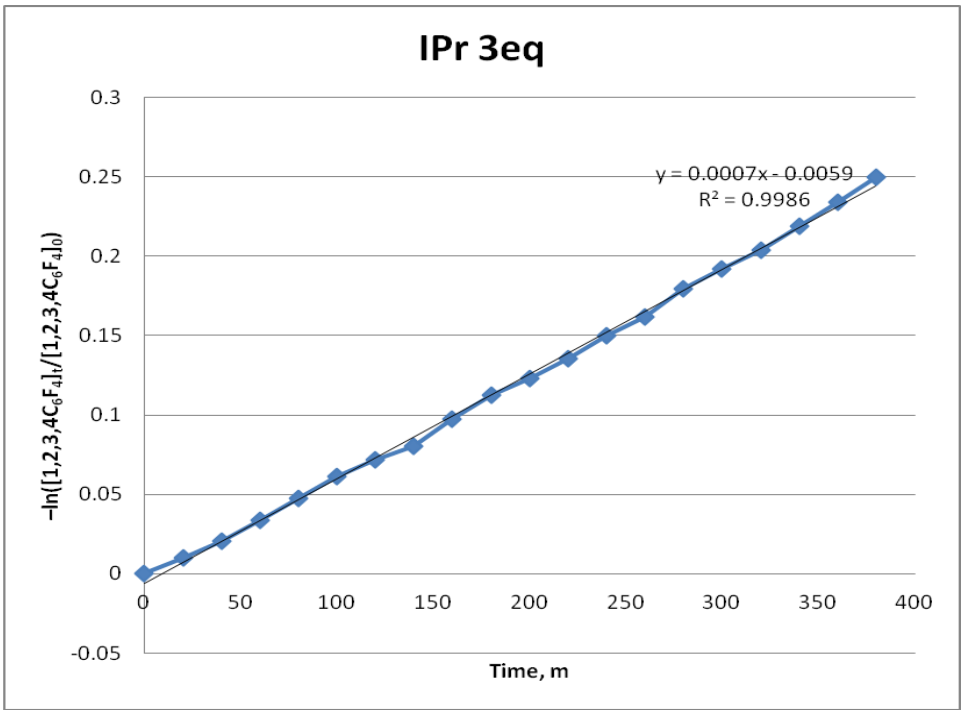

Figure XII- 25. Plot $-\ln([1,2,3,4C_6F_4]_t/[1,2,3,4C_6F_4]_0)$ versus time under pseudo-

first order conditions (30 equivs of IPA, 3eq of IPr)

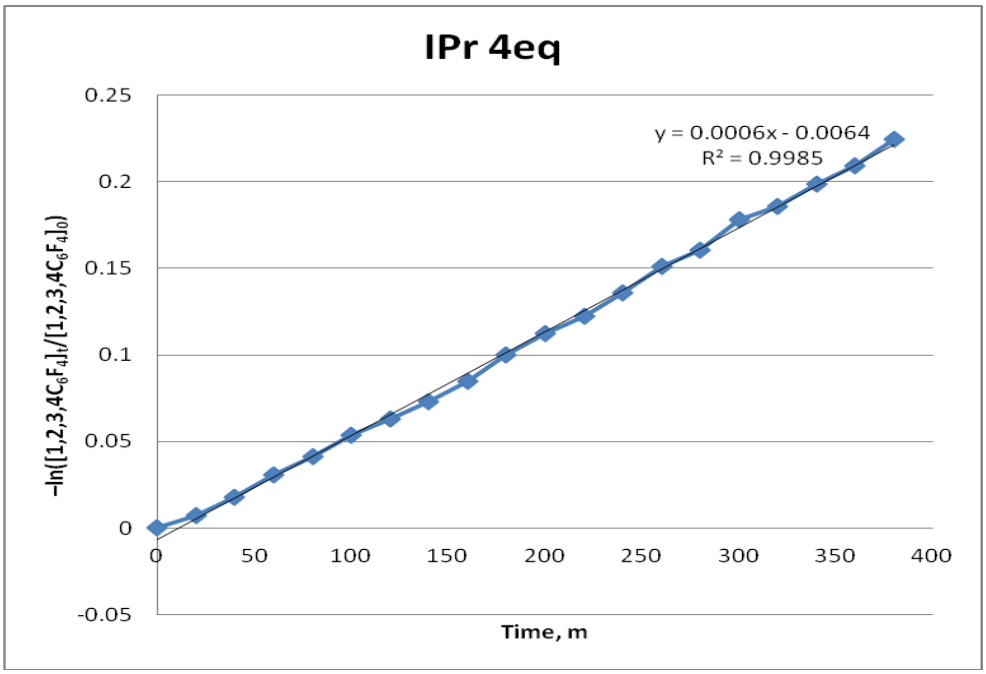

Figure XII- 26. Plot $-\ln([1,2,3,4C_6F_4]_t/[1,2,3,4C_6F_4]_0)$ versus time under pseudo-first order conditions (30 equivs of IPA, 4eq of IPr)

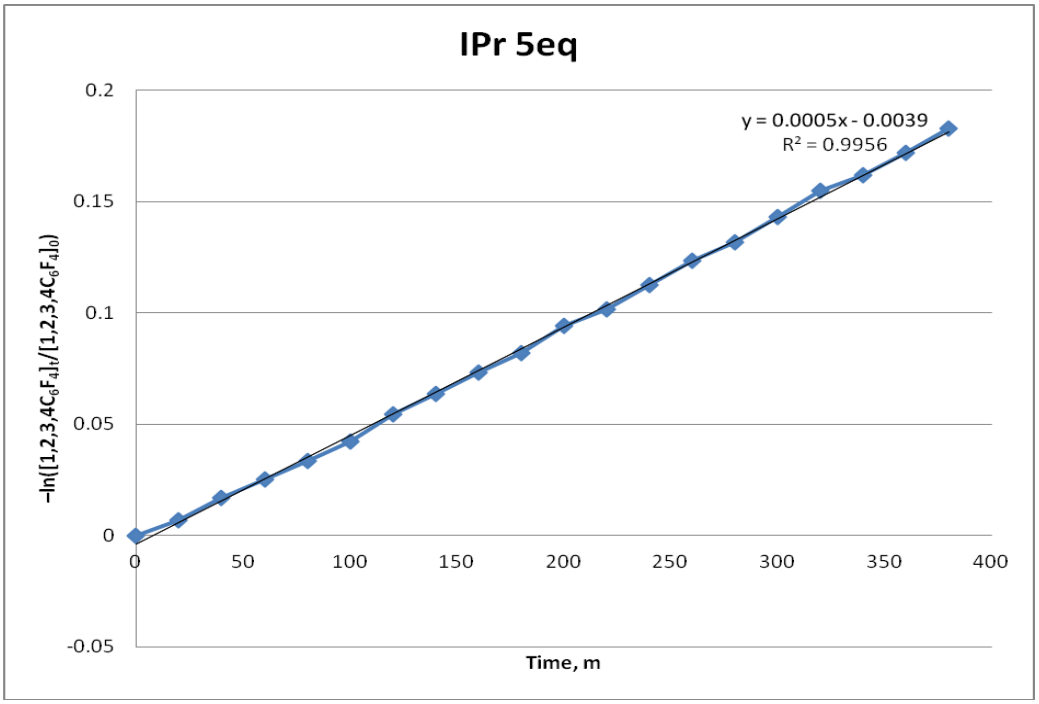

Figure XII- 27. Plot $-\ln([1,2,3,4C_6F_4]_t/[1,2,3,4C_6F_4]_0)$ versus time under pseudo-first order conditions (30 equivs of IPA, 5eq of IPr)

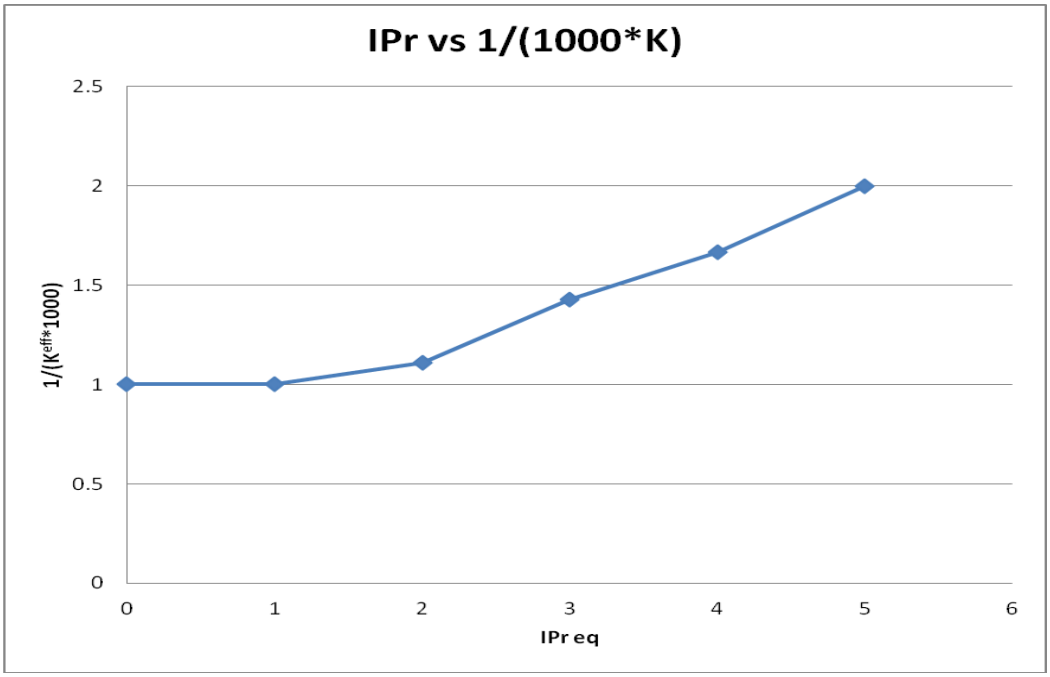

Figure XII- 28. Dependence of the HDF of 1,2,3,4-tetrafluorobenzene on the amount of IPA.

XII.2 Selected NMR spectra

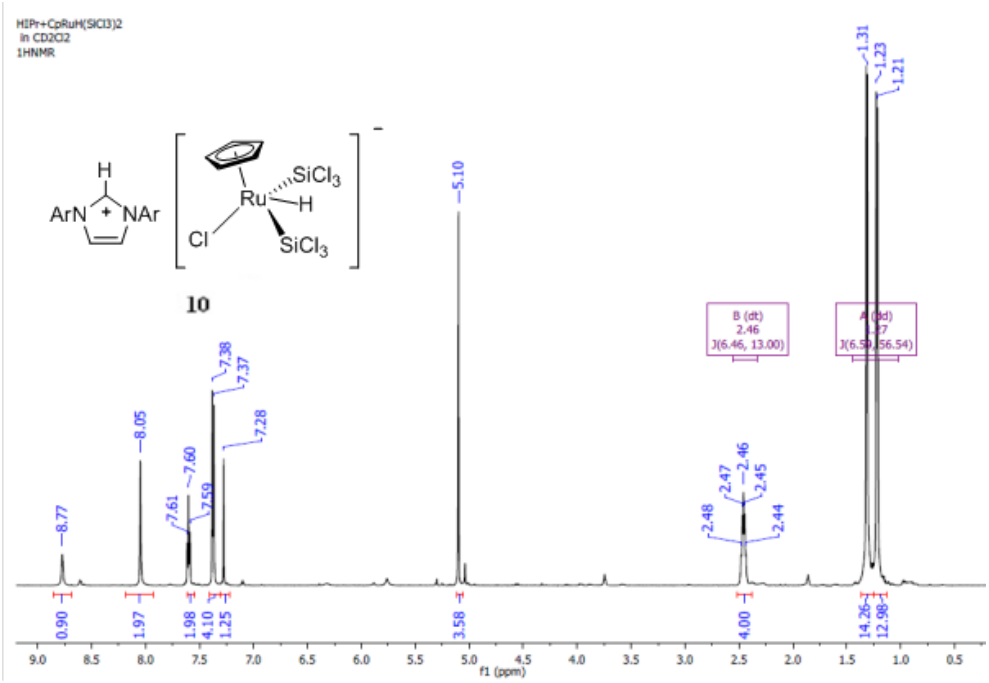

Figure XII- 29. ^{1}H NMR (600 MHz, 22°C, CD_2Cl_2) of $[IPrH][CpRuCl(H)(SiCl_3)_2]$ (**VIII-12**)

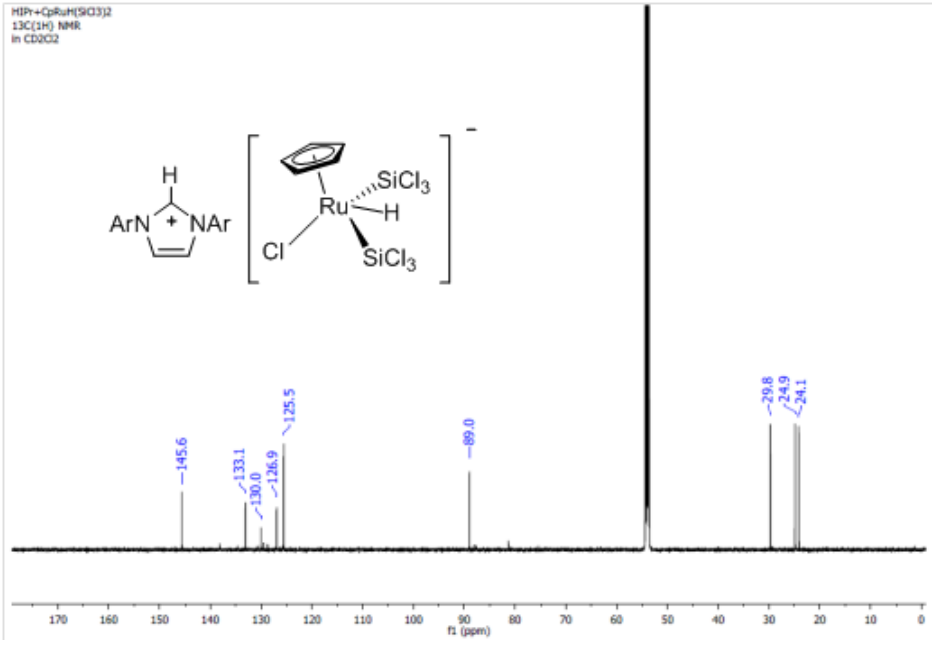

Figure XII- 30. $^{13}C\{^{1}H\}$ NMR (600 MHz, 22°C, CD_2Cl_2) of

[IPrH][CpRuCl(H)($SiCl_3$)$_2$] (**VIII-12**)

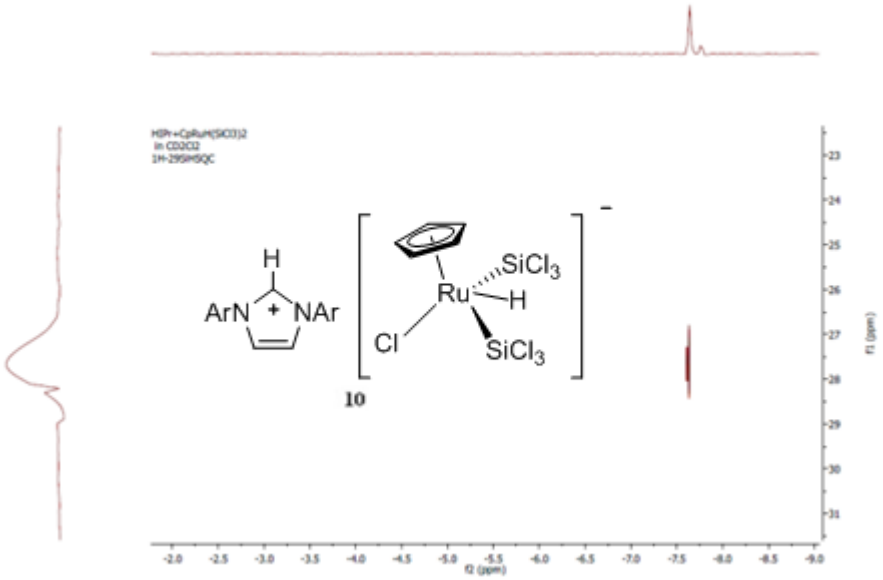

Figure XII- 31. ^{1}H - ^{29}Si HSQC NMR (119.2 MHz, 22°C, CD_2Cl_2) of [IPrH][CpRuCl(H)($SiCl_3$)$_2$] (**VIII-12**)

Cp(IPr)RuCl(η^2-$HSiCl_3$) (VIII-9a)

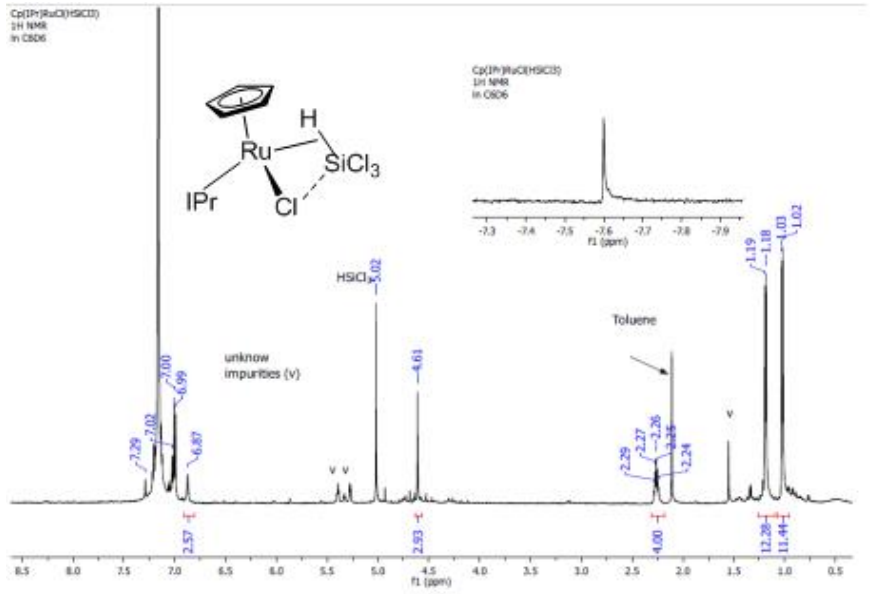

a)

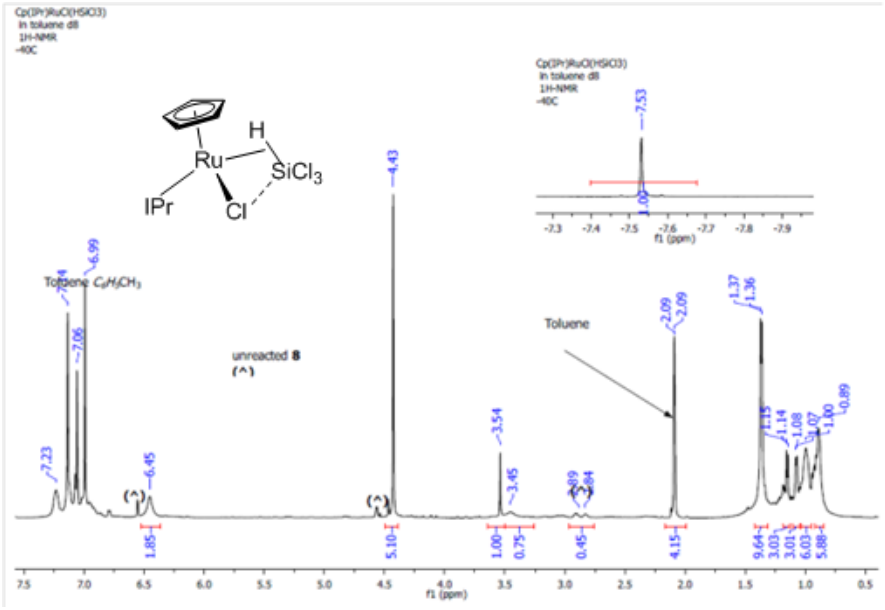

b)

Figure XII- 32.a) ^{1}H NMR (600 MHz, 22°C, C_6D_6) of Cp(IPr)RuCl(η^2-$HSiCl_3$); (b) ^{1}H NMR (600 MHz, -40 °C, $C_6D_5CD_3$) of *in situ* generated Cp(IPr)RuCl(η^2-$HSiCl_3$).

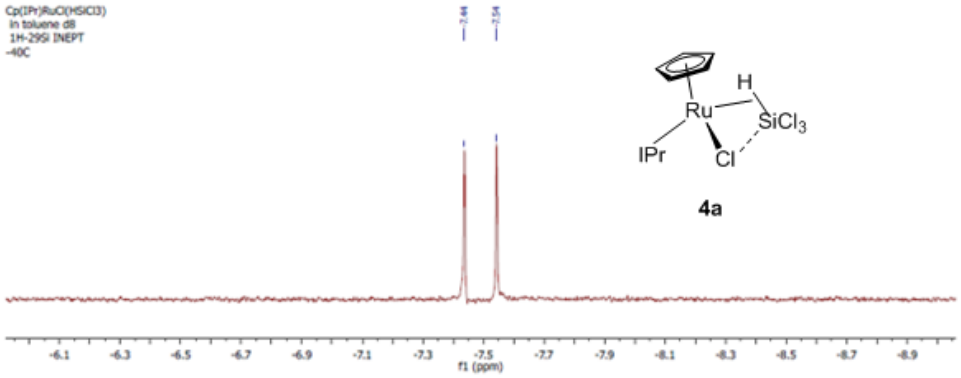

Figure XII- 33. ^{1}H - ^{29}Si INEPT NMR (119.2 MHz, -40 °C, $C_6D_5CD_3$) of Cp(IPr)RuCl(η^2-$HSiCl_3$)

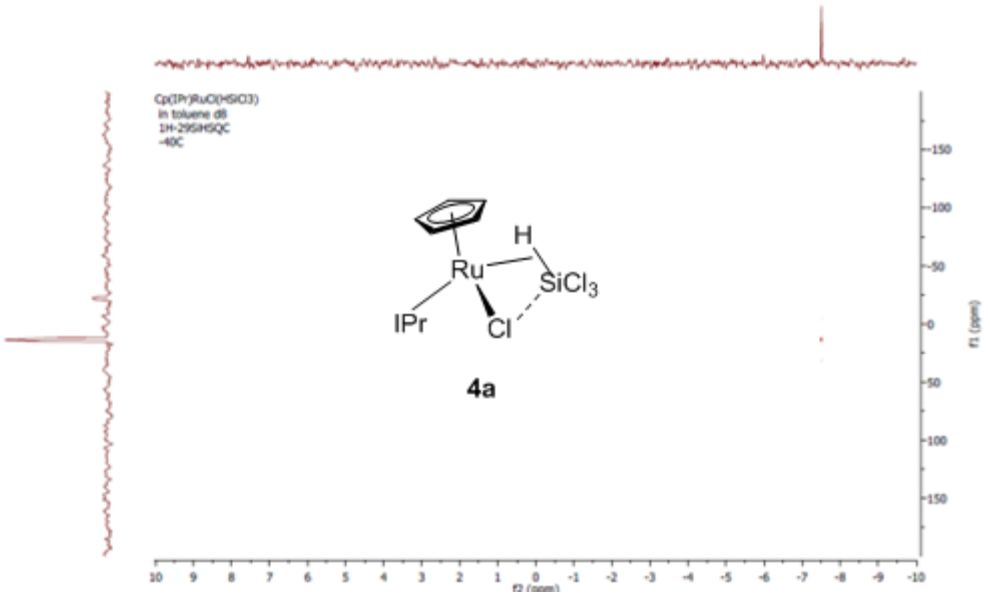

Figure XII- 34. ^{1}H - ^{29}Si HSQC NMR (119.2 MHz, -40 °C, $C_6D_5CD_3$) of $Cp(IPr)RuCl(\eta^2\text{-}HSiCl_3)$

$Cp(IPr)RuCl(\eta^2\text{-}HSiCl_2Me)$ (VIII-9b)

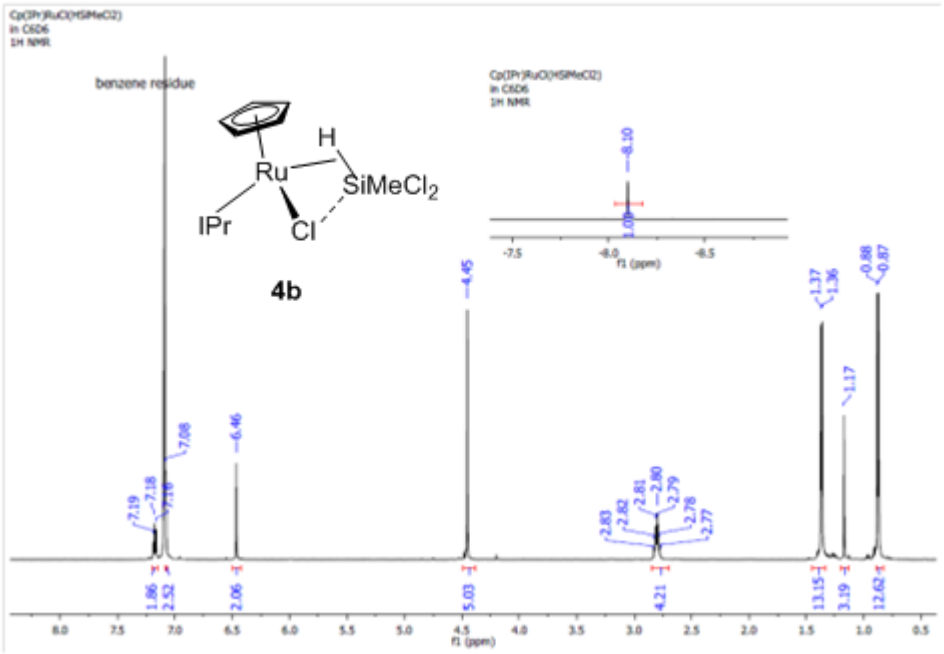

a)

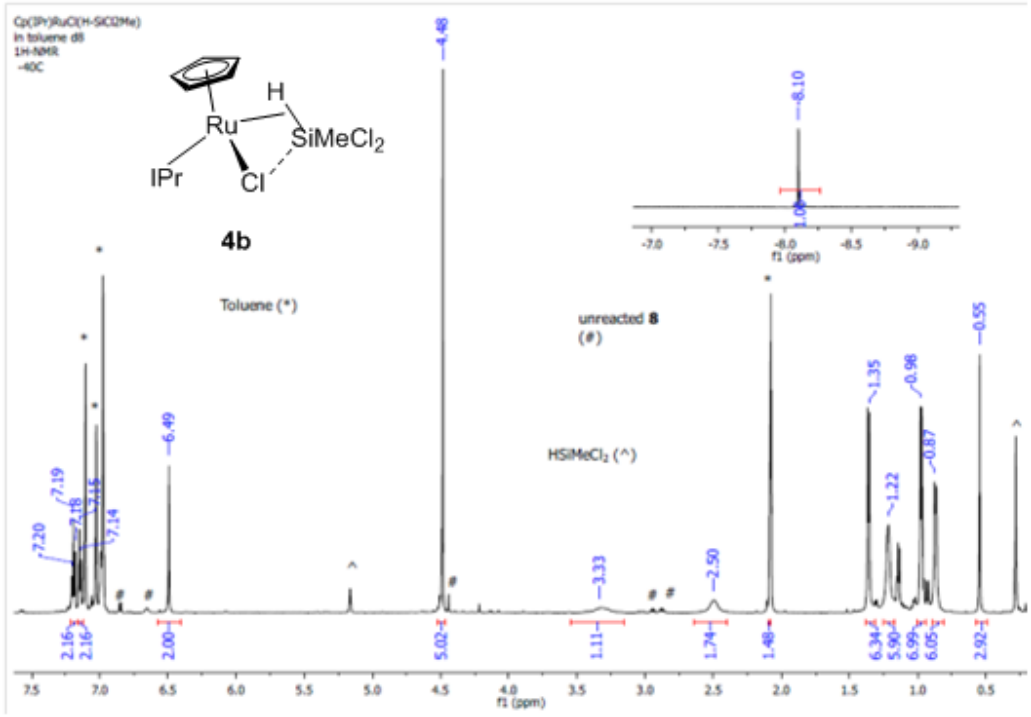

b)

Figure XII- 35. (a) ^{1}H NMR (600 MHz, 22°C, in C_6D_6) of Cp(IPr)RuCl(η^2-$HSiCl_2Me$) ; (b) ^{1}H NMR (600 MHz, -40°C, $C_6D_5CD_3$) of *in situ* generated Cp(IPr)RuCl(η^2-$HSiCl_2Me$).

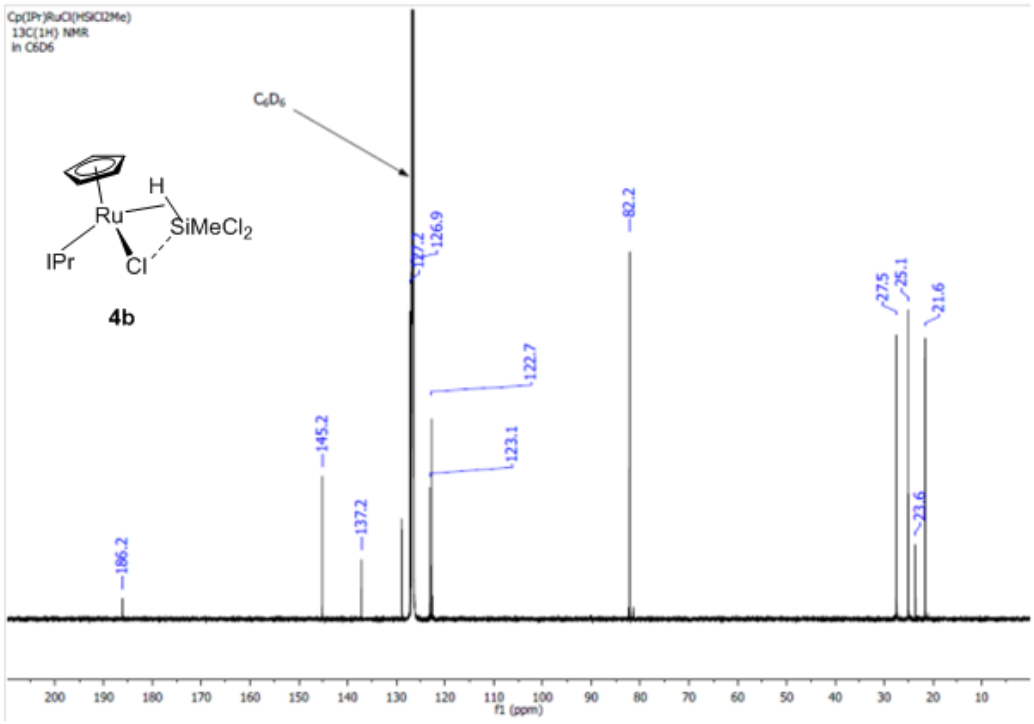

Figure XII- 36. $^{13}C\{^{1}H\}$ NMR (600 MHz, 22°C, in C_6D_6) of Cp(IPr)RuCl(η^2-

$HSiCl_2Me$).

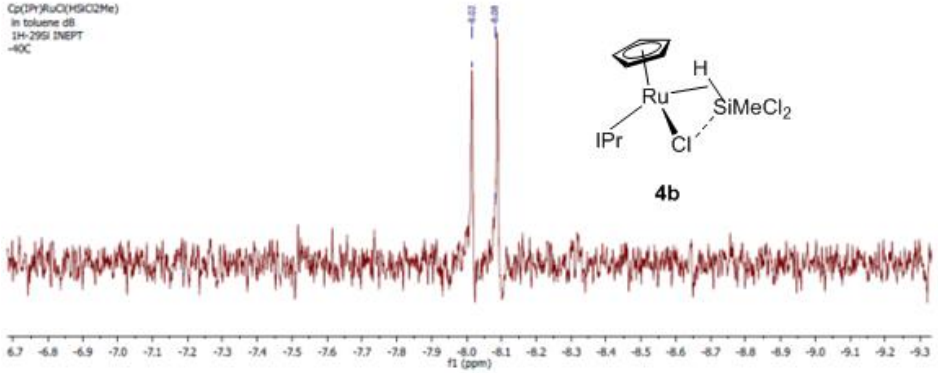

Figure XII- 37. ^{1}H - ^{29}Si INEPT NMR (119.2 MHz; -40°C, $C_6D_5CD_3$) of $Cp(IPr)RuCl(\eta^2\text{-}HSiCl_2Me)$.

$Cp(IPr)RuCl(\eta^2\text{-}HSiClMe_2)$ (VIII-9c)

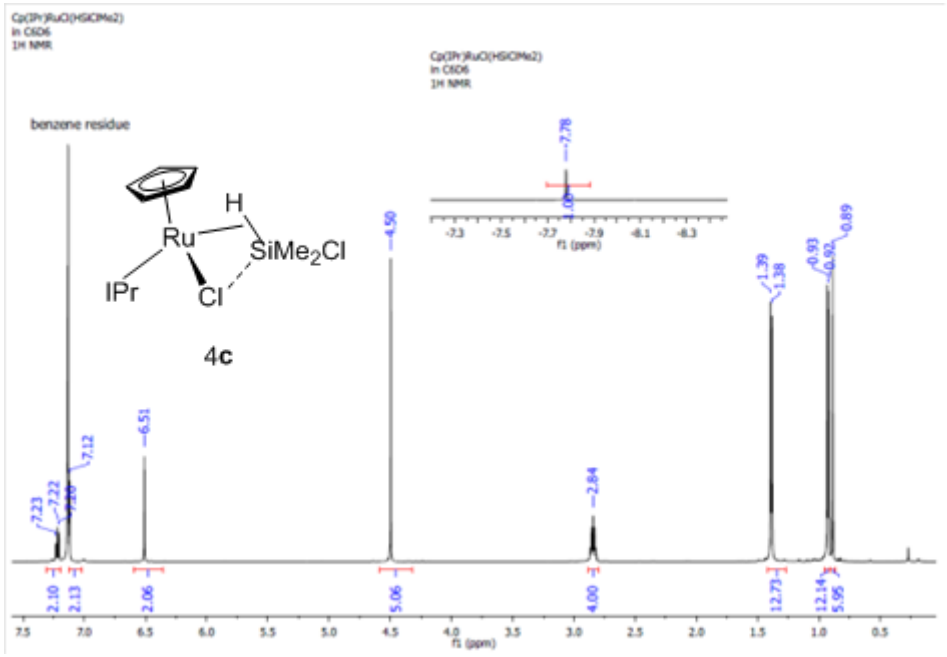

a)

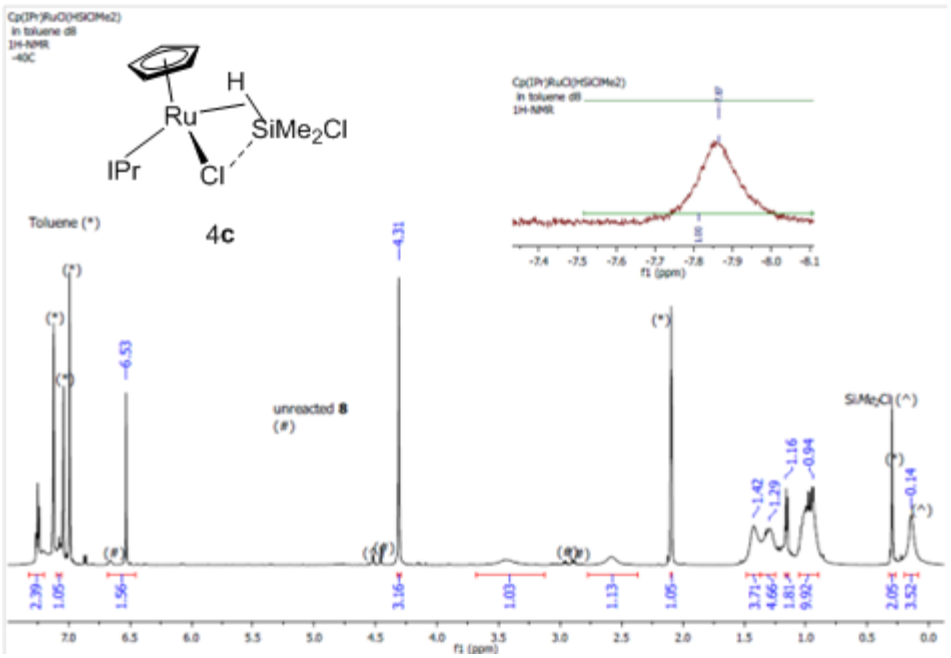

b)

Figure XII- 38. (a) ^{1}H NMR (600 MHz, 22°C, in C_6D_6) of Cp(IPr)RuCl(η^2-HSiClMe$_2$); (b) ^{1}H NMR (600 MHz, -40°C, $C_6D_5CD_3$) of *in situ* generated Cp(IPr)RuCl(η^2-HSiClMe$_2$).

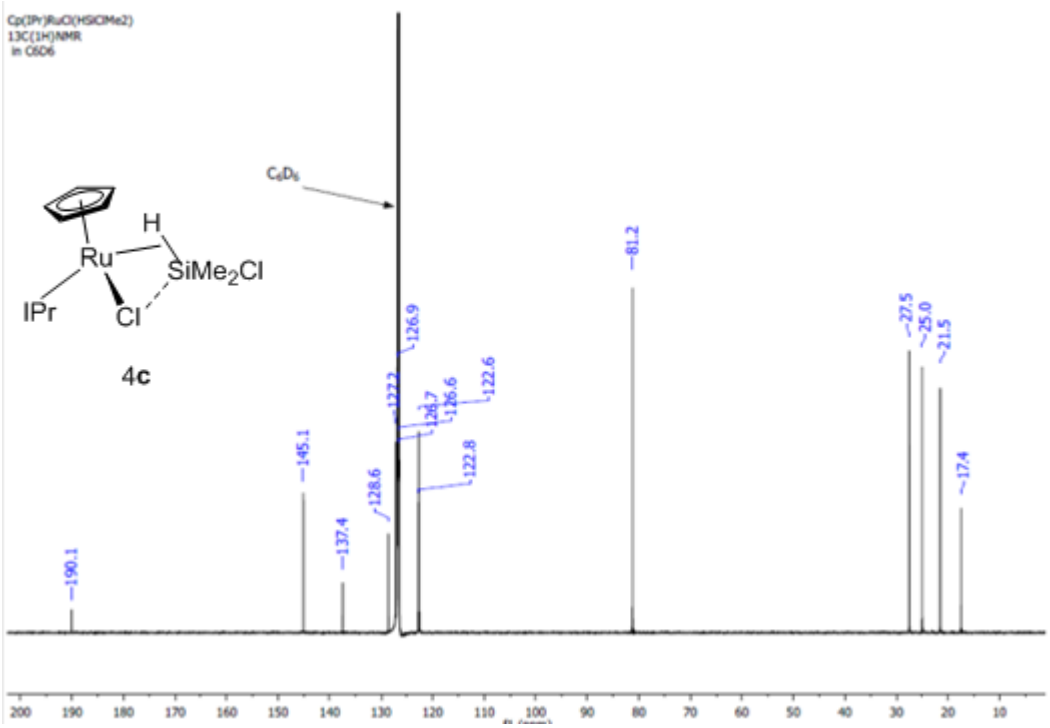

Figure XII- 39. $^{13}C\{^{1}H\}$ NMR (600 MHz, 22°C, in C_6D_6) of Cp(IPr)RuCl(η^2-HSiClMe$_2$).

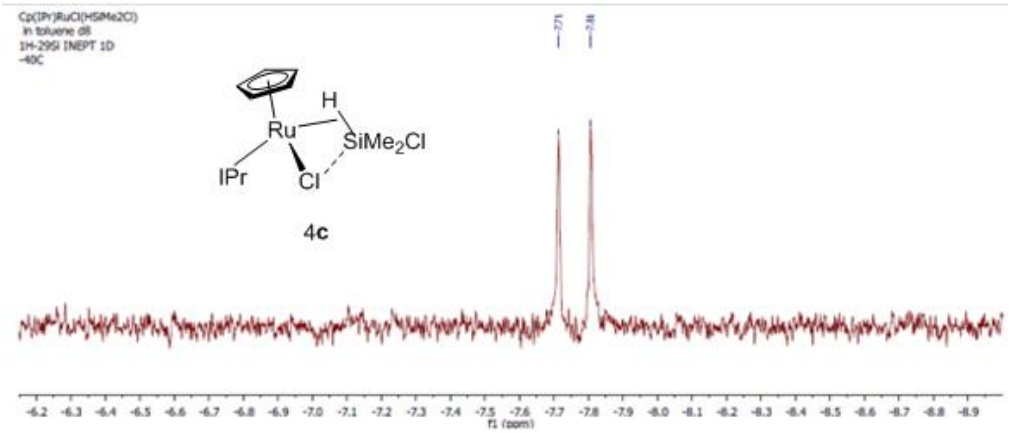

Figure XII- 40. ^{1}H - ^{29}Si INEPT NMR (119.2 MHz, -40°C, $C_6D_5CD_3$) of Cp(IPr)RuCl(η^2-HSiClMe$_2$).

Cp(IPr)RuCl(η^2-HSiH$_2$Ph) (VIII-9d)

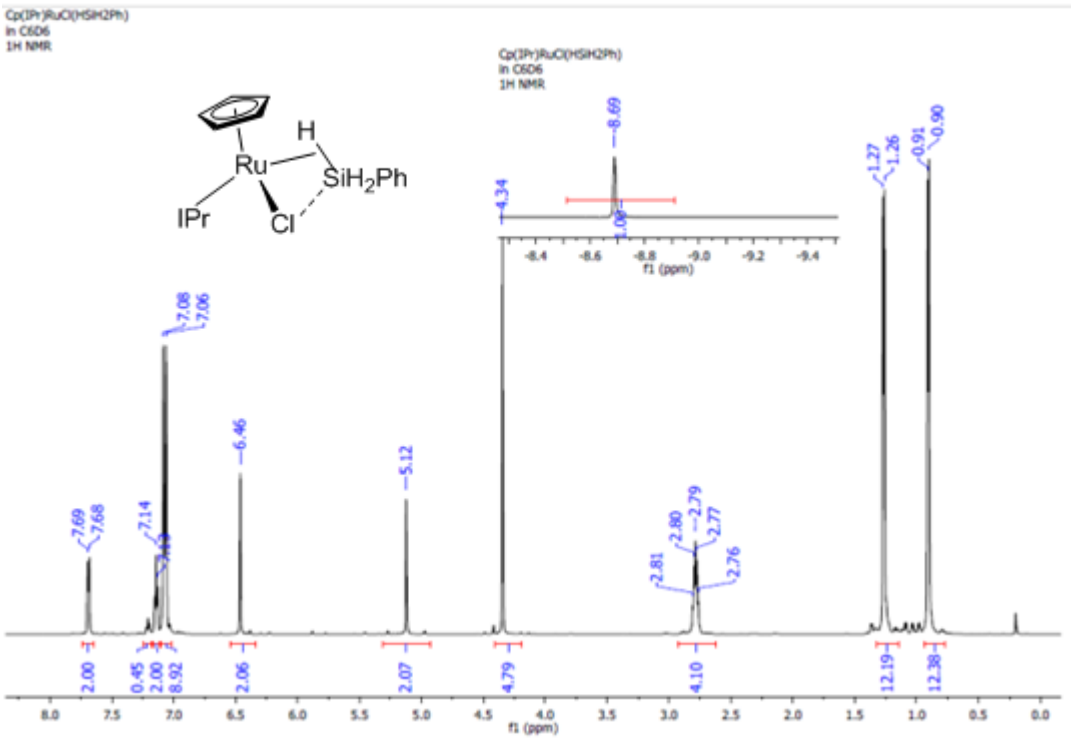

a)

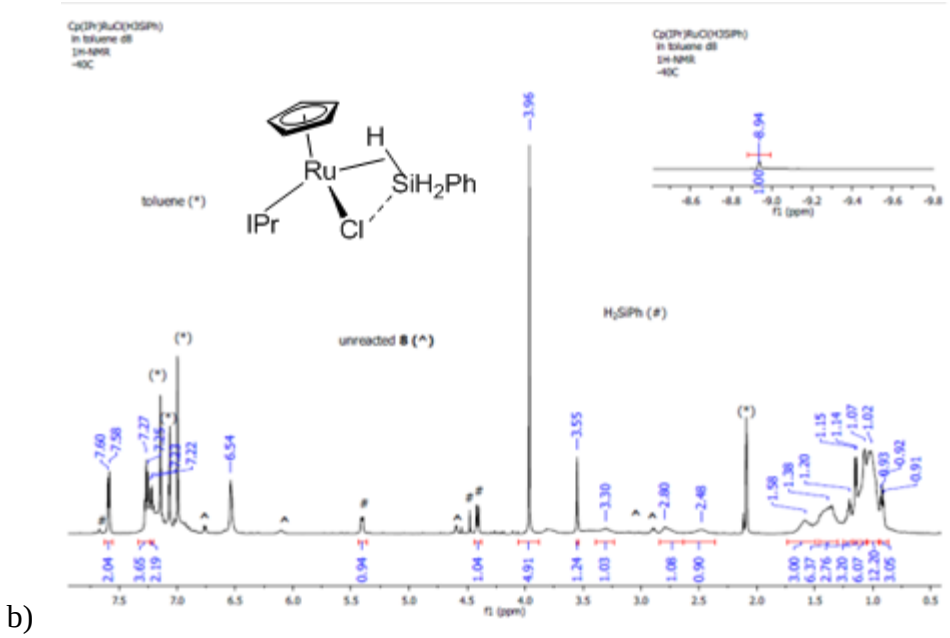

b)

Figure XII- 41. (a) ^{1}H NMR (600 MHz, 22°C, C_6D_6) of Cp(IPr)RuCl(η^2-H_3SiPh); (b) ^{1}H NMR (600 MHz, -40°C, $C_6D_5CD_3$) of *in situ* generated Cp(IPr)RuCl(η^2-H_3SiPh).

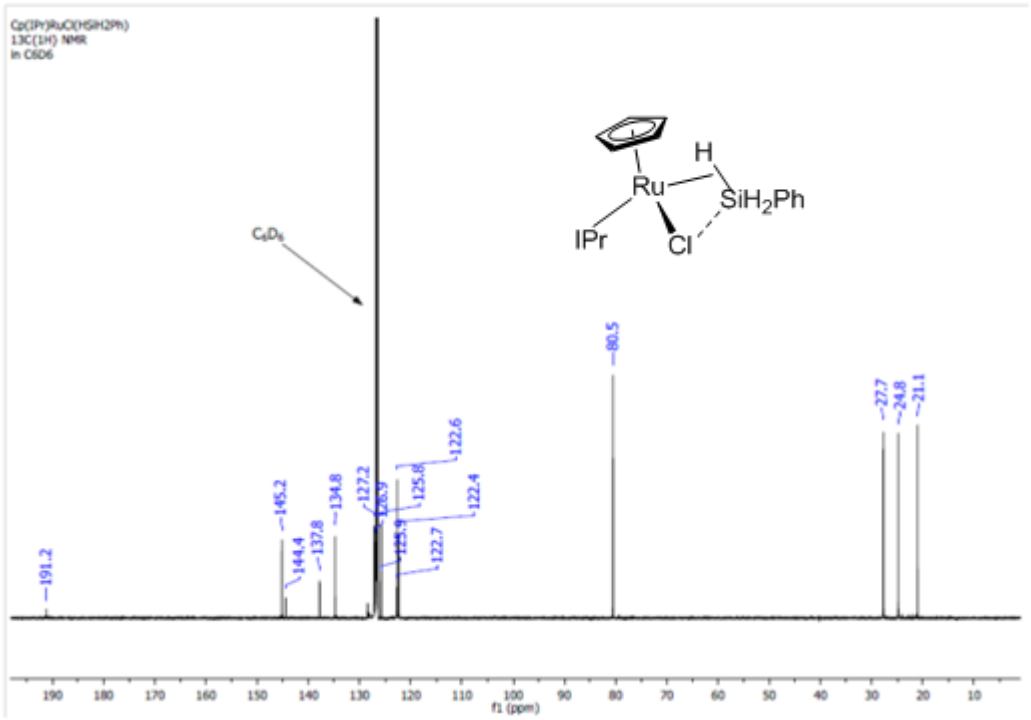

Figure XII- 42. ^{13}C{^{1}H} NMR (600 MHz, 22°C, C_6D_6) of Cp(IPr)RuCl($HSiH_2Ph$).

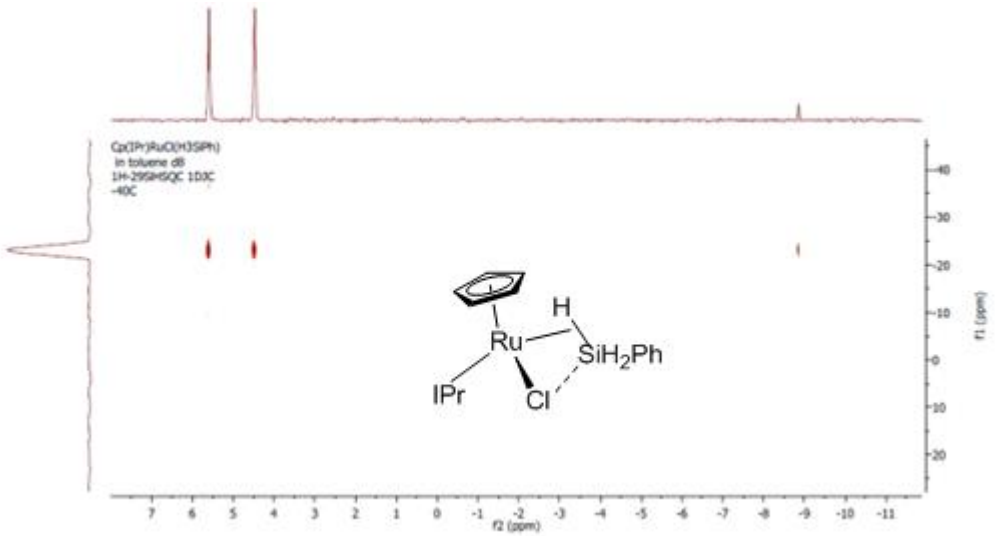

Figure XII- 43. ^{1}H - ^{29}Si INEPT NMR (119.2 MHz, -40°C, $C_6D_5CD_3$) of $Cp(IPr)RuCl(\eta^2\text{-}HSiH_2Ph)$

$[Cp(IPr)Ru(NCCH_3)(\eta^2\text{-}HSiCl_3)]BArF_4$ (VIII-13a)

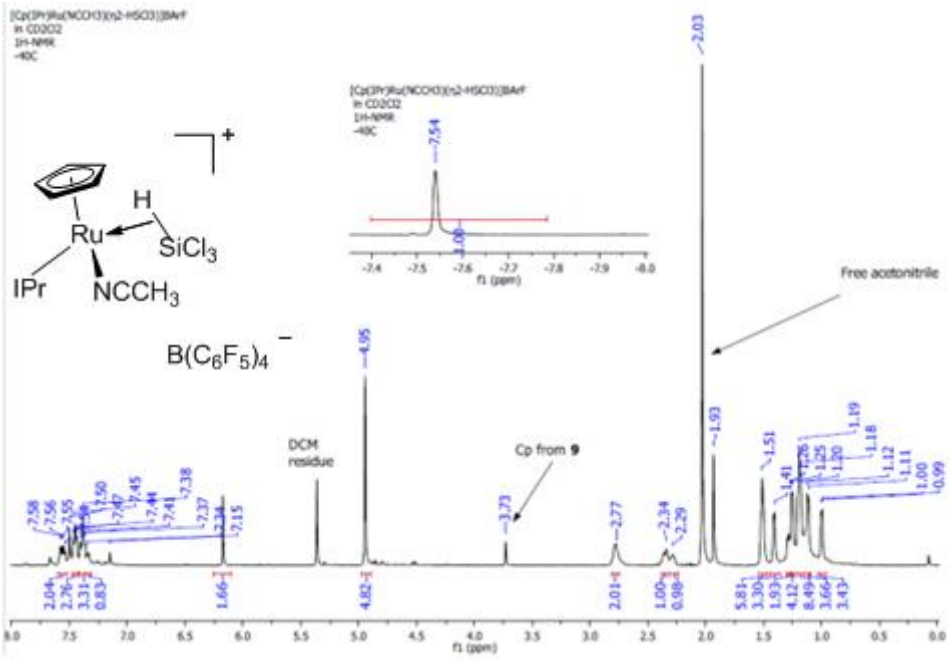

Figure XII- 44. ^{1}H NMR (600 MHz, -40°C, CD_2Cl_2) of *in situ* generated $[Cp(IPr)Ru(NCCH_3)(\eta^2\text{-}HSiCl_3)]BArF_4$

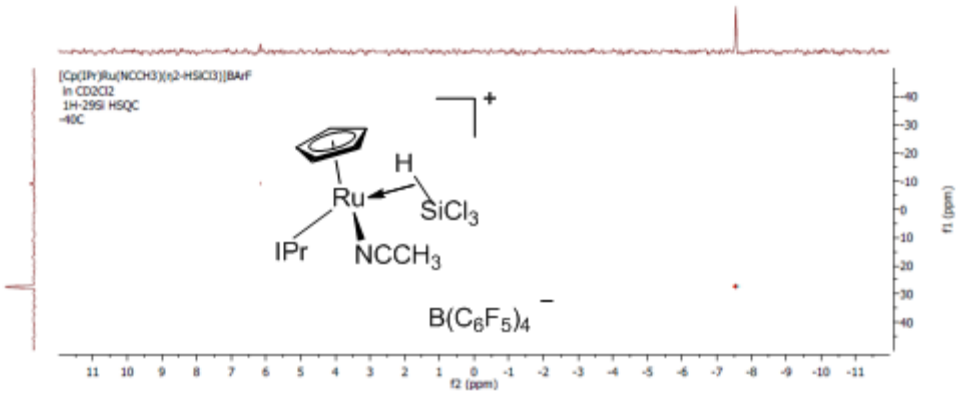

Figure XII- 45. ^{1}H - ^{29}Si HSQC NMR (119.2 MHz, -40°C, CD_2Cl_2) of $[Cp(IPr)Ru(NCCH_3)(\eta^2\text{-}HSiCl_3)]BArF_4$

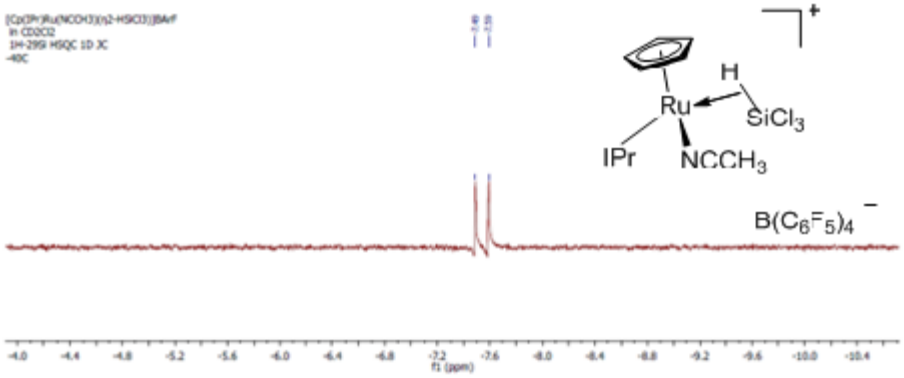

Figure XII- 46. ^{1}H - ^{29}Si INEPT NMR (119.2 MHz, -40°C, CD_2Cl_2) of $[Cp(IPr)Ru(NCCH_3)(\eta^2\text{-}HSiCl_3)]BArF_4$

$[Cp(IPr)Ru(NCCH_3)(\eta^2\text{-}HSiH_2Ph)]BArF_4$ (VIII-13d)

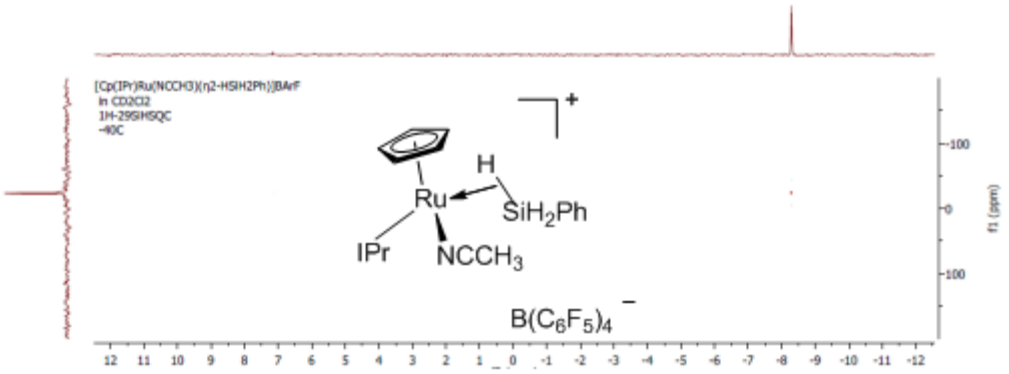

Figure XII- 47. ^{1}H - ^{29}Si IHSQC NMR (119.2 MHz, -40°C, CD_2Cl_2) of $[Cp(IPr)Ru(NCCH_3)(\eta^2\text{-}H_2SiPh)]BArF_4$

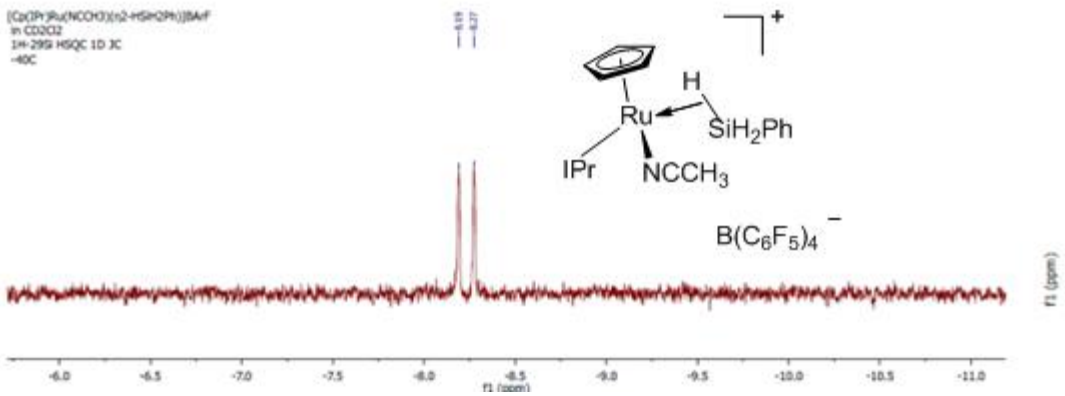

Figure XII- 48. ^{1}H - ^{29}Si INEPT NMR (119.2 MHz, -40°C, CD_2Cl_2) of $[Cp(IPr)Ru(NCCH_3)(\eta^2\text{-}H_3SiPh)]BArF_4$

$[Cp(IPr)Ru(NCCH_3)(\eta^2\text{-}HSiHMePh)]BArF_4$ (VIII-13e)

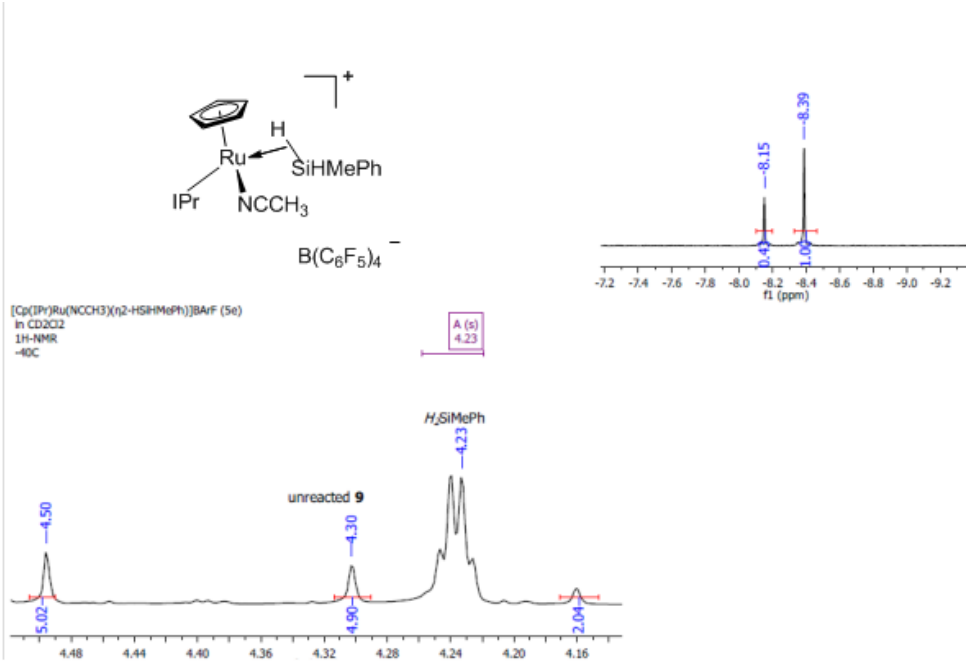

Figure XII- 49. ^{1}H NMR (600 MHz, -40°C, CD_2Cl_2) of *in situ* generated $[Cp(IPr)Ru(NCCH_3)(\eta^2\text{-}HSiHMePh)]BArF_4$ (two isomers).

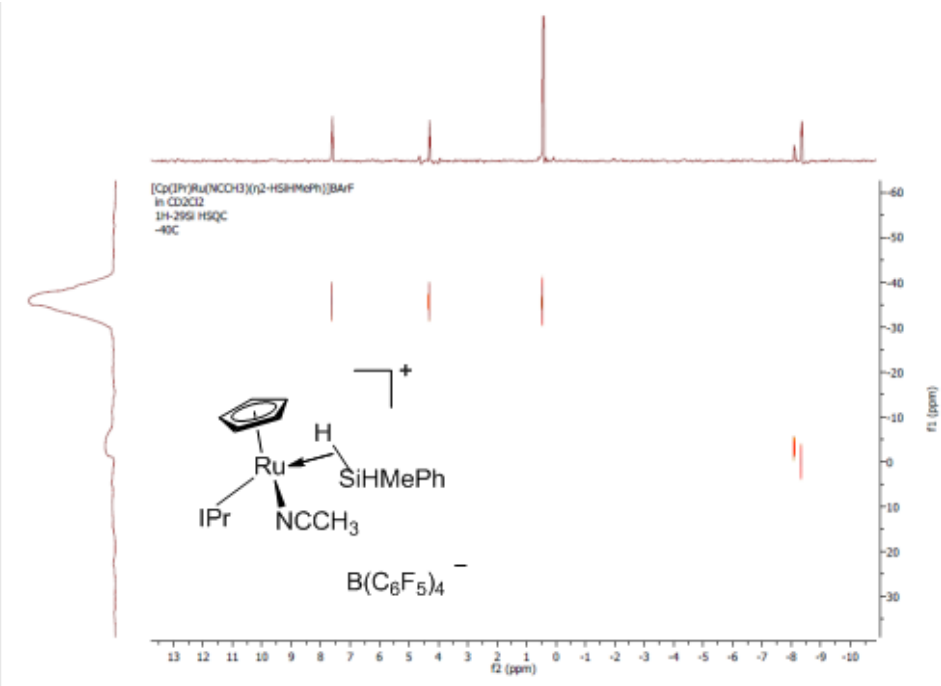

Figure XII- 50. ^{1}H - ^{29}Si INEPT NMR (119.2 MHz, -40°C, CD_2Cl_2) of $[Cp(IPr)Ru(NCCH_3)(\eta^2\text{-}HSiHMePh)]BArF_4$

$[Cp(IPr)Ru(NCCH_3)_2]BArF_4$ (VIII-6a)

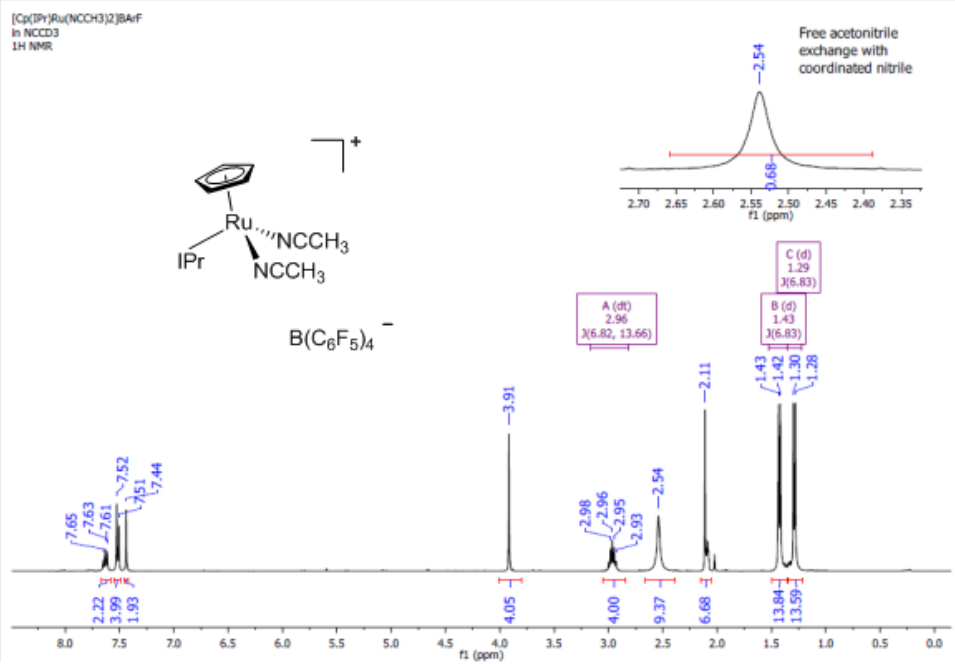

Figure XII- 51. ^{1}H NMR (600 MHz, 22°C, $NCCD_3$) of $[Cp(IPr)Ru(NCCH_3)_2]BArF_4$

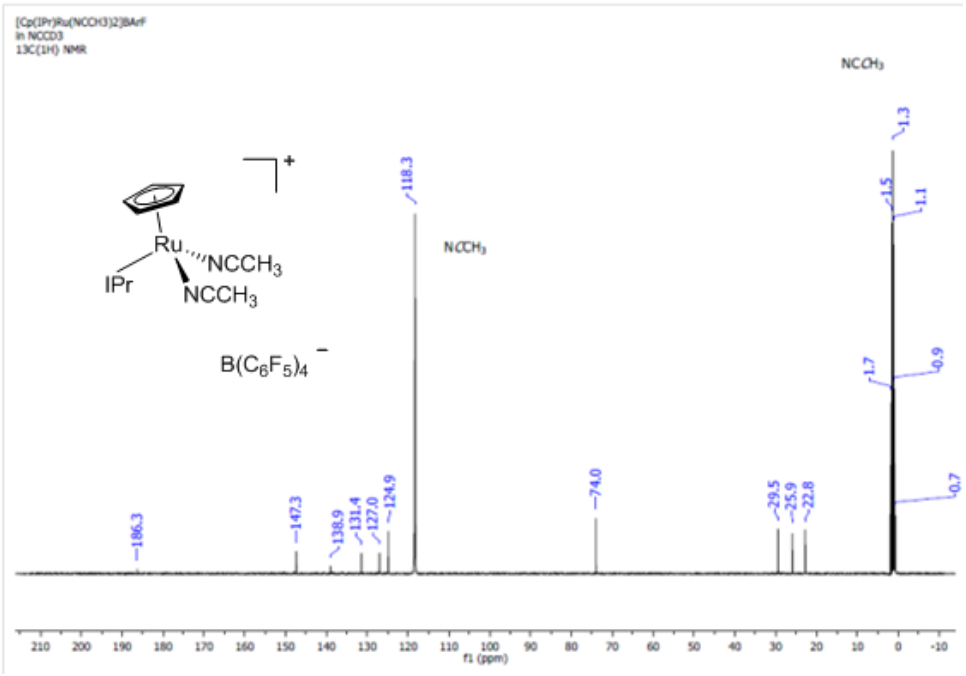

Figure XII- 52. $^{13}C\{^{1}H\}$ NMR spectrum (151 MHz, 22°C, $NCCD_3$) of $[Cp(IPr)Ru(NCCH_3)_2]BArF_4$

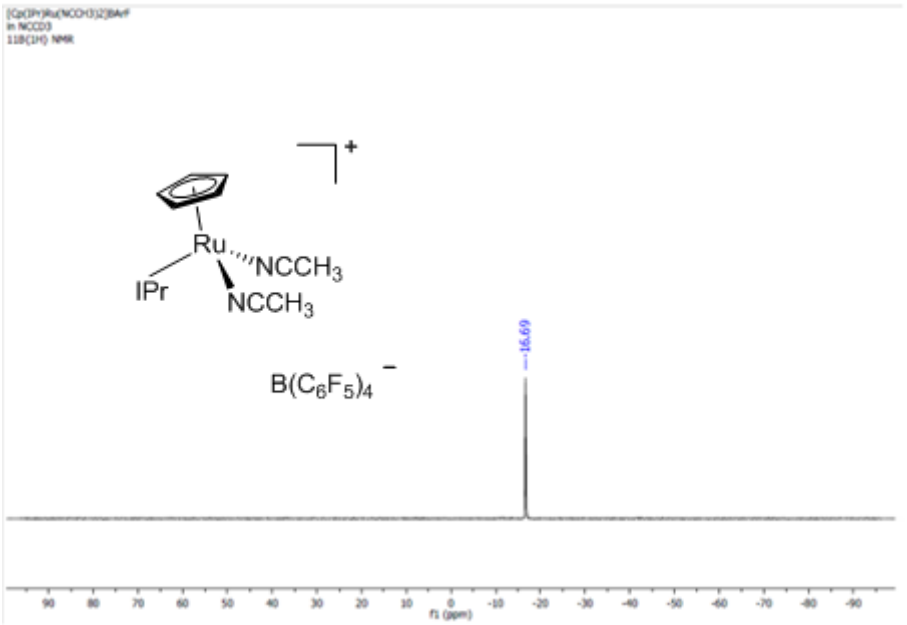

Figure XII- 53. $^{11}B\{^{1}H\}$ NMR spectrum (151 MHz, $NCCD_3$) of $[Cp(IPr)Ru(NCCH_3)_2]BArF_4$

[IPrH][CpRuCl(H)(SiCl$_3$)$_2$] (VIII-12)

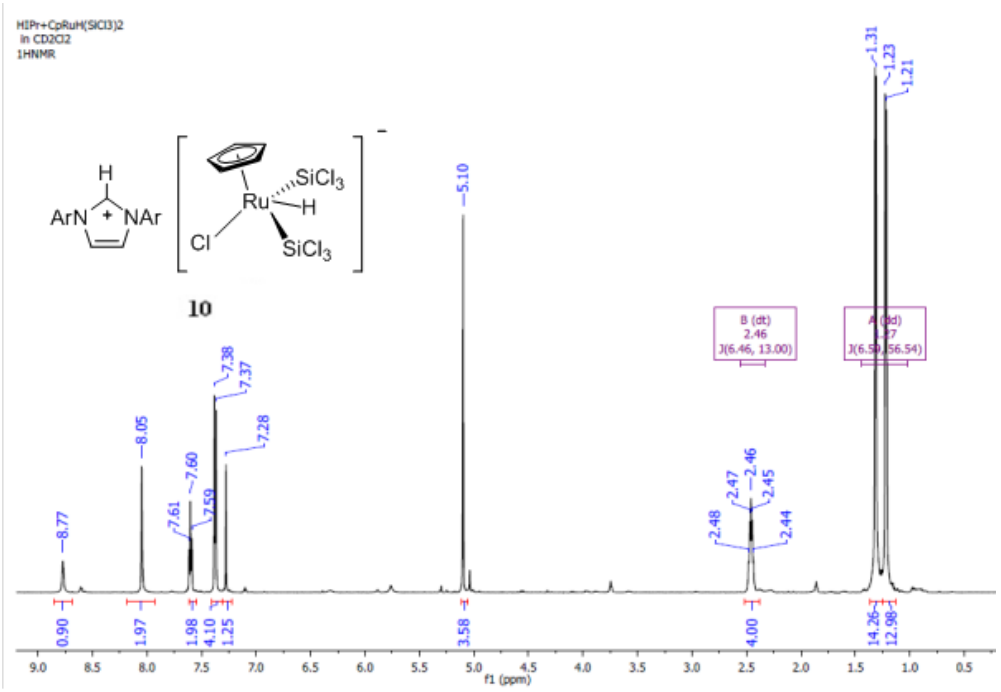

Figure XII- 54. ^{1}H NMR (600 MHz, 22°C, CD_2Cl_2) of [IPrH][CpRuCl(H)(SiCl$_3$)$_2$] (10)

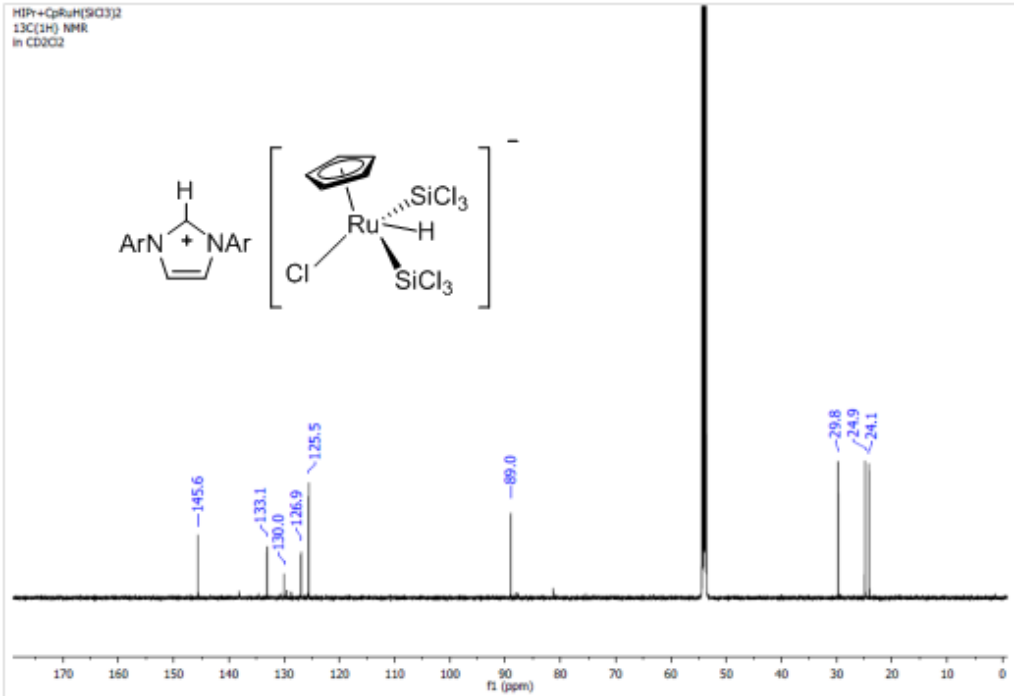

Figure XII- 55. $^{13}C\{^{1}H\}$ NMR (600 MHz, 22°C, CD_2Cl_2) of [IPrH][CpRuCl(H)($SiCl_3$)$_2$]

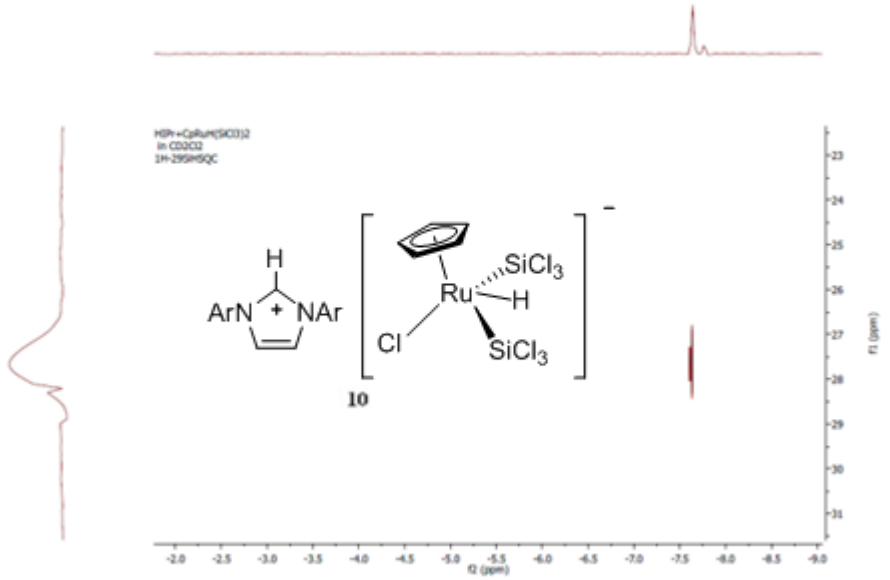

Figure XII- 56. ^{1}H - ^{29}Si HSQC NMR (119.2 MHz, 22°C, CD_2Cl_2) of [IPrH][CpRuCl(H)($SiCl_3$)$_2$]

Cp(IPr)RuH_3 (VI-1)

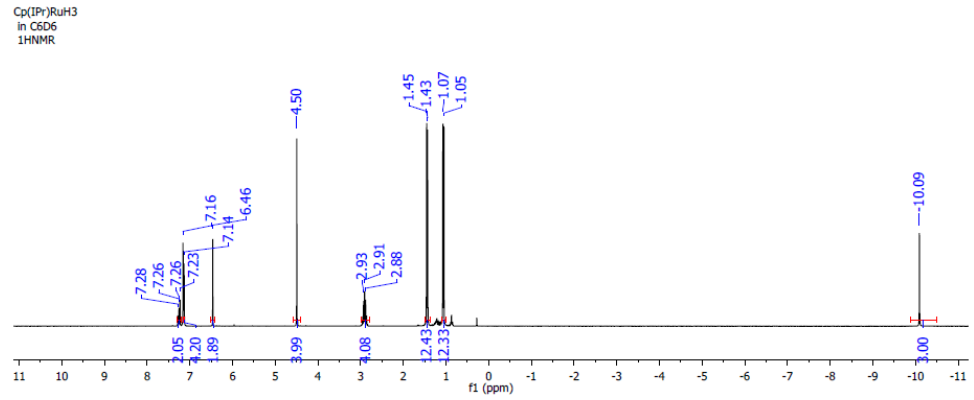
Cp(IPr)RuH3
in C6D6
1HNMR
-4.50
1.45
1.43
1.07
1.05
7.16
7.14
6.46
7.28
7.26
7.26
7.23
2.93
2.91
2.88
-10.09
2.05
4.20
1.89
3.99
4.08
12.43
12.33
3.00
f1 (ppm)

a)

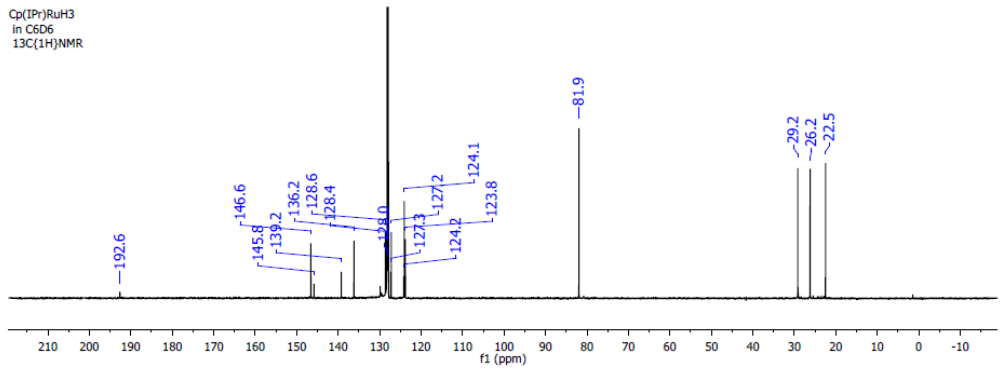
Cp(IPr)RuH3
in C6D6
13C{1H}NMR
-192.6
146.6
145.8
139.2
136.2
128.6
128.4
128.0
127.3
127.2
124.2
124.1
123.8
-81.9
29.2
26.2
22.5
f1 (ppm)

b)

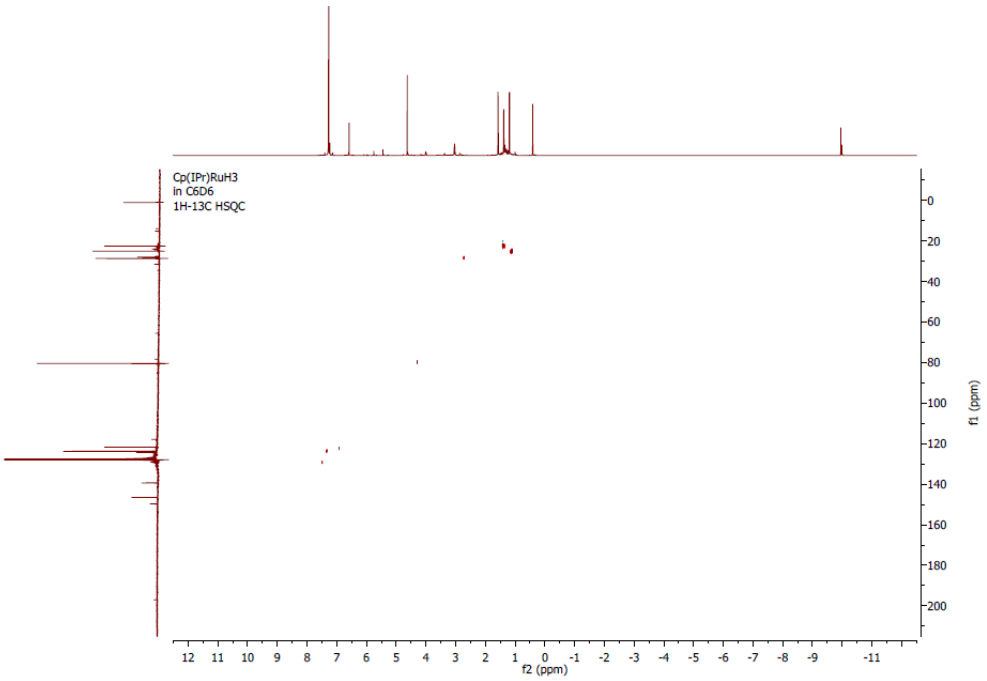

c)

Figure XII- 57. NMR spectra for Cp(IPr)RuH_3 a) ^{1}H- NMR, b) ^{13}C -NMR, c) ^{1}H-^{13}C HSQC

Cp(IPr)$RuH_2(SiCl_3)$ (VII-2a)

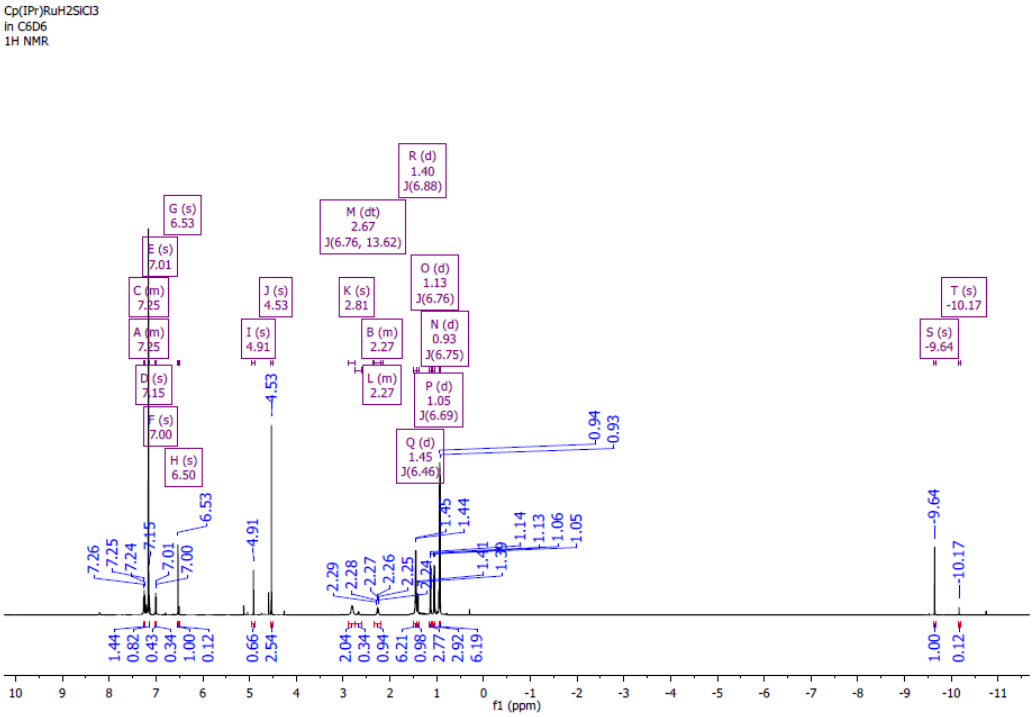

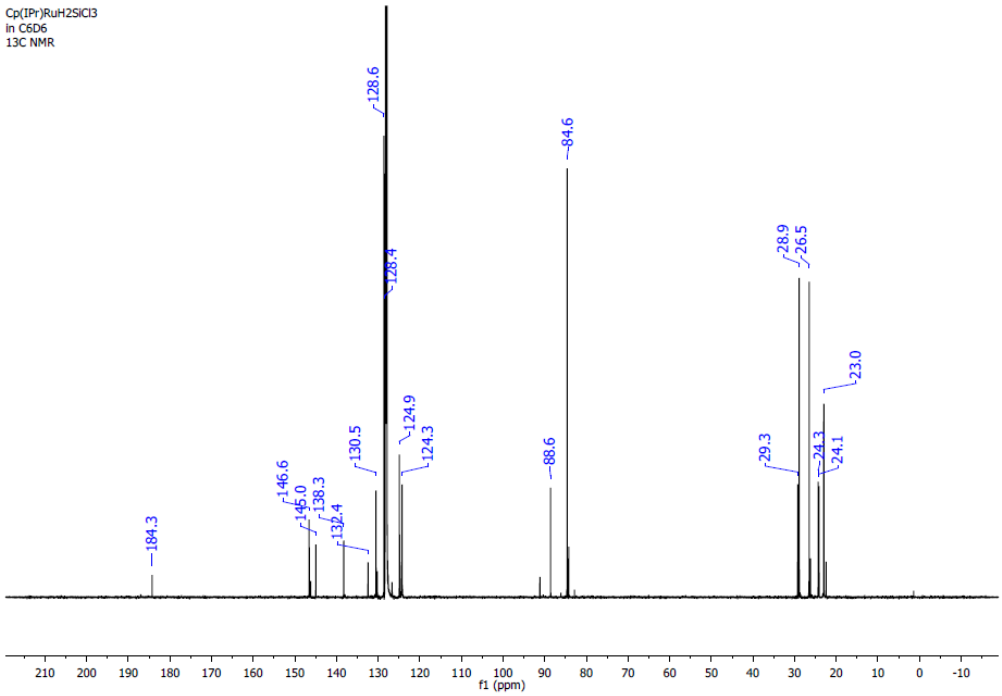
Cp(IPr)RuH2SiCl3
in C6D6
13C NMR
184.3
146.6
146.0
138.3
132.4
130.5
128.6
128.4
124.9
124.3
88.6
84.6
29.3
28.9
26.5
24.3
24.1
23.0
f1 (ppm)

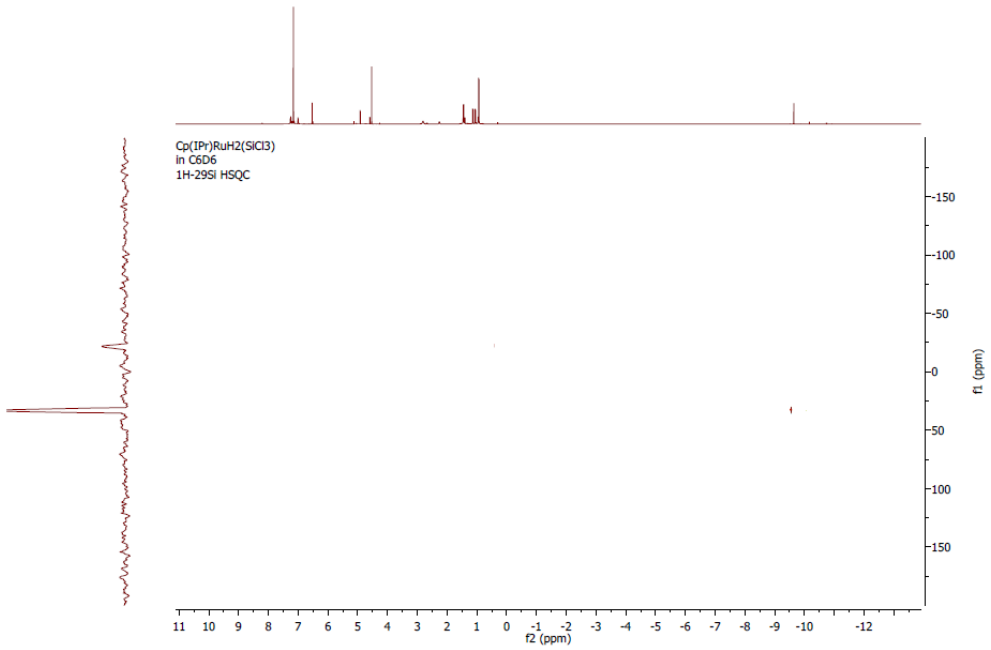
Cp(IPr)RuH2(SiCl3)
in C6D6
1H-29Si HSQC
f2 (ppm)
f1 (ppm)

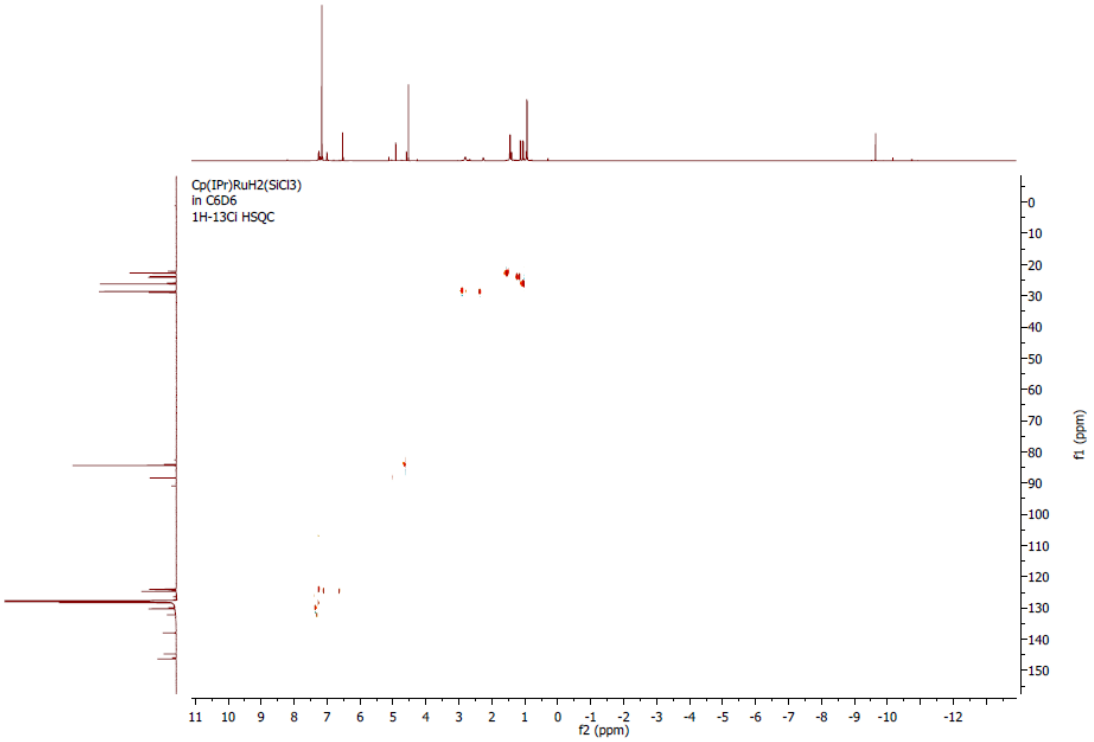

Figure XII- 58. NMR spectra for $Cp(IPr)RuH_2(SiCl_3)$, a) ^{1}H- NMR, b) ^{13}C -NMR, c) ^{1}H-^{13}C HSQC, d) ^{1}H-^{29}Si HSQC

$Cp(IPr)RuH_2(SiCl_2Me)$ (VII-2b)

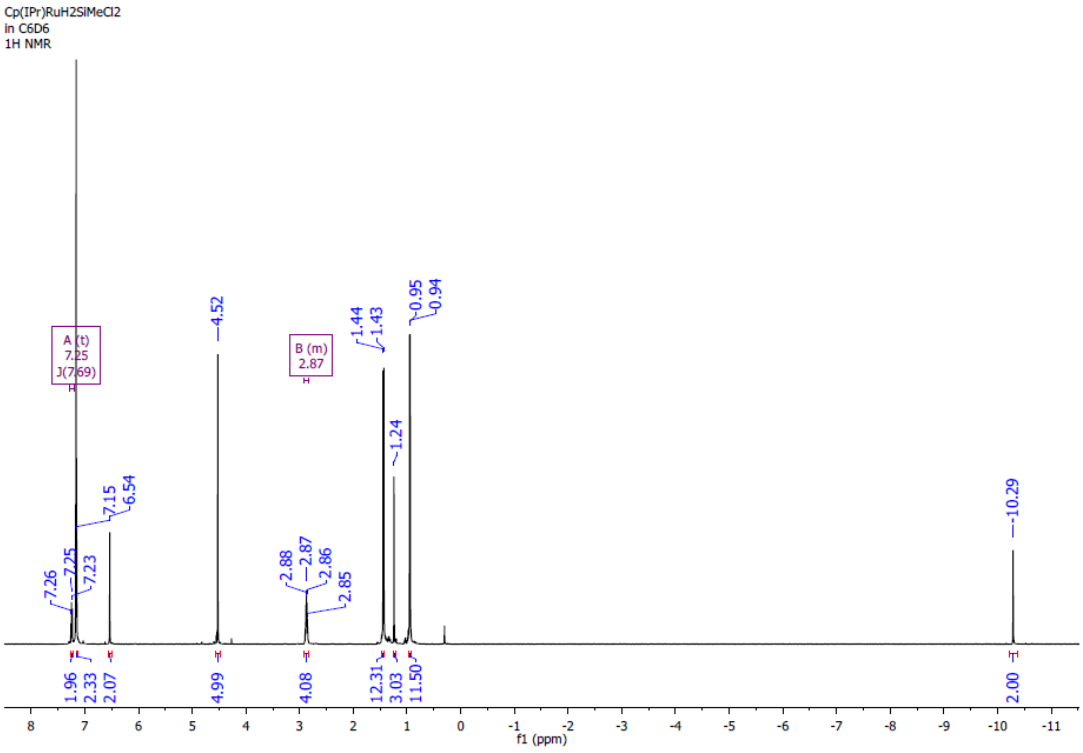

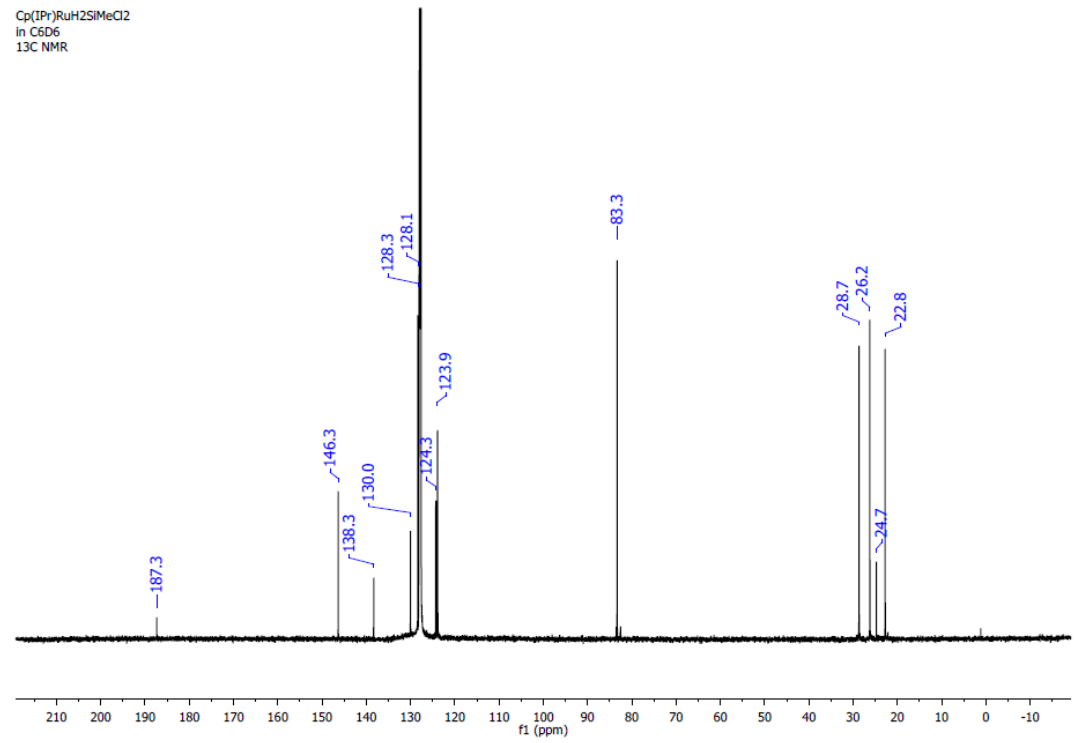
Cp(IPr)RuH2SiMeCl2
in C6D6
13C NMR
187.3
146.3
138.3
130.0
128.3
128.1
124.3
123.9
83.3
28.7
26.2
24.7
22.8
f1 (ppm)

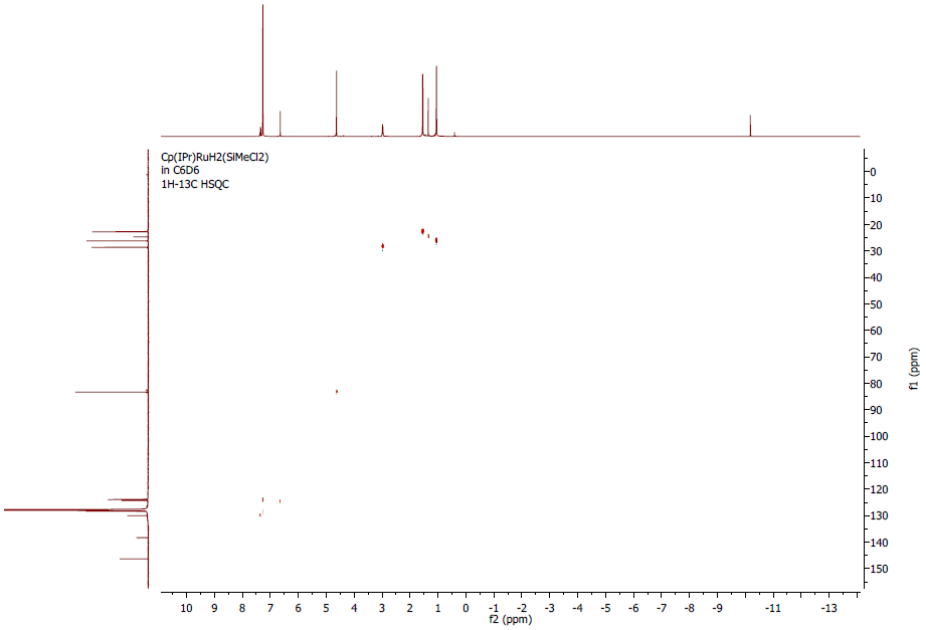
Cp(IPr)RuH2(SiMeCl2)
in C6D6
1H-13C HSQC
f2 (ppm)
f1 (ppm)

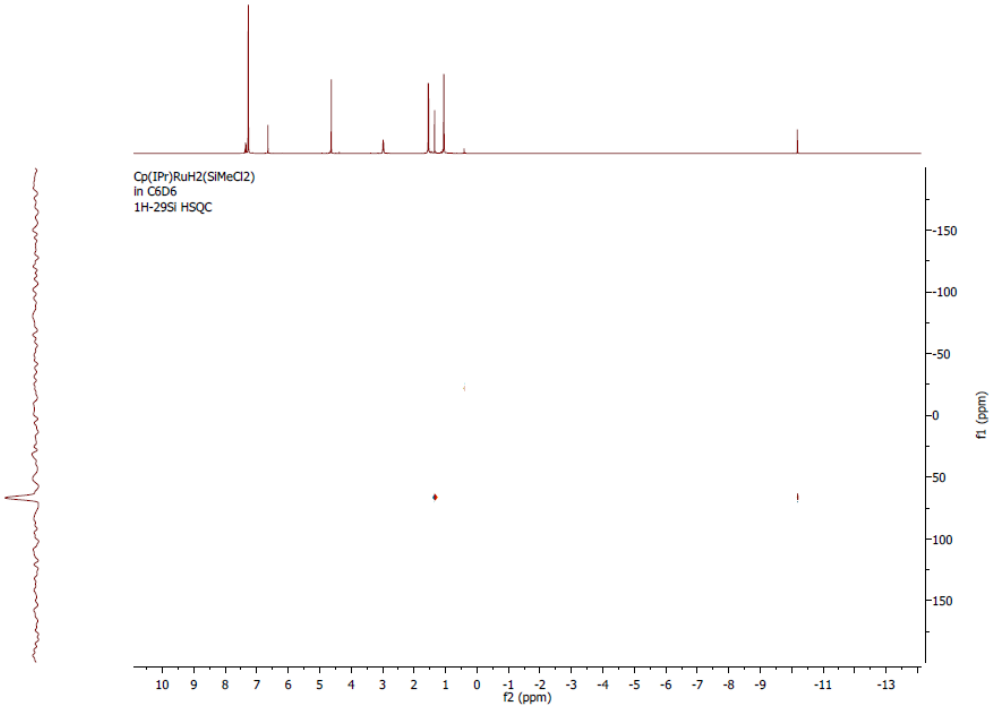

Figure XII- 59. NMR spectra for $Cp(IPr)RuH_2(SiCl_2Me)$ a) ^{1}H- NMR, b) ^{13}C - NMR, c) ^{1}H-^{13}C HSQC, d) ^{1}H-^{29}Si HSQC

$Cp(IPr)RuH_2(SiClMe_2)$ (VII-2c)

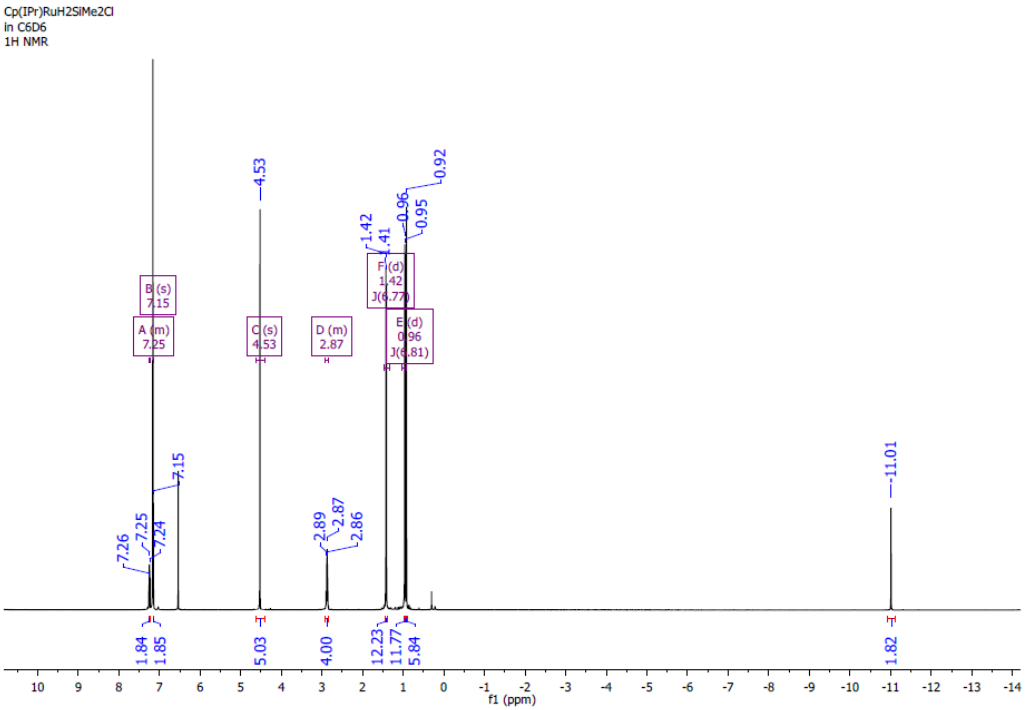

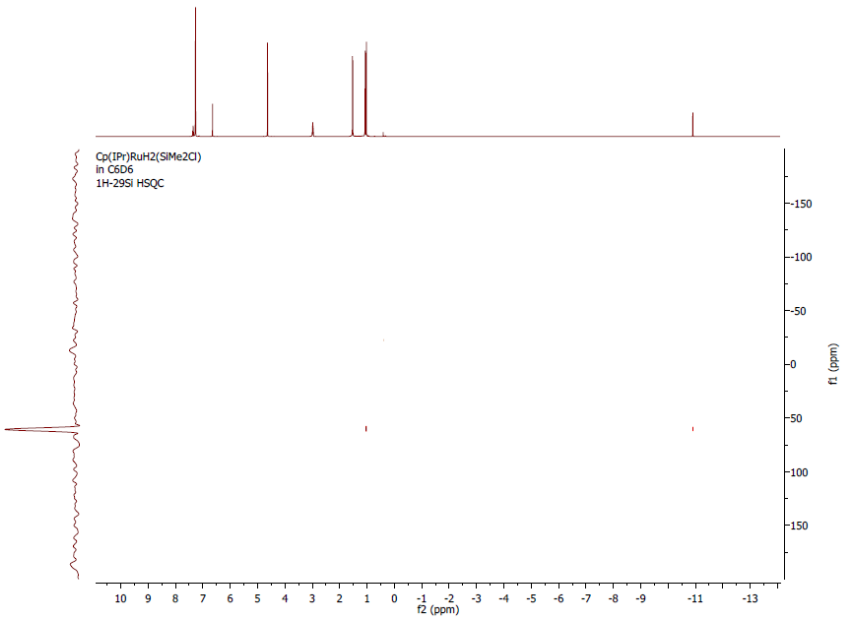
Cp(IPr)RuH2(SiMe2Cl)
in C6D6
1H-29Si HSQC
f1 (ppm)
f2 (ppm)

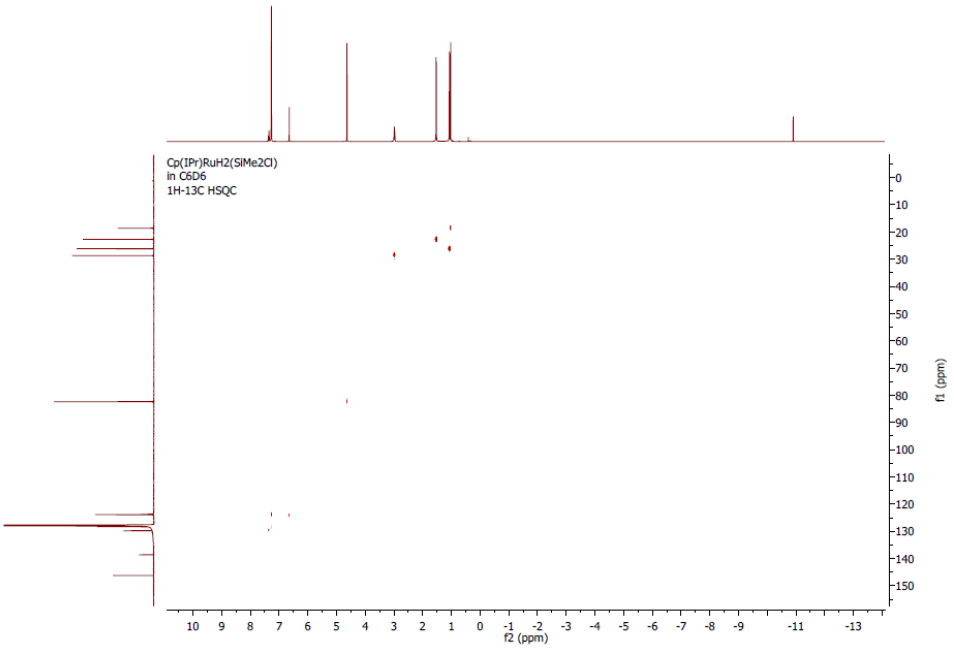
Cp(IPr)RuH2(SiMe2Cl)
in C6D6
1H-13C HSQC
f1 (ppm)
f2 (ppm)

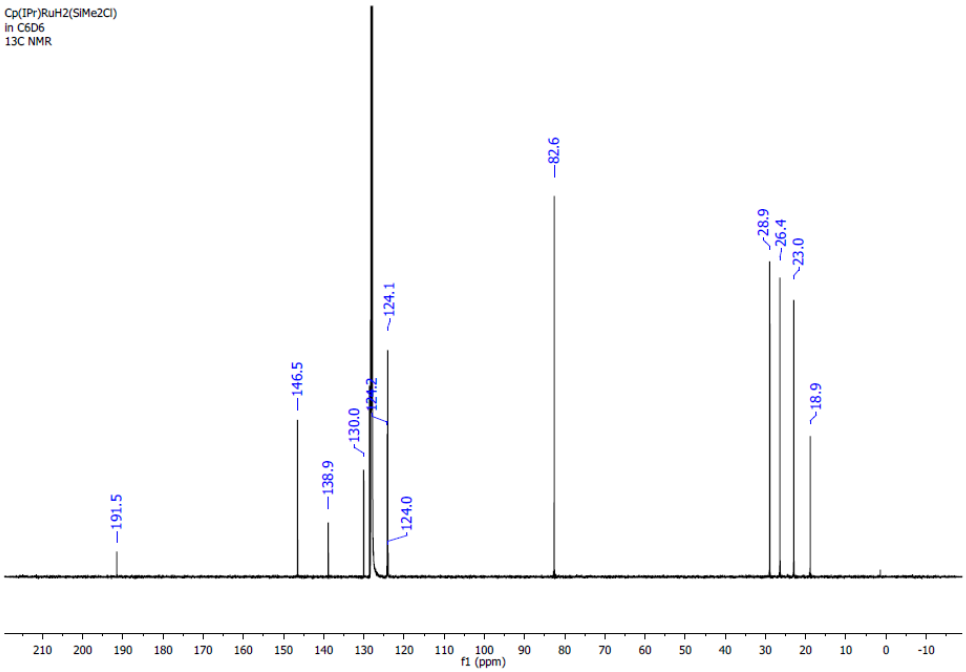

Figure XII- 60. NMR spectra for Cp(IPr)RuH$_2$(SiClMe$_2$) a) ^{1}H- NMR, b) ^{13}C - NMR, c) ^{1}H-^{13}C HSQC, d) ^{1}H-^{29}Si HSQC

Cp(IPr)RuH$_2$(SiH$_2$Ph) (VII-2d)

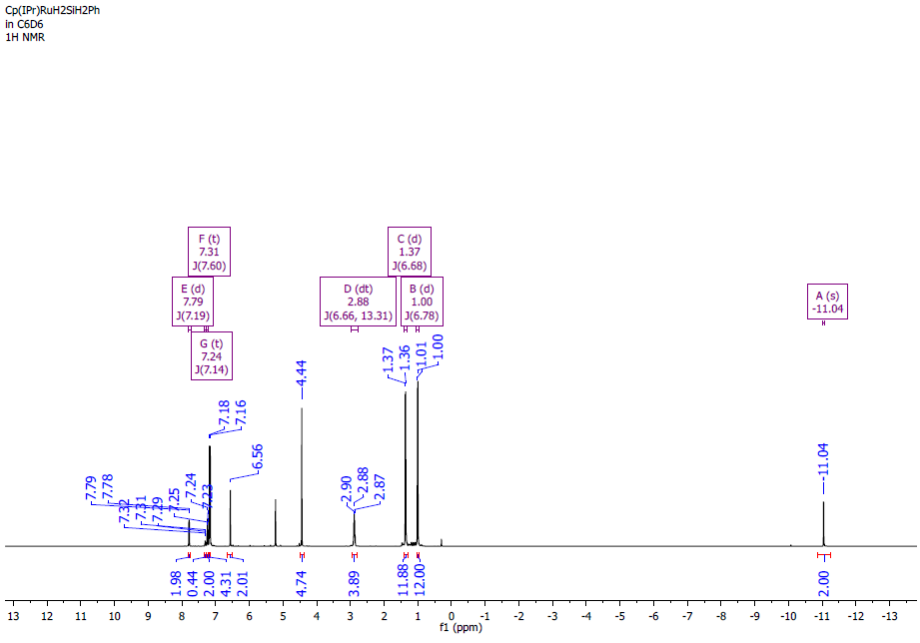

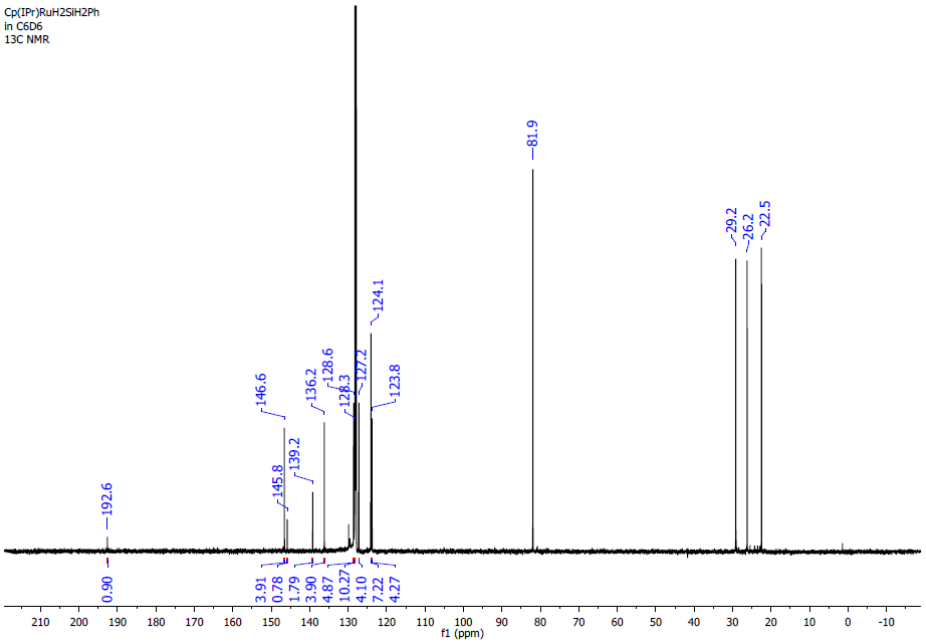
Cp(IPr)RuH2SiH2Ph
in C6D6
13C NMR
192.6
146.6
145.8
139.2
136.2
128.6
128.3
127.2
124.1
123.8
81.9
29.2
26.2
22.5
0.90
3.91
0.78
1.79
3.90
4.87
10.27
4.10
7.22
4.27
f1 (ppm)

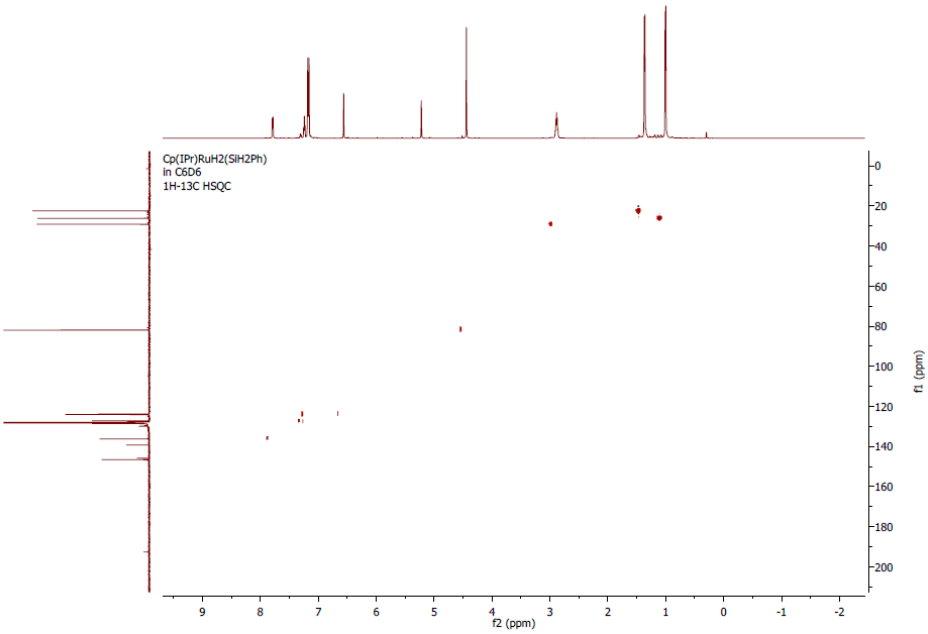
Cp(IPr)RuH2(SiH2Ph)
in C6D6
1H-13C HSQC
f2 (ppm)
f1 (ppm)

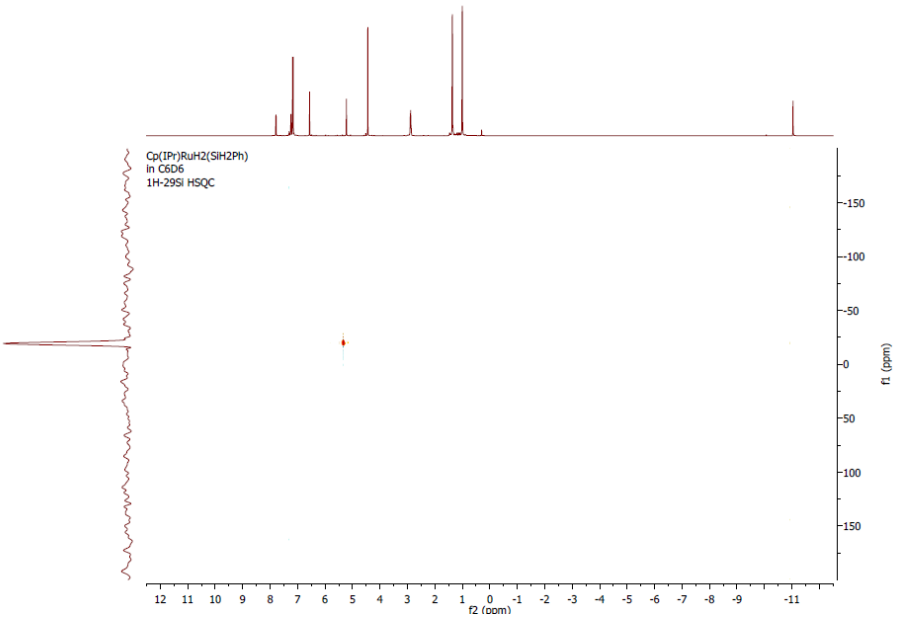

Figure XII- 61. NMR spectra for Cp(IPr)RuH$_2$(SiH$_2$Ph) a) ^{1}H- NMR, b) ^{13}C - NMR, c) ^{1}H-^{13}C HSQC, d) ^{1}H-^{29}Si HSQC

Cp(IPr)RuH$_2$(SiHMePh) (VII-2e)

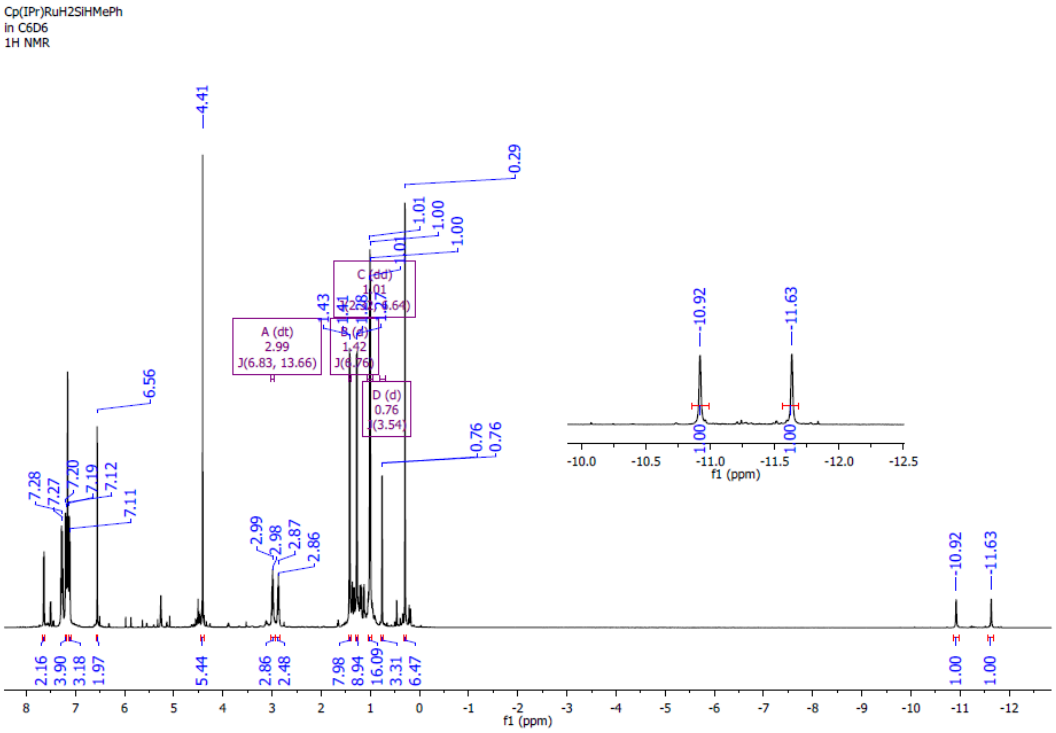

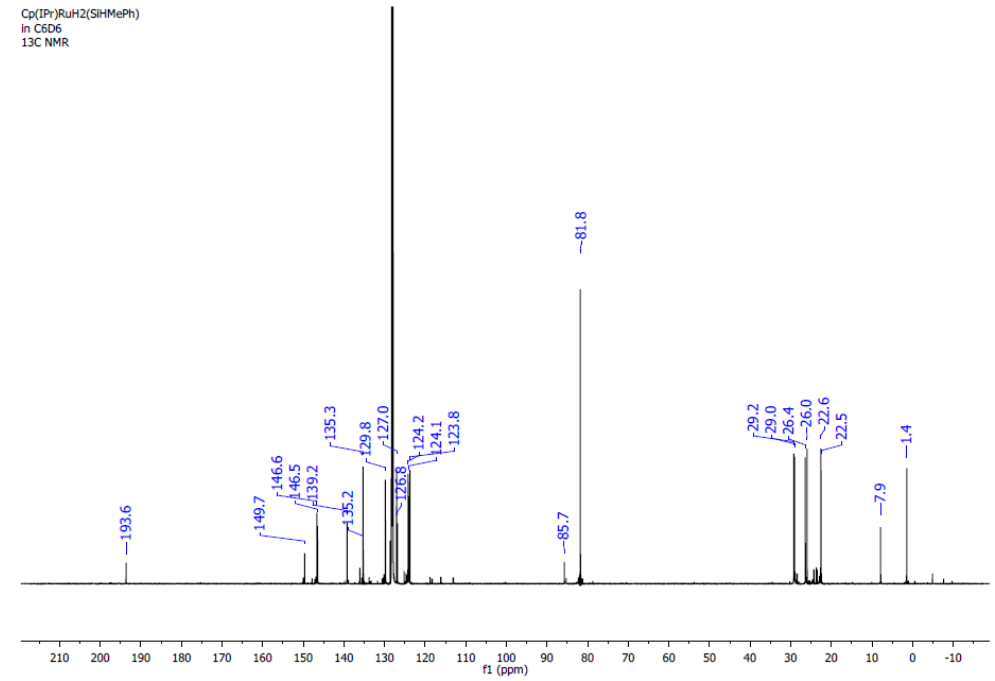
Cp(IPr)RuH2(SiHMePh)
in C6D6
13C NMR
193.6
149.7
146.6
146.5
139.2
135.3
135.2
129.8
127.0
126.8
124.2
124.1
123.8
85.7
81.8
29.2
29.0
26.4
26.0
22.6
22.5
7.9
1.4
f1 (ppm)

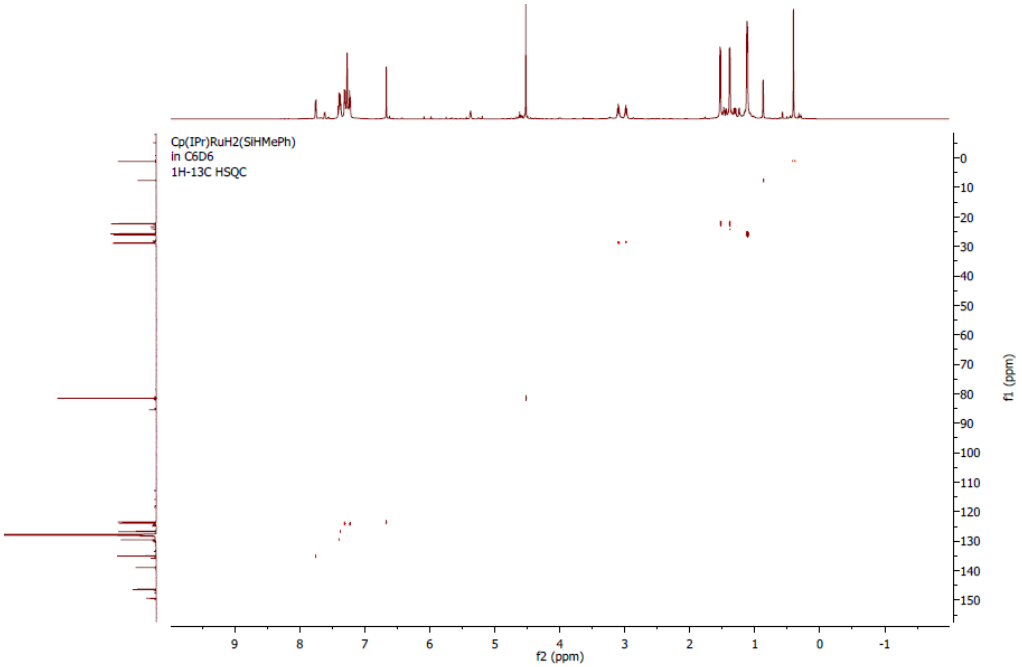
Cp(IPr)RuH2(SiHMePh)
in C6D6
1H-13C HSQC
f2 (ppm)
f1 (ppm)

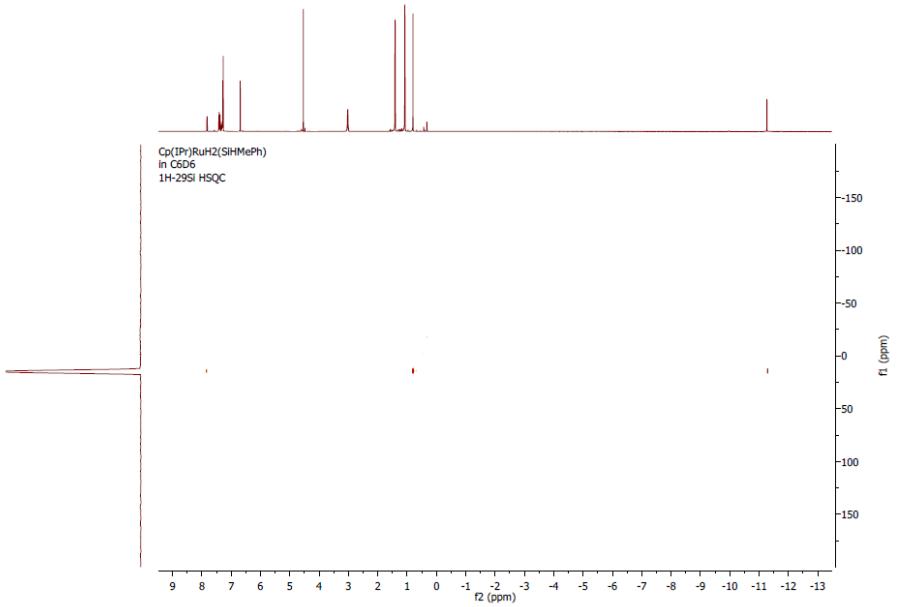

Figure XII- 62. NMR spectra for Cp(IPr)RuH$_2$(SiHMePh) a) ^{1}H- NMR, b) ^{13}C - NMR, c) ^{1}H-^{13}C HSQC, d) ^{1}H-^{29}Si HSQC

Cp(IPr)RuH$_2$(SiMe$_2$Ph) (VII-2f)

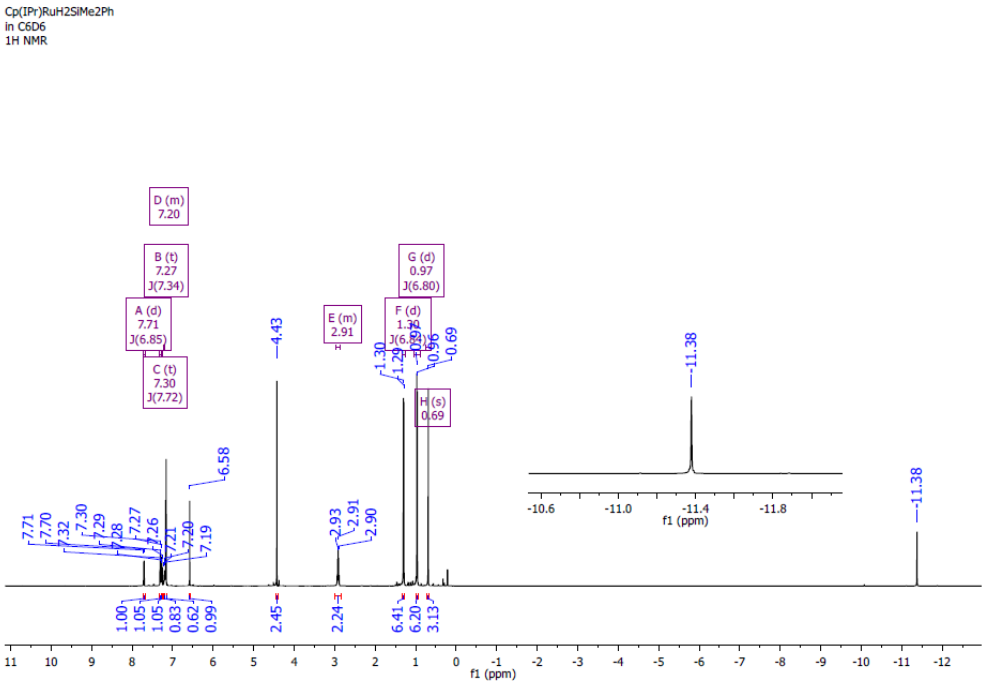

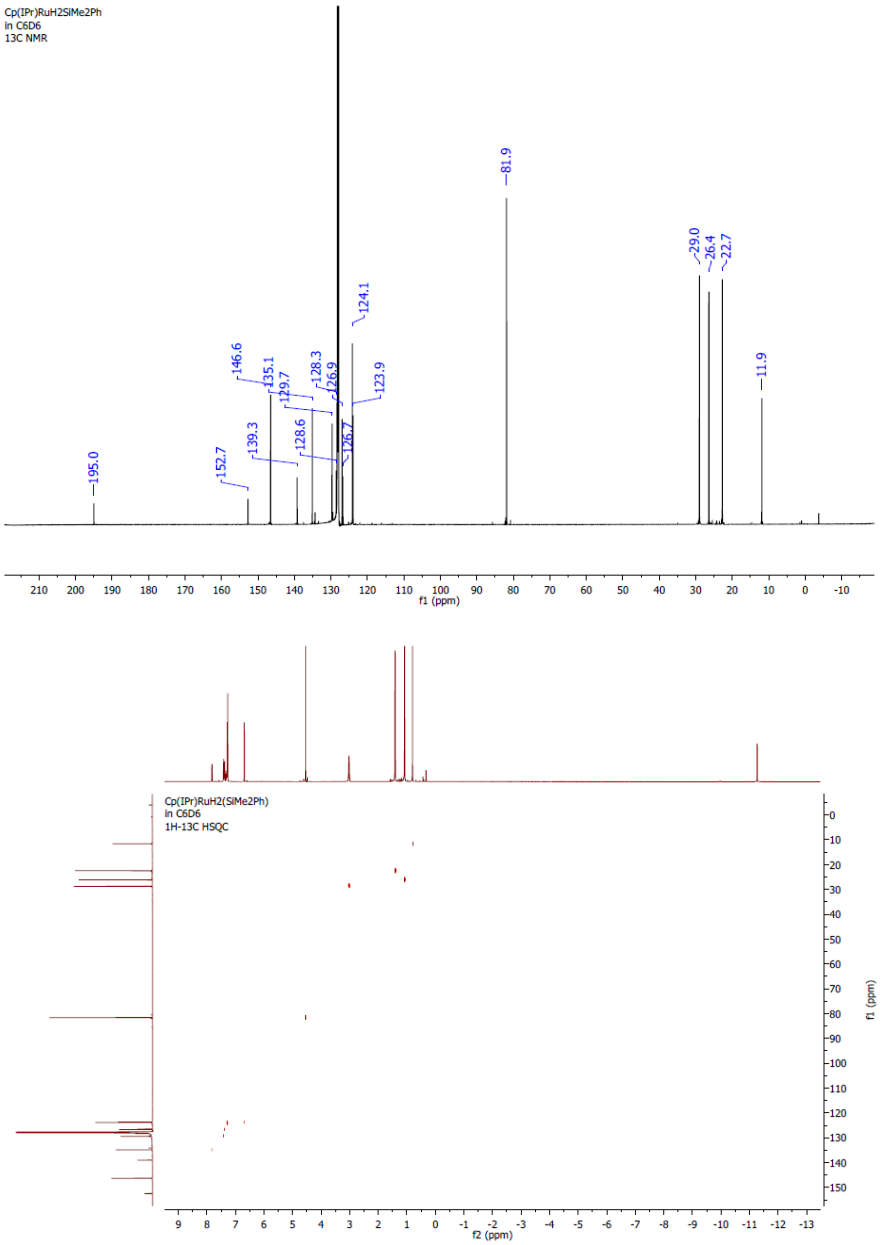
Cp(IPr)RuH2SiMe2Ph
in C6D6
13C NMR
195.0
152.7
146.6
139.3
135.1
129.7
128.6
128.3
126.9
126.7
124.1
123.9
81.9
29.0
26.4
22.7
11.9
f1 (ppm)
Cp(IPr)RuH2(SiMe2Ph)
in C6D6
1H-13C HSQC
f2 (ppm)
f1 (ppm)

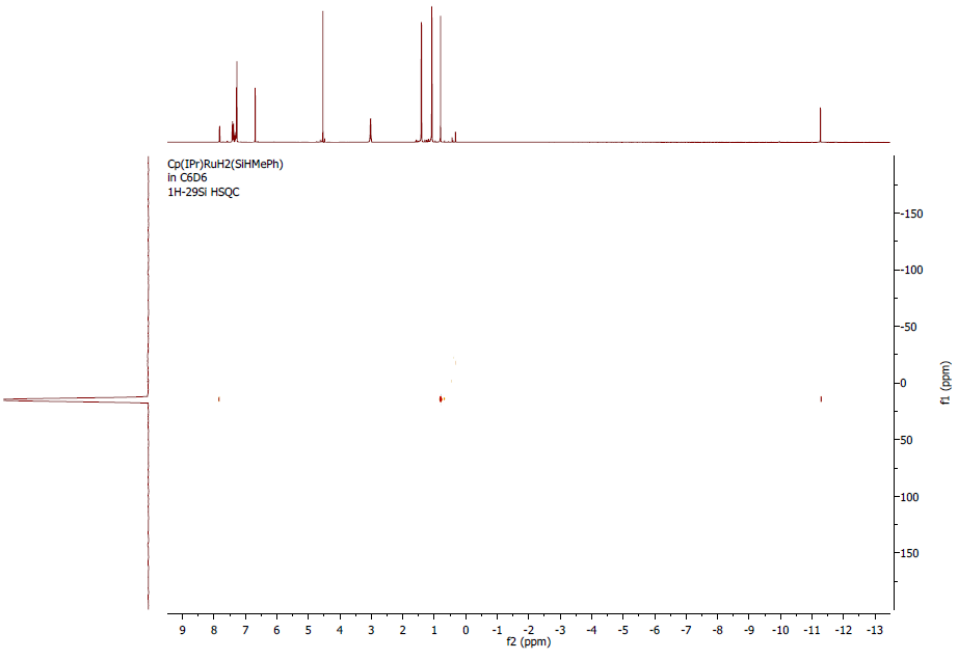

Figure XII- 63. NMR spectra for Cp(IPr)$RuH_2(SiMe_2Ph)$ a) ^{1}H- NMR, b) ^{13}C - NMR, c) ^{1}H-^{13}C HSQC, d) ^{1}H-^{29}Si HSQC

Isolated ammonium salts and amines

$CH_3(CH_2)_5NH_3Cl$

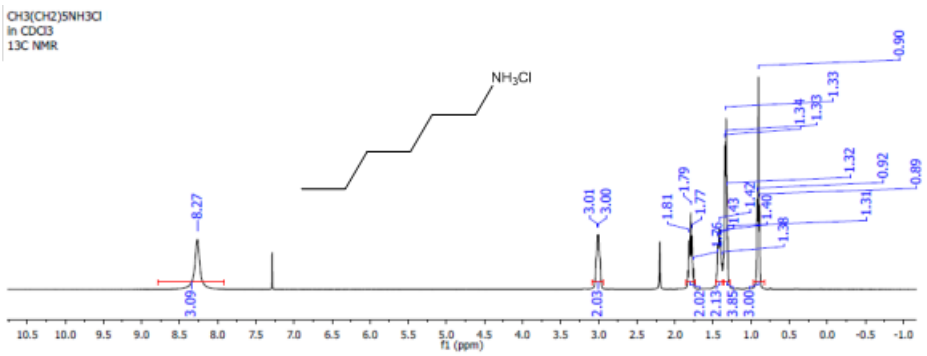

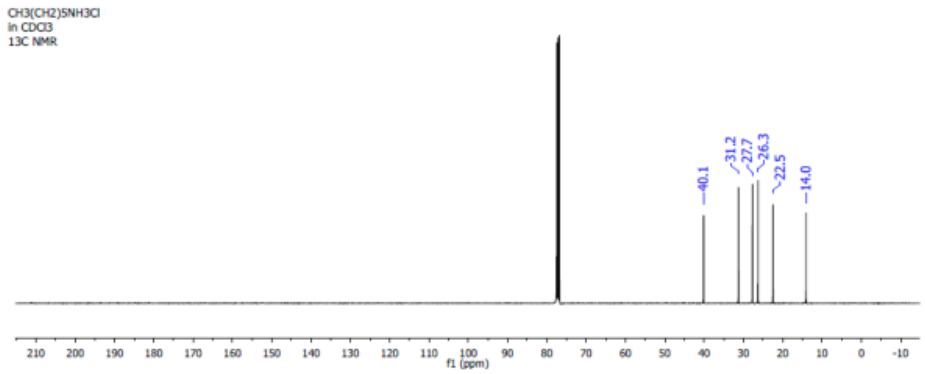

Figure XII- 64. ^{1}H (400 MHz, $CDCl_3$) and $^{13}C\{^{1}H\}$(100.6 MHz, $CDCl_3$) NMR spectra of $CH_3(CH_2)_5NH_3Cl$

$CH_3(CH_2)_3NH_2$

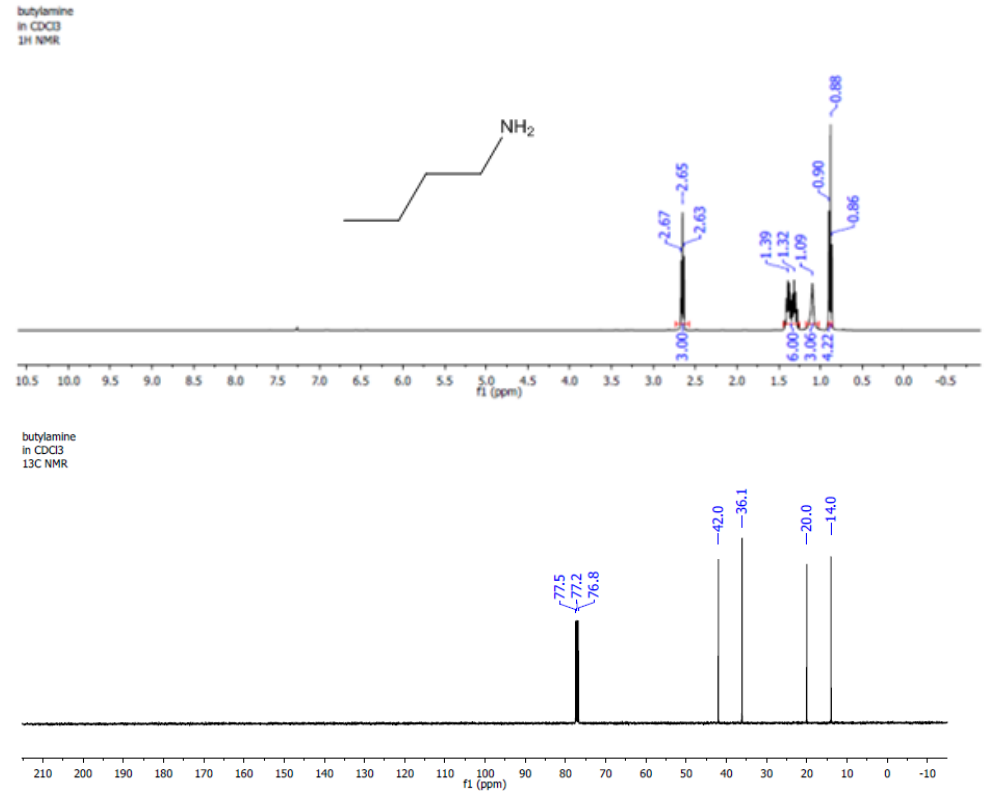

Figure XII- 65. ^{1}H (400 MHz, $CDCl_3$) and $^{13}C\{^{1}H\}$(100.6 MHz, $CDCl_3$) NMR spectra $CH_3(CH_2)_4NH_2$

4-(CH_3O)$C_6H_4CH_2NH_3Cl$

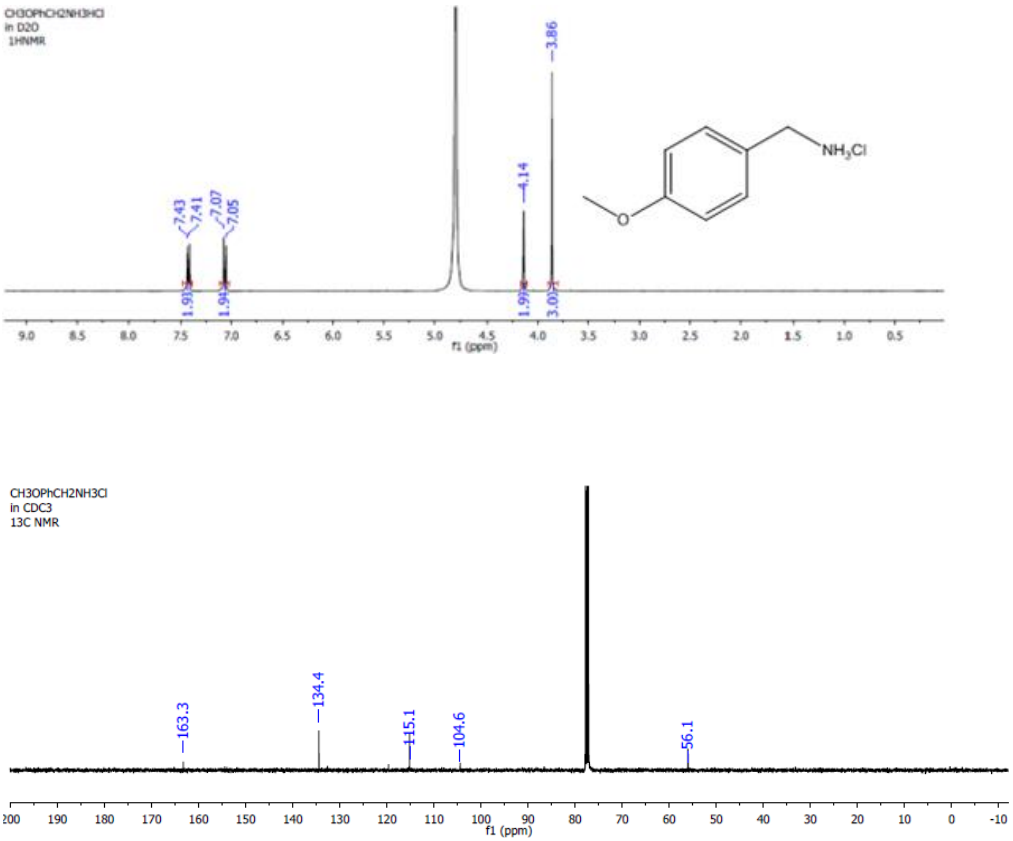

Figure XII- 66. ^{1}H (400 MHz, D_2O) and $^{13}C\{^{1}H\}$(100.6 MHz, $CDCl_3$) NMR spectra of 4-(CH_3O)$C_6H_4CH_2NH_3Cl$

4-(NH_2)$C_6H_4CH_2NH_3Cl$

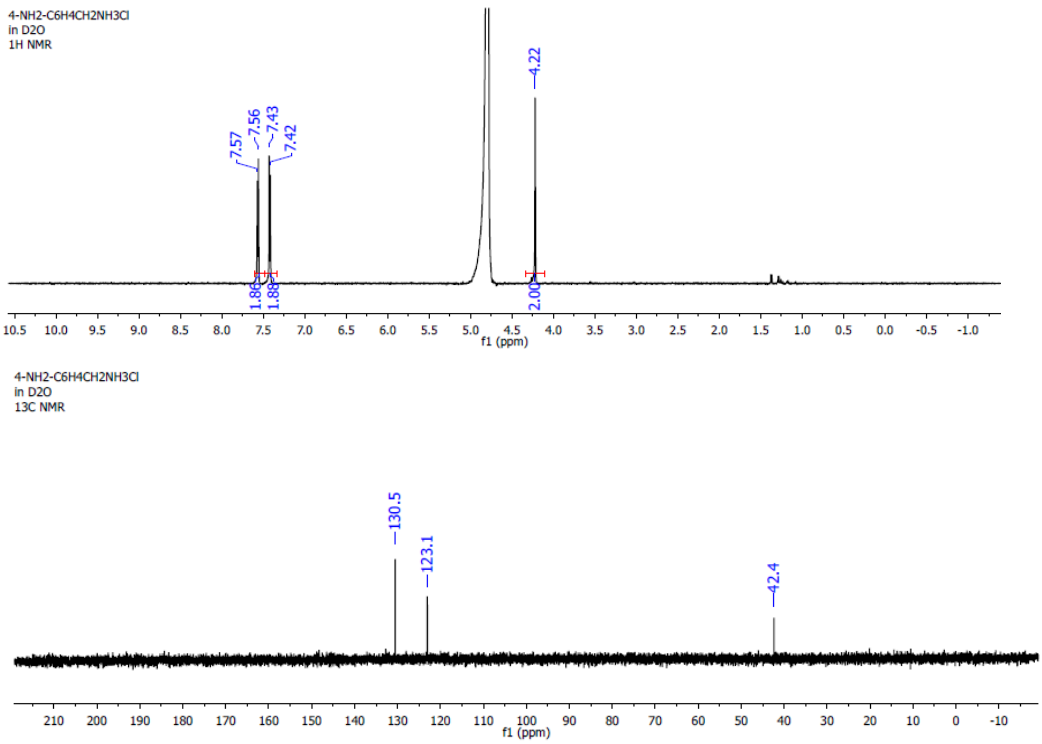

Figure XII- 67. ^{1}H (400 MHz, D_2O) and $^{13}C\{^{1}H\}$(100.6 MHz, D_2O) NMR spectra of 4-(NH_2)$C_6H_4CH_2NH_3Cl$

$C_6H_5CH_2NH_3Cl$

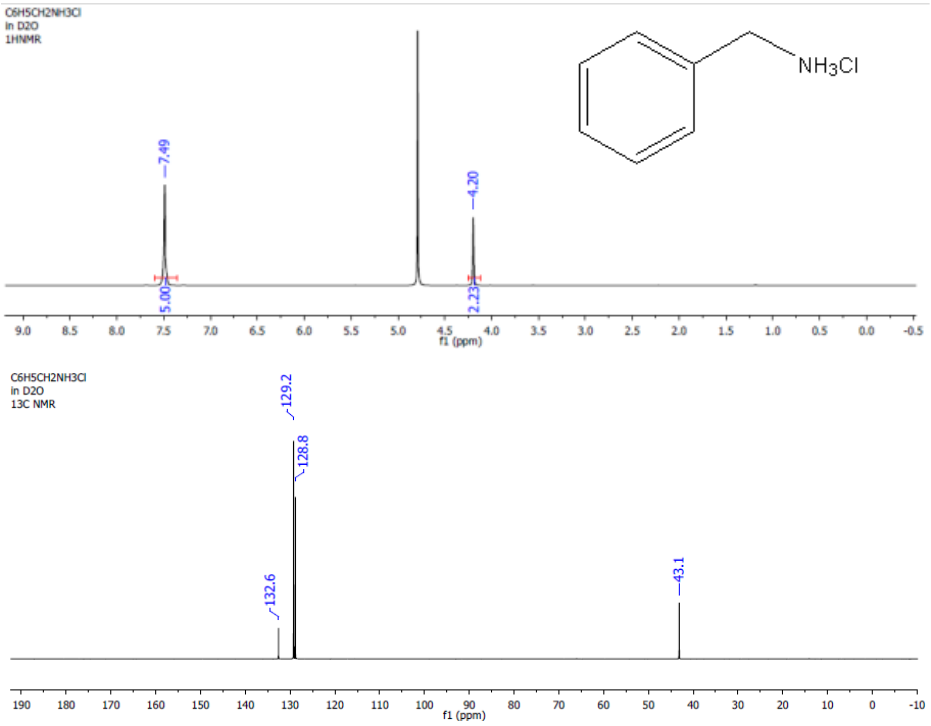

Figure XII- 68. ^{1}H (400 MHz, D_2O) and $^{13}C\{^{1}H\}$(100.6 MHz, D_2O) NMR spectra of $C_6H_5CH_2NH_3Cl$

1,2,3,4-tetrahydroquinoline

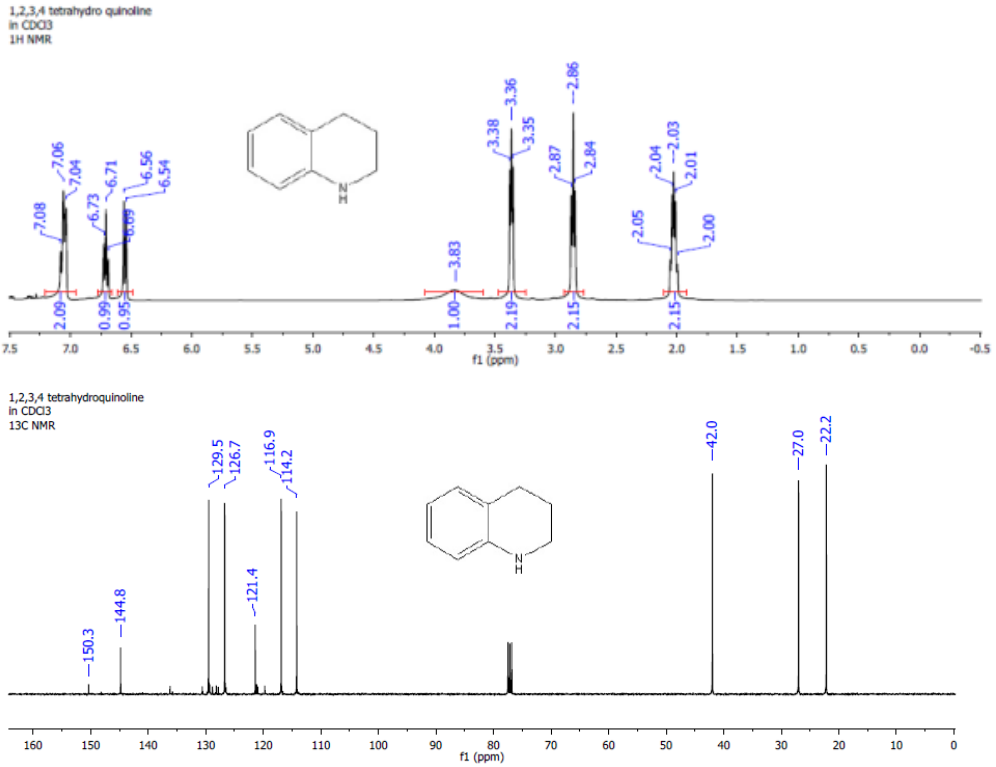

Figure XII- 69. ^{1}H (400 MHz, $CDCl_3$) and $^{13}C\{^{1}H\}$(100.6 MHz, $CDCl_3$) NMR spectra of 1,2,3,4-tetrahydroquinoline

Hydrogenated conjugated olefins

Ethylbutyrate

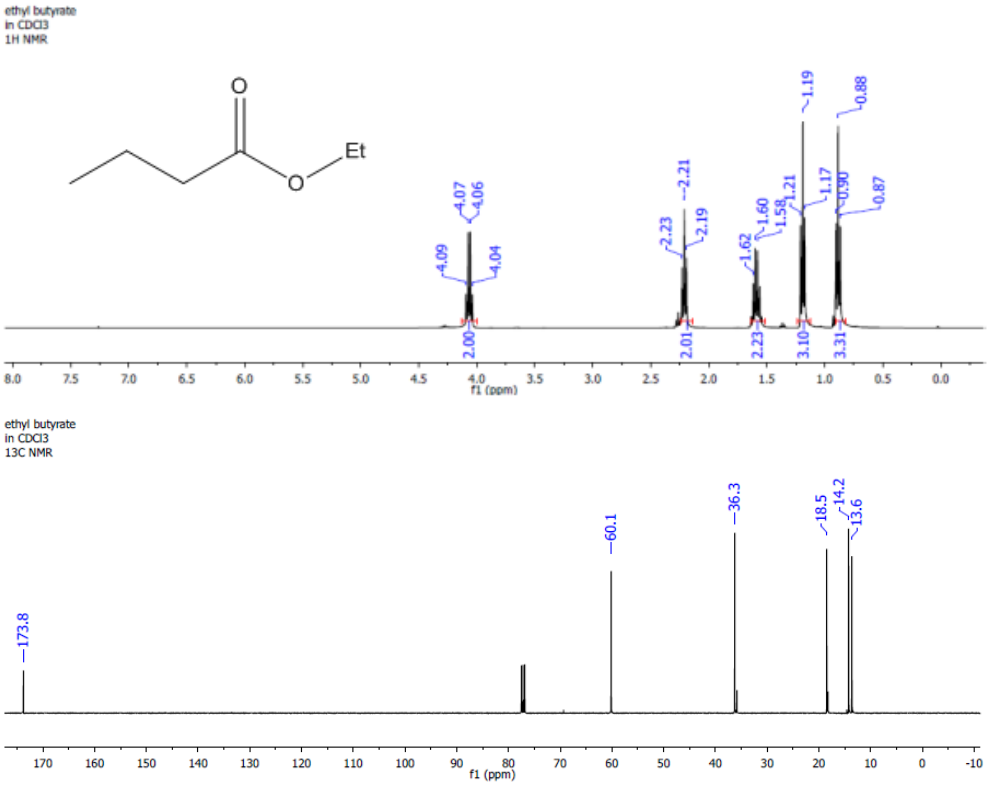

Figure XII- 70. ^{1}H (400 MHz, $CDCl_3$) and $^{13}C\{^{1}H\}$(100.6 MHz, $CDCl_3$) NMR spectra of ethylbutyrate

Isopropyl isobutyrate

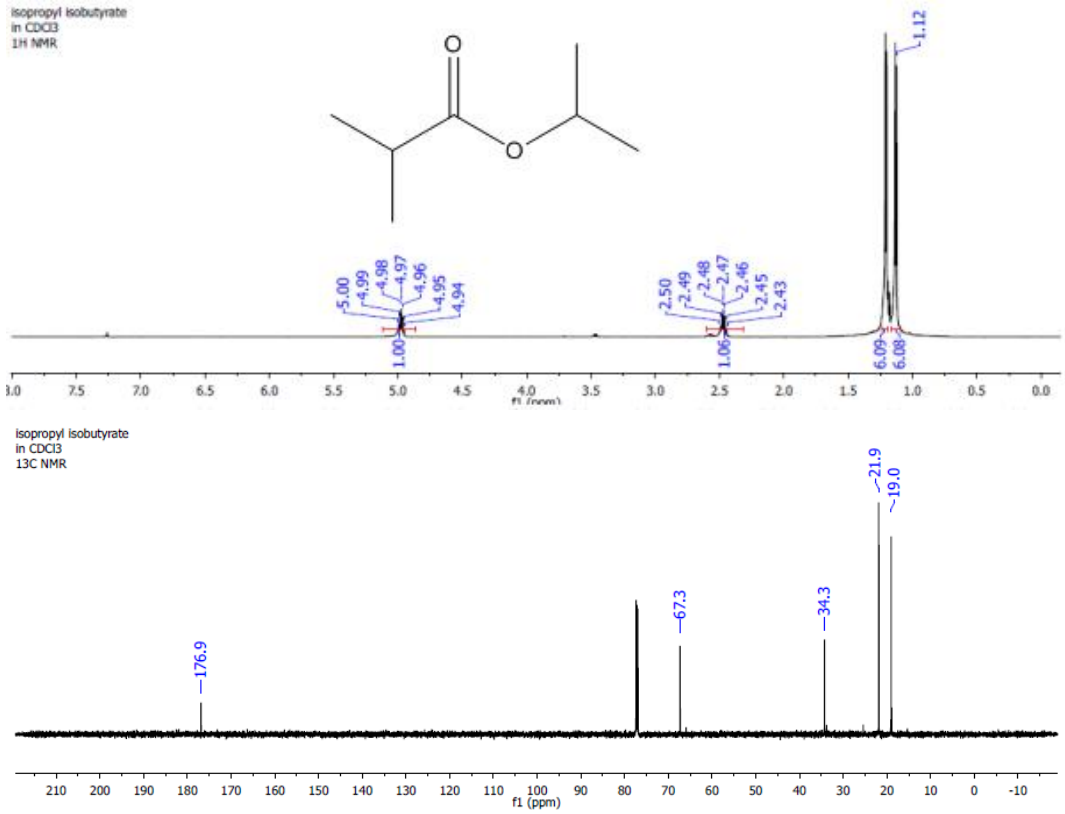

Figure XII- 71. ^{1}H (400 MHz, $CDCl_3$) and $^{13}C\{^{1}H\}$(100.6 MHz, $CDCl_3$) NMR spectra of isopropyl isobutyrate

Propionamide

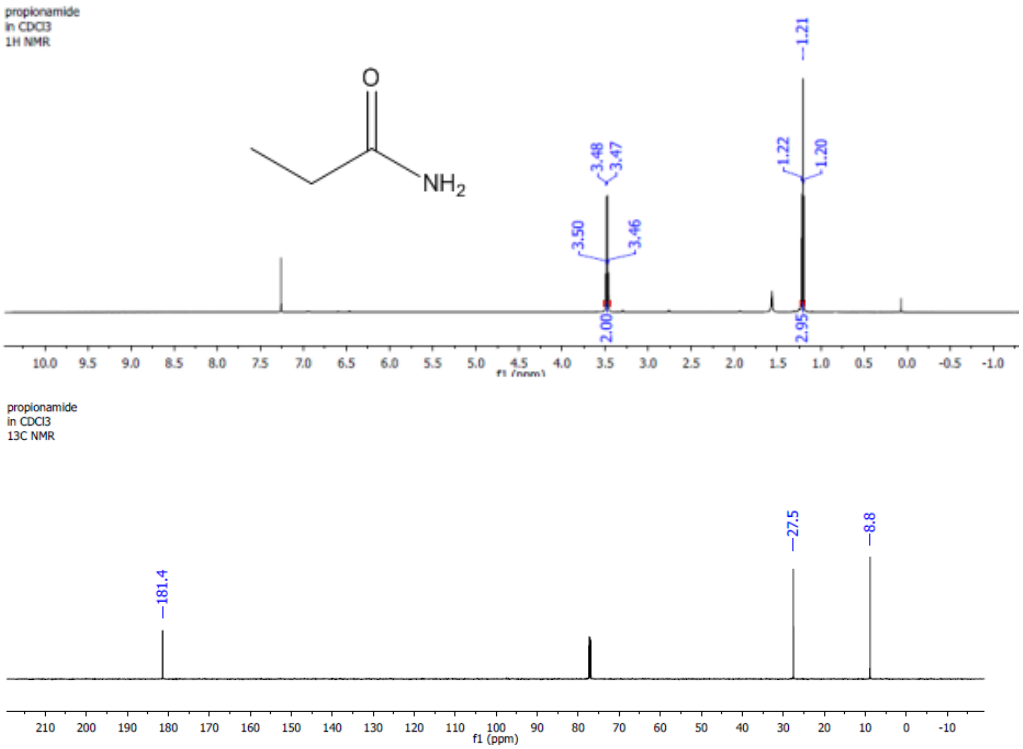

Figure XII- 72. ^{1}H (400 MHz, $CDCl_3$) and $^{13}C\{^{1}H\}$(100.6 MHz, $CDCl_3$) NMR spectra of propionamide

Isobutyramide

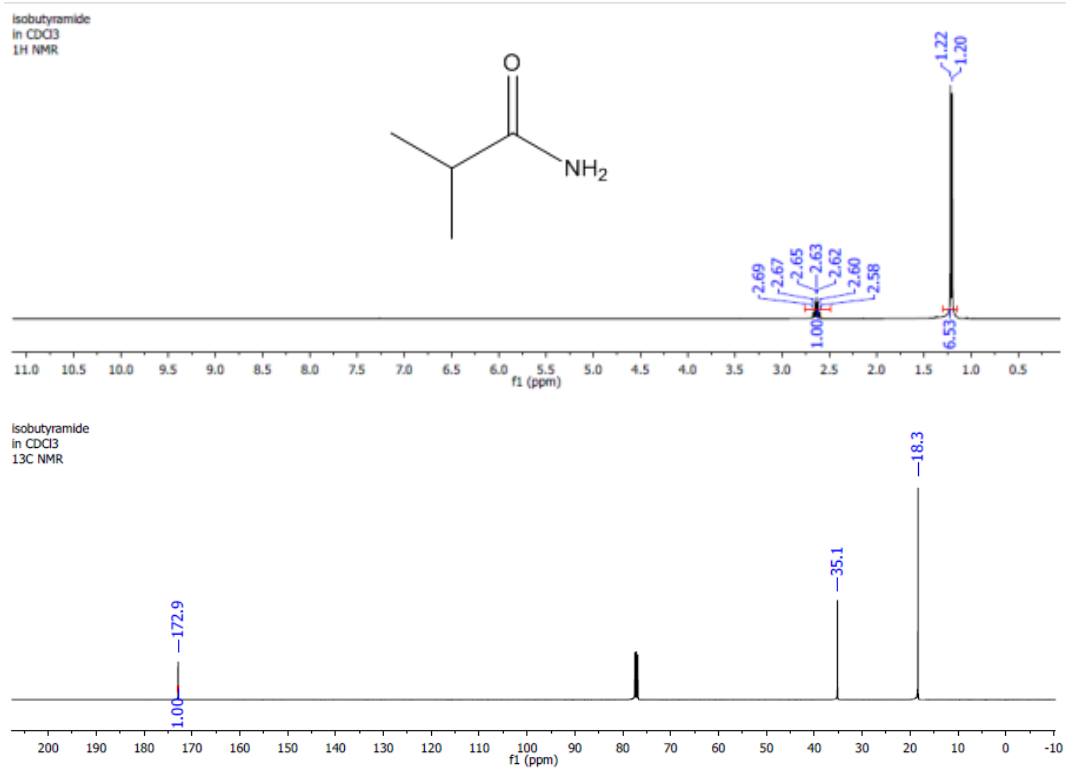

Figure XII- 73. ^{1}H (400 MHz, $CDCl_3$) and $^{13}C\{^{1}H\}$(100.6 MHz, $CDCl_3$) NMR spectra of isobutyramide

Ethyl isobutyrate

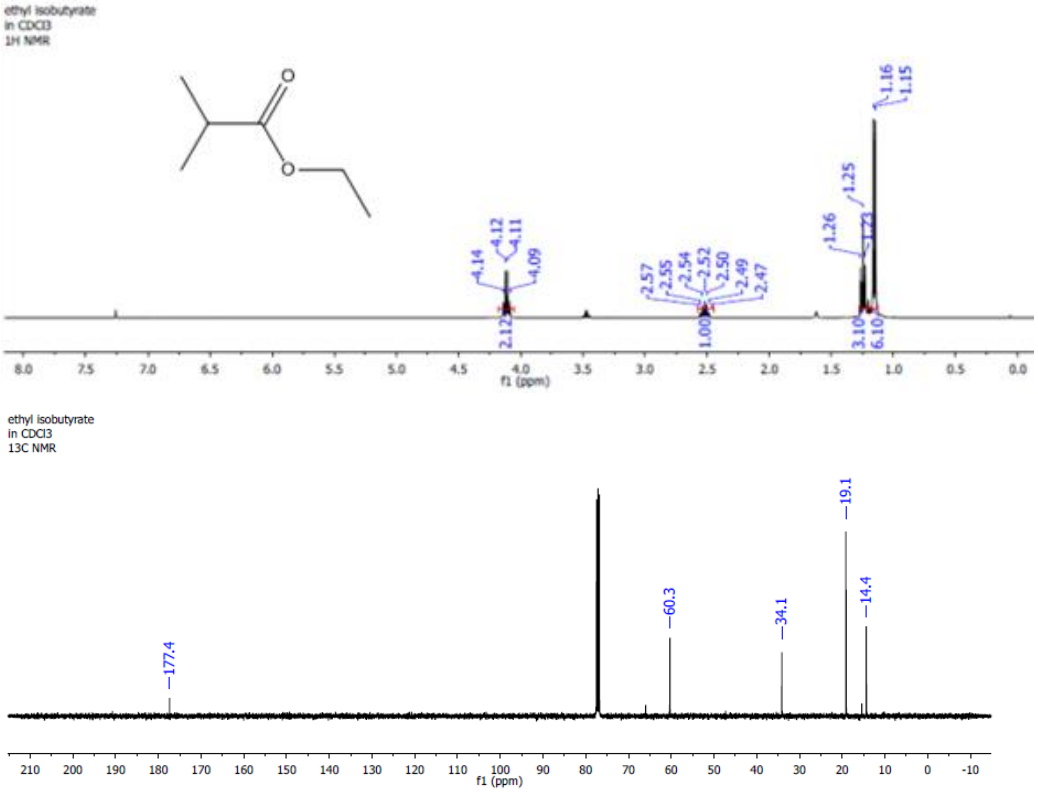

Figure XII- 74. ^{1}H (400 MHz, $CDCl_3$) and $^{13}C\{^{1}H\}$(100.6 MHz, $CDCl_3$) NMR spectra of ethyl isobutyrate

Methyl propionate

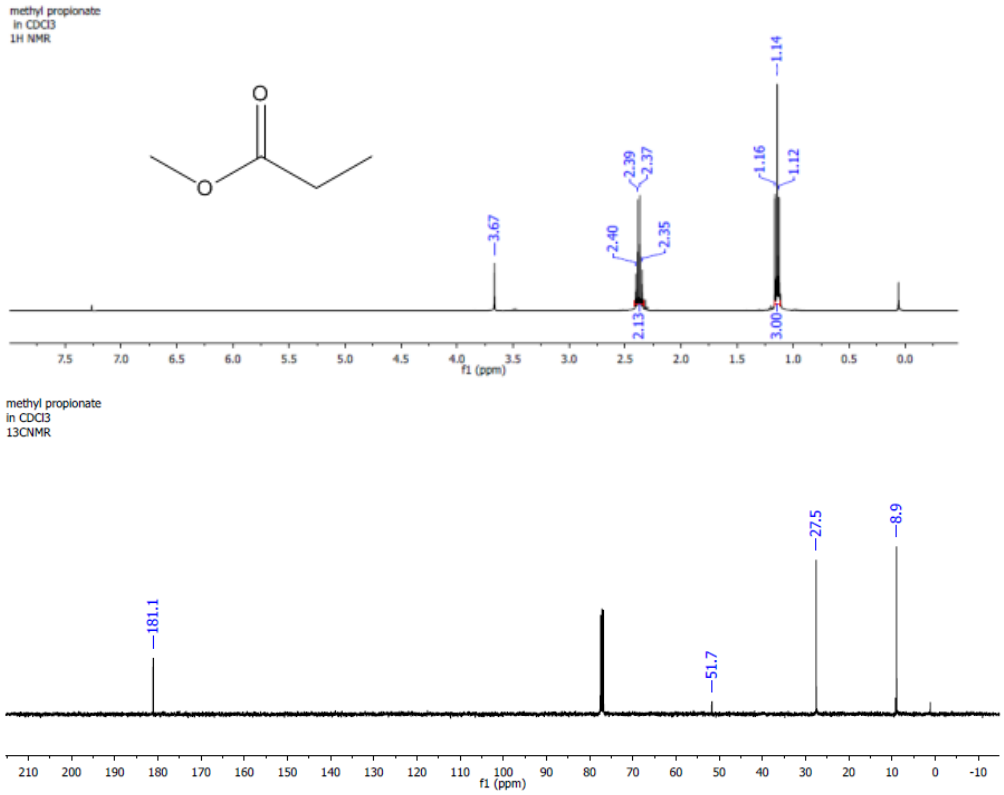

Figure XII- 75. ^{1}H (400 MHz, $CDCl_3$) and $^{13}C\{^{1}H\}$(100.6 MHz, $CDCl_3$) NMR spectra of methyl propionate

Ethyl propionate

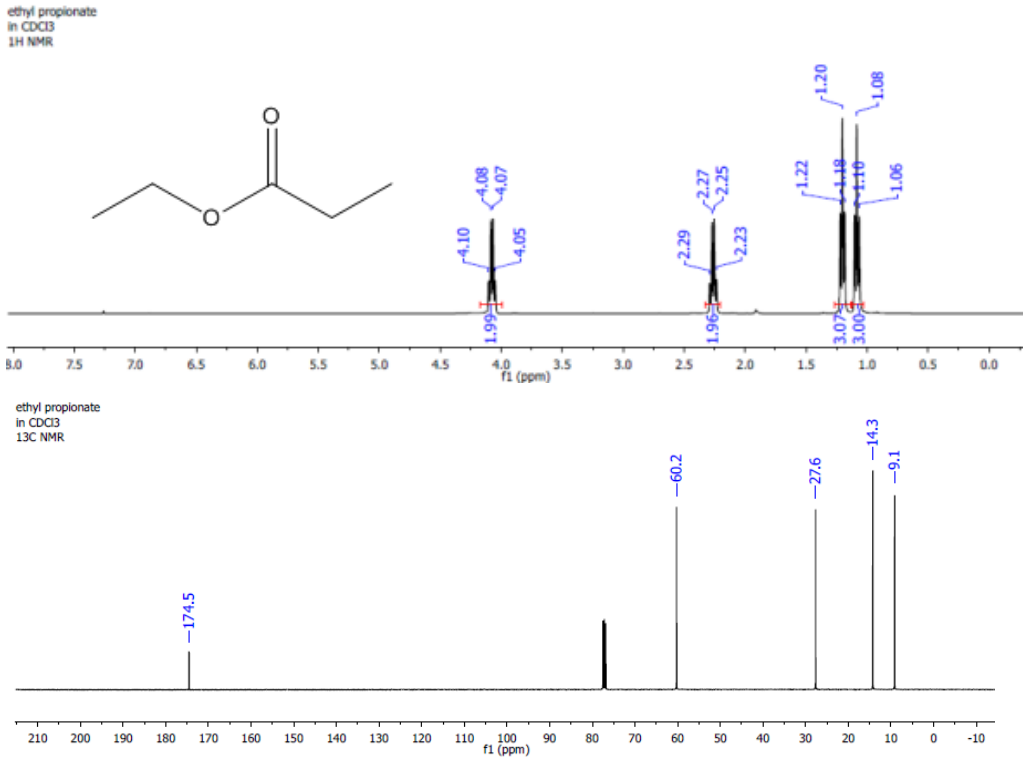

Figure XII- 76. ^{1}H (400 MHz, $CDCl_3$) and $^{13}C\{^{1}H\}$(100.6 MHz, $CDCl_3$) NMR spectra of ethyl propionate

$[Cp^*(IPr)Ru(NCCH_3)_2]PF_6$ (VI-8)

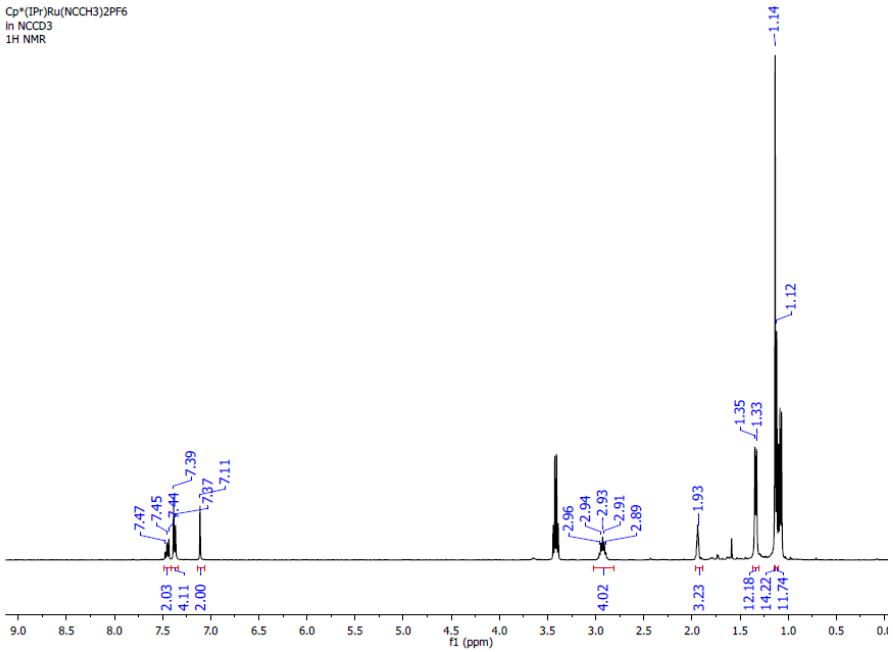

Figure XII- 77. ^{1}H NMR (600 MHz, $NCCD_3$) spectrum of

[Cp*(IPr)Ru(NCCH$_3$)$_2$]PF$_6$. (**VI-8**)

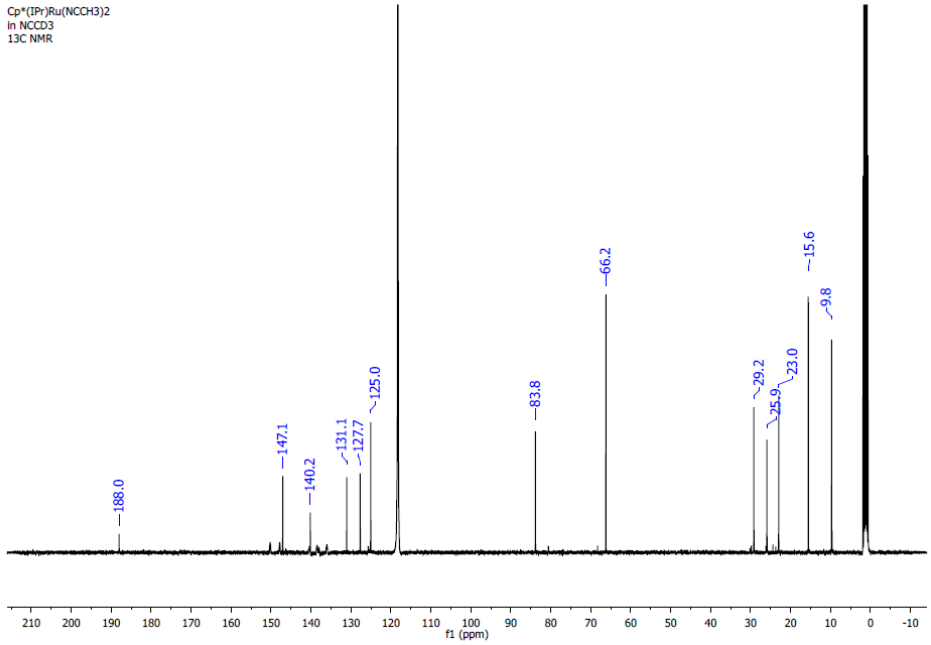

Figure XII- 78. ^{13}C NMR (600 MHz, NCCD$_3$) spectrum of [Cp*(IPr)Ru(NCCH$_3$)$_2$]PF$_6$. (**VI-8**)

Cp(IMes)RuH$_3$ (VI-17)

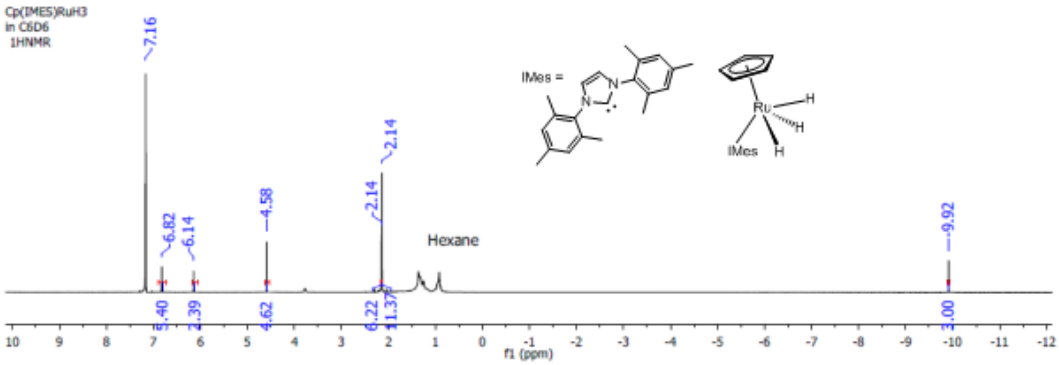

Figure XII- 79. ^{1}H NMR (600 MHz, C$_6$D$_6$) spectrum of Cp(IMes)RuH$_3$.

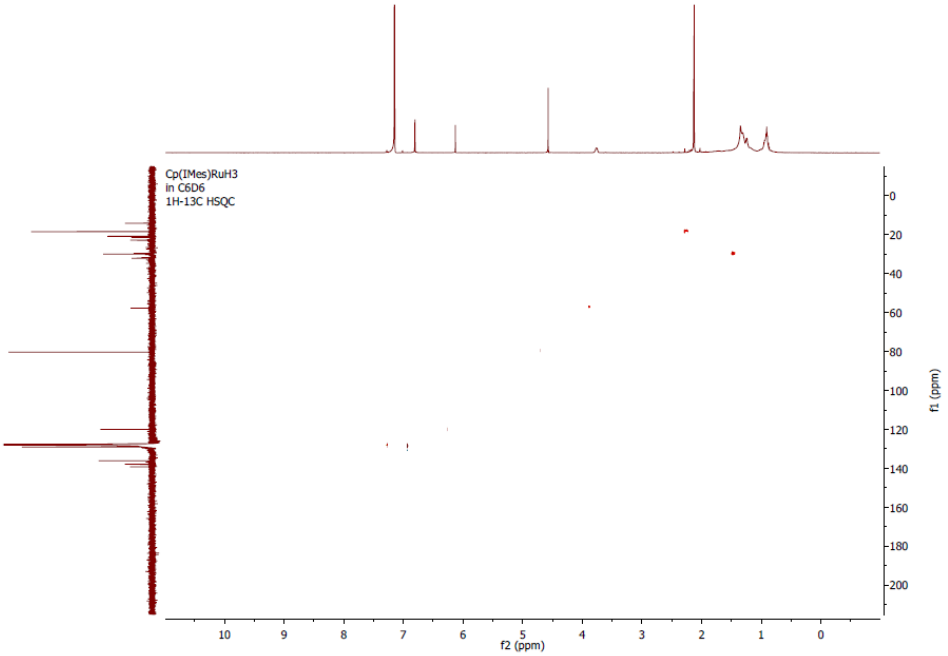

Figure XII- 80. ^{1}H- ^{13}C HSQC NMR (600 MHz, C_6D_6) spectrum of Cp(IMes)RuH_3.

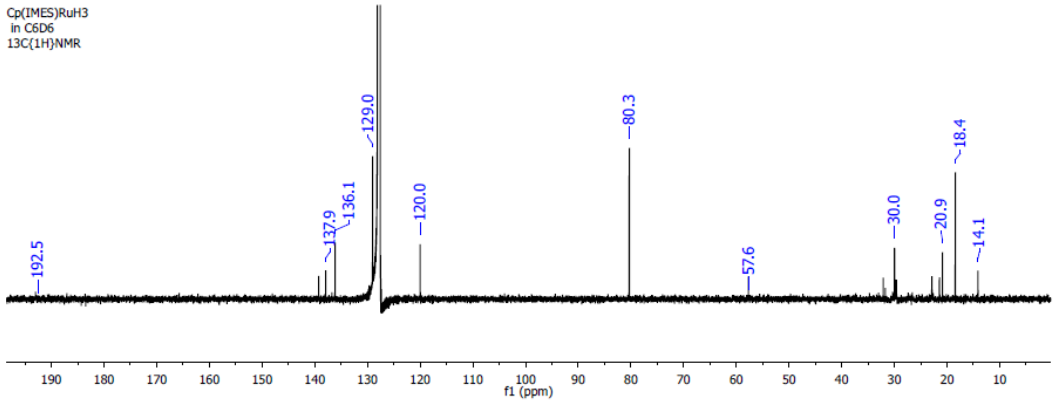

Figure XII- 81. $^{13}C\{^{1}H\}$ NMR spectrum (151 MHz, C_6D_6) spectrum of Cp(IMes)RuH_3.

Cp*(IPr)RuH_3 (VI-15)

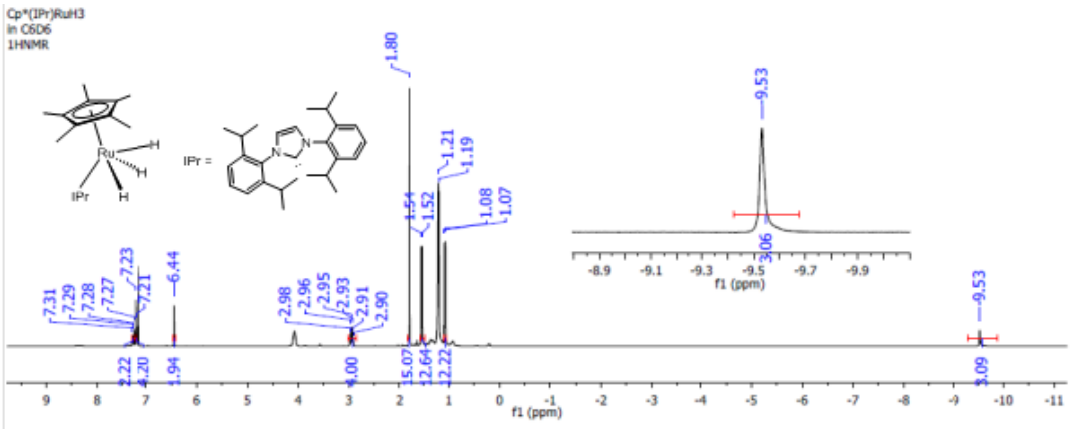

Figure XII- 82. ^{1}H NMR (600 MHz, C_6D_6) spectrum of Cp*(IPr)RuH_3.

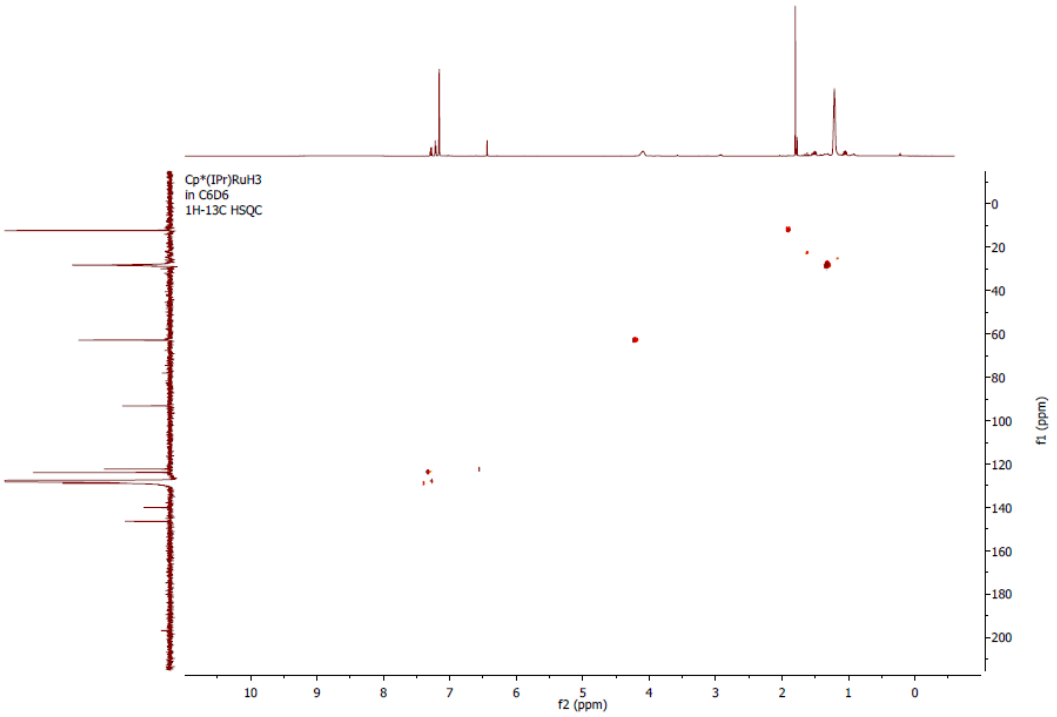

Figure XII- 83. ^{1}H- ^{13}C HSQC NMR (600 MHz, C_6D_6) spectrum of Cp*(IPr)RuH_3.

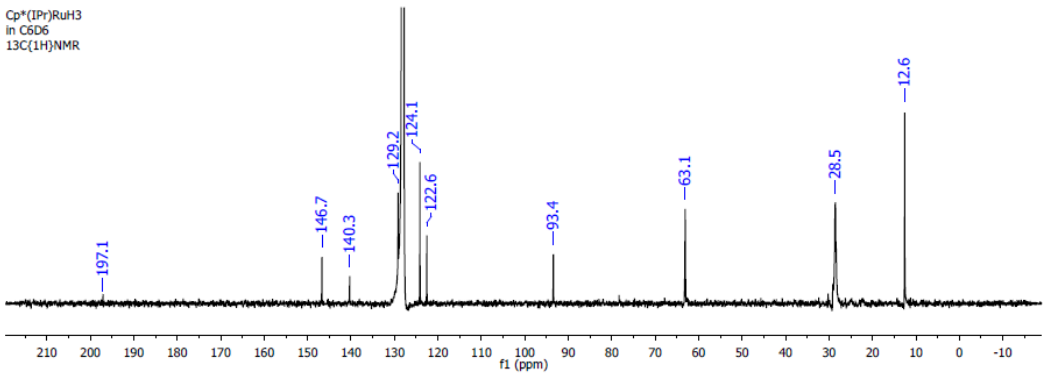

Figure XII- 84. $^{13}C\{^{1}H\}$ NMR spectrum (151 MHz, C_6D_6) spectrum of Cp*(IPr)RuH_3.

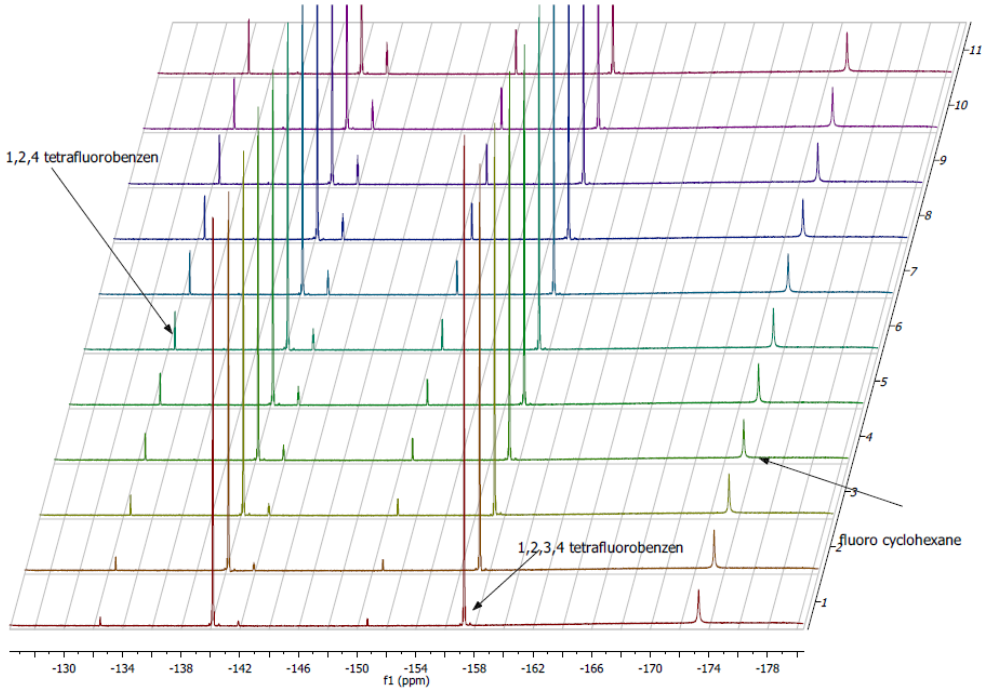

Figure XII- 85. Stacked $^{19}F\{^{1}H\}$ NMR spectra from kinetic study

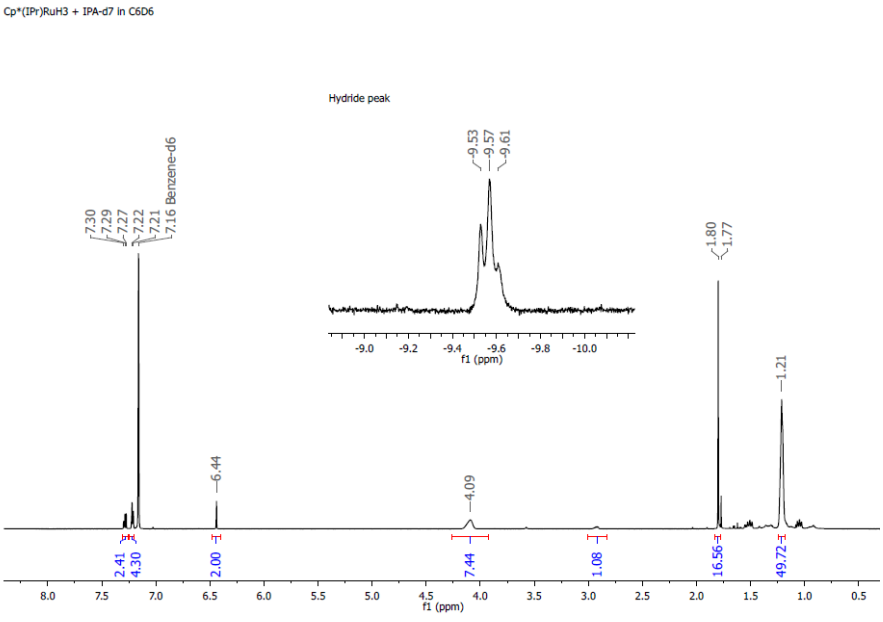

Figure XII- 86. ^{1}H NMR spectrum of D-labelled Cp*(IPr)Ru(H_x/D_{3-x})

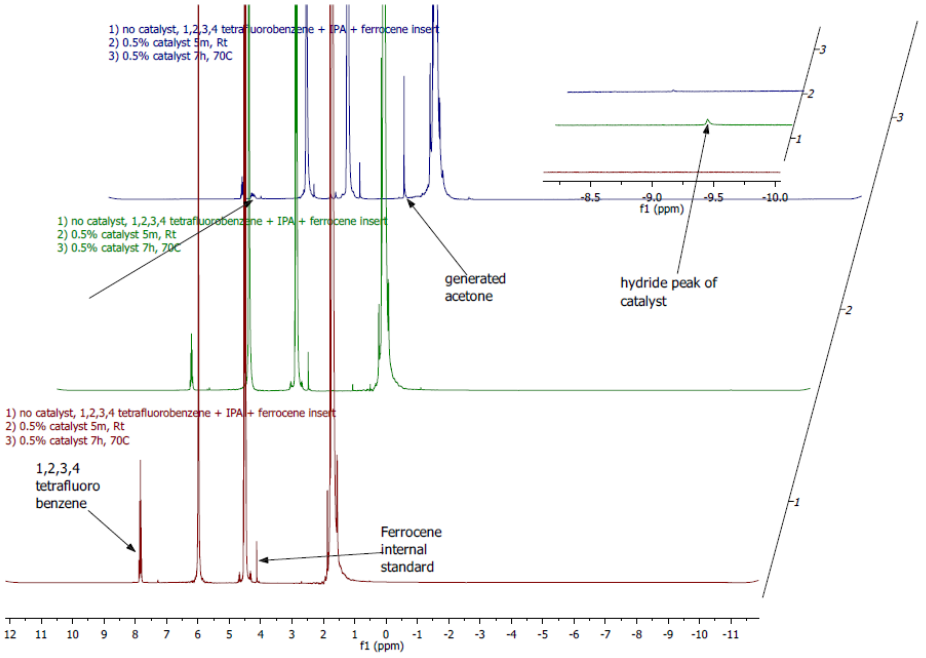

Figure XII- 87. ^{1}H-NMR spectrum for HDF catalytic reaction of 1,2,4,5-tetrafluorobenzen in IPA + ferrocene internal standard.

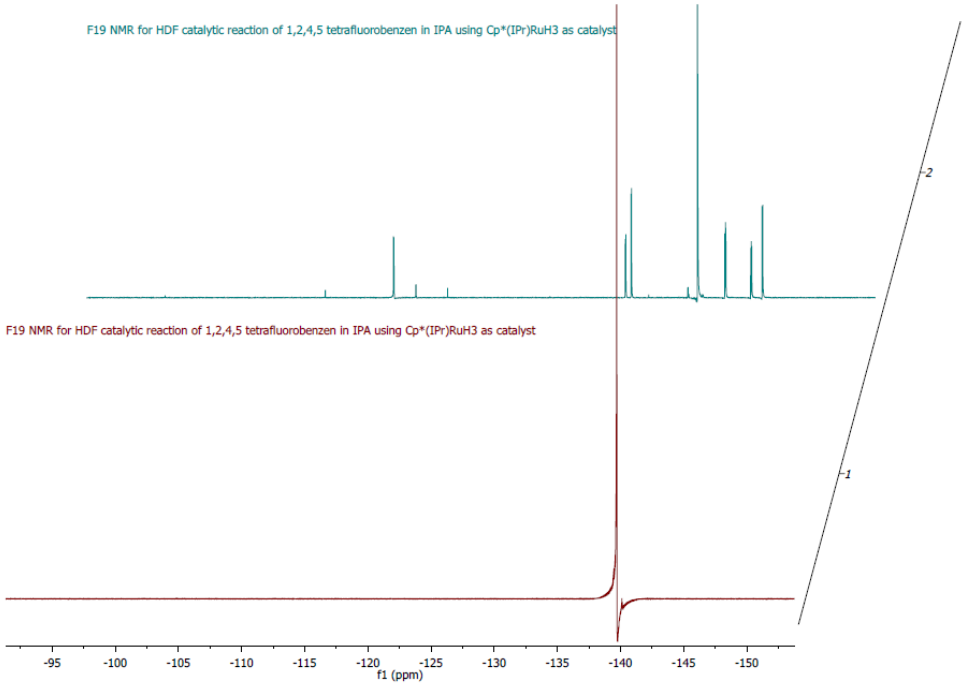

Figure XII- 88. ^{19}F-NMR spectrum for HDF catalytic reaction of 1,2,4,5-tetrafluorobenzen in IPA + ferrocene internal standard.

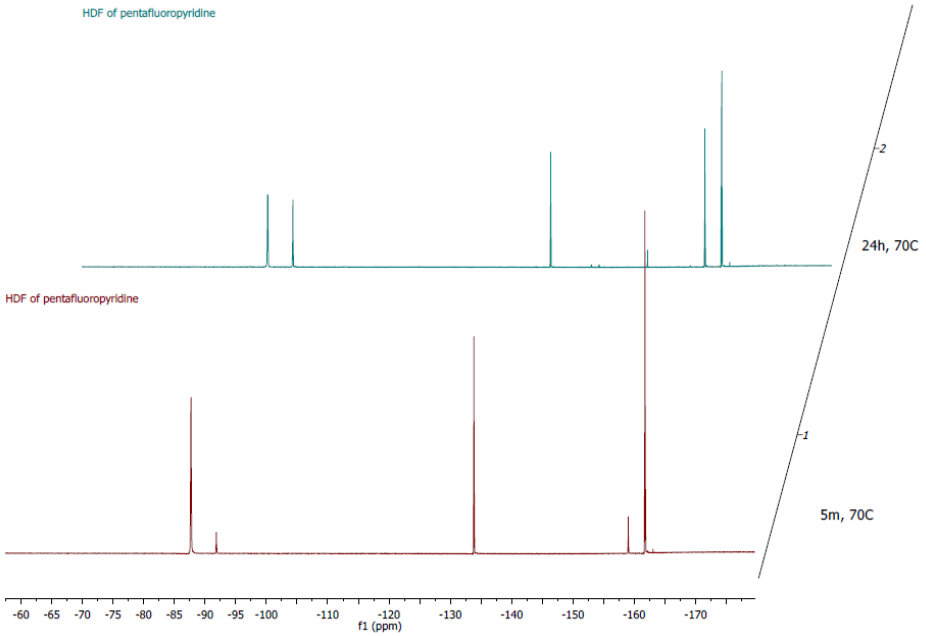

Figure XII- 89. ^{19}F-NMR spectrum for HDF catalytic reaction of pentafluoropyridine.

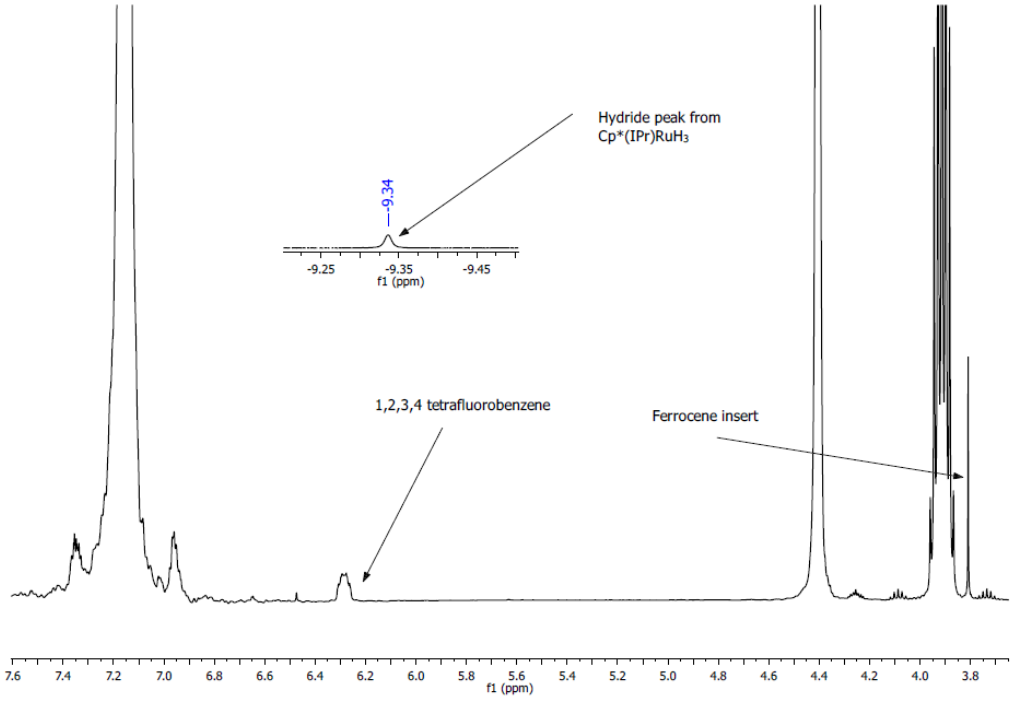

Figure XII- 90. ^{1}H-NMR spectrum for HDF kinetic sample with 30eq of IPA (without H_2 gas).

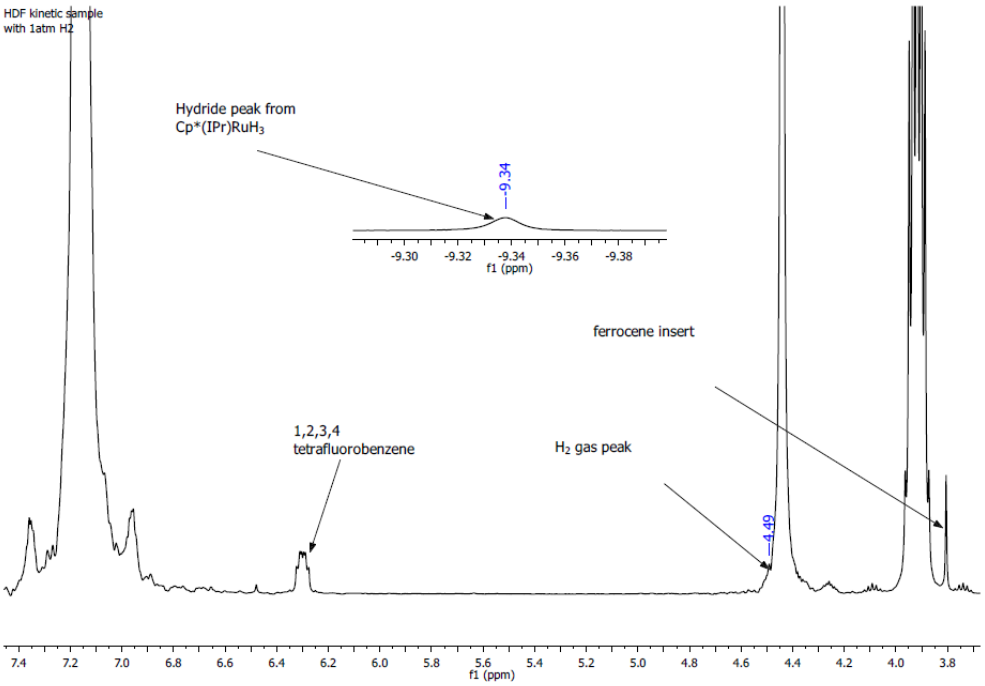

Figure XII- 91. ^{1}H-NMR spectrum for HDF kinetic sample with 30eq of IPA (with H_2 gas).

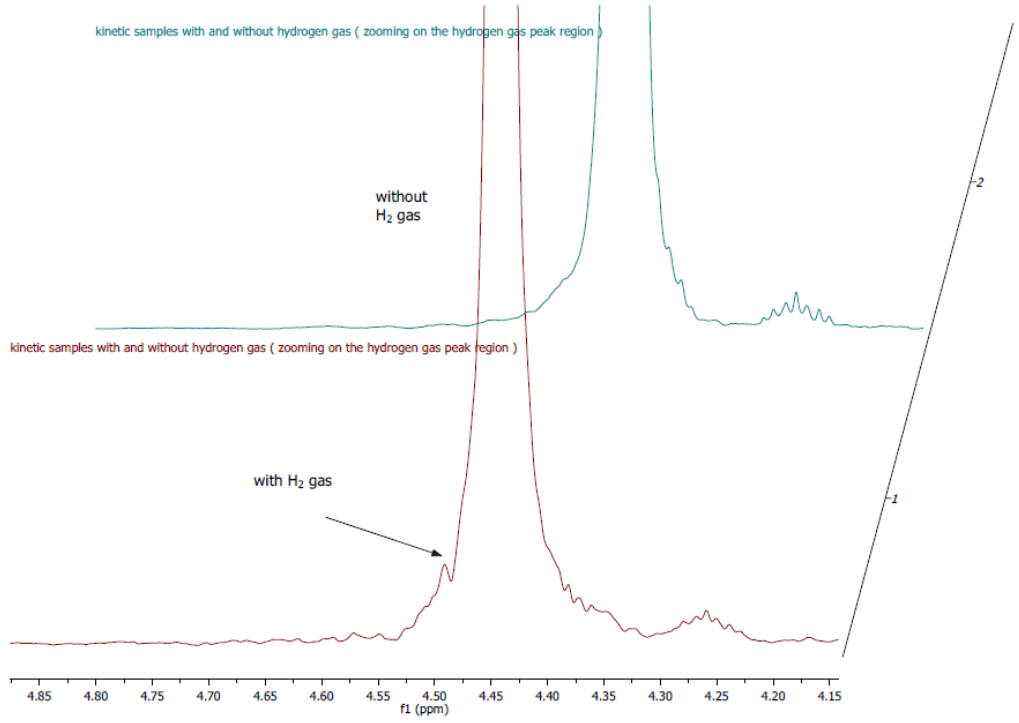

Figure XII- 92. Stacked ^{1}H-NMR spectrum for HDF kinetic sample with 30eq of IPA (with and without H_2 gas, zooming on hydrogen peak region).

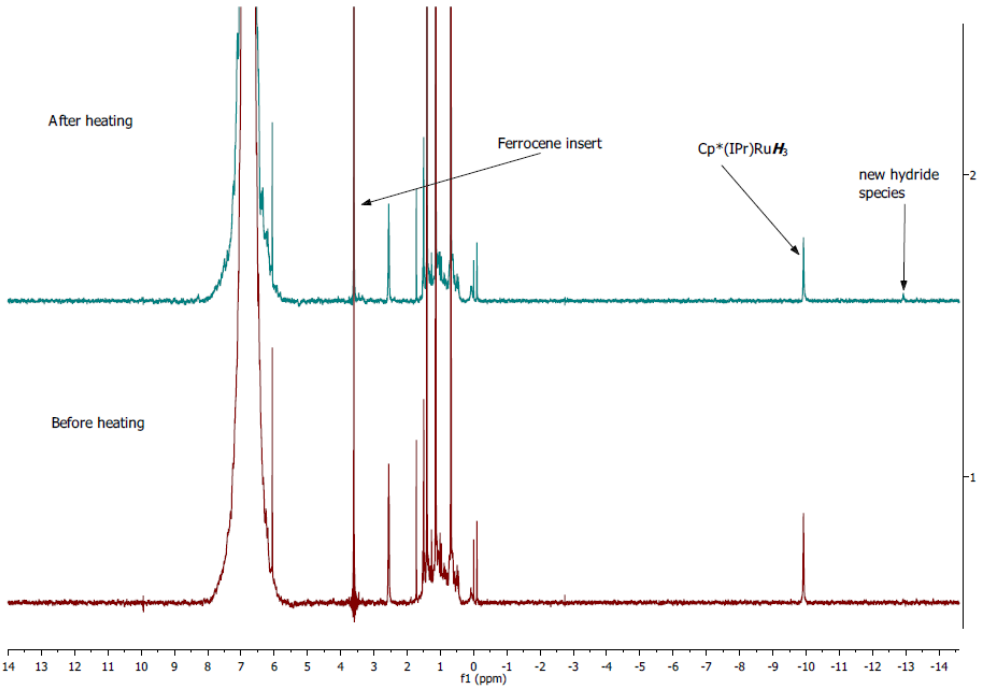

Figure XII- 93. Stacked ^{1}H-NMR spectrum for Cp*(IPr)RuH_3, in benzene before heating and after heating with Ferrocene insert.

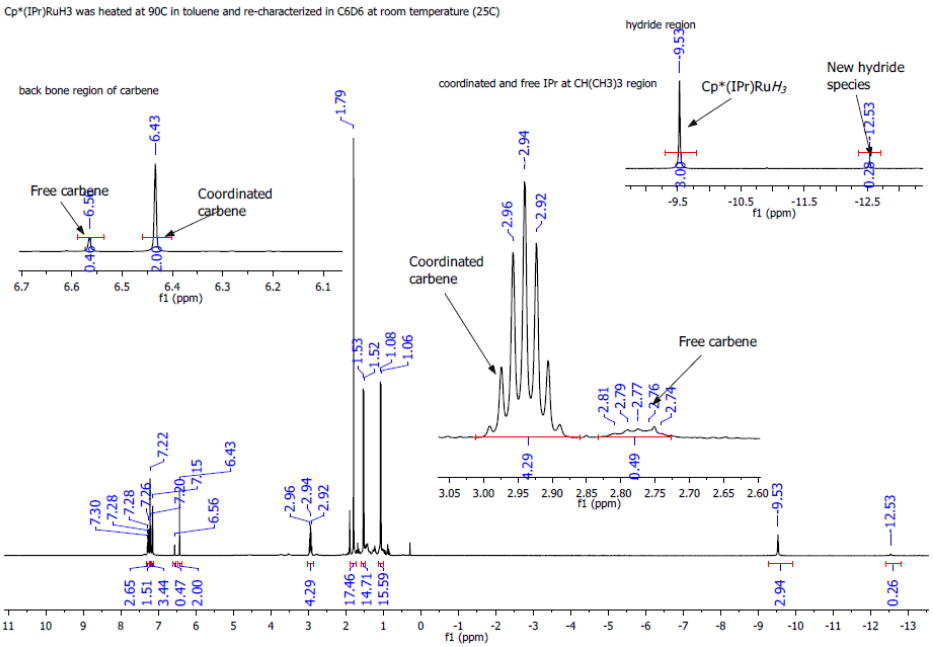

Figure XII- 94. ^{1}H-NMR spectrum for Cp*(IPr)RuH_3 at 23 °C after being heated at 90 °C for 8h in protio-benzene and then redissolved in C_6D_6. Note: the new hydride species at -12.53 ppm could be the hydride signal from $[Cp^*RuH_4]_2$

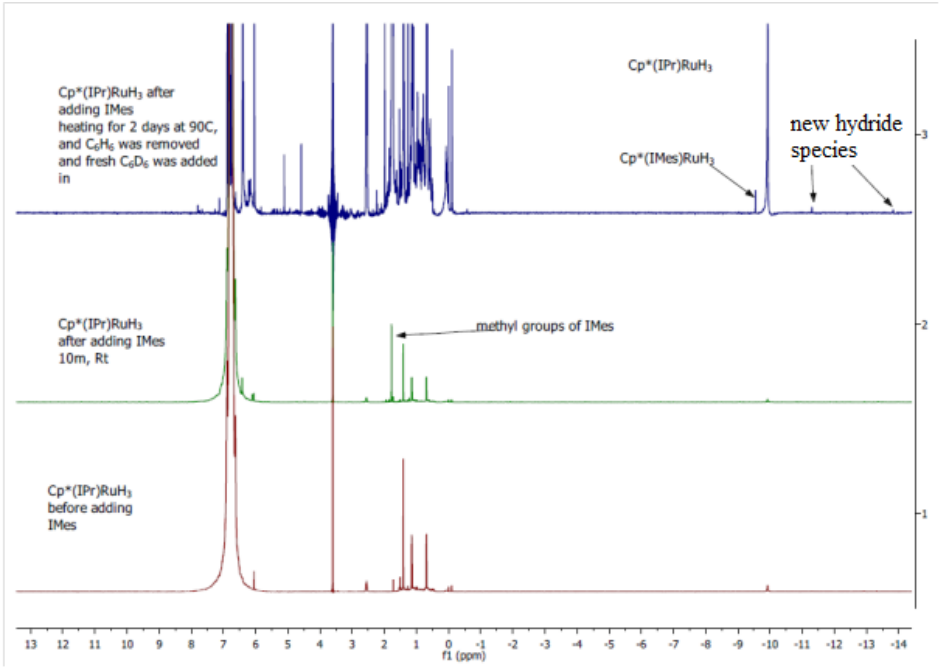

Figure XII- 95. Stacked ^{1}H-NMR spectrum for a 1:1 mixture of Cp*(IPr)RuH$_3$ and IMes in C_6H_6 before heating and after heating at 90 °C (with ferrocene insert).

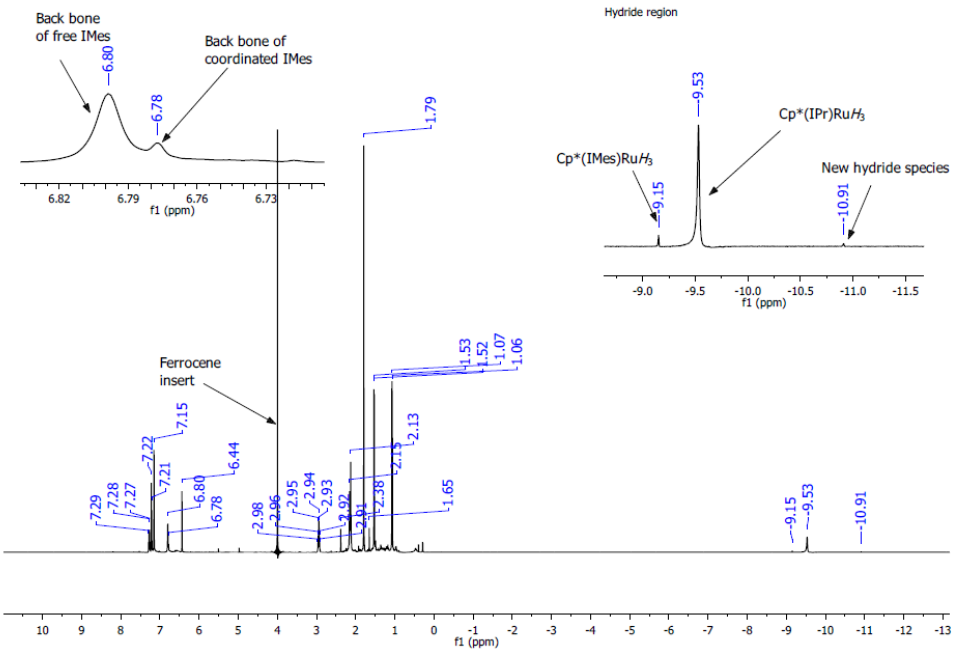

Figure XII- 96. ^{1}H-NMR spectrum for Cp*(IPr)RuH$_3$ +IMes in benzene after heating at 90°C for 2 days, C_6H_6 was removed and fresh C_6D_6 was added

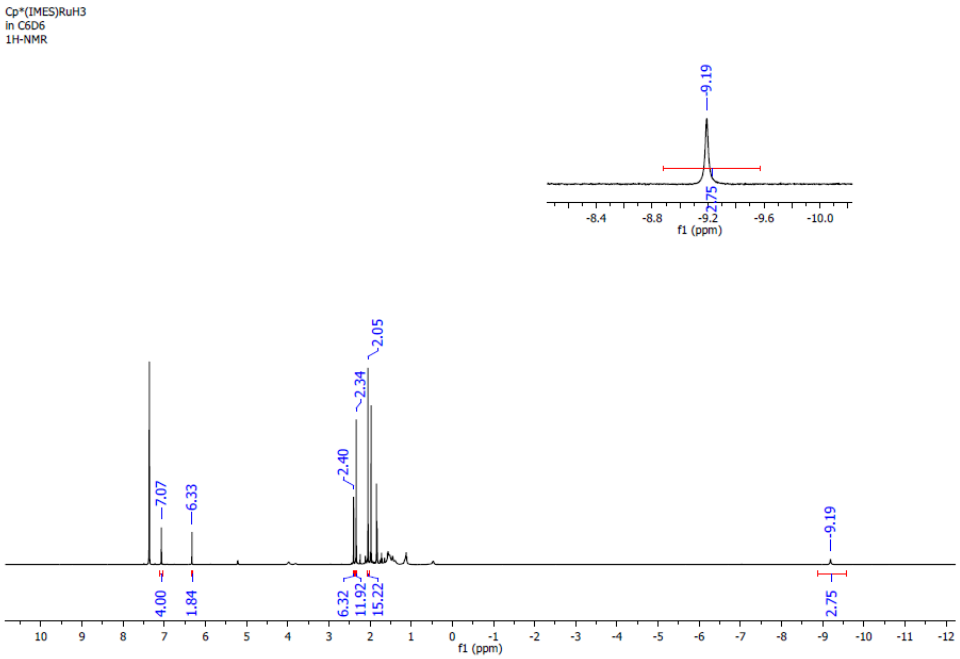

Figure XII- 97. ^{1}H-NMR spectrum for Cp*(IMes)RuH$_3$ in C_6D_6.

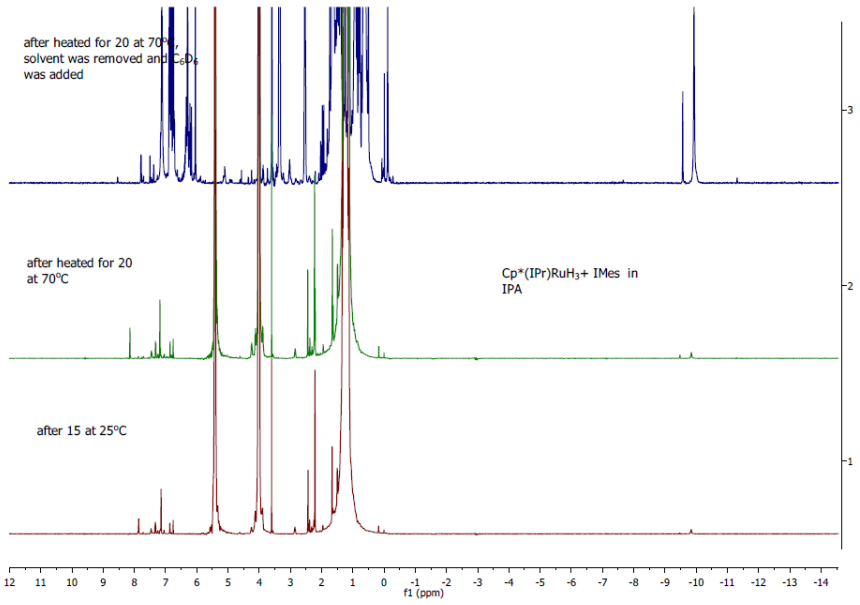

Figure XII- 98. Stacked ^{1}H-NMR spectrum for a 1:1 mixture of Cp*(IPr)RuH3 and IMes in IPA before heating and after heating at 90 °C (with ferrocene insert).

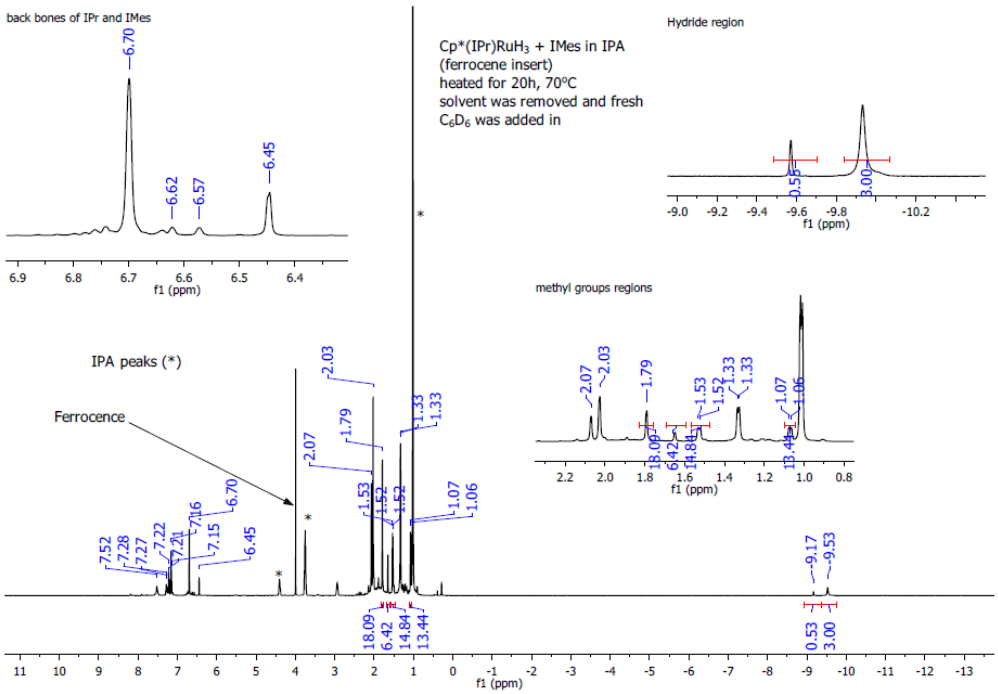

Figure XII- 99. ^{1}H-NMR spectrum for Cp*(IPr)RuH$_3$ +IMes in IPA after heating at 70°C for 20h, IPA was removed and fresh C_6D_6 was added.

XII.3 Crystal and structure refinement data

Table XII- 5. Selected crystal and structure refinement data

Empirical formula	$C_{33}H_{45}Cl_3N_2RuSi$	$C_{76}H_{98}Cl_2N_4Ru_2Si_2$	$C_{32}H_{41}ClN_2Ru$	$C_{32}H_{43}Cl_7N_2RuSi_2$
Formula weight	705.22	1396.80	590.19	861.08
colour, habit	yellow, block	yellow-red, block	blue, block	colourless, block
Crystal size, mm^3	0.28x0.26x0.24	0.17x0.11x0.08	0.11x0.09x0.06	0.23x0.18x0.18
Crystal system	Orthorhombic	triclinic	monoclinic	triclinic
Space group	Pna2(1)	P-1	P2(1)/c	P-1
Unit cell dimensions:				
a, Å	17.4593(11)	11.4152(6)	12.6112(3)	11.2074(4)
b, Å	12.4412(8)	15.9638(9)	14.8442(4)	11.2257(4)
c, Å	15.8779(10)	19.8855(10)	16.5695(4)	18.4143(6)
α, deg.	90	95.4893(17)	90	83.2160(15)
β, deg.	90	98.2770(16)	104.4642(14)	88.0443(15)
γ deg.	90	91.0324(16)	90	60.9801(13)
Volume, Å3	3448.9(4)	3567.7(3)	3003.55(13)	2010.96(12)
Z	4	2	4	2

Density (calculated), g/cm3	1.358	1.300	1.305	1.422
Absorption coefficient, mm-1	0.746	0.576	0.633	0.939
F(000)	1464	1464	1232	880
Diffractometer	Bruker SMART	Bruker SMART	Bruker SMART	Bruker SMART
Temperature, K	200(2)	200(2)	200(2)	200(2)
Radiation, (lambda, Å)	(0.71073) Mo Kα	(0.71073) Mo Kα	(0.71073) Mo Kα	(0.71073) Mo Kα
Scan mode	ω	ω	ω	ω
Scan step (in omega), deg	0.3	0.3	0.3	0.3
Time per step, sec.	15	15	15	15
Theta range for data collection, deg	2.01 to 28.32	1.28 to 28.33	1.87 to 28.32	1.11 to 28.35
Index ranges	-21≤*h*≤23, -16≤ *k* ≤ 16, -20≤ *l* ≤21	-15≤*h*≤15, -21≤ *k* ≤ 21, -25≤ *l* ≤26	-16≤*h*≤15, -19≤ *k* ≤ 19, -22≤ *l* ≤22	-14≤*h*≤13; -14≤*k*≤ 14; -24≤*l*≤24
Reflections collected	25082	46453	43544	19434
Independent reflections	8210 [R(int) = 0.0288]	17610 [R(int) = 0.0318]	7448 [R(int) = 0.0503]	9949 [R(int) = 0.0389]
Absorption correction	multi-scan	multi-scan	multi-scan	multi-scan
Max. transmission	0.7457	0.955	0.7457	0.7457

Min. transmission	0.6356	0.908	0.6838	0.6282
Refinement method	Full-matrix least-squares on F^2 (SHELXTL-Plus)	Full-matrix least-squares on F^2 (SHELXTL-Plus)	Full-matrix least-squares on F^2 (SHELXTL-Plus)	Full-matrix least-squares on F^2 (SHELXTL-Plus)
Data / restraints / parameters	8210/1/361	17610/0/755	7448/0/325	9949/0/397
Goodness-of-fit on F^2	1.030	1.010	1.021	1.063
Final R indices [I>2sigma(I)]	R_1 = 0.0296, wR_2 = 0.0662	R_1 = 0.0461, wR_2 = 0.1057	R_1 = 0.0352, wR_2 = 0.0775	R_1 = 0.0466, wR_2 = 0.1221
R indices (all data)	R_1 = 0.0329, wR_2 = 0.0678	R_1 = 0.0735, wR_2 = 0.1195	R_1 = 0.0565, wR_2 = 0.0871	R_1 = 0.0755, wR_2 = 0.1291
Largest diff. peak and hole, e.$Å^{-3}$	0.366, -0.400	1.272, -1.214	0.622, -0.493	1.069, -0.586

XIII. References

1. Andersson, P. G.; Munslo, I. J., *Modern Reduction Methods*. **2008**.

2. Kuivila, H. G., *Synthesis* **1970**, *1970*, 499.

3. Trost, B. M.; Fleming, I., *Comprehensive organic synthesis: reduction*. Elsevier: **1991**; Vol. 8.

4. Hudlicky, M., *Reductions in organic chemistry*. Ellis Horwood Chichester: **1984**.

5. Brieger, G.; Nestrick, T. J., *Chem. Rev.* **1974**, *74*, 567.

6. Cerveny, L., *Catalytic Hydrogenation*. **1986**.

7. de Vries, J. G.; Elsevier, C. J., *The Handbook of Homogeneous Hydrogenation*. **2007**.

8. Krische, M. J.; Sun, Y., Hydrogenation and Transfer Hydrogenation. *Acc. Chem. Res.* **2007**, *40*, 1237-1237.

9. Rylander, P. N., *Catalytic Hydrogenation in Organic Synthesis*. **1979**.

10. Dash, A. K.; Wang, J. Q.; Eisen, M. S.,*Organometallics* **1999**, *18*, 4724.

11. Marciniec, B., *Hydrosilylation*. **2007**.

12. Marciniec, B., *Hydrosilylation: A Comprehensive Review on Recent Advances*. **2009**.

13. Marciniec, B.; Gulinski, J.; Urbaniak, W.; Kornetka, Z. W., *Comprehensive Handbook on Hydrosilylation*. **1992**.

14. Brown, H. C., *Hydroboration: with supplement, Nobel lecture, December 8, 1979*. Benjamin-Cummings Publishing Company: **1962**.

15. Dhillon, R. S., *Hydroboration and Organic Synthesis: 9-Borabicyclo [3.3. 1] nonane (9-BBN)* **2007**, 59.

16. Männig, D.; Nöth, H., *Angew. Chem., Int. Ed. Engl.* **1985**, *24*, 878.

17. Nace, H. R., Hydroboration (Brown, Herbert C.). *J. Chem. Educ* **1963**, *40*, A72.

18. Sondheimer, F., Hydroboration. *J. Am. Chem. Soc.* **1962**, *84*, 4996.

19. Johnstone, R. A.; Wilby, A. H.; Entwistle, I. D., *Chem. Rev.* **1985**, *85*, 129.

20. Kubas, G. J., *Catal. Lett.* **2005**, *104*, 79.

21. Lee, S. H.; Nikonov, G. I., *ChemCatChem* **2015**, *7*, 107.

22. Uematsu, N.; Fujii, A.; Hashiguchi, S.; Ikariya, T.; Noyori, R., *J. Am. Chem. Soc.* **1996**, *118*, 4916.

23. Wang, D.; Astruc, D., *Chem. Rev.* **2015**, *115*, 6621.

24. Hartung, W. H.; Simonoff, R., *Organic Reactions* **1953**.

25. Espmark, K., The Nobel Prize in Literature. *The Nobel Prize: The First 100 Years* **1999**, 137.

26. Blaser, H. U.; Federsel, H. J., *Asymmetric Catalysis on Industrial Scale*. 2010.

27. Noyori, R., *Angew. Chem., Int. Ed.* **2002**, *41*, 2008.

28. Anderson, J. A.; Castaldi, M. J.; Spivey, J. J.; Dooley, K., *Catalysis*. Royal Society of Chemistry: **2009**; Vol. 21.

29. Blaser, H. U.; Pugin, B.; Spindler, F.; Cornils, B.; Herrmann, W. A., *Applied Homogeneous Catalysis with Organometallic Compounds*. **2000**.

30. Bond, G. C., Heterogeneous catalysis. **1987**.

31. Bond, G. C., *Catalysis by metals*. Academic Press: **1962**.

32. Le Page, A., *Applied heterogeneous catalysis*. **1988**.

33. Noyori, R., *Asymmetric Catalysis in Organic Synthesis*. **1994**. Dub, P. A.; Henson, N. J.; Martin, R. L.; Gordon, J. C., *J. Am. Chem. Soc.* **2014,** *136*, 3505.

34. Satterfield, C. N., *Heterogeneous catalysis in industrial practice*. **1991**.

35. Satterfield, C. N., *Heterogeneous catalysis in practice*. McGraw-Hill Companies: **1980**.

36. Smith, G. V.; Notheisz, F., *Heterogeneous catalysis in organic chemistry*. Academic Press: **1999**.

37. Thomas, J. M.; Thomas, W. J.; Salzberg, H., *J. Electrochem. Soc.* **1967**, *114*, 279C.

38. Tichit, D.; Corma, A.; Iborra, S.; Brunel, D.; Derouane, E., *Catalysis*. **2006**; 171.

39. Trovarelli, A., *Catalysis by ceria and related materials*. World Scientific: **2002**; Vol. 2.

40. Climent, M. J.; Corma, A.; Iborra, S., *Chem. Rev.* **2011**, *111*, 1072.

41. Mozingo, R., Catalyst, Raney Nickel, W-2. *Organic Syntheses* **1941**, 15.

42. Berkessel, A.; Gröger, H., *Asymmetric organocatalysis: from biomimetic concepts to applications in asymmetric synthesis*. John Wiley & Sons: **2006**.

43. Christmann, M.; Bräse, S., *Asymmetric synthesis: the essentials*. Wiley-VCH: **2008**; Vol. 1.

44. Morrison, J., *Asymmetric synthesis*. Elsevier: **2012**; Vol. 3.

45. Ojima, I., *Catalytic asymmetric synthesis*. John Wiley & Sons: **2004**.

46. Procter, G., *Asymmetric synthesis*. Oxford University Press on Demand: **1996**.

47. Bullock, R. M., *Catalysis Without Precious Metals*. **2010**.

48. Choi, J.; Goldman, A. S.; Andersson, P. G., *Iridium Catalysis*. **2011**.

49. Oro, L. A.; Carmona, D.; Fraile, J. M.; Chiusoli, G. P.; Maitlis, P. M., *In Metal-Catalysis in Industrial Organic Processes*. **2006**; p 79.

50. Cotton, F. A.; Wilkinson, G.; Murillo, C. A.; Bochmann, M., *Advanced Inorganic Chemistry*. **1999**.

51. Chalk, A. J.; Halpern, J., *J. Am. Chem. Soc.* **1959**, *81*, 5846.

52. Chalk, A. J.; Harrod, J. F., *J. Am. Chem. Soc.* **1965**, *87*, 16.

53. Koga, N.; Daniel, C.; Han, J.; Fu, X.; Morokuma, K., *J. Am. Chem. Soc.* **1987**, *109*, 3455.

54. Moineau, G.; Granel, C.; Dubois, P.; Jérôme, R.; Teyssié, P., *Macromolecules* **1998**, *31*, 542.

55. Osborn, J.; Wilkinson, G.; Mrowca, J., Chlorotris (triphenylphosphine) rhodium (I)(Wilkinson's catalyst). *Inorganic Syntheses: Reagents for Transition Metal Complex and Organometallic Syntheses, Volume 28* **1990**, 77.

56. Debenham, S. D.; Toone, E. J., *Tetrahedron: Asymmetry* **2000**, *11*, 385.

57. Fish, R. H.; Tan, J. L.; Thormodsen, A. D., *Organometallics* **1985**, *4*, 1743.

58. Sharma, U.; Kumar, P.; Kumar, N.; Kumar, V.; Singh, B., *Adv. Synth. Catal.* **2010**, *352*, 1834.

59. Gu, P.; Wang, W.; Wang, Y.; Wei, H., *Organometallics* **2013**, *32*, 47.

60. Kawanami, Y.; Sonoda, Y.; Mori, T.; Yamamoto, K., *Org. Lett.* **2002**, *4*, 2825.

61. Werkmeister, S.; Bornschein, C.; Junge, K.; Beller, M., R, *Eur. J. Org. Chem.* **2013**, *2013*, 3671.

62. Anderson, C. M.; Crespo, M.; Ferguson, G.; Lough, A. J.; Puddephatt, R., *J. Organometallics* **1992**, *11*, 1177.

63. Meerwein, H.; Schmidt, R., *Liebigs Ann. Chem.* **1925**, *444*, 221.

64. Miyashita, A.; Yasuda, A.; Takaya, H.; Toriumi, K.; Ito, T.; Souchi, T.; Noyori, R., *J. Am. Chem. Soc.* **1980**, *102*, 7932.

65. Sharpless, K. B.; Amberg, W.; Bennani, Y. L.; Crispino, G. A.; Hartung, J.; Jeong, K. S.; Kwong, H. L.; Morikawa, K.; Wang, Z. M., *J. Org. Chem.* **1992**, *57*, 2768.

66. Armstrong, S. K.; Brown, J. M.; Burk, M. J., *Tetrahedron letters* **1993**, *34*, 879.

67. Vineyard, B. D.; Knowles, W. S.; Sabacky, M. J.; Bachman, G. L.; Weinkauff, D. J., *J. Am. Chem. Soc.* **1977**, *99*, 5946.

68. Anderson, C. M.; Crespo, M.; Jennings, M. C.; Lough, A. J.; Ferguson, G.; Puddephatt, R., *J. Organometallics* **1991**, *10*, 2672.

69. Anderson, D. J.; McDonald, R.; Cowie, M., *Angew. Chem.* **2007**, *119*, 3815.

70. Ayllon, J. A.; Guari, Y.; Sayers, S. G.; Sabo-Etienne, S.; Chaudret, B.; Grundemann, S.; Limbach, H. H. *Dihydrogen bonds and proton transfer in ruthenium hydride complexes*, American Chemical Society: **1998**; 318.

71. Balakrishna, M. S.; Ramaswamy, K.; Abhyankar, R. M., *J. Organomet. Chem.* **1998**, *560*, 131.

72. Guan, H.; Iimura, M.; Magee, M. P.; Norton, J. R.; Zhu, G., *J. Am. Chem. Soc.* **2005**, *127*, 7805.

73. Kitamura, M.; Noyori, R.; Murahashi, S. I., *Ruthenium in Organic Synthesis*. **2004**.

74. Kumar, P.; Gupta, R. K.; Pandey, D. S., *Chem. Soc. Rev.* **2014**, *43*, 707.

75. Raghuraman, K.; Krishnamurthy, S. S.; Nethaji, M., *J. Chem. Soc., Dalton Trans.* **2002**, 4289.

76. Reguillo, R.; Grellier, M.; Vautravers, N.; Vendier, L.; Sabo-Etienne, S., *J. Am. Chem. Soc.* **2010**, *132*, 7854.

77. Shaw, A. P.; Norton, J. R.; Buccella, D.; Sites, L. A.; Kleinbach, S. S.; Jarem, D. A.; Bocage, K. M.; Nataro, C., *Organometallics* **2009**, *28*, 3804.

78. Silantyev, G. A.; Filippov, O. A.; Tolstoy, P. M.; Belkova, N. V.; Epstein, L. M.; Weisz, K.; Shubina, E. S., *Inorg. Chem.* **2013**, *52*, 1787.

79. Yi, C. S.; Liu, N., *Synlett* **1999**, 281

80. Dick, T. J.; Luke, A. M.; Peterson, A. A. *Rhodium catalyzed hydrogenation of fluoroarenes in mild condition*, American Chemical Society: **2016**; 902.

81. Yu, Y.-H.; Chiu, P. In *Catalytic reduction of fluoroethene: Kinetics, pathway, and mechanism*, American Chemical Society: **2014**; 18.

82. Church, T. L.; Andersson, P. G.; Nugent, T. C., *Chiral Amine Synthesis*. **2010**; p 179.

83. Li, J. Q.; Quan, X.; Andersson, P. G., *Chem.-Eur. J.* **2012,** *18*, 10609.

84. Verendel, J. J.; Andersson, P. G., *Dalton Trans.* **2007**, 5603.

85. Gutsulyak, D. V.; Churakov, A. V.; Kuzmina, L. G.; Howard, J. A. K.; Nikonov, G. I., *Organometallics* **2009**, *28*, 2655.

86. Gutsulyak, D. V.; Kuzmina, L. G.; Howard, J. A. K.; Vyboishchikov, S. F.; Nikonov, G. I., *J. Am.Chem. Soc.* **2008**, *130*, 3732.

87. Nikonov, G. I., Recent Advances in Nonclassical Interligand Si… H Interactions. *Adv. Organomet. Chem.* **2005**, *53*, 217.

88. Osipov, A. L.; Gutsulyak, D. V.; Kuzmina, L. G.; Howard, J. A. K.; Lemenovskii, D. A.; Suess-Fink, G.; Nikonov, G. I., *J. Organomet. Chem.* **2007**, *692*, 5081.

89. Osipov, A. L.; Vyboishchikov, S. F.; Dorogov, K. Y.; Kuzmina, L. G.; Howard, J. A. K.; Lemenovskii, D. A.; Nikonov, G. I., *Chem. Commun.* **2005**, 3349.

90. Bakhmutov, V. I.; Howard, J. A. K.; Keen, D. A.; Kuzminia, L. G.; Leech, M. A.; Nikonov, G. I.; Vorontsov, E. V.; Wilson, C. C., *J. Chem. Soc., Dalton Trans.* **2000**, 1631.

91. Lee, S. H., *Half-sandwich Complexes of Ruthenium; Synthesis and Application to Catalysis*. **2014**.

92. Caputo, C. B.; Stephan, D. W. In *Phosphonium Lewis acids: Hydrodefluorination, hydrosilylation, and dehydrocoupling reactions catalyzed by [(C$_6$F$_5$)$_3$PF][B(C$_6$F$_5$)$_4$]*, American Chemical Society: **2014**; 151.

93. Gountchev, T. I.; Tilley, T. D., *Organometallics* **1999**, *18*, 5661.

94. Lachaize, S.; Vendier, L.; Sabo-Etienne, S., *Dalton Trans.* **2010**, *39*, 8492.

95. Riener, K.; Högerl, M. P.; Gigler, P.; Kühn, F. E., *ACS Catalysis* **2012**, *2*, 613.

96. Sakaki, S.; Takayama, T.; Sumimoto, M.; Sugimoto, M., *J. Am. Chem. Soc*. **2004**, *126*, 3332.

97. Yang, Y.-F.; Chung, L. W.; Zhang, X.; Houk, K. N.; Wu, Y.-D., Ligand-Controlled Reactivity, *J. Org. Chem.* **2014**, *79*, 8856.

98. Hill, R. M., *Silicone surfactants*. CRC Press: **1999**; Vol. 86.

99. Zelisko, P. M.; Brook, M. A., *Langmuir* **2002**, *18*, 8982.

100. Frampton, M. B.; Zelisko, P. M., Organosilicon biotechnology. *Silicon* **2009**, *1*, 147.

101. Ojima, I.; Kogure, T.; Kumagai, M.; Horiuchi, S.; Sato, T., *J. Organomet. Chem.* **1976**, *122*, 83.

102. Ojima, I.; Nihonyanagi, M.; Kogure, T.; Kumagai, M.; Horiuchi, S.; Nakatsugawa, K.; Nagai, Y., *J. Organomet. Chem.* **1975**, *94*, 449.

103. Corey, J. Y., *Chem. Rev.* **2011**, *111*, 863.

104. Delpech, F.; Sabo-Etienne, S.; Daran, J.-C.; Chaudret, B.; Hussein, K.; Marsden, C. J.; Barthelat, J.-C., *J. Am. Chem. Soc.* **1999**, *121*, 6668.

105. McGrady, G. S.; Sirsch, P.; Chatterton, N. P.; Ostermann, A.; Gatti, C.; Altmannshofer, S.; Herz, V.; Eickerling, G.; Scherer, W., *Arch., Phys.* **2008**, 1,

106. McGrady, G. S.; Sirsch, P.; Chatterton, N. P.; Ostermann, A.; Gatti, C.; Altmannshofer, S.; Herz, V.; Eickerling, G.; Scherer, W., *Inorg Chem* **2009**, *48*, 1588.

107. Woo, H. G.; Walzer, J. F.; Tilley, T. D., *J. Am. Chem. Soc.* **1992**, *114*, 7047.

108. Gutsulyak, D. V.; Vyboishchikov, S. F.; Nikonov, G. I., *J. Am. Chem. Soc.* **2010**, *132* , 5950.

109. Lin, Z., *Chem Soc Rev* **2002**, *31*, 239.

110. Perrin, L.; Eisenstein, O.; Maron, L., *New J. Chem.* **2007**, *31*, 549.

111. Sadow, A. D.; Tilley, T. D., *J. Am. Chem. Soc.* **2005**, *127*, 643.

112. Lachaize, S.; Caballero, A.; Vendier, L.; Sabo-Etienne, S., *Organometallics* **2007**, *26*, 3713.

113. Lachaize, S.; Sabo-Etienne, S., *Eur. J. Inorg. Chem.* **2006**, 2115.

114. Perutz, R. N.; Sabo-Etienne, S., *Angew. Chem. Int. Ed.* **2007**, *46*, 2578.

115. Ignatov, S. K.; Rees, N. H.; Tyrrell, B. R.; Dubberley, S. R.; Razuvaev, A. G.; Mountford, P.; Nikonov, G. I., *Chem. - Eur. J.* **2004**, *10*, 4991.

116. Nikonov, G. I., *Angew. Chem. Int. Ed.* **2001**, *40*, 3353.

117. Nikonov, G. I., *J. Organomet. Chem.* **2001**, *635*, 24.

118. Nikonov, G. I.; Vyboishchikov, S. F.; Shirobokov, O. G.; Simionescu, R., *Eur. J. Inorg. Chem.* **2014**, *2014*, 2896.

119. Dorogov, K. Y.; Churakov, A. V.; Kuzmina, L. G.; Howard, J. A. K.; Nikonov, G. I., *Eur. J. Inorg. Chem.* **2004**, 771.

120. Nikonov, G. I.; Mountford, P.; Green, J. C.; Cooke, P. A.; Leech, M. A.; Blake, A. J.; Howard, J. A. K., *Eur. J. Inorg. Chem.* **2000**, 1917.

121. Ignatov, S. K.; Rees, N. H.; Merkoulov, A. A.; Dubberley, S. R.; Razuvaev, A. G.; Mountford, P.; Nikonov, G. I., *Chem. Eur. J.* **2008**, *14*, 296.

122. Gutsulyak, D. V.; Kuzmina, L. G.; Howard, J. A.; Vyboishchikov, S. F.; Nikonov, G. I., *J. Am. Chem. Soc.* **2008**, *130*, 3732.

123. Lee, T. Y.; Dang, L.; Zhou, Z.; Yeung, C. H.; Lin, Z.; Lau, C. P., *Eur. J. Inorg. Chem.* **2010**, 5675.

124. Gutsulyak, D. V.; Nikonov, G. I., *Angew. Chem. Int. Ed.* **2010**, *49*, 7553.

125. Gutsulyak, D. V.; van der Est, A.; Nikonov, G. I., *Angew. Chem.* **2011**, *123*, 1420.

126. Lee, S.-H.; Gutsulyak, D. V.; Nikonov, G. I., *Organometallics* **2013**, *32*, 4457.

127. Mai, V. H.; Kuzmina, L. G.; Churakov, A. V.; Korobkov, I.; Howard, J. A. K.; Nikonov, G. I., *Dalton Trans.* **2016**, *45*, 208.

128. Nikonov, G. I.; Kuzmina, L. G.; Howard, J. A. K., *J. Chem. Soc., Dalton Trans.* **2002**, 3037.

129. Abdel-Magid, A. F., *Reductions in organic synthesis*. American Chemical Society: **1996**.

130. Meyer, G. R., *J. Chem. Educ* **1981**, *58*, 628.

131. Weber, W., *Silicon reagents for organic synthesis*. Springer Science & Business Media: **2012**; Vol. 14.

132. Brown, H. C., *Boranes in organic chemistry*. Cornell University Press Ithaca, NY: **1972**; Vol. 13.

133. Samec, J. S.; Bäckvall, J.-E.; Andersson, P. G.; Brandt, P., *Chem. Soc. Rev.* **2006**, *35*, 237.

134. Kochi, J., *Organometallic mechanisms and catalysis: the role of reactive intermediates in organic processes*. Elsevier: **2012**.

135. Bolm, C.; Beller, M., *Transition metals for organic synthesis*. Wiley-VCH: Weinheim: **2004**.

136. Peterson, R. J., *Hydrogenation Catalysts*. Noyes Publications: 1977.

137. Bower, J. F.; Krische, M. J., In *Iridium Catalysis*, Springer: 2011; pp 107-138.

138. Noyori, R.; Hashiguchi, S., *Acc. Chem. Res.* **1997**, *30*, 97.

139. Noyori, R., *Angew. Chem. Int. Ed.* **2002,** *41*, 2008.

140. Noyori, R.; Takaya, H., *Acc. Chem. Res.* **1990**, *23*, 345.

141. Hashiguchi, S.; Fujii, A.; Takehara, J.; Ikariya, T.; Noyori, R., *J. Am. Chem. Soc.* **1995**, *117*, 7562.

142. Noyori, R., *Science* **1990,** *248*, 1194.

143. Noyori, R.; Hashiguchi, S., *Acc. Chem. Res.* **1997**, *30*, 97-102.

144. Haack, K. J.; Hashiguchi, S.; Fujii, A.; Ikariya, T.; Noyori, R., *Angew. Chem. Int. Ed. Engl.* **1997**, *36*, 285.

145. Seyden-Penne, J., *Reductions by the Alumino- and Borohydrides in Organic Synthesis*. **1997**.

146. Rylander, P. N., *Hydrogenation Methods*. **1985**.

147. Akiyama, T.; Atobe, K.; Shibata, M.; Mori, K., *J. Fluorine Chem.* **2013**, *152*, 81.

148. Baumgartner, R.; McNeill, K., *Environ Sci Technol* **2012**, *46*, 10199.

149. Braun, T.; Ahrens, M.; Kallane, S.; Teltewskoi, M.; Zamostna, L. In *C-F, C-H, and S-F bond activations of fluorinated compounds at rhodium(I) complexes*, American Chemical Society: **2014**; 28.

150. Braun, T.; Noveski, D.; Ahijado, M.; Wehmeier, F., *Dalton Trans.* **2007**, 3820.

151. Douvris, C.; Nagaraja, C. M.; Chen, C.-H.; Foxman, B. M.; Ozerov, O. V., *J. Am. Chem. Soc.* **2010**, *132*, 4946.

152. Garcia, J. J.; Arevalo, A.; Tlahuext, A. *Hydrodefluorination of fluoroarenes with nickel compounds: The true role of the ancillary ligand*, American Chemical Society: **2014**; 771.

153. Weaver, J. D., *Synlett* **2014**, *25*, 1946.

154. Weaver, J. D.; Singh, A.; Senaweera, S. *Photocatalytic hydrodefluorination: Facile access to partially fluorinated aromatics*, American Chemical Society: **2014**.

155. Whittlesey, M. K.; Peris, E., *ACS Catal.* **2014**, *4*, 3152.

156. Yang, H.; Gao, H.; Angelici, R. J., *Organometallics* **1999**, *18*, 2285.

157. Yow, S.; Gates, S. J.; White, A. J. P.; Crimmin, M. R., *Angew Chem Int Ed Engl* **2012**, *51*, 12559.

158. Du, G.; Abu-Omar, M. M., *Organometallics* **2006**, *25*, 4920.

159. Shirobokov, O. G.; Kuzmina, L. G.; Nikonov, G. I., *J. Am. Chem. Soc.* **2011**, *133*, 6487.

160. Knoevenagel, E.; Bergdolt, B., *Chem. Ber.* **1903**, *36*, 2857.

161. Braude, E. A.; Linstead, R. P., *J. Chem. Soc.* **1954**, 3544.

162. De Bellefon, C.; Fouilloux, P., *Catal. Rev.* **1994**, *36*, 459.

163. Ponndorf, W., *Angew. Chem.* **1926**, *39*, 138.

164. Verley, A., *Bull. Soc. Chim. Fr.* **1925**, *37*, 537.

165. Chowdhury, R. L.; Bäckvall, J. E., *J. Chem. Soc., Chem. Commun.* **1991**, 1063.

166. Handgraaf, J. W.; Meijer, E. J., *J. Am. Chem. Soc.* **2007**, *129*, 3099.

167. Baratta, W.; Bosco, M.; Chelucci, G.; Zotto, A. D.; Siega, K.; Toniutti, M.; Zangrando, E.; Rigo, P., *Organometallics* **2006**, *25*, 4611.

168. Baratta, W.; Ros, P. D.; Zotto, A. D.; Sechi, A.; Zangrando, E.; Rigo, P., *Angew. Chem., Int. Ed.* **2004**, *43*, 3584.

169. Ohkuma, T.; Tsutsumi, K.; Utsumi, N.; Arai, N.; Noyori, R.; Murata, K., *Org. Lett.* **2007**, *9*, 255.

170. Gowda, S.; Gowda, D. C., *Tetrahedron* **2002**, *58*, 2211.

171. Szmant, H., *Organic Buliding Blocks of the Chemical Industry*. **1989**.

172. Raney, M., *Method of producing finely-divided nickel.* Patents: **1927**.

173. Diesen, J. S.; Andersson, P. G.; Andersson, P. G.; Munslow, I. J., *Modern Reduction Methods*. **2008**.

174. Beebe, T. R.; Adkins, R.; Baldridge, R.; Hensley, V.; MacMillen, D.; Morris, D.; Noe, R.; Ng, F. W.; Powell, G.; Spielberger, C.; Stolte, M., *J. Org. Chem.* **1987**, *52*, 5472.

175. Bishop, B. C.; Brands, K. M. J.; Gibbs, A. D.; Kennedy, D. J., *Synthesis* **2004**, 43.

176. V. Hong, Y. L. V., *Catalytic hydrogenation of nitriles.* Patents: **1964**.

177. Beatty, R. P.; Paciello, R. A., Ruthenium hydrogenation catalysts. Google Patents: **1996**.

178. Takemoto, S.; Kawamura, H.; Yamada, Y.; Okada, T.; Ono, A.; Yoshikawa, E.; Mizobe, Y.; Hidai, M., *Organometallics* **2002**, *21*, 3897.

179. Toti, A.; Frediani, P.; Salvini, A.; Rosi, L.; Giolli, C.; Giannelli, C., *Rendu Chem.* **2004**, *7*, 769.

180. Li, T.; Bergner, I.; Haque, F. N.; Zimmer-De Iuliis, M.; Song, D.; Morris, R. H., *Organometallics* **2007**, *26*, 5940.

181. Enthaler, S.; Addis, D.; Junge, K.; Erre, G.; Beller, M., *Chemistry – A European Journal* **2008**, *14*, 9491.

182. Enthaler, S.; Junge, K.; Addis, D.; Erre, G.; Beller, M., *ChemSusChem* **2008**, *1*, 1006.

183. Addis, D.; Enthaler, S.; Junge, K.; Wendt, B.; Beller, M., *Tetrahedron Lett.* **2009**, *50*, 3654.

184. Werkmeister, S.; Junge, K.; Beller, M., *Org. Proc. Res. Dev.* **2014**, *18*, 289.

185. Gunanathan, C.; Milstein, D., *Acc. Chem. Res.* **2011**, *44*, 588.

186. Srimani, D.; Mukherjee, A.; Goldberg, A. F.; Leitus, G.; Diskin-Posner, Y.; Shimon, L. J.; Ben David, Y.; Milstein, D., *Angew. Chem., Int. Ed.* **2015**, *54*, 12357.

187. Vilches-Herrera, M.; Werkmeister, S.; Junge, K.; Borner, A.; Beller, M., *Catal. Sci. Technol.* **2014**, *4*, 629.

188. Yoshida, T.; Thorn, D. L.; Okano, T.; Otsuka, S.; Ibers, J. A., *J. Am. Chem. Soc.* **1980**, *102*, 6451.

189. Chin, C. S.; Lee, B., *Catal. Lett.* **1992**, *14*, 135.

190. Woodmansee, D.; Pfaltz, A.; Andersson, P. G., *Iridium Catalysis*. **2011**; Vol. 34.

191. Sato, Y.; Kayaki, Y.; Ikariya, T., *Organometallics* **2016**, *35*, 1257.

192. Bornschein, C.; Werkmeister, S.; Wendt, B.; Jiao, H.; Alberico, E.; Baumann, W.; Junge, H.; Junge, K.; Beller, M., *Nat Commun* **2014**, *5*.

193. Zell, T.; Ben-David, Y.; Milstein, D., *Catal. Sci. Technol.* **2015**, *5*, 822.

194. Mukherjee, A.; Srimani, D.; Chakraborty, S.; Ben-David, Y.; Milstein, D., *J. Am. Chem. Soc.* **2015**, *137*, 8888.

195. Elangovan, S.; Topf, C.; Fischer, S.; Jiao, H.; Spannenberg, A.; Baumann, W.; Ludwig, R.; Junge, K.; Beller, M., *J. Am. Chem. Soc.* **2016**.

196. Adam, R.; Alberico, E.; Baumann, W.; Drexler, H. J.; Jackstell, R.; Junge, H.; Beller, M., *Chem. Eur. J.* **2016**, *22*, 4991.

197. Carlier, P. R., *J. Nat. Prod.* **2001**, *64*, 1257.

198. Bird, C. W., *Tetrahedron* **1992**, *48*, 335.

199. Zhou, H.; Li, Z.; Wang, Z.; Wang, T.; Xu, L.; He, Y.; Fan, Q. H.; Pan, J.; Gu, L.; Chan, A. S. C., *Angew. Chem., Int. Ed.* **2008**, *47*, 8464.

200. Wang, D.-S.; Chen, Q.-A.; Lu, S.-M.; Zhou, Y.-G., *Chem. Rev.* **2012**, *112*, 2557-2590.

201. Wang, B.; Zhu, B.; Zhang, J.; Xu, S.; Zhou, X.; Weng, L., *Organometallics* **2003**, *22*, 5543.

202. Minato, M.; Zhou, D. Y.; Zhang, L. B.; Hirabayashi, R.; Kakeya, M.; Matsumoto, T.; Harakawa, A.; Kikutsuji, G.; Ito, T., *Organometallics* **2005**, *24*, 3434.

203. Long, J.; Zhou, Y.; Li, Y., *Chem. Commun.* **2015**, *51*, 2331.

204. Stephan, D. W., Frustrated Lewis Pairs: From Concept to Catalysis. *Acc. Chem. Res.* **2015**, *48*, 306.

205. Erker, G.; Stephan, D. W., *Frustrated Lewis Pairs I: Uncovering and Understanding*. **2013**; Vol. 332.

206. Erker, G.; Stephan, D. W., *Frustrated Lewis Pairs II: Expanding the Scope*. **2013**; Vol. 334.

207. Murata, S.; Sugimoto, T.; Matsuura, S., *Heterocycles* **1987**, *26*, 763.

208. Bianchini, C.; Barbaro, P.; Scapacci, G.; Farnetti, E.; Graziani, M., *Organometallics* **1998**, *17*, 3308.

209. Wang, W. B.; Lu, S. M.; Yang, P. Y.; Han, X. W.; Zhou, Y. G., *J. Am. Chem. Soc.* **2003**, *125*, 10536.

210. Man, M. L.; Zhou, Z.; Ng, S. M.; Lau, C. P., *Dalton Trans.* **2003**, 3727.

211. Friedman, D.; Masciangioli, T.; Olson, S., *The role of the chemical sciences in finding alternatives to critical resources: A workshop summary*. National Academies Press: **2012**.

212. Yang, P. Y.; Zhou, Y. G., *Tetrahedron: Asymmetry* **2004**, *15*, 1145.

213. Wang, Z. J.; Zhou, H. F.; Wang, T. L.; He, Y. M.; Fan, Q. H., *Green Chem.* **2009,** *11*, 767.

214. Baeza, A.; Pfaltz, A., *Chem.-Eur. J.* **2010**, *16*, 2036.

215. Baeza, A.; Pfaltz, A., *Chem.-Eur. J.* **2009**, *15*, 2266.

216. Kuwano, R.; Kashiwabara, M.; Sato, K.; Ito, T.; Kaneda, K.; Ito, Y., *Tetrahedron: Asymmetry* **2006**, *17*, 521.

217. Duan, Y.; Chen, M. W.; Ye, Z. S.; Wang, D. S.; Chen, Q. A.; Zhou, Y. G., *Chem.-Eur. J.* **2011**, *17*, 7193.

218. Lu, S. M.; Wang, Y. Q.; Han, X. W.; Zhou, Y. G., *Angew. Chem., Int. Ed.* **2006**, *45*, 2260.

219. Tang, W. J.; Xu, L. J.; Fan, Q. H.; Wang, J.; Fan, B. M.; Zhou, Z. Y.; Lam, K. H.; Chan, A. S. C., *Angew. Chem., Int. Ed.* **2009**, *48*, 9135.

220. Wang, X. B.; Zeng, W.; Zhou, Y. G., *Tetrahedron Lett.* **2008**, *49*, 4922.

221. Kuwano, R.; Kashiwabara, M.; Ohsumi, M.; Kusano, H., *J. Am. Chem. Soc.* **2008**, *130*, 808.

222. Kuwano, R.; Kameyama, N.; Ikeda, R., *J. Am. Chem. Soc.* **2011**, *133*, 7312.

223. Bullock, R. M., *Science* **2013**, *342*, 1054.

224. Enthaler, S.; Junge, K.; Beller, M., *Angew. Chem., Int. Ed.* **2008**, *47*, 3317.

225. (a) Chakraborty, S.; Brennessel, W. W.; Jones, W. D., *J. Am. Chem. Soc.* **2014**, *136*, 8564. (b) Xu, R.; Chakraborty, S.; Yuan, H.; Jones, W. D., *ACS Catal.* **2015,** *5* , 6350. (c) Xu, R.; Chakraborty, S.; Bellows, S. M.; Yuan, H.; Cundari, T. R.; Jones, W. D., *ACS Catal.* **2016,** *6*, 2127.

226. Wang, Y. Q.; Lu, S. M.; Zhou, Y. G., *J. Org. Chem.* **2007**, *72*, 3729.

227. (a) Wang, D. S.; Zhou, Y. G., *Tetrahedron Lett.* **2010**, *51*, 3014. (b) Talwar, D.; Li, H. Y.; Durham, E.; Xiao, J., *Chem. - Eur. J.* **2015**, *21*, 5379.

228. Xu, R.; Chakraborty, S.; Bellows, S. M.; Yuan, H.; Cundari, T. R.; Jones, W. D., *ACS Catal.* **2016**, *6*, 2127.

229. Parekh, V.; Ramsden, J. A.; Wills, M., *Tetrahedron Asym.* **2010**, *21*, 1549.

230. Mai, V. H.; Nikonov, G. I., *Organometallics* **2016**, *35*, 943.

231. Verendel, J. J.; Pàmies, O.; Diéguez, M.; Andersson, P. G., *Chem. Rev.* **2014**, *114*, 2130.

232. Lau, C. P.; Ng, S. M.; Jia, G.; Lin, Z., *Coord. Chem. Rev.* **2007**, *251*, 2223.

233. Heller, D.; de Vries, A. H. M.; de Vries, J. G.; de Vries, J. G.; Elsevier, C. J., *Handbook of Homogeneous Hydrogenation*. **2007**.

234. Ohkuma, T.; Ooka, H.; Ikariya, T.; Noyori, R., *J. Am. Chem. Soc.* **1995**, *117*, 10417.

235. Takaya, H.; Otha, T.; Noyori, R.; Ojima, I., *Catalytic Asymmetric Synthesis*. **1993**.

236. Knowles, W. S.; Sabacky, M. J.; Vineyard, B. D.; Weinkauff, D. J., *J. Am. Chem. Soc.* **1975**, *97*, 2567.

237. Dang, T. P.; Kagan, H. B., *J. Chem. Soc. D* **1971**, 481.

238. Broene, R. D.; Buchwald, S. L., *J. Am. Chem. Soc.* **1993**, *115*, 12569.

239. Troutman, M. V.; Appella, D. H.; Buchwald, S. L., *J. Am. Chem. Soc.* **1999**, *121*, 4916.

240. Crabtree, R. H.; Gautier, A.; Giordano, G.; Khan, T., *J. Organomet. Chem.* **1977**, *141*, 113.

241. Schnider, P.; Koch, G.; Prétôt, R.; Wang, G.; Bohnen, F. M.; Krüger, C.; Pfaltz, A., *Chem.-Eur. J.* **1997**, *3*, 887.

242. Lightfoot, A.; Schnider, P.; Pfaltz, A., *Angew. Chem., Int. Ed.* **1998**, *37*, 2897.

243. (a) Bart, S. C., Lobkovsky, E.; Chirik, P. J. *J. Am. Chem. Soc.* **2004**, *126*, 13794; (b) Daida, E. J.; Peters, J. C., *Inorganic Chemistry* **2004**, *43*, 7474.

244. Friedfeld, M. R.; Shevlin, M.; Hoyt, J. M.; Krska, S. W.; Tudge, M. T.; Chirik, P. J., *Science* **2013**, *342*, 1076.

245. Gärtner, D.; Welther, A.; Rad, B. R.; Wolf, R.; Jacobi von Wangelin, A., *Angew. Chem., Int. Ed.* **2014**, *53*, 3722.

246. Vasudevan, K. V.; Scott, B. L.; Hanson, S. K., *Eur. J. Inorg. Chem.* **2012,** *2012*, 4898.

247. Grützmacher, H., *Angew. Chem., Int. Ed.* **2008**, *47*, 1814.

248. Horn, S.; Gandolfi, C.; Albrecht, M., *Eur. J. Inorg. Chem.* **2011**, 2863.

249. Zhang, G.; Yin, Z.; Tan, J., *RSC Adv.* **2016**, *6*, 22419.

250. Hiyama, T., *Organofluorine Compounds: Chemistry and Applications*. **2000**.

251. Uneyama, K., *Organofluorine Chemistry*. **2006**.

252. Fried, J.; Sabo, E. F., *J. Am. Chem. Soc.* **1954**, *76*, 1455.

253. Welch, J. T.; Eswarakrishnan, S., *Fluorine in Bioorganic Chemistry*. **1991**.

254. Thrasher, J. S.; Strauss, S. H., *Inorganic Fluorine Chemistry: Toward the 21st Century*. **1994**.

255. Banks, R. E., *Fluorine Chemistry at the Millennium: Fascinated by Fluorine*. 2000.

256. Hiyama, T.; Kanie, K.; Kusumoto, T.; Morizawa, Y.; Shimizu, M., *Organofluorine Compounds: Chemistry and Application*. **2000**.

257. Chambers, R. D., *Fluorine in Organic Chemistry*. **2004**.

258. Soloshonok, V. A., *Fluorine-Containing Synthons*. **2005**.

259. Bégué, J. P.; Bonnet-Delpon, D., *Bioorganic and Medicinal Chemistry of Fluorine*. **2008**.

260. Uneyama, K., *Organofluorine Chemistry*. **2008**.

261. Ohashi, M.; Ogoshi, S., Catalytic transformations of fluorinated olefins. In *Organometallic Fluorine Chemistry*, Braun, T.; Hughes, P. R., Eds. Springer International Publishing: Cham, **2015**; pp 197.

262. Braun, T.; Hughes, R. P., *Organometallic Fluorine Chemistry*. Springer: **2015**; Vol. 52.

263. Ritter, T.; Furuya, T.; Tang, P. Fluorination of organic compounds., **2010**.

264. Hu, J.-Y.; Zhang, J.-L., *Top. Organomet. Chem.* **2015**, *52* (Organometallic Fluorine Chemistry), 143.

265. Baumgartner, R.; McNeill, K. In *Hydrodefluorination of fluorinated arenes using a heterogeneous rhodium-based catalyst*, American Chemical Society: **2011**; 215.

266. Caputo, C. B.; Hounjet, L. J.; Dobrovetsky, R.; Stephan, D. W., *Science* **2013**, *341*, 1374.

267. Kraft, B. M.; Lachicotte, R. J.; Jones, W. D. In *Carbon-fluorine bond activation using Cp*$_2$ZrH$_2$*, American Chemical Society: **2001**; 390.

268. Kraft, B. M.; Lachicotte, R. J.; Jones, W. D., *J. Am. Chem. Soc.* **2000**, *122*, 8559.

269. Yamada, T.; Saito, K.; Akiyama, T., *Adv. Synth. Catal.* **2016**, *358*, 62.

270. McKay, D.; Riddlestone, I. M.; Macgregor, S. A.; Mahon, M. F.; Whittlesey, M. K., *ACS Catal.* **2015**, *5*, 776.

271. Ahrens, T.; Kohlmann, J.; Ahrens, M.; Braun, T., *Chem. Rev.* **2015**, *115*, 931.

272. Ekkert, O.; Strudley, S. D. A.; Rozenfeld, A.; White, A. J. P.; Crimmin, M. R., *Organometallics* **2014**, *33*, 7027.

273. Kuhnel, M. F.; Lentz, D., *Angew. Chem. Int. Ed.* **2010**, *49*, 2933.

274. Braun, T.; Salomon, M. A.; Altenhoner, K.; Teltewskoi, M.; Hinze, S., *Angew. Chem., Int. Ed.* **2009**, *48*, 1818.

275. Brown, S. D.; Richmond, T. G., *Chemtracts* **2000,** *13*, 134.

276. Zhu, J.; Perez, M.; Caputo, C. B.; Stephan, D. W., *Angew. Chem., Int. Ed.* **2016**, *55*, 1417.

277. Luo, Y. R., *Comprehensive handbook of chemical bond energies*. **2010**.

278. Swarts, F., *Bull. Cl. Sci., Acad. R. Belg.* **1920**, 399.

279. Aizenberg, M.; Milstein, D., *Science* **1994**, *265*, 359.

280. Edelbach, B. L.; Jones, W. D., *J. Am. Chem. Soc.* **1997**, *119*, 7734.

281. Whittlesey, M. K.; Perutz, R. N.; Moore, M. H., *Chem. Commun.* **1996**, 787.

282. Reade, S. P.; Mahon, M. F.; Whittlesey, M. K., *J Am Chem Soc* **2009**, *131*, 1847.

283. Panetier, J. A.; MacGregor, S. A.; Whittlesey, M. K., *Angew. Chem. Int. Ed.* **2011**, *50*, 2783.

284. Raza, A. L.; Panetier, J. A.; Teltewskoi, M.; MacGregor, S. A.; Braun, T., *Organometallics* **2013**, *32*, 3795.

285. Braun, T.; Noveski, D.; Ahijado, M.; Wehmeier, F., *Dalton Trans.* **2007**, 3820.

286. Nova, A.; Erhardt, S.; Jasim, N. A.; Perutz, R. N.; Macgregor, S. A.; McGrady, J. E.; Whitwood, A. C., *J. Am. Chem. Soc.* **2008**, *130*, 15499.

287. (a) Braun, T.; Noveski, D.; Neumann, B.; Stammler, H. G., *Angew. Chem.* **2002,** *114*, 2870; (b) Braun, T.; Perutz, R. N.; Sladek, M. I., *Chem. Commun.* **2001**, 2254.

288. Chen, Z.; He, C.-Y.; Yin, Z.; Chen, L.; He, Y.; Zhang, X., *Angew. Chem., Int. Ed.* **2013**, *52*, 5813.

289. Sabater, S.; Mata, J. A.; Peris, E., *Nat. Commun.* **2013**, *4*, 3553, 7.

290. Fahey, D. R.; Mahan, J. E., *J. Am. Chem. Soc.* **1977**, *99*, 2501.

291. Cronin, L.; Higgitt, C. L.; Karch, R.; Perutz, R. N., *Organometallics* **1997**, *16*, 4920.

292. Johnson, S. A.; Huff, C. W.; Mustafa, F.; Saliba, M., *J. Am. Chem. Soc.* **2008**, *130*, 17278.

293. Johnson, S. A.; Mroz, N. M.; Valdizon, R.; Murray, S., *Organometallics* **2011**, *30*, 441.

294. Fischer, P.; Goetz, K.; Eichhorn, A.; Radius, U., *Organometallics* **2012**, *31*, 1374.

295. Zheng, T.; Sun, H.; Chen, Y.; Li, X.; Dürr, S.; Radius, U.; Harms, K., *Organometallics* **2009**, *28*, 5771.

296. Schaub, T.; Fischer, P.; Steffen, A.; Braun, T.; Radius, U.; Mix, A., C−F *J. Am. Chem. Soc.* **1999**, *130*, 9304.

297. Prikhod'ko, S. A.; Adonin, N. Y.; Parmon, V. N., *Russ. Chem. Bull.* **2009**, *58*, 2304.

298. Prikhod'ko, S. A.; Adonin, N. Y.; Parmon, V. N., *Tetrahedron Lett.* **2010**, *51*, 2265.

299. Wu, J.; Cao, S., *ChemCatChem* **2011**, *3*, 1582.

300. Ding, K.; Dugan, T. R.; Brennessel, W. W.; Bill, E.; Holland, P. L., *Organometallics* **2009**, *28*, 6650.

301. Li, X.; Sun, H.; Yu, F.; Flörke, U.; Klein, H.-F., *Organometallics* **2006**, *25*, 4695.

302. Furuya, T.; Klein, J. E. M. N.; Ritter, T., *Synthesis* **2010**, *2010*, 1804.

303. Arunan, E.; Desiraju, G. R.; Klein, R. A.; Sadlej, J.; Scheiner, S.; Alkorta, I.; Clary, D. C.; Crabtree, R. H.; Dannenberg, J. J.; Hobza, P., *Pure Appl. Chem.* **2011**, *83*, 1637.

304. Li, J.; Zheng, T.; Sun, H.; Xu, W.; Li, X., *Dalton Trans.* **2013**, *42*, 5740.

305. Lu, F.; Li, J.; Sun, H.; Li, X., *Inorg. Chim. Acta* **2014**, *416*, 222.

306. Vela, J.; Smith, J. M.; Yu, Y.; Ketterer, N. A.; Flaschenriem, C. J.; Lachicotte, R. J.; Holland, P. L., *J. Am. Chem. Soc.* **2005**, *127*, 7857.

307. Kubas, G. J.; Ryan, R. R.; Swanson, B. I.; Vergamini, P. J.; Wasserman, H. J., *J. Am. Chem. Soc.* **1984**, *106*, 451.

308. Kubas, G. J., *Metal Dihydrogen and σ-Bond Complexes: Structure, Theory, and Reactivity*. **2001**.

309. Kubas, G. J., *Metal Dihydrogen and σ-bond Complexes*. **2007**.

310. Hoyano, J. K.; Elder, M.; Graham, W. A. G., *J. Am. Chem. Soc.* **1969**, *91*, 4568.

311. Kubas, G. J., *J. Organomet. Chem.* **2001**, *635*, 37.

312. Corey, J. Y.; Braddock-Wilking, J., *Chem. Rev.* **1999**, *99*, 175.

313. Luo, X.-L.; Kubas, G. J.; Bryan, J. C.; Burns, C. J.; Unkefer, C. J., *J. Am. Chem. Soc.* **1994**, *116*, 10312.

314. Nikonov, G. I., *Adv. Organomet. Chem.* **2005**, *53*, 217.

315. Alcaraz, G.; Sabo-Etienne, S., *Coord. Chem. Rev.* **2008**, *252*, 2395.

316. Schubert, U., *Adv. Organomet. Chem.* **1990**, *30*, 151.

317. Tanaka, I.; Ohhara, T.; Nimura, N.; Ohashi, Y.; Jiang, Q.; Berry, D. H., *J. Chem. Res.* **1999**, *4*, 14.

318. Mork, B. V.; Tilley, T. D.; Schultz, A. J.; Cowan, J. A., *J. Am. Chem. Soc.* **2004**, *126*, 10428.

319. Scherer, W.; Eickerling, G.; Tafipolsky, M.; McGrady, G. S.; Sirsch, P.; Chatterton, N. P., *Chem. Commun.* **2006**, 2986.

320. Bourg, S.; Roury, B.; Carré, F.; Corriu, R. J. P., *Organometallics* **1997**, *16*, 3097.

321. Freeman, S. T. N.; Lemke, F. R.; Brammer, L., *Organometallics* **2002**, *21*, 2030.

322. Park, S.; Brookhart, M., *Organometallics* **2010**, *29*, 6057.

323. Luo, X. L.; Crabtree, R. H., *J. Am. Chem. Soc.* **1989**, *111*, 2527.

324. Lemke, F. R., *J. Am. Chem. Soc.* **1994**, *116*, 11183.

325. Freeman, S. T. N.; Lemke, F. R.; Brammer, L., *Organometallics* **2002**, *21*, 2030.

326. Brook, M. A., *Silicon in Organic, Organometallic, and Polymer Chemistry*. **2000**.

327. Takao, T.; Yoshida, S.; Suzuki, H., *Chem. Lett.* **2001**, 1100.

328. Junk, T.; Catallo, W. J., *Chem. Soc. Rev.* **1997**, *26*, 401.

329. Siskin, M.; Katritzky, A. R., *Chem. Rev.* **2001**, *101*, 825.

330. Crabtree, R. H., *J. Organomet. Chem.* **2004**, *689*, 4083.

331. Ribas, X.; Xifra, R.; Parella, T.; Poater, A.; Solà, M.; Llobet, A., *Angew. Chem.* **2006**, *118*, 3007.

332. Atzrodt, J.; Derdau, V.; Fey, T.; Zimmermann, J., *Angew. Chem. Int. Ed.* **2007**, *46*, 7744.

333. Elander, N.; Jones, J. R.; Lu, S.-Y.; Stone-Elander, S., Microwave-enhanced radiochemistry. *Chem. Soc. Rev.* **2000**, *29*, 239.

334. Thulasiram, H. V.; Phan, R. M.; Rivera, S. B.; Poulter, C. D., *J. Org. Chem.* **2006**, *71*, 1739.

335. Moriconi, E. J.; St. George, J. P.; Forbes, W. F., *Can. J. Chem* **1966**, *44*, 759.

336. Munz, D.; Webster-Gardiner, M.; Fu, R.; Strassner, T.; Goddard, W. A.; Gunnoe, T. B., *ACS Catal.* **2015,** *5*, 769.

337. Bai, W.; Lee, K.-H.; Tse, S. K. S.; Chan, K. W.; Lin, Z.; Jia, G., *Organometallics* **2015**, *34*, 3686.

338. Eguillor, B.; Esteruelas, M. A.; Garcia-Raboso, J.; Olivan, M.; Onate, E., *Organometallics* **2009**, *28*, 3700.

339. Ariza, X.; Asins, G.; Garcia, J.; Hegardt, F. G.; Makowski, K.; Serra, D.; Velasco, J., *J. Labelled Compd. Radiopharm.* **2010**, *53*, 556.

340. Attygalle, A. B.; Gangam, R.; Pavlov, J., *Anal. Chem. (Washington, DC, U. S.)* **2014**, *86*, 928.

341. Buskens, P.; Giunta, D.; Leitner, W., *Inorg. Chim. Acta* **2004**, *357*, 1969.

342. Lee, S. H.; Gorelsky, S. I.; Nikonov, G. I., *Organometallics* **2013**, *32*, 6599.

343. Piola, L.; Fernandez-Salas, J. A.; Manzini, S.; Nolan, S. P., *Org. Biomol. Chem.* **2014**, *12*, 8683.

344. Shilov, A. E.; Shul'pin, G. B., *Chem. Rev.* **1997**, *97*, 2879.

345. Lehman, M. C.; Gary, J. B.; Boyle, P. D.; Sanford, M. S.; Ison, E. A., *ACS Catalysis* **2013**, *3*, 2304.

346. Rhinehart, J. L.; Manbeck, K. A.; Buzak, S. K.; Lippa, G. M.; Brennessel, W. W.; Goldberg, K. I.; Jones, W. D., *Organometallics* **2012**, *31*, 1943.

347. Iluc, V. M.; Fedorov, A.; Grubbs, R. H., *Organometallics* **2012**, *31*, 39.

348. Hickman, A. J.; Cismesia, M. A.; Sanford, M. S., *Organometallics* **2012**, *31*, 1761.

349. Klei, S. R.; Golden, J. T.; Tilley, T. D.; Bergman, R. G., *J. Am. Chem. Soc.* **2002**, *124*, 2092.

350. Becker, E.; Stingl, V.; Mereiter, K.; Kirchner, K., *Organometallics* **2006**, *25* (17), 4166.

351. Derrah, E. J.; Giesbrecht, K. E.; McDonald, R.; Rosenberg, L., *Organometallics* **2008**, *27*, 5025.

352. Dubey, A.; Khaskin, E., *ACS Catal.* **2016**, *6*, 3998.

353. Baratta, W.; Ballico, M.; Zotto, A. D.; Siega, K.; Magnolia, S.; Rigo, P., *Chem.—Eur. J.* **2008**, *14*, 2557.

354. Lundgren, R. J.; Stradiotto, M., *Chem.—Eur. J.* **2008**, *14*, 10388.

355. Huang, J.; Schanz, H.-J.; Stevens, E. D.; Nolan, S. P., *Organometallics* **1999**, *18*, 2370.

356. Gutsulyak, D. V.; Vyboishchikov, S. F.; Nikonov, G. I., *J. Am. Chem. Soc.* **2010**, *132*, 5950.

357. Vyboishchikov, S. F.; Nikonov, G. I., *Organometallics* **2007**, *26*, 4160.

358. Corey, J. Y., *Chem. Rev.* **2011**, *111*, 863.

359. Corey, J. Y.; Braddock-Wilking, J., *Chem. Rev.* **1999**, *99*, 175.

360. Taw, F. L.; Bergman, R. G.; Brookhart, M., *Organometallics* **2004**, *23*, 886.

361. Albinati, A.; Bakhmutov, V. I.; Belkova, N. V.; Bianchini, C.; de los Rios, I.; Epstein, L.; Gutsul, E. I.; Marvelli, L.; Peruzzini, M.; Rossi, R., *Eur. J. Inorg. Chem.* **2002**, *2002*, 1530.

362. Campion, B. K.; Heyn, R. H.; Tilley, T. D.; Rheingold, A. L., *J. Am. Chem. Soc.* **1993**, *115*, 5527.

363. Mork, B. V.; Tilley, T. D., *J. Am. Chem. Soc.* **2001**, *123*, 9702.

364. Shilov, A. E.; Shul'pin, G. B., *Chem. Rev.* **1997**, *97*, 2879.

365. Scott, N. M.; Nolan, S. P., *Eur. J. Inorg. Chem.* **2005**, *10*, 1815.